

Technical Report Documentation Page

1. REPORT No.

TE 70-5

2. GOVERNMENT ACCESSION No.**3. RECIPIENT'S CATALOG No.****4. TITLE AND SUBTITLE**

Asphalt Mixture Behavior In Repeated Flexure

5. REPORT DATE

December 1970

6. PERFORMING ORGANIZATION**7. AUTHOR(S)**

Carl Monismith, J.A. Epps, D.A. Kasianchuk, and D.B. McLean

8. PERFORMING ORGANIZATION REPORT No.

TE 70-5

9. PERFORMING ORGANIZATION NAME AND ADDRESS

Office of Research Services
University of California, Berkeley

10. WORK UNIT No.**11. CONTRACT OR GRANT No.****12. SPONSORING AGENCY NAME AND ADDRESS****13. TYPE OF REPORT & PERIOD COVERED****14. SPONSORING AGENCY CODE****15. SUPPLEMENTARY NOTES**

Prepared in cooperation with the United States Department of Transportation, Federal Highway Administration

16. ABSTRACT

Introduction:

This report describes research completed during the period 1966- 1970 on the project concerned with (1) factors affecting the fatigue response of asphalt paving mixtures and (2) incorporation of the fatigue factor in the design of asphalt concrete pavements.

During this period considerable information has been developed on the factors affecting the fatigue response of mixtures representative of the type used in California and an attempt has been made to summarize these results into a form usable for design purposes.

Secondly the investigation has been concerned with the definition of a subsystem to consider the fatigue mode of distress in the structural design of new pavements and in the analysis of existing pavements. The authors consider this to be one of the significant results stemming from the study. General considerations for this subsystem have been summarized and the most recent developments required to use the subsystem have been included to make the process as realistic and reasonable for engineering use as practicable.

Finally, in order that considerations of fatigue may eventually be incorporated in asphalt mixture design requirements, a brief discussion is included of alternative ways in which fatigue response might be controlled or defined through a direct tension test, a test which is much less time consuming and simpler to perform than conventional fatigue tests.

17. KEYWORDS**18. No. OF PAGES:**

302

19. DRI WEBSITE LINK

<http://www.dot.ca.gov/hq/research/researchreports/1969-1970/te70-5.pdf>

20. FILE NAME

TE70-5.pdf

SOIL MECHANICS AND BITUMINOUS MATERIALS
RESEARCH LABORATORY



ASPHALT MIXTURE BEHAVIOR IN
REPEATED FLEXURE

by
C. L. MONISMITH
J. A. EPPS
D. A. KASIANCHUK
and
D. B. McLEAN

REPORT NO. TE 70-5
to

THE MATERIALS A
DIVISIO
STATE

PREPARED IN
THE UNITED STATES DE
FEDERAL HIGH
BUREAU

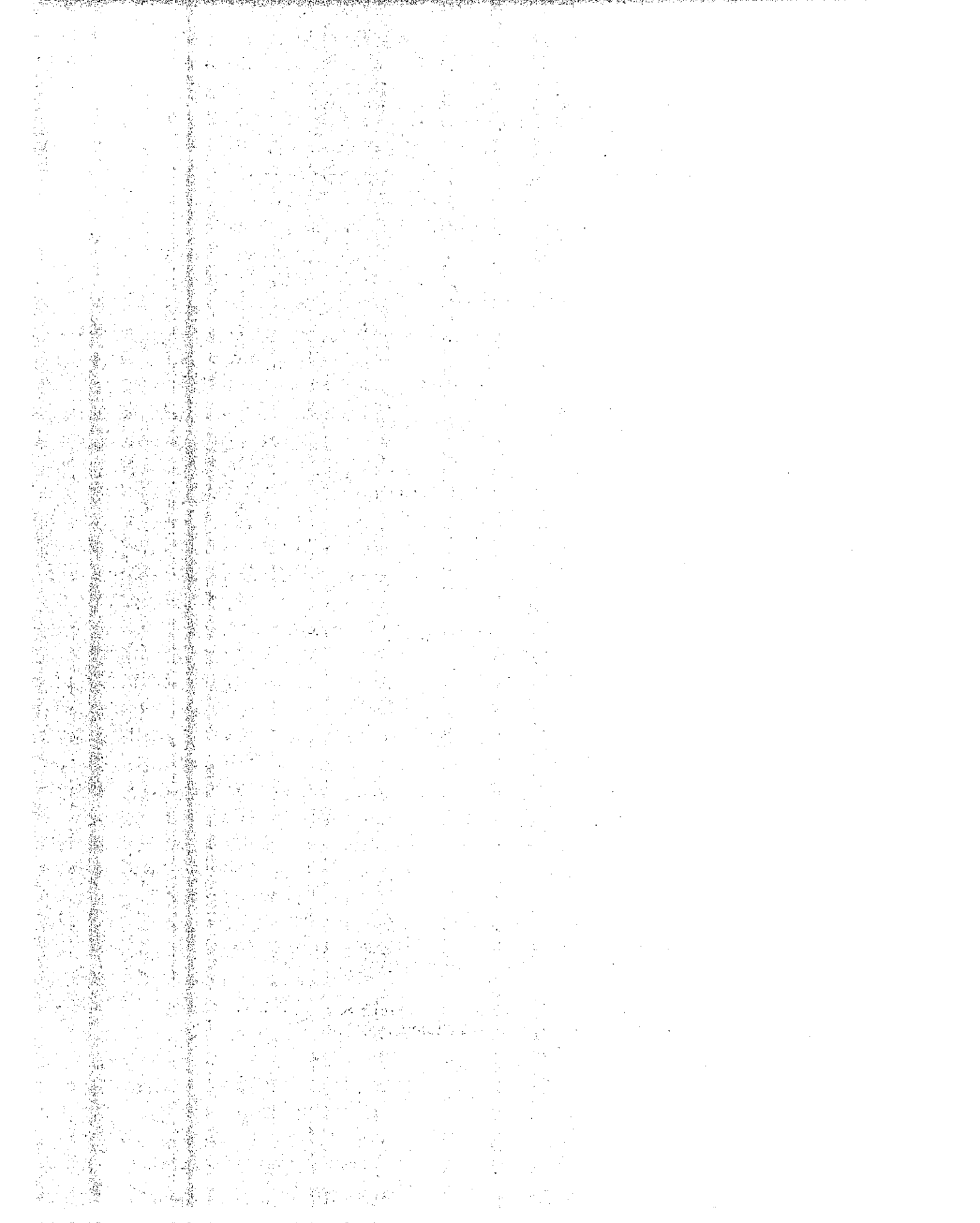
**TE
70-5**

DEPARTMENT C
INSTITUTE OF TRANSPORTA

G



University of California • Berkeley



Soil Mechanics and Bituminous Materials
Research Laboratory

ASPHALT MIXTURE BEHAVIOR IN REPEATED FLEXURE

A report on an investigation

by

C. L. Monismith
Professor of Civil Engineering and
Research Engineer

J. A. Epps
Assistant Professor of Civil Engineering
Texas A & M University, College Station, Texas
formerly Research Assistant

D. A. Kasianchuk
Associate Professor of Engineering
Carleton University, Canada
formerly Research Assistant

and

D. B. McLean
Research Assistant

to

The Materials and Research Department
Division of Highways
State of California

under

State of California Standard Agreement M and R 633153
Research Technical Agreement 13945-13002

Prepared in cooperation with
The United States Department of Transportation
Federal Highway Administration

Report No. TE 70-5, Office of Research Services
University of California, Berkeley, California

December 1970

MEMORANDUM FOR THE RECORD

DATE: 10/15/54

TO: SAC, NEW YORK

FROM: SA [Name obscured]

SUBJECT: [Subject obscured]

[Text obscured]

INTRODUCTION

This report describes research completed during the period 1966-1970 on the project concerned with (1) factors affecting the fatigue response of asphalt paving mixtures and (2) incorporation of the fatigue factor in the design of asphalt concrete pavements.

During this period considerable information has been developed on the factors affecting the fatigue response of mixtures representative of the type used in California and an attempt has been made to summarize these results into a form usable for design purposes.

Secondly the investigation has been concerned with the definition of a subsystem to consider the fatigue mode of distress in the structural design of new pavements and in the analysis of existing pavements. The authors consider this to be one of the significant results stemming from the study. General considerations for this subsystem have been summarized and the most recent developments required to use the subsystem have been included to make the process as realistic and reasonable for engineering use as practicable.

Finally, in order that considerations of fatigue may eventually be incorporated in asphalt mixture design requirements, a brief discussion is included of alternative ways in which fatigue response might be controlled or defined through a direct tension test, a test which is much less time consuming and simpler to perform than conventional fatigue tests.

PAVEMENT DESIGN SYSTEMS — GENERAL CONSIDERATIONS

Pavement design, like other aspects of engineering design requires that engineers have the ability to analyze pavement structures in terms of significant parameters. Moreover it is necessary that such analyses incorporate essential features of observed pavement performance and appropriately measured values of the parameters to make the necessary quantitative evaluations required for design. It is generally recognized, however, that the parameters involved together with their interrelationships are complex.

It is possible to formulate, in a systematic manner, pavement design systems which bring these factors together. A schematic representation of one such formulation is illustrated in Fig. 1 (1). Some solutions for this system have been generated using a relatively simple representation for the effects of load and environment on reduction of serviceability in the pavement structure (1,2) and include considerations for certain of the decision criteria (e. g. , maintenance requirements and material costs).

An alternative approach is to develop a series of subsystems, the goal of each is to minimize a particular form of distress. Using this approach a pavement structure may be selected to minimize one distress mode and then checked to insure that other modes do not occur or are in themselves minimal. If the potential for other forms of distress do exist (to an intolerable degree), the design may be modified to preclude or reduce these effects.

Table 1 lists the three principal distress modes which can lead to a decrease in the serviceability of asphalt pavements with time. From an extensive evaluation of the performance of asphalt pavements throughout the United States, Finn (3) has suggested that the distress mechanisms which appear to be most significant in contributing to a reduction in pavement serviceability are:

1. Fracture from repeated loading (fatigue in treated materials).
2. Distortion which is traffic associated.
3. Fracture resulting from non-traffic associated factors (e. g. , temperature changes or moisture changes in subgrade soil).

Specific formats for design frameworks (subsystems) are shown in Figs. 2 through 4 to consider these three distress modes. It will be noted that these subsystems parallel the conventional structural engineering approach in which a structure is selected (designed)*, its behavior under anticipated service conditions analyzed, and its adequacy with respect to the specific distress criterion determined.

*The State of California pavement design procedure can serve as the starting point for such an analysis.

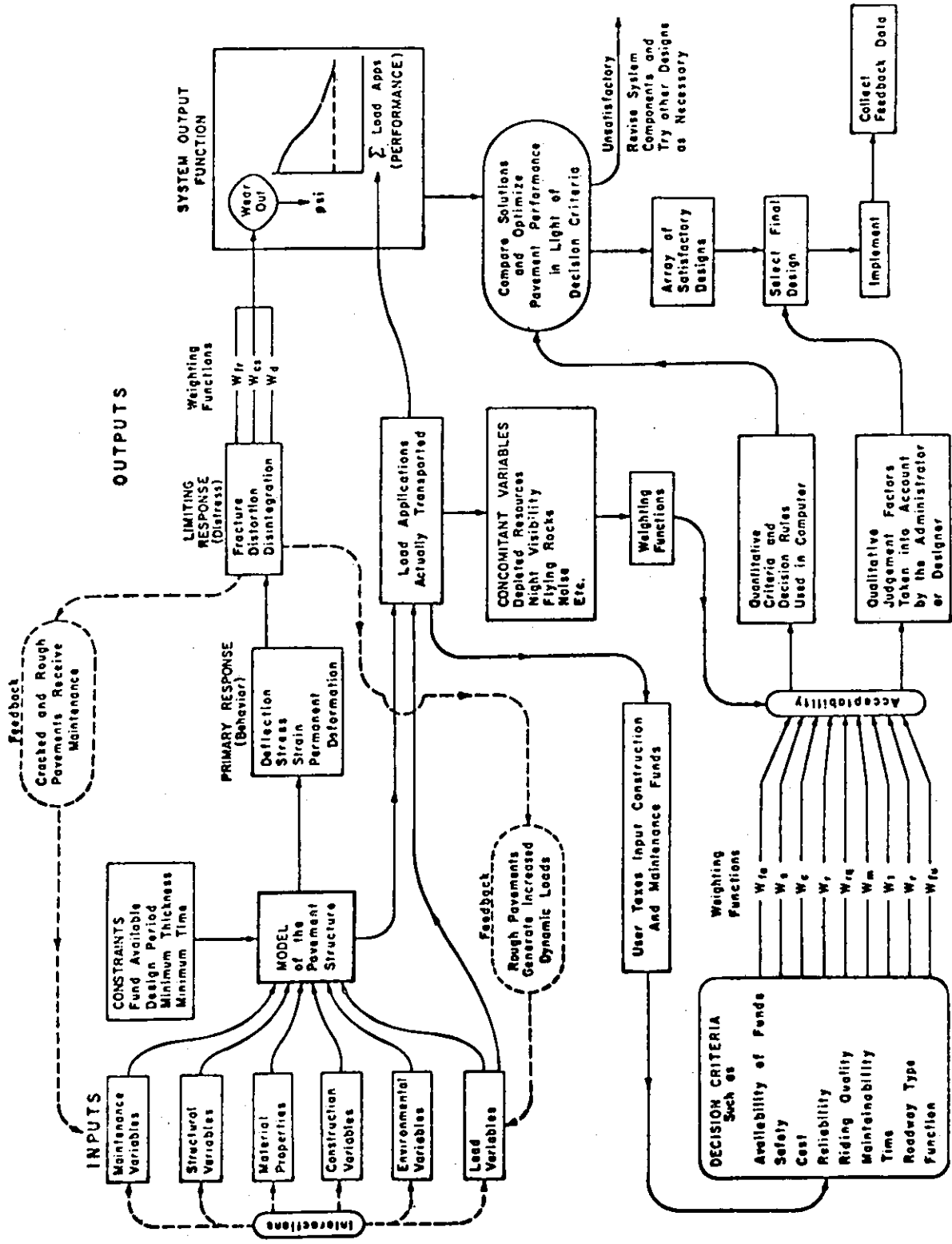


Fig. 1 -- Block diagram of conceptual pavement system. (After NCHRP Project 1-101.)

TABLE 1 — CATEGORIES OF DISTRESS FOR ASPHALT PAVEMENTS⁽¹⁾

<u>Distress Mode</u>	<u>Distress Manifestation</u>	<u>Examples of Distress Mechanism</u> ⁽²⁾
Fracture ——— Cracking	Traffic-load associated	Repeated Loading (fatigue) Excessive Loading Slippage (horizontal forces)
	Non-traffic associated	Moisture Changes Thermal Changes Shrinkage
Distortion ——— Permanent Deformation	Traffic-load associated	Excessive Loading (shear distortion) Time-dependent Deformation (e.g., creep) Densification (i. e., compaction)
	Non-traffic associated	Swelling Consolidation of underlying materials
Disintegration ——— Raveling, Stripping	Traffic-load associated	Abrasion by Traffic Aggregate Degradation
	Non-traffic associated	Adhesion (i. e., loss of bond) Chemical Reactivity Asphalt Durability

(1) Adapted from Finn, Hudson, McCullough and Nair.

(2) Not intended to be a complete listing of all possible distress mechanisms.

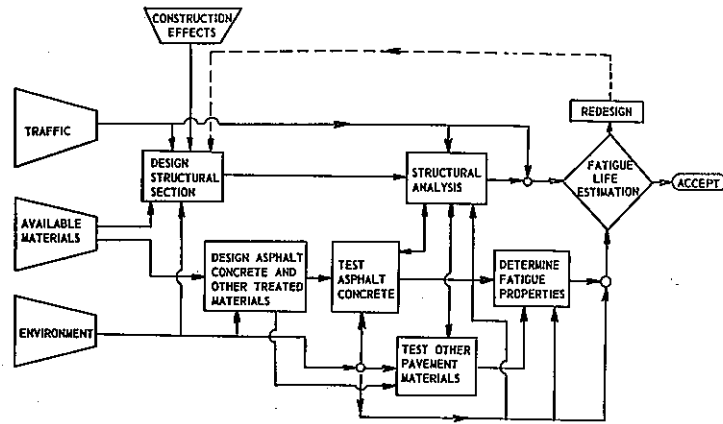


Fig. 2 — Block diagram of a fatigue subsystem.

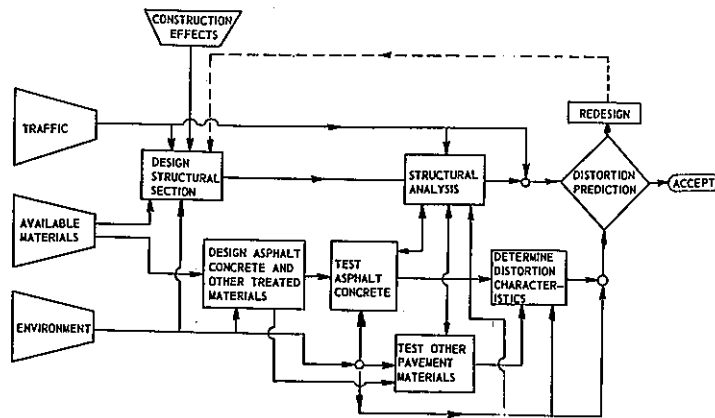


Fig. 3 — Block diagram of a distortion subsystem.

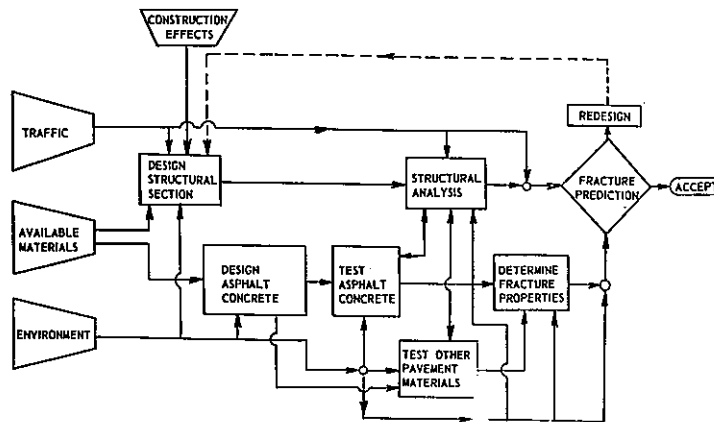


Fig. 4 — Block diagram of a fracture subsystem.

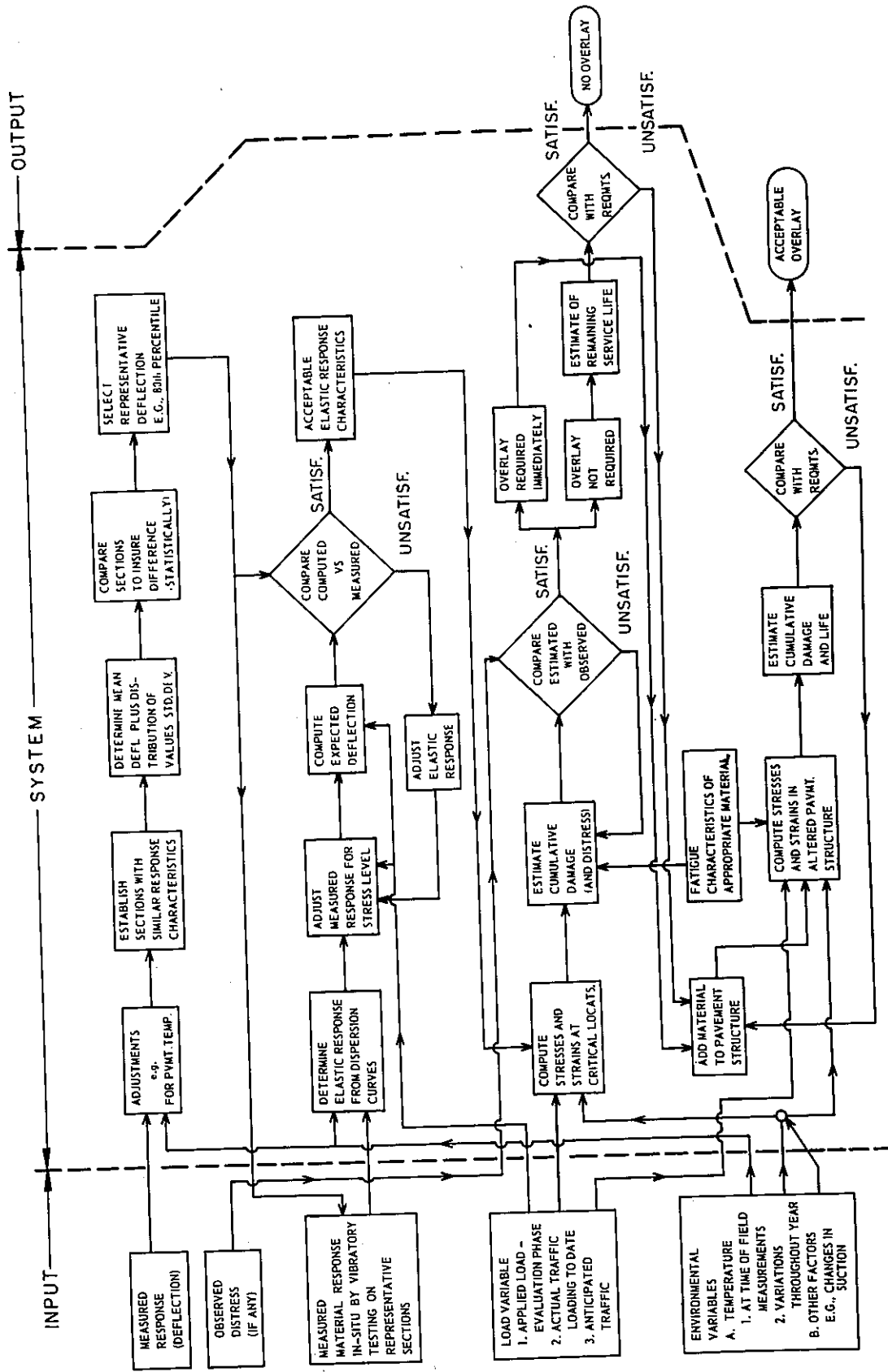


Fig. 5 — Example of an overlay design subsystem of the pavement design and management system.

In the next section a detailed discussion is presented for the fatigue subsystem. Available information is summarized for each phase of the design process. Hopefully the material which has been summarized will illustrate how available theory can be blended with present experience to make reasonable engineering decisions at this stage in time.

At this point it should also be noted that such an approach is not only applicable for the design of new pavements, but also can be used to evaluate existing pavements and to design overlay pavements.

In Fig. 5 is illustrated a simplified flow diagram for the overlay design subsystem to consider the fatigue mode of distress. It will be noted that this system is an extension of the overlay design procedure developed by the State of California (4).

It should be emphasized that this approach to pavement design is not intended to develop a replacement for existing methods rather it is hoped that such a technique or others like it as they are developed will be used in conjunction with existing procedures in order that engineers will have the capabilities to:

1. Accommodate continually changing loading requirements (including both changes in weight and repetitions).
2. Better utilize available materials.
3. Accommodate new materials which might be developed.
4. Better define the role of construction.
5. Improve the reliability for performance prediction (or of the design estimate).

FATIGUE SUBSYSTEM

In this section the fatigue subsystem shown in Fig. 2 will be discussed in detail. Information required and data available from this investigation as well as material developed from other studies are summarized. The material contained herein is intended to provide the engineer with a general overview of the procedure whereby the potential for fatigue in an existing or new pavement can be ascertained utilizing recently developed information. For convenience the information will be summarized in subsections corresponding to the various steps shown in Fig. 2.

Traffic

For highway pavements the following traffic information is required:

1. Axle load distribution.
2. Wheel and axle configurations (dual or single tires and single or tandem axles*).
3. Contact pressures (or tire pressures) of the various classes of vehicles.
4. Distribution of truck traffic throughout day, month, and year.
5. Vehicular velocities.
6. Lane distribution of truck traffic for multilane facilities.
7. Tracking of traffic in wheel paths.

The most desirable solution would be to have this data available for the specific highway to be designed. Alternatively traffic data contained in statewide or local traffic surveys may have to be utilized if data for the specific highway is not available (e. g. , loadometer studies, contained in the W-4 Table).

To estimate fatigue damage attributable to specific traffic, it is necessary to establish the correspondence between traffic repetitions and stress applications developed at some critical point in the layer which may be damaged by fatigue. Thus the lateral placement (wheel path tracking) and distribution of traffic among the lanes of a multilane facility must be determined.

The distribution of truck traffic in the lanes of multilane highways has been investigated by Taragin (6) and Fig. 6 illustrates data developed by him for a four-lane divided highway.

The State of California utilizes such considerations for design purposes and the proportion of truck traffic assigned to each lane is shown in Table 2 (no consideration for traffic volume, however, as seen in Fig. 6. and proportions are therefore conservative).

*Dual axles considered as two repetitions of a single axle as is done in the State of California Design Procedure (5).

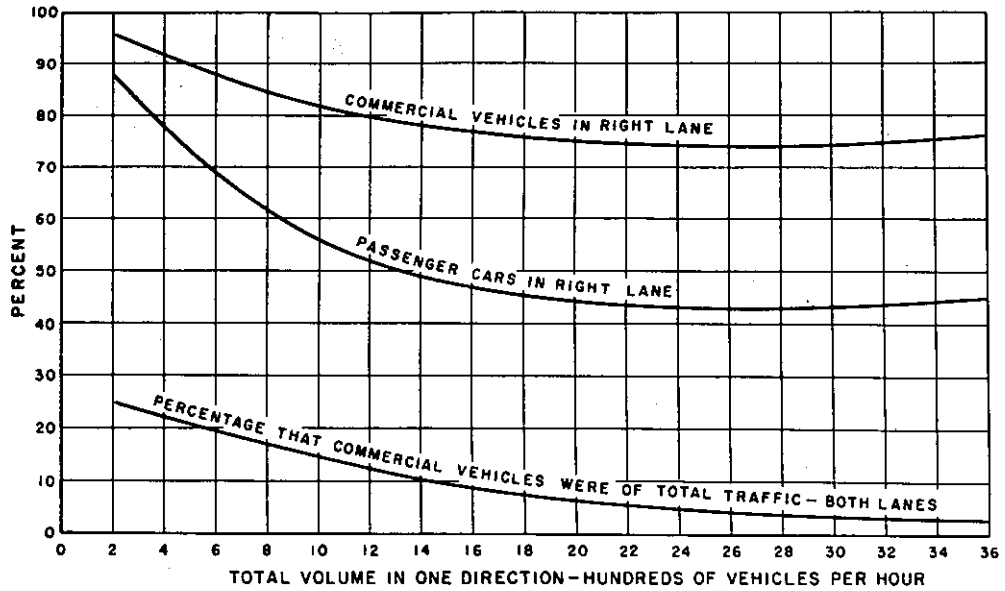


Fig. 6 - Proportion of commercial vehicles using the right lane of divided four-lane highways as a function of total traffic volume. (After Taragin)

**DISTRIBUTION OF TRUCK WHEEL PLACEMENTS
RELATIVE TO PAVEMENT EDGE**

(Right side of contact area, 12' right lane)

Distance from edge of pavement in inches	Frequency %
0*	0.03
0-1	0.03
0-2	0.1
0-3	0.2
0-4	0.3
0-5	0.4
0-6	0.6

10" x 20" Tire
Tire width = 11.7"
Contact area width = 7.2"
Truck width = 95"
Truck to outside edge of contact area = 45.25"

* with right side of contact area at or beyond the pavement edge

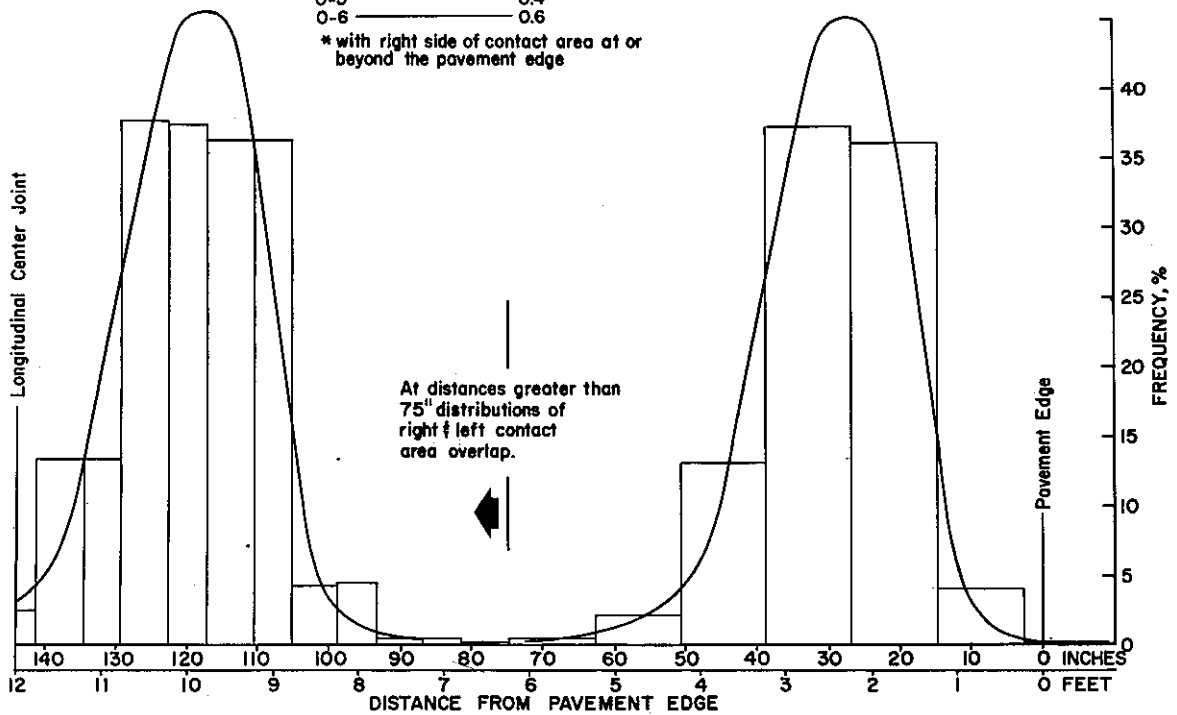


Fig. 7 - Lateral distribution of trucks within a traffic lane. (After Fordyce and Packard.)

TABLE 2 — LANE DISTRIBUTION FACTORS ON MULTILANE ROADS

Number of lanes in both directions	Factors to be applied to EWL percent			
	Lane 1*	Lane 2	Lane 3	Lane 4
2	100	-	-	-
4	100	100	-	-
6	20	80	80	-
8	20	20	80	80

(after State of California, Planning Manual)

*Lane 1 is next to the centerline or median on the driver's left.

The correspondence between the number of vehicle passages within the design lane and the number of load repetitions at some critical point, e. g. the center of the outer wheel path, is dependent on the tracking of the vehicles using the lane. Taragin (6) has shown that the center of the average truck is located within 0.2 feet of the center of a 12-foot wide lane and that about 75 percent of the trucks maintained a lateral position within one foot of the center of the lane. He also notes that little difference occurs in this pattern on slight curves and that the placement in two and four lane highways is approximately the same.

Fordyce and Packard (7) have examined the variation in the lateral location of the wheels of a typical truck. Fig. 7 shows this lateral distribution. If the smooth curves shown in this figure are assumed to represent a normal distribution of the center of the loaded area about the center of the wheel path, a standard deviation of about 9 inches will yield the frequency distribution shown for the tail of the curve.

Analyses such as that shown in Fig. 8 indicate that the stress level at the underside of the asphalt concrete layer is relatively constant over the section from outside to outside of the tires. If we now assume that a typical dual tire spacing is 14 in. center to center of the tires and that each of the tires has an effective load radius of 4 in., we can see that the center of the wheel path is strained near its maximum for every passage of a dual tire within 11 in. of the center of the wheel path. Assuming the normal distribution of lateral locations based on Fordyce and Packard's curve, this indicates that about 80 percent of all passages will result in this strain level at the center of the wheel path. Since the dual dimensions assumed above might be considered as minimum spacing, it is reasonable to assume that each passage of such a load will result in near maximum strain at the critical location. The remainder of the wheel load passages will result in some lesser strain level at the critical location in the design lane.

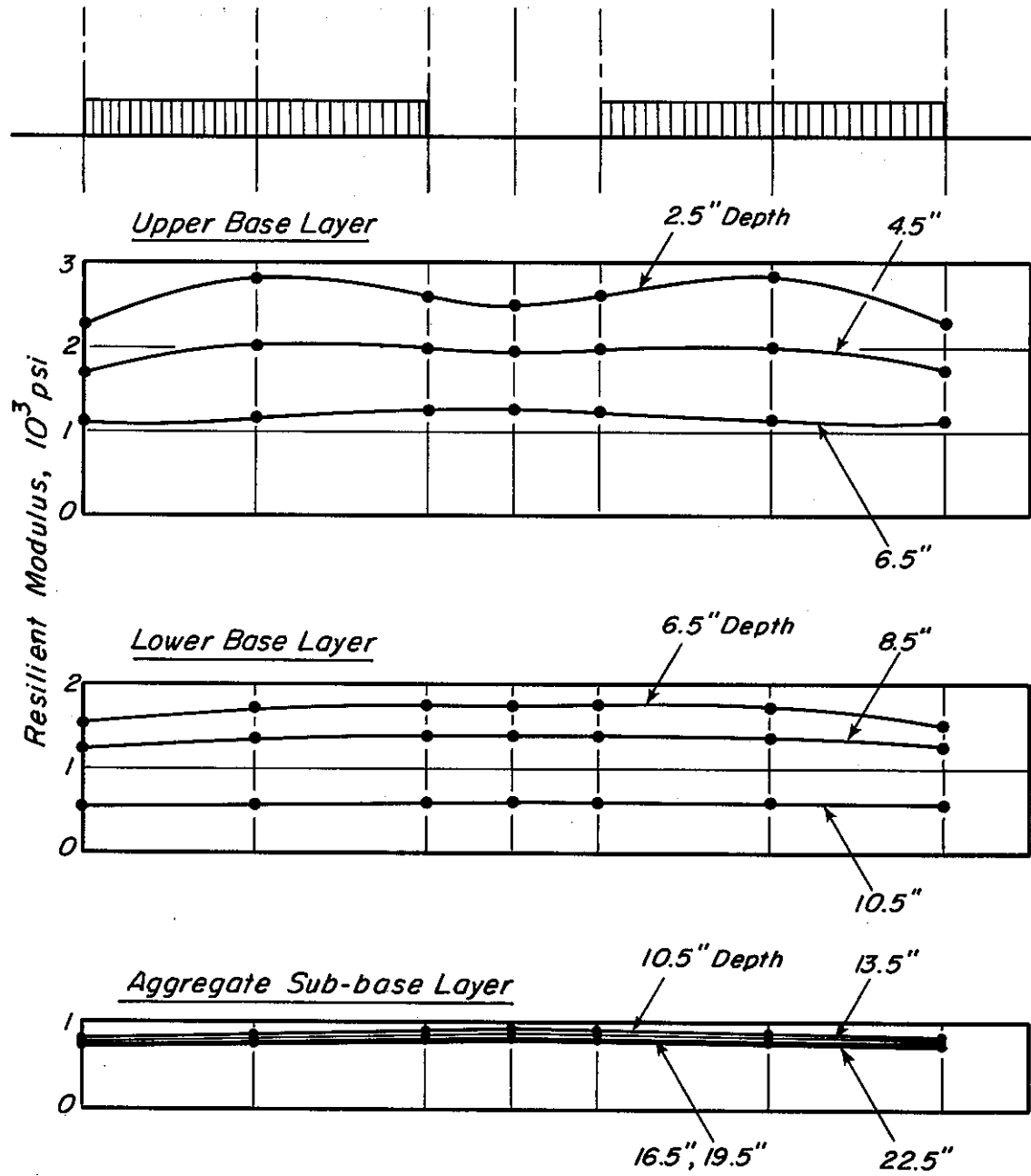


Fig. 8 — Variation of modulus across loaded area.

From this argument one can see that it is not unduly conservative to use a one-to-one relationship between wheel load passages in the design lane and load repetitions at the center of the wheel path. More sophisticated treatment of the lateral location variation does not seem justified when one considers the accuracy that can be expected from the estimates of traffic that will be used.

Environment

Since the response of asphalt concrete to load is dependent on temperature, distributions of temperature within the asphalt-bound layer must be obtained. In addition, the influence of environment as it influences the water contents (or effective stresses) of materials comprising pavement sections must be ascertained. While there are other environmental effects, such as aging (or curing) of treated materials and changes in characteristics of treated or untreated materials due to the effects of water other than those caused by changes in water content or effective stress, these will not be discussed at this time even though such effects may be important as far as the ultimate performance of the pavement structure is concerned.

Temperature. The distribution of temperature in an asphalt-bound layer can be determined using a form of the heat conduction equation where the temperature input is assumed independent of the x and y coordinates, i. e. ,

$$\frac{\partial^2 \phi}{\partial z^2} = \frac{c\rho}{k} \frac{\partial \phi}{\partial t}$$

where:

- ϕ = temperature field
- c = specific heat of the material
- k = thermal conductivity
- ρ = density of the material

Available data (8) indicate that c is of the order of 0.2 BTU per lb per °F and k is of the order of 0.7 BTU per ft² per hr per °F, ft. It is possible to include not only daily temperature variations (assumed to vary sinusoidally about the daily mean) but also the effects of solar insolation, sky (or cloud) cover, and wind velocity (9).

The generalized equation is for a semi-infinite mass in contact with air at a temperature $T_M + T_V \sin 0.2625t$; the 24 hr periodic temperature of the mass is (9):

$$T = T_M + T_V \cdot \frac{He^{-xC}}{\sqrt{(H+C)^2 + C^2}} \sin \left(0.262t - xC - \arctan \frac{C}{H+C} \right) \dots (2)$$

where:

- T = temperature of mass, °F
 T_M = mean effective air temperature, °F
 T_V = maximum variation in temperature from mean, °F
 t = time from beginning of cycle, hours
 x = depth below surface, ft
 H = h/k
 h = surface coefficient, BTU per sq ft per hr, °F
 k = conductivity, BTU per sq ft per hr, °F per ft
 C = $\sqrt{0.131 \text{ per } b}$
 b = diffusivity, sq ft per hr = $k/c\rho$
 c = specific heat, BTU per lb, °F
 ρ = density, lbs per cu ft

To include the other effects noted above:

1. The effects of forced convection due to wind and average reradiation from the surface are accounted for by stating the surface coefficient as:

$$h = 1.3 + 0.62v^{0.75}$$

where:

v = wind velocity, miles per hour

2. The affect of solar radiation can be included by defining the effective air temperature to include solar radiation as:

$$T_E = T_a + \frac{dI}{h}$$

where::

- T_E = effective air temperature, °F
 T_a = air temperature, °F
 d = absorptivity of surface to solar radiation
 I = solar radiation, BTU per sq ft hr

Solar radiation on a horizontal surface is reported in Langleys per day. *

* One Langley per day = one calory per sq cm day or 3.69 BTU per sq ft day.

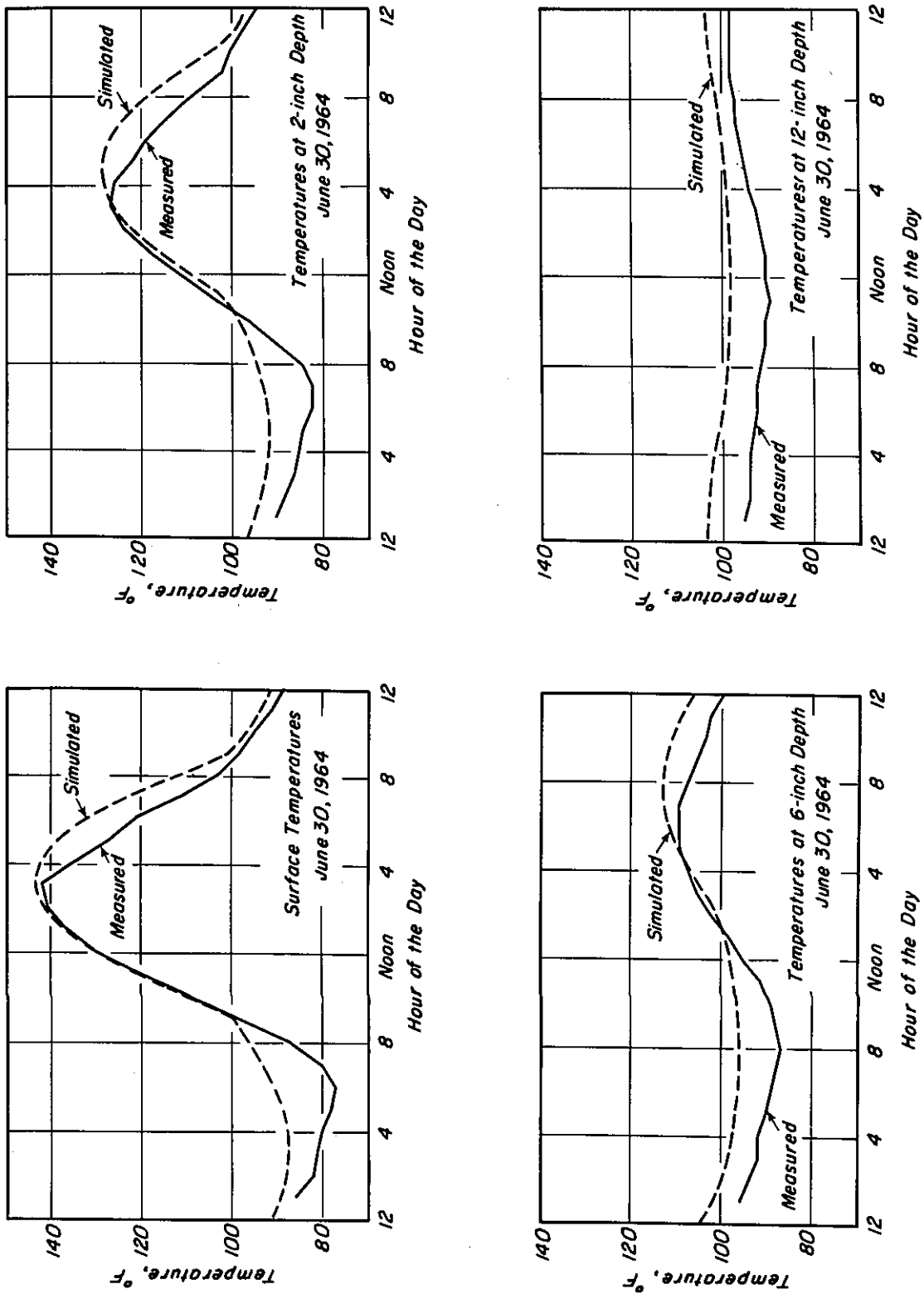


Fig. 9 — Comparison of computed and measured daily temperature variation. College Park, Maryland - June 1964. (After Kasianchuk.)

There is an average net loss by long-wave reradiation of about $1/3$, so that R, the average contribution to T_E , is:

$$R = 0.67b \frac{3.69L}{24h}$$

where:

L - solar radiation, Langleys per day

The deviation of R from the average may be roughly approximated by a sine wave with a half amplitude of $3R$. The maximum temperature obtained is then

$$T_M = T_A + R$$

where:

T_A = average air temperature, $^{\circ}F$

T_V = $0.5 T_R + 3R$

T_R = daily range in air temperature, $^{\circ}F$

Comparison of computed and measured data are shown in Figs. 9 and 10 using the available weather data (Table 3) and assumed properties for the asphalt concrete (Table 4). The reasonableness of the comparisons would indicate that temperature profiles can be computed with a reasonable degree of confidence at least in asphalt-bound layers to 12-in. in thickness.

TABLE 3 — WEATHER DATA, COLLEGE PARK, MARYLAND

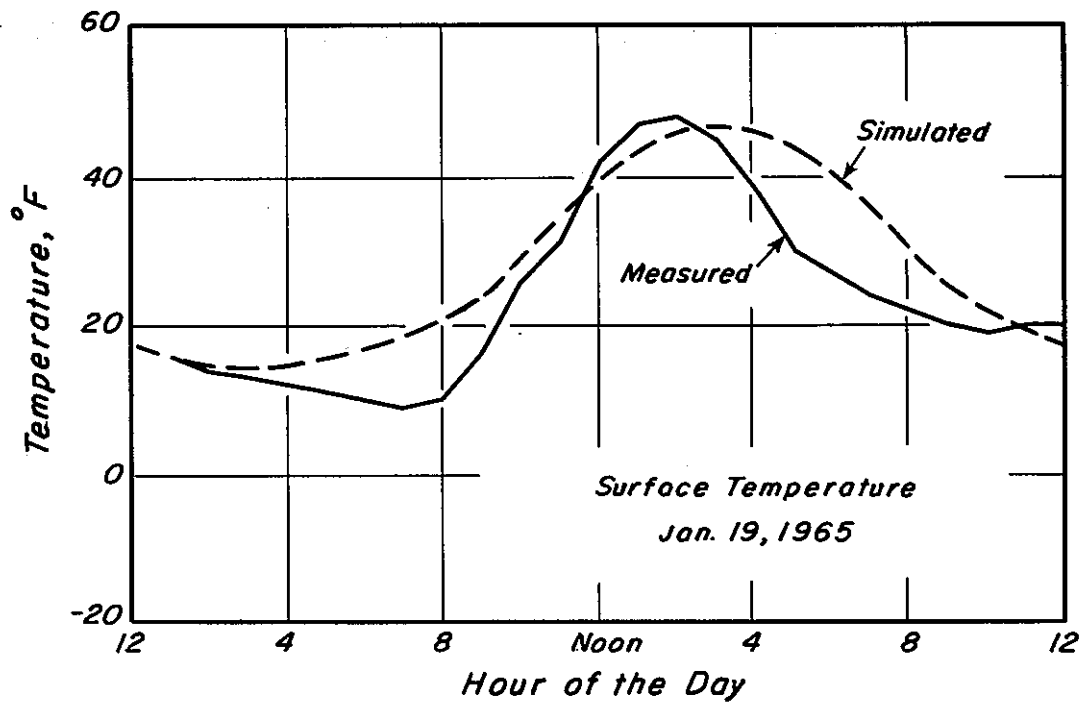
June 30, 1964

Mean Air Temperature	83.4 $^{\circ}F$
Diurnal Range	35.0 $^{\circ}F$
Mean Wind Velocity*	7.2 mph
Solar Insolation*	660 Langleys per day

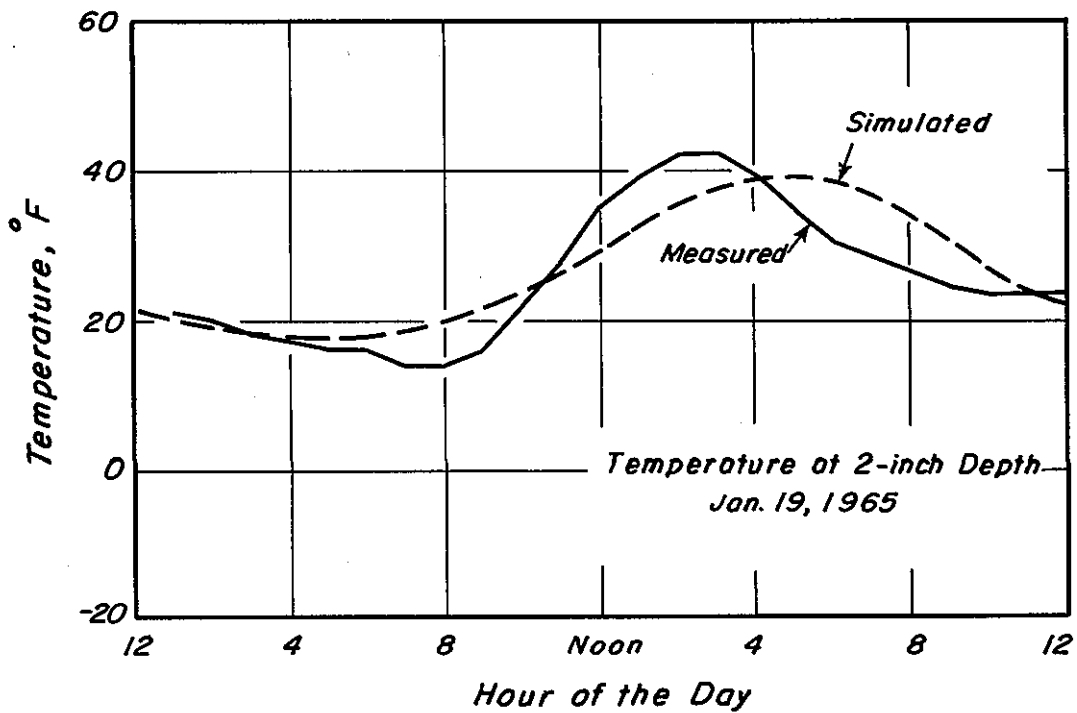
January 19, 1965

Mean Air Temperature	17.3 $^{\circ}F$
Diurnal Range	28.0 $^{\circ}F$
Mean Wind Velocity*	7.2 mph
Solar Insolation*	270 Langleys per day

* Estimated data



a.



b.

Fig. 10 — Comparison of computed and measured daily temperature variation, College Park, Maryland. (After Kasianchuk)

TABLE 4 — ASPHALT CONCRETE MIXTURE PROPERTIES,
COLLEGE PARK, MARYLAND TEMPERATURE STUDY

Unit Weight	143.2 lbs/cu ft
Asphalt Content (total mix)	4.9 percent
Air Voids Content	9.1 percent
Penetration	42 dmm
Ring and Ball Softening Point	138°F
Thermal Conductivity	0.70 BTU ft/ft ² , °F, hr
Specific Heat	0.22 BTU/lb, °F
Surface Coefficient	9.95

Alternatively, an extension of the finite element procedure (10) developed originally by Wilson (11) for temperature profiles can be used. This particular procedure has the advantage that it can be applied to layered systems in which the individual layers have different conductivities. Results of an analysis by Pretorius (10) are shown in Fig. 11.

This latter procedure may have some advantage in thick asphalt-bound layers (> 12 in.) where the temperature of the underlying materials may have some influence on the temperature variation in the lower portion of the bound-layer.

Moisture Considerations. One of the most important environmental effects is that of water, particularly as it influences the response of materials in the pavement section to load and as it may cause undesirable volume changes.

For structural design purposes the influence of water has generally been considered to the extent that properties of untreated materials are measured at water contents which are assumed to be representative of those which may develop at some time subsequent to construction, e. g. , the use of the exudation pressure in the State of California design procedure (5) or the use of soaked samples in the CBR design procedure (12). In some instances these procedures may lead to soil conditions which are not representative of those which develop in the field (13). Accordingly it is desirable to have alternative procedures available which would provide the pavement design engineer with estimates of expected in-situ moisture conditions together with an indication of how these conditions might develop (e. g. , some measure of the rate of increase (or decrease) in water content of a subgrade soil with time).

For areas like California or portions of the lower half of the United States where little or no freezing of the subgrade occurs, considerations of soil moisture suction may provide

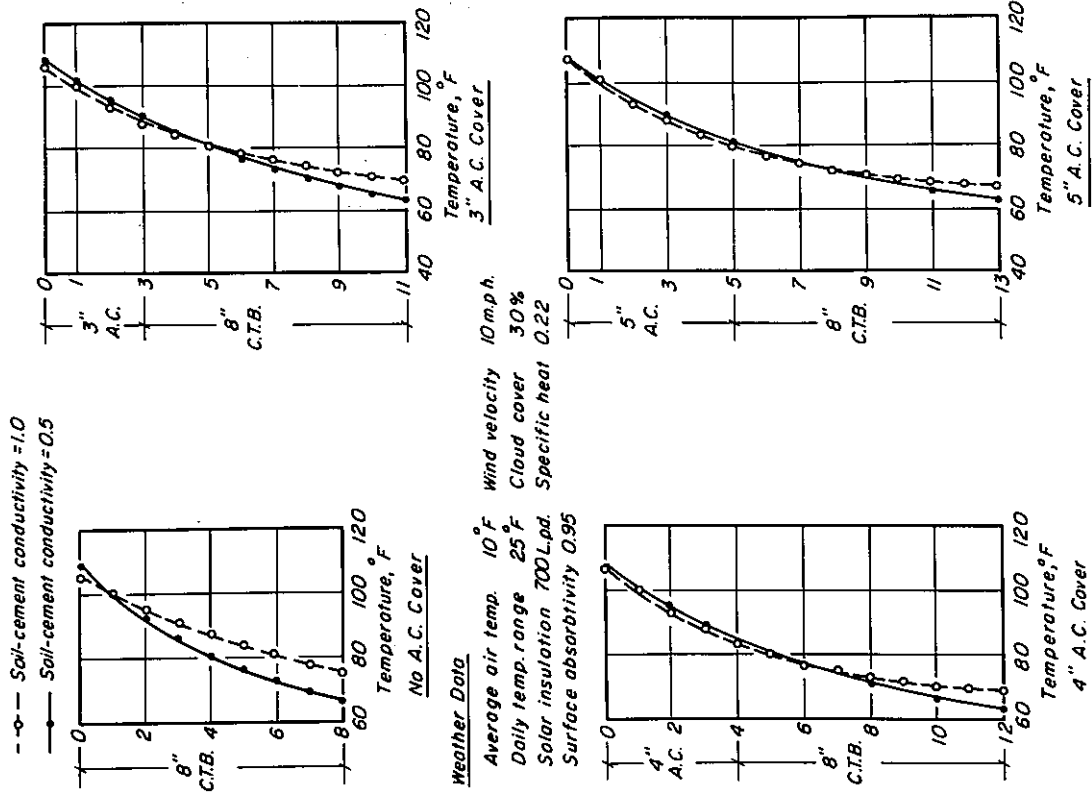


Fig. 11b - Influence of soil-cement conductivity on pavement temperature. (After Pretorius.)

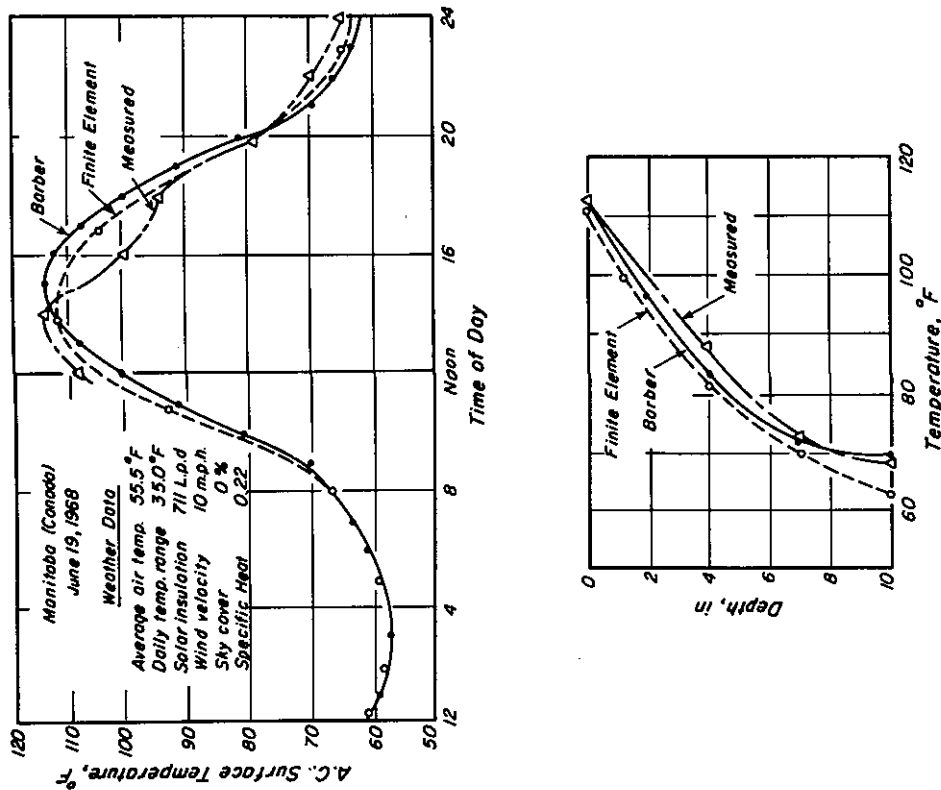


Fig. 11a - Comparison of recorded and predicted temperatures in a 10-in. asphalt concrete layer (After Pretorius.)

a useful (and practical) approach to the estimation of equilibrium moisture conditions in fine-grained soils, particularly under treated impervious layers (e. g. , asphalt concrete or asphalt-treated material resting directly on compacted fine-grained subgrade soils).

A number of investigators (e. g. , (13), (14)) have suggested procedures whereby the equilibrium suction profile can be estimated depending on the location of the groundwater table and the environment. Richards (13) has summarized these procedures as follows based primarily on the results of Australian (13) and British investigations (14).

For shallow water tables (20 ft in clay, 10 ft in sandy clays and silts, and 3 ft in sand), regardless of climate, the equilibrium suction profile can be estimated from:

$$(\text{matrix suction})_z = (\text{depth to G. W. T.}) - z \dots\dots\dots (3)$$

where:

z = depth, measured from bottom of impervious surface,
at which suction is desired. (Fig. 12a)

For deep water tables, the suction profile is controlled by the moisture balance between rainfall and evapotranspiration. In areas where no permanent surface desiccation exists, the profile can be expressed approximately by the relation (Fig. 12b):

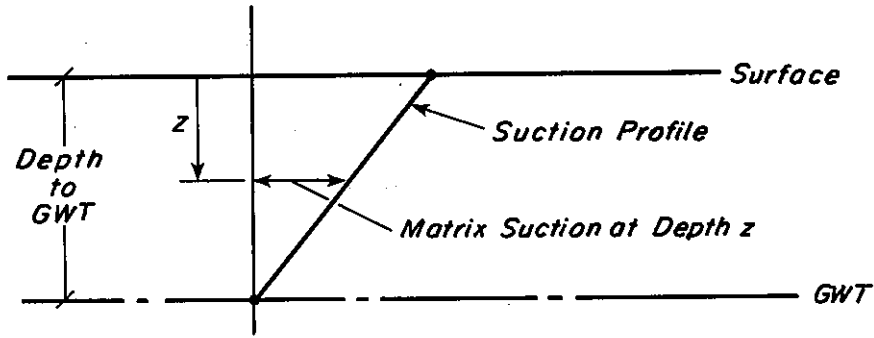
$$\begin{array}{l} \text{Suction at} \\ \text{depth } z \end{array} = \begin{array}{l} \text{Suction at a depth} \\ \text{greater than depth} \\ \text{of seasonal variation} \end{array} + z_0 - z \dots\dots\dots (4)$$

Alternatively it has been determined that total suction (and therefore matrix suction) beneath covered areas can be related approximately to climate by Thornthwaite's moisture index I**, shown in Fig. 13. It should be noted that large departures can occur from this relationship due to local environmental factors; however, it may prove useful for preliminary estimates of suction.

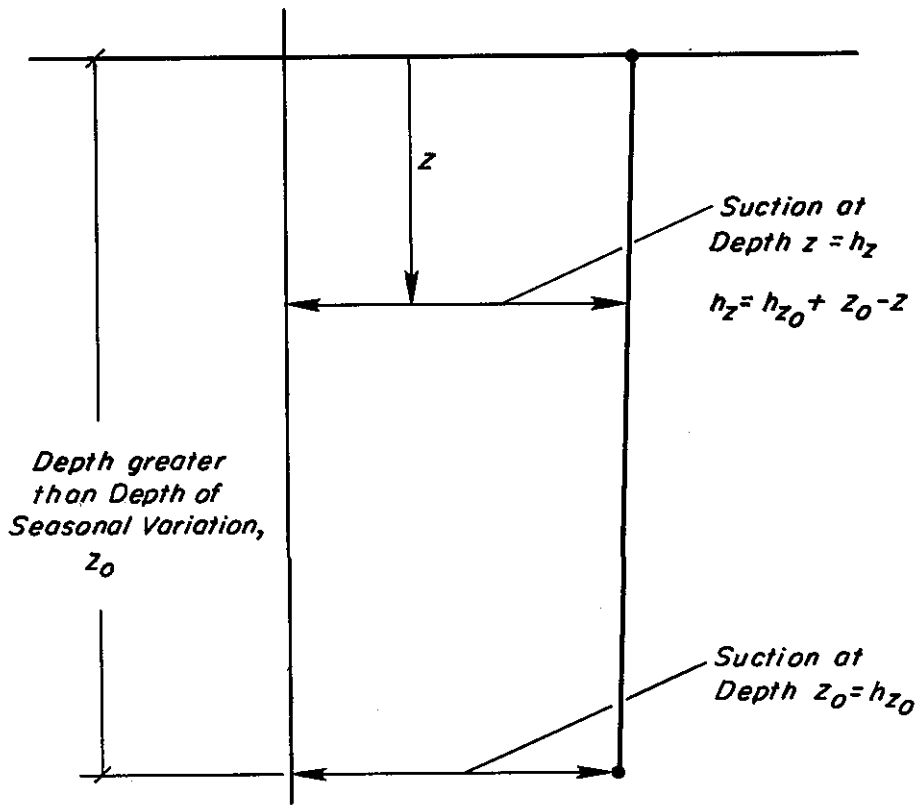
* Total suction is equal to the sum of matrix (or soil water) suction and osmotic suction. In the absence of dissolved salts, the osmotic suction is zero; for uniform salt concentrations the osmotic suction can be neglected. Under these circumstances, therefore, the total suction can be considered equal to the matrix suction.

$$** I = \frac{100D - 60d}{E_p}$$

where: D = soil drainage, inches
d = soil moisture deficit, inches
E_p = potential evapotranspiration, inches



a. Shallow water table.



b. Deep water table.

Fig. 12 — Suction profiles.

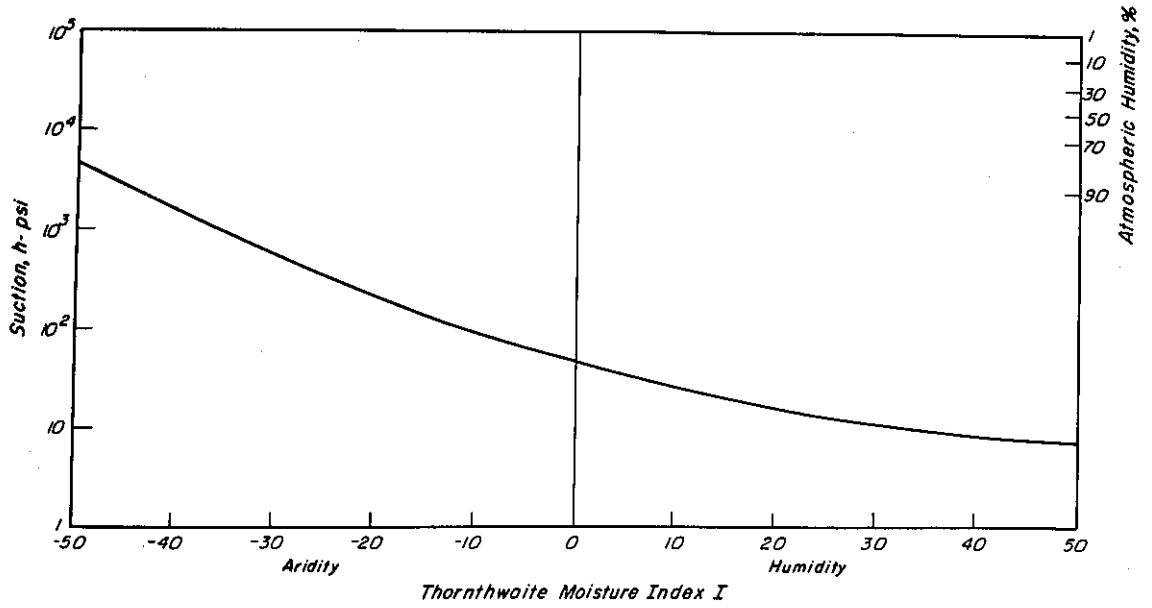


Fig. 13 – Equilibrium suction beneath the center of sealed road pavements at 18-in. depth, as a function of Thornthwaite moisture index. (After Richards.)

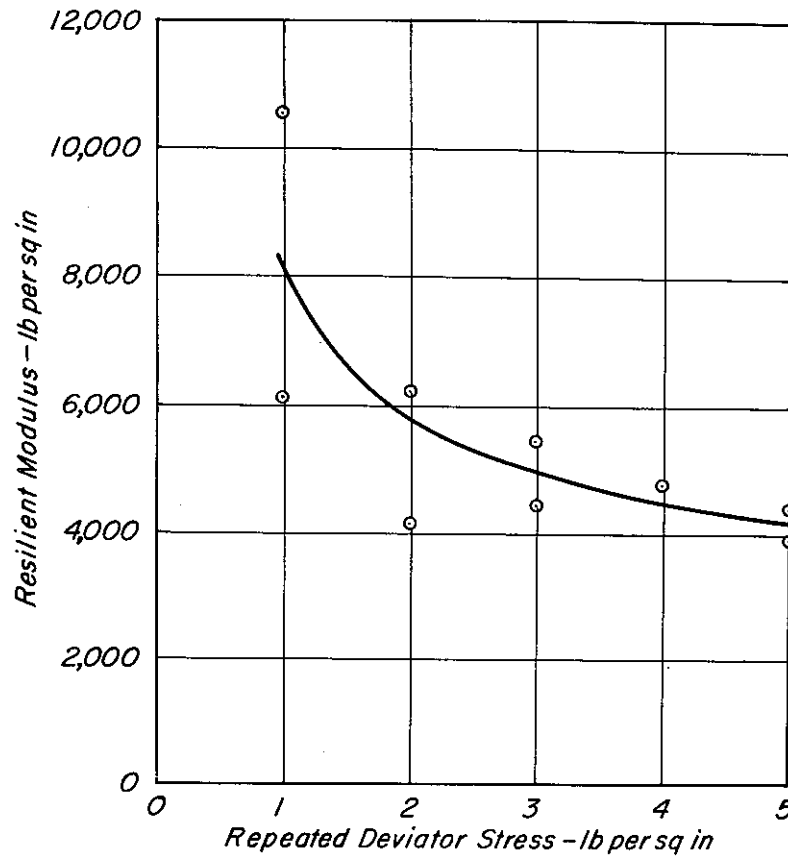


Fig. 14 – Results of repeated load tests, Ygnacio Valley Road subgrade soil.

In a subsequent section data will be presented illustrating a relationship between suction and the response of soils to repeated loading (as measured by resilient modulus).

It should also be noted that an assessment of distortion of the pavement structure due to volume changes in the subgrade can be estimated from suction data. (Richards (13) has presented a technique whereby heave or settlement of the pavement surface can be estimated provided the suction profile at the time of construction, the equilibrium suction profile, and the moisture content (void ratio) vs. matrix suction relation for the subgrade are known.

Materials Characterization

The steps labeled Available Materials, Design Asphalt Concrete and Other Treated Materials, Test Asphalt Concrete, and Test Other Pavement Materials are interrelated. While one must consider as a part of the design process related to these steps the following:

1. Survey of subgrade soils traversed by the proposed route and the performance of identification and classification tests.
2. Selection of the most economic materials to be used in the construction of the highway.
3. Design of the asphalt concrete mixture to be used.

emphasis in this section will be placed on aspects of materials characterization, aspects necessary to examine the fatigue mode of distress in the pavement structure. Moreover, it should be noted that the design of the asphalt concrete mixture to be used is related to the type of pavement in which the material is utilized; accordingly it must be emphasized that mixture design and structural pavement design must be treated as a part of the same process. Fig. 2 shows this in stepwise progression.

The characterization technique presently utilized as a part of the fatigue subsystem (to determine the so-called "elastic" properties* of paving materials) can be considered as a process whereby significant properties are measured to permit prediction of response under special (and/or limited) loading conditions, rather than the process whereby fundamental properties are measured to predict response under any system of applied loads. This latter characterization technique has not been accomplished as yet for conventional paving materials. The complexity of such a process will be illustrated briefly later in the report, by showing the type of data required to develop a nonlinear elastic characterization of subgrade soils (20).

*Considerable evidence has been presented in recent years that elastic theory produces, at least to an engineering approximation, a reasonable indication of pavement response to moving wheel loads (15 through 19).

While a number of procedures now exist to describe the "elastic" response of materials comprising the structural pavement section, a test procedure developed originally by Seed and Fead (21) for subgrade soils is utilized herein for the characterization process (for both fine-grained soils and untreated granular materials). From the test a resilient modulus is determined which is defined as the quotient of the repeated axial stress and the recoverable axial strain after some number of stress repetitions (usually in the range 100 to 1000), that is,

$$M_R = \frac{\text{Repeated axial stress}}{\text{Recoverable axial strain}} \quad (\text{psi})$$

Fine-grained (cohesive) Soils. For cohesive subgrade soils which have been tested to date, the resilient modulus is stress-dependent, i. e. , $M_R = f(\sigma_d)$, where σ_d = repeatedly applied stress, particularly in the range of stresses to which the subgrade soils of well-designed pavements are subjected (i. e. , less than 3 to 5 psi). Results of tests on undisturbed samples of an existing subgrade soil from the Ygnacio Valley Road are shown in Fig. 14 to illustrate this point.

Data developed by Seed et al (22) to illustrate the effects of initial compaction conditions are presented in Fig. 15 for materials representative of the AASHO (23) and WASHO (24) Test Road subgrades and for Vicksburg silty clay used extensively in test pavements at the Corps of Engineers Waterways Experiment Station (25). In general it can be seen that the resilient deformation increases with an increase in degree of saturation and decrease in density. (Note: the resilient modulus which is proportional to the reciprocal of this deformation will decrease in the same fashion.)

While the data presented in Fig. 15 indicate that the modulus of soils is dependent on water content it may be worthwhile to examine its relationship to soil moisture suction which, as noted earlier, can be predicted in-situ to a degree of certainty, useful from an engineering standpoint.

Data obtained by Dehlen (20) for undisturbed specimens from the subgrade of the San Diego Test Road are presented in Figs. 16 and 17. In both figures the distinct relationship between modulus and suction is noted. Sauer (26) has developed similar data for a glacial till and his data, also reflecting the dependence of resilient modulus on suction, are shown in Fig. 18.

Recent studies of the influence of water content and dry density on suction in the as-compacted condition have been developed by Morris et al (27) and Richards (28). Results of these investigations are shown in Figs. 19 through 21. Interestingly the location of the lines of equal suction approximately parallel the lines of constant resilient deformation, see Fig. 15. As will be noted on these figures, density as well as effective stress

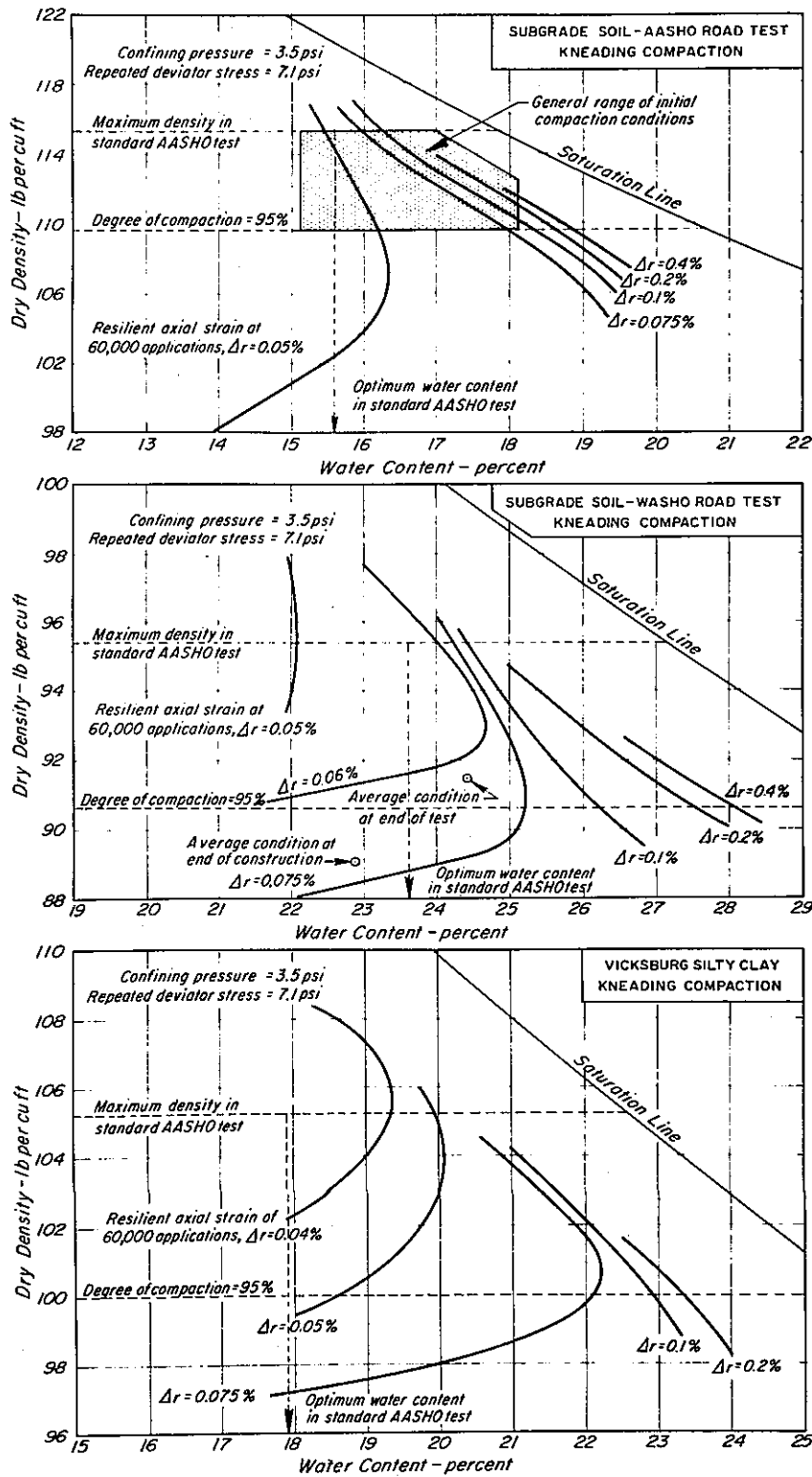
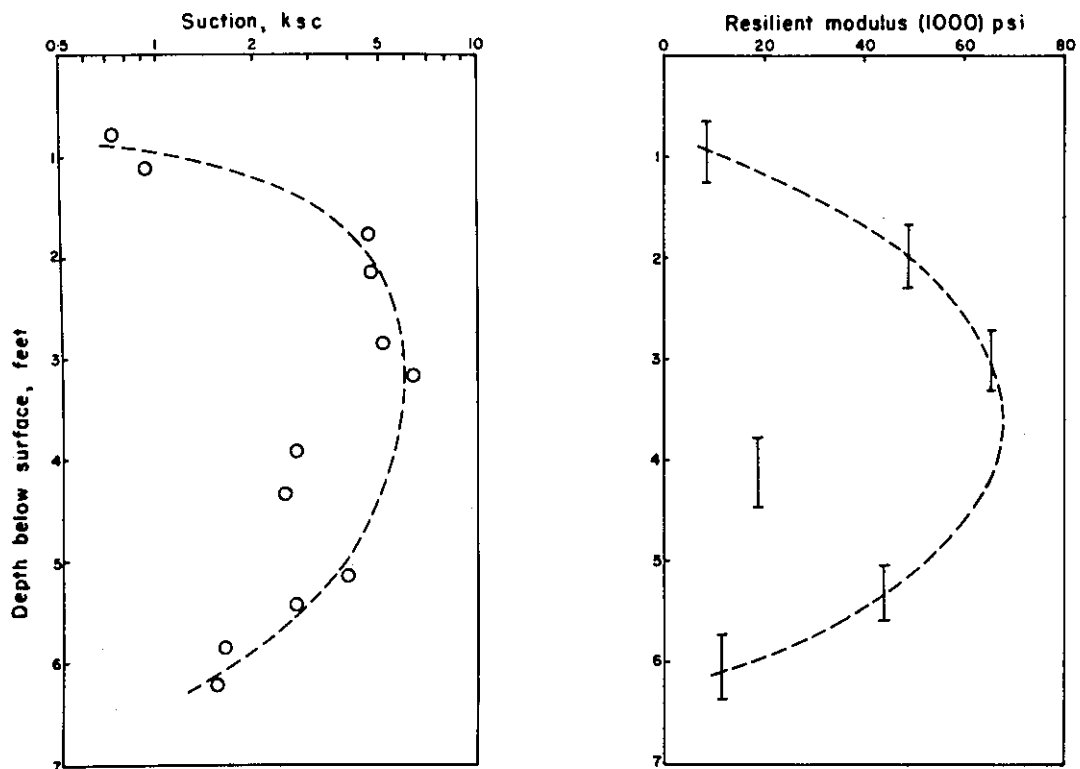
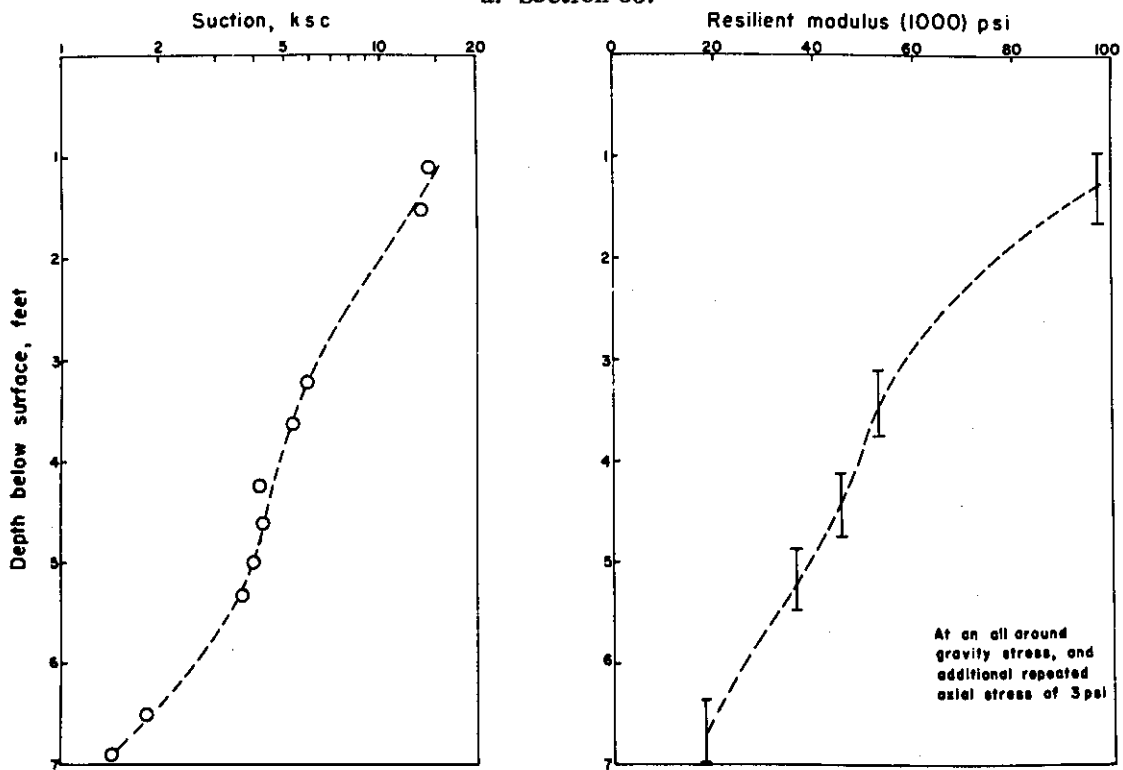


Fig. 15 - Effect of compaction conditions on resilience characteristics. (After Seed, Chan and Lee)



a. Section 35.



b. Section 2.

Fig. 16 — Suction and resilient modulus. (After Dehlen.)

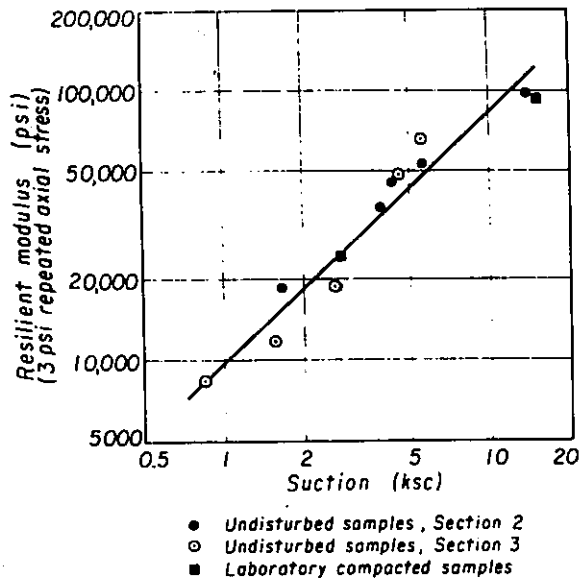


Fig. 17 - Relation between resilient modulus and suction, San Diego road test subgrade soil. (Reference (29).)

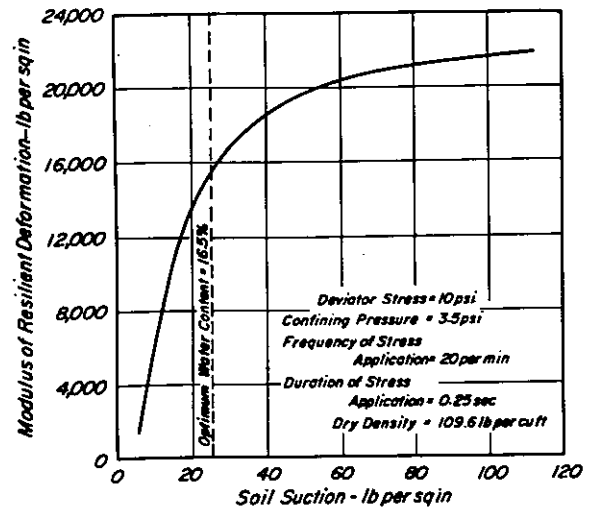


Fig. 18 - Relationship between resilient deformation and soil suction for laboratory compacted specimens of till from Qu'Appelle Moraine, Saskatchewan, Canada.

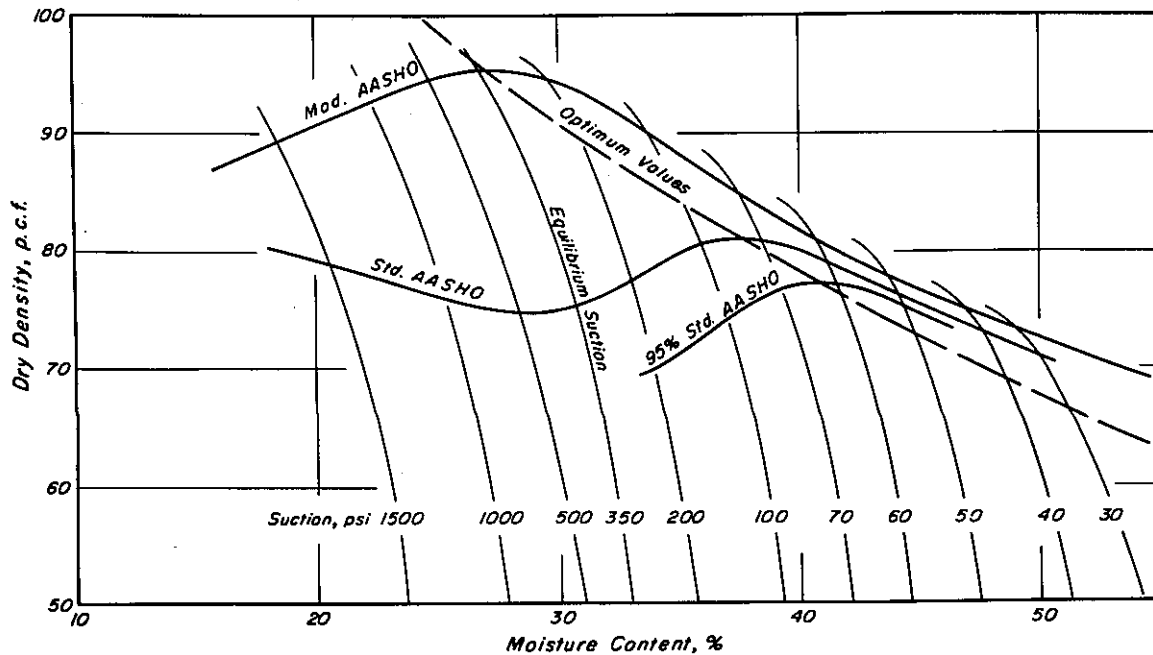
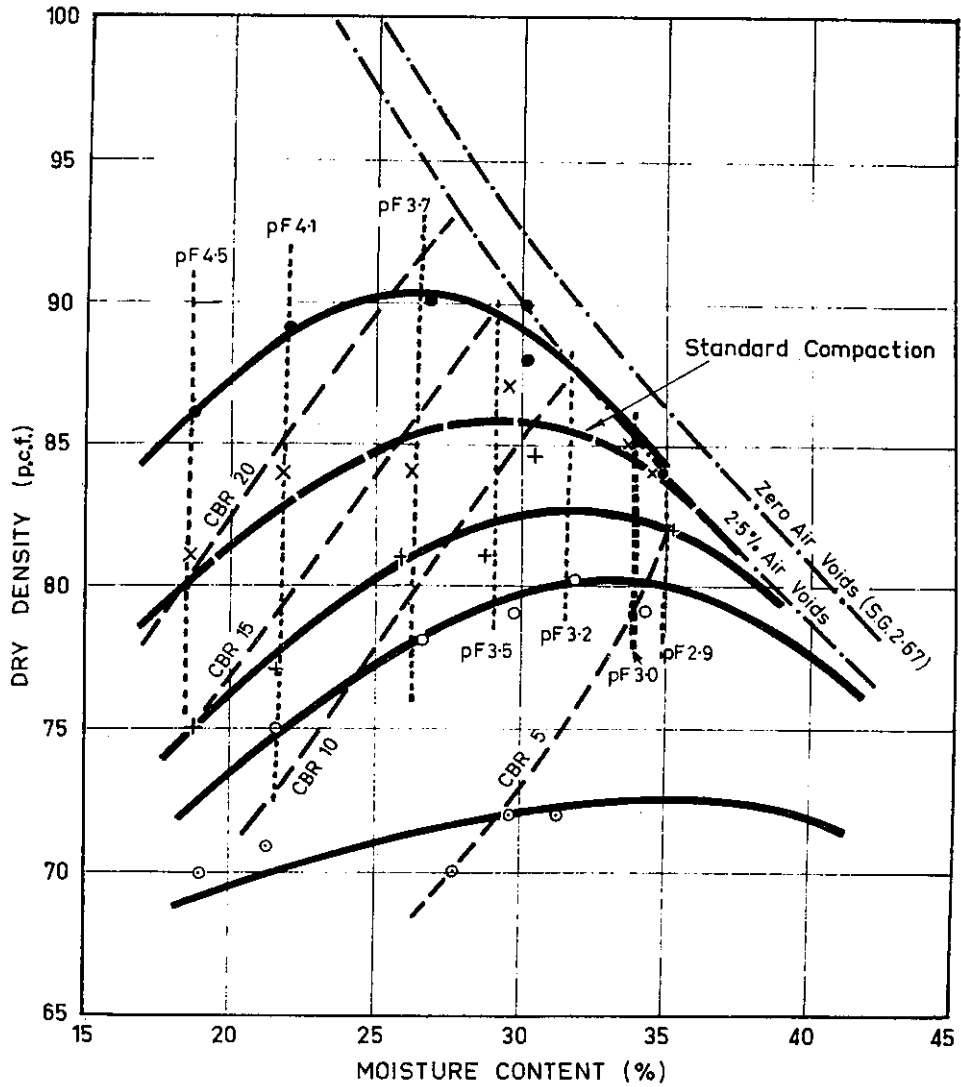


Fig. 19 - Compaction curves with initial soil suction contours for a composite sample of subgrade material. (After Richards, et al.)



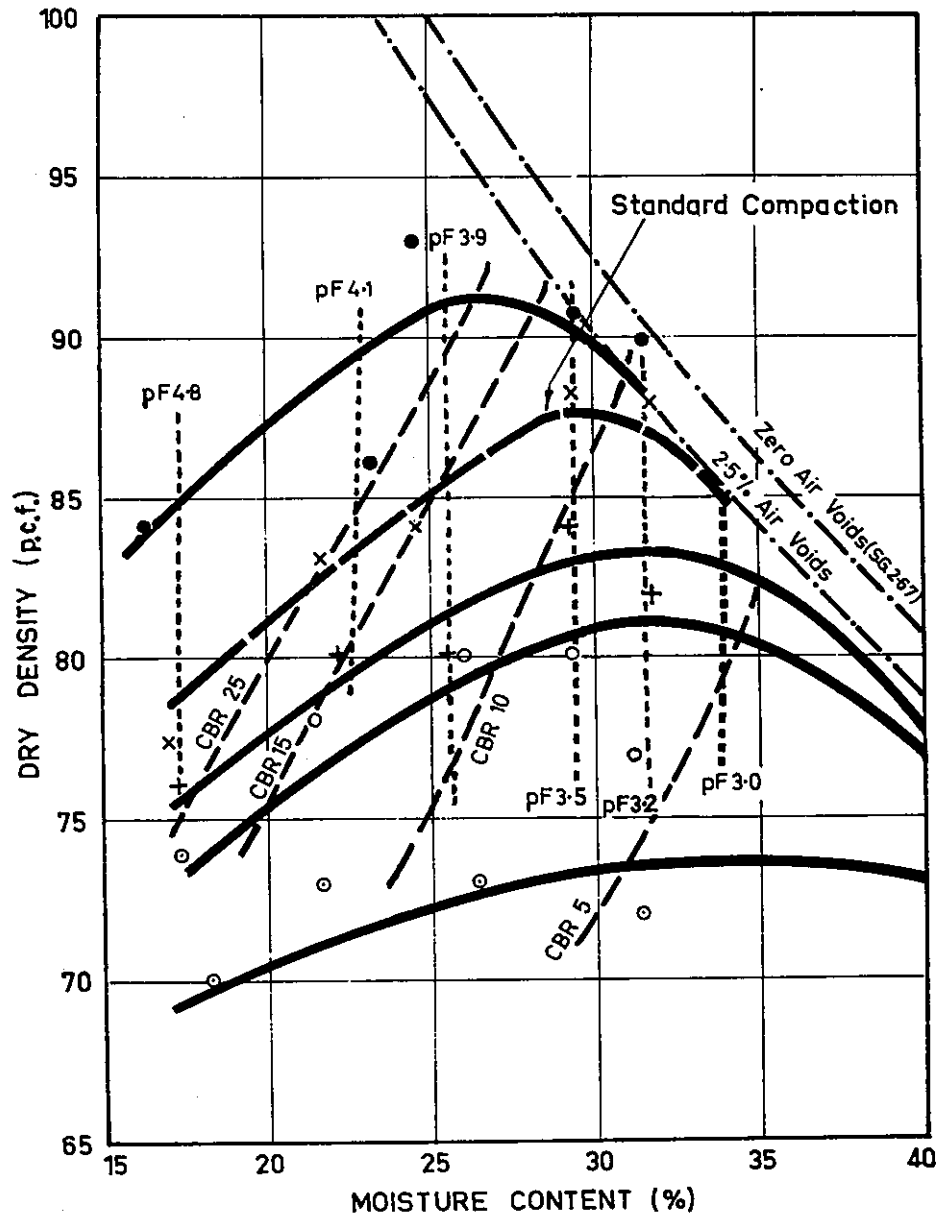
LEGEND

----- Matrix suction lines
 - - - - CBR lines

Soil compacted in CBR mould in 3 layers using:-

- 112 blows per layer
- x 56 " " " (Standard compaction)
- + 37 " " "
- 28 " " "
- 14 " " "

Fig. 20 — Dry density, moisture content, CBR and suction relationships for a grey brown soil being wet up from 15 to 35 percent moisture content. Note: moisture content determined after CBR testing and taking of suction samples. (After Morris, Tynan and Cowan)



LEGEND

- Matrix suction lines
- CBR lines

Soil compacted in CBR mould in 3 layers using :-

- 112 blows per layer.
- x 56 " " " (Standard compaction)
- + 37 " " "
- 28 " " "
- 14 " " "

Fig. 21 — Dry density, moisture content, CBR and suction relationships for a grey brown soil being dried back from 35 to 15 percent moisture content. Note: moisture content determined after CBR testing and taking of suction samples. (After Morris, Tynan and Cowan)

(suction) has an influence on the resilient response. At a specific density, however, it is conceivable that if the suction could be anticipated in the field (Fig. 12) and duplicated in the laboratory (based on compaction requirements) then the modulus of the material could be ascertained for design purposes. Thus the concept of soil moisture suction may be an extremely useful device whereby the influence of environment as it influences the stress vs strain characteristics of fine-grained soils (through changes in suction rather than changes in water content) can be utilized for the design of pavements. Implementation of field and laboratory studies are required to insure that such concepts are valid (e. g. of the type described in Ref. (28)).

While not a part of the materials characterization process for the fatigue subsystem, it should be noted again that the suction concept provides a means whereby an assessment of distortion of the pavement structure due to volume change in the subgrade can be estimated. Richards (13) has developed a method whereby this heave or settlement can be determined provided the suction profile at the time of construction, the equilibrium suction profile, and the water content (void ratio) vs. matrix suction relation for the material are known. In effect this procedure can be considered as a portion of the distortion subsystem of Fig. 3. An example of the estimation procedure is included in Appendix A to illustrate the applicability of this useful concept.

As noted earlier, the technique used to characterize fine-grained soils for use in analyses associated with the fatigue subsystem assumes the material to be linear elastic at a particular level of stress or strain. To consider non-linear response characteristics, additional testing will be required.

Dehlen (20) has developed a procedure for characterizing fine-grained soils as non-linear elastic and has examined the response of the subgrade soil from the San Diego Test Road (29) within this framework. In this process the stress state has an important influence on material response. Thus in order to minimize testing it is most desirable to cover only the range which occurs in a pavement under the anticipated traffic.

Fig. 22a illustrates a range in stress paths which might be selected for laboratory testing and Fig. 22b illustrates typical data obtained from a pattern of stressing corresponding to (c) of Fig. 22a. It should also be noted that the triaxial test may define the constitutive relationships for materials at points beneath the center of an axisymmetrically loaded area, these results may be inadequate for conditions elsewhere in the structure since the triaxial test permits only two normal stresses to be varied independently, and the resulting two strains to be measured, while for complete characterization for use with this type of loading, three normal and one shear stress would have to be varied independently, and the resulting four strains measured.

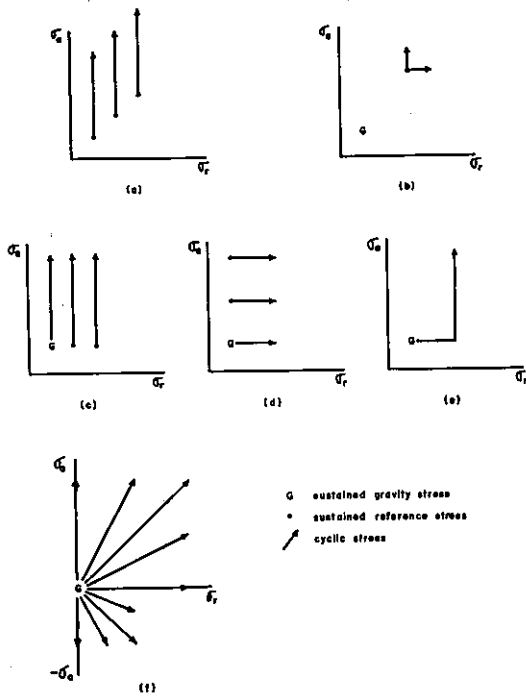


Fig. 22a - Stress paths in laboratory tests.

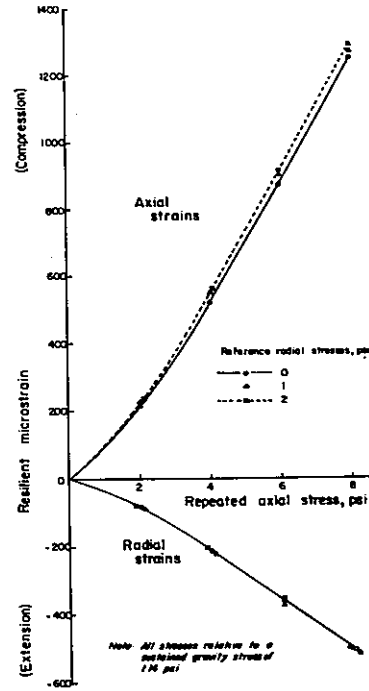


Fig. 22b - Variation of axial and radial strains with axial stress.

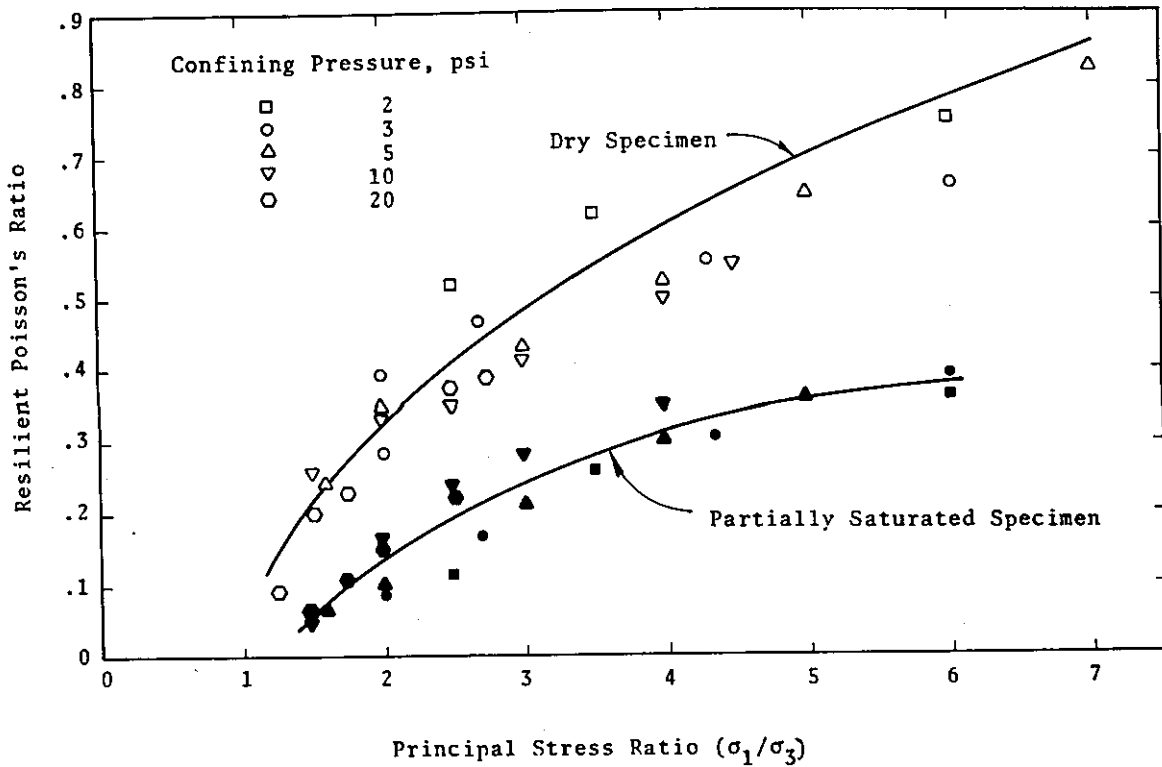


Fig. 23 - Secant Poisson's ratio as a function of principal stress ratio. (Partially crushed aggregate, low density, coarse grading.)

As will be seen subsequently there appears to be little advantage in characterizing a material within such a framework at this stage in time. However, such considerations must be recognized as an additional iteration in the materials characterization process.

Untreated Granular (Cohesionless) Materials. The response of untreated granular materials has also been shown to be dependent on stress. The resilient modulus for such materials can be expressed either in terms of the confining pressure (in triaxial compression) or the sum of the principal stresses according to the following relationships:

$$M_R = k \cdot \sigma_3^n \quad \text{or} \quad M_R = k'(\theta)^{n'} \dots\dots\dots (5)$$

where:

$$\theta = \theta = \sigma_1 + \sigma_2 + \sigma_3$$

or

$$\theta = \sigma_1 + 2\sigma_3 \quad \text{for the type of test utilized in this study.}$$

Hicks (30) has studied the response of granular materials within such a framework and determined the influence of a number of aggregate characteristics on resilient modulus. His study included an investigation of the effects of aggregate density, aggregate gradation (percent passing No. 200 sieve), and degree of saturation on the resilient response of two aggregates representative of those used in the construction of asphalt pavements in California. Results of this study indicate that at a given stress level the resilient modulus increased with increasing density, increasing particle angularity or surface roughness, decreasing fines content, and decreasing degree of saturation.

This investigation also included a study of the effect of a number of load and mix variables on the resilient Poisson's ratio*. The influence of stress on Poisson's ratio can be approximated as follows:

$$\nu = A_0 \pm A_1 \left(\frac{\sigma_1}{\sigma_3} \right) + A_2 \left(\frac{\sigma_1}{\sigma_3} \right)^2 + A_3 \left(\frac{\sigma_1}{\sigma_3} \right)^3 \dots\dots\dots (6)$$

where:

A_0, A_1, A_2 and A_3 are coefficients determined by means of a regression analysis.

*Resilient Poisson's ration (ν) is defined as the quotient of the recoverable radial strain (ϵ_r) divided by the recoverable axial strain (ϵ_a), i. e., $\nu = \epsilon_r / \epsilon_a$.

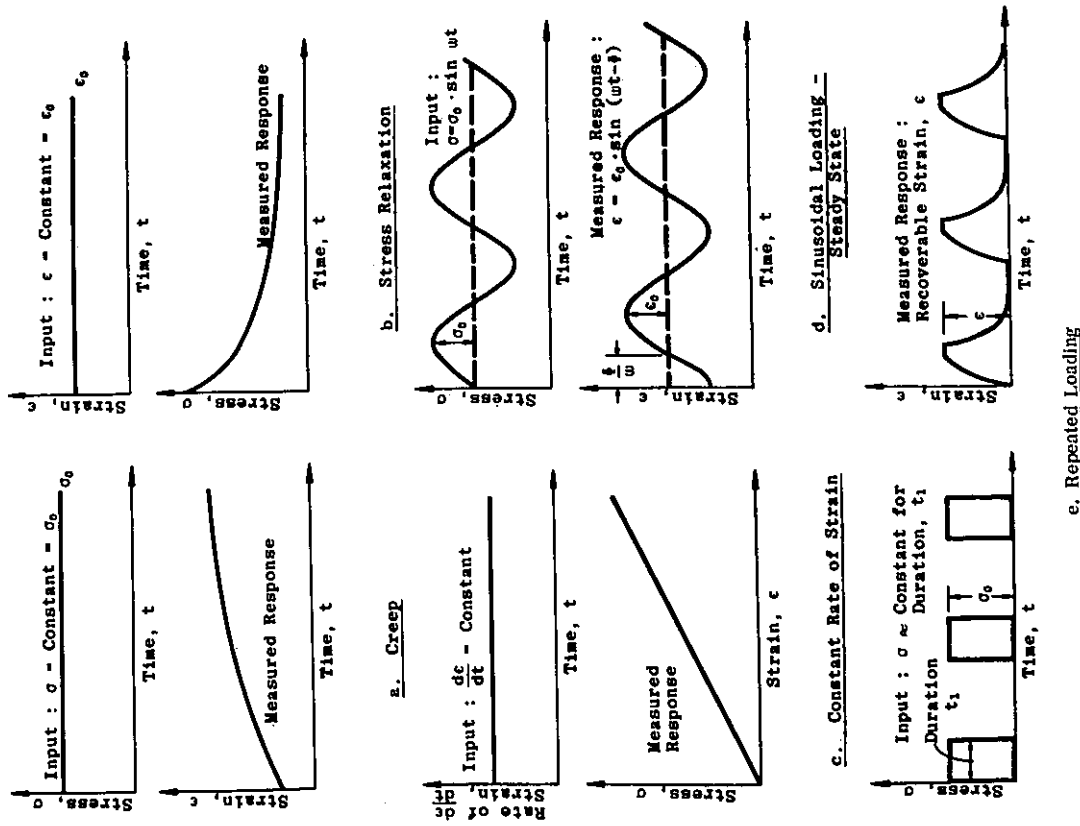


Fig. 25 - Types of loading to measure stiffness characteristics of asphalt mixtures.

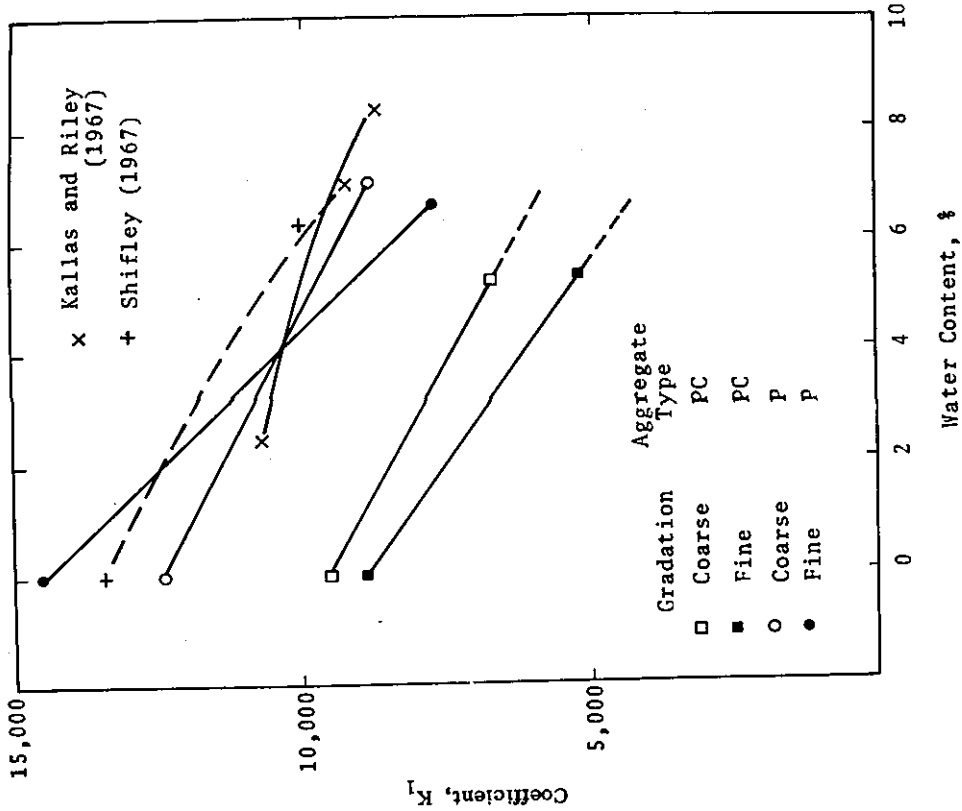


Fig. 24 - Variation in regression constant (K_1) $M_r = K_1 \sigma_1^3 K_2$ with water content.

This variation is illustrated in Fig. 23 for specimens in both a dry and partially saturated condition. Poisson's ratio also was slightly influenced by density, generally decreased as the fines content increased, and generally decreased as the degree of saturation increased.

These studies indicated that as the degree of saturation of the aggregate increased, the resilient modulus decreased in essentially a linear fashion with no large reductions occurring under repetitive loading when the specimens were completely saturated. Some earlier evidence (31) had suggested the potential for the development of large pore water pressures under repetitive loading. Such was not the case in Hick's study as seen in Fig. 24. Also shown in this figure are the results of studies by Kallas and Riley (32) and Shifley (33) substantiating this observation.

Hick's data also suggest that to define the response of a granular material to load using equation (5) it may be necessary to test only one specimen since his data provide some basis for adjustments to k or k' of equation (5). While not illustrated in this section, Appendix B contains a suggestion as to how the adjustments might be accomplished.

Asphalt-Bound Materials. For asphalt-bound materials utilizing asphalt cements, stiffness as defined by the relation

$$S(t, T) = \frac{\sigma}{\epsilon} \dots\dots\dots (7)$$

where:

$S(t, T)$ = mixture stiffness at a particular time of loading
and temperature

σ, ϵ = axial stress and strain respectively.

can be used at this stage in time (1970) and either measured directly or estimated using the procedure developed by the Shell investigators (34, 35).

Table 5 contains a summary of the various methods by means of which the stiffness (or modulus) of asphalt concrete can be measured and the methods are illustrated schematically in Fig. 25.

Generally for the short times of loading associated with moving traffic, non-linear effects such as those due to stress or to differences in tensile and compressive response may be considered unimportant from an engineering standpoint. Thus it is suggested that the stiffness be selected at a time of loading which is representative for conditions associated with moving traffic applied to the pavement. It will be necessary, however, to determine stiffnesses over a range in temperatures, such as the relationship illustrated in Fig. 26, since (as seen in the figure) the effect of temperature at a particular time of loading is significant. This, in turn, may considerably influence the response of the pavement structure to load.

TABLE 5 - SUMMARY OF METHODS TO MEASURE RHEOLOGIC BEHAVIOR OF ASPHALTIC CONCRETE

A. DIRECT MEASUREMENT				
Method of Test	Input	Measured Response	Measure of Rheologic Behavior	Remarks
Creep:	Tension and Compression:	Strain as a function of time, $\epsilon(t)$	(a) Creep compliance, $D(t) = \frac{\epsilon(t)}{\sigma_0}$	(a) Necessary to use superposition principle ^a to relaxation modulus, $E_T(t)$, from compliance, $D(t)$.
(a) Axial loading	Constant stress, σ_0		(b) Creep modulus, $E_C(t) = \frac{\sigma_0}{\epsilon(t)}$	(b) $E_C(t) = E_T(t)$ only at short and long loading times.
(b) Bending	Flexure: Constant moment		(c) Creep modulus in flexure, $E_R(t) = \frac{1}{I} M \frac{[\epsilon_t + \epsilon_c](t)}{h}$	(c) $E_R(t) = E_T(t)$ only at short loading times for asphaltic concrete
Relaxation:	Tension and compression:	Stress as a function of time, $\sigma(t)$	Relaxation modulus, $E_T(t) = \frac{\sigma(t)}{\epsilon_0}$	(a) Analogous to van der Poel's stiffness.
(a) Axial loading	Constant strain, σ_0			(b) Difficult to perform true stress relaxation test on asphaltic concrete.
Constant rate-of-strain:	Tension and compression:	Stress and strain, σ and ϵ	Relaxation modulus, $E_T(t) = d\sigma/d\epsilon$ at different values for $d\epsilon/dt$	
(a) Axial loading	Constant rate-of-strain, $d\epsilon/dt$			
Dynamic loading	Tension and compression:	For stress input:	Complex modulus, $ E^* = \sigma_0/\epsilon_0$	(a) $ E^* = E_T(t)$ only at short and long loading times. Necessary to use another form of superposition principle to determine $E_T(t)$ for intermediate times.
(a) Axial loading	Sinusoidally varying stress, $\sigma = \sigma_0 \sin \omega t$; or sinusoidally varying strain $\epsilon = \epsilon_0 \sin \omega t$. Range in frequencies	Sinusoidally varying strain, $\epsilon = \epsilon_0 \sin (\omega t - \phi)$ at particular frequency where $\phi =$ phase shift $\omega =$ frequency	and phase shift ϕ for a range in frequencies	(b) By plotting $ E^* $ as a function of $1/\omega$, a curve similar in shape to $E_T(t)$ is obtained; will be displaced somewhat from $E_T(t)$ curve for intermediate times as noted in (a) above.
Repeated loading:	Compression:	Compression:	Compression:	(a) Should produce comparable moduli to those measured by other means noted above, particularly at short loading times.
(a) Axial loading	Axial stress, σ_d	Recoverable strain after a specific number of load applications, ϵ_R	Resilient modulus: $MR = \sigma_d/\epsilon_R$	
(b) Flexure	Flexure: Applied load, P	Flexure: Recoverable deflection after a specific number of load applications, Δ_R	Flexural stiffness: $S = K \frac{P}{I \Delta_R}$ where K = constant depending on loading conditions	
B. INDIRECT DETERMINATION				
Stiffness (Shell investigators)	Penetration and ring-and-ball softening point of recovered asphalt volume concentration of aggregate, C_v percent air voids.		Stiffness, $S(t, T) = \sigma/\epsilon$	(a) Analogous to relaxation modulus.

^a One statement of superposition principle: $\int_0^t D(t - \tau) E(t) d\tau = \int_0^t \epsilon(t - \tau) D(t) \tau = t$

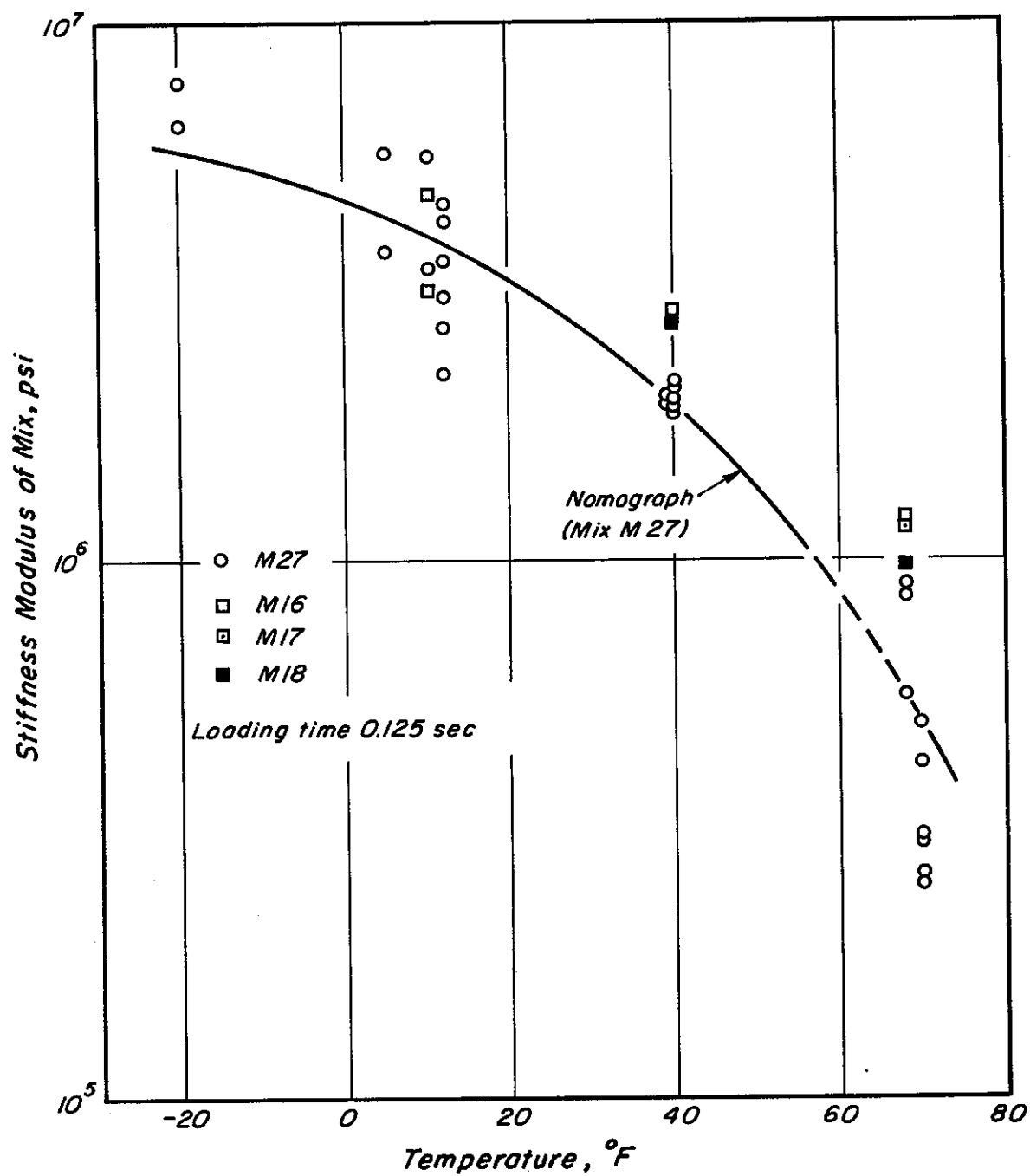


Fig. 26 — Stiffness modulus of asphalt concrete at various temperatures.

To estimate stiffness using the method developed by the Shell investigators requires that the properties of asphalt cement contained in the mix (penetration and ring and ball softening point) together with the volume concentration of the aggregate and the percent air voids in the compacted mixture be known.

For mixtures with air void contents of about 3 percent the mixture stiffness can be estimated from the following relationship:

$$\frac{S_{\text{mix}}}{S_{\text{asp}}} = \left(1 + \frac{2.5}{n} \cdot \frac{C_v}{1 - C_v} \right)^n \dots \dots \dots (8)$$

where:

$$n = 0.83 \log \left(\frac{4 \cdot 10^5}{S_{\text{asp}}} \right)$$

S_{asp} = stiffness of asphalt, kg per cm^2 (obtained from Fig. 27)

S_{mix} = stiffness of compacted mix, kg per cm^2

C_v = volume concentration of the aggregate = $\frac{\text{vol. aggregate}}{\text{vol. aggregate} + \text{vol. asphalt}}$

The expression is also limited to volume concentrations of aggregate in the range 0.7 to 0.9.

For air void contents larger than 3 percent, van Draat and Sommer (36) have suggested the use of a corrected volume concentration of aggregate, C'_v , defined as:

$$C'_v = \frac{C_v}{1 - \Delta_{\text{air void content}}}$$

where:

$\Delta_{\text{air void content}}$ = actual air void content - 0.03
(expressed in decimal form)

This expression is applicable so long as:

$$C_B \geq \frac{2}{3} (1 - C'_v) \dots \dots \dots (10)$$

where:

$C_B = \frac{\text{vol. asphalt}}{\text{vol. aggregate} + \text{vol. asphalt}}$

Van Draat and Sommer note that when $C_B = \frac{1}{3} (1 - C'_v)$ the stiffness may only be one-half the value as estimated from equation (8).

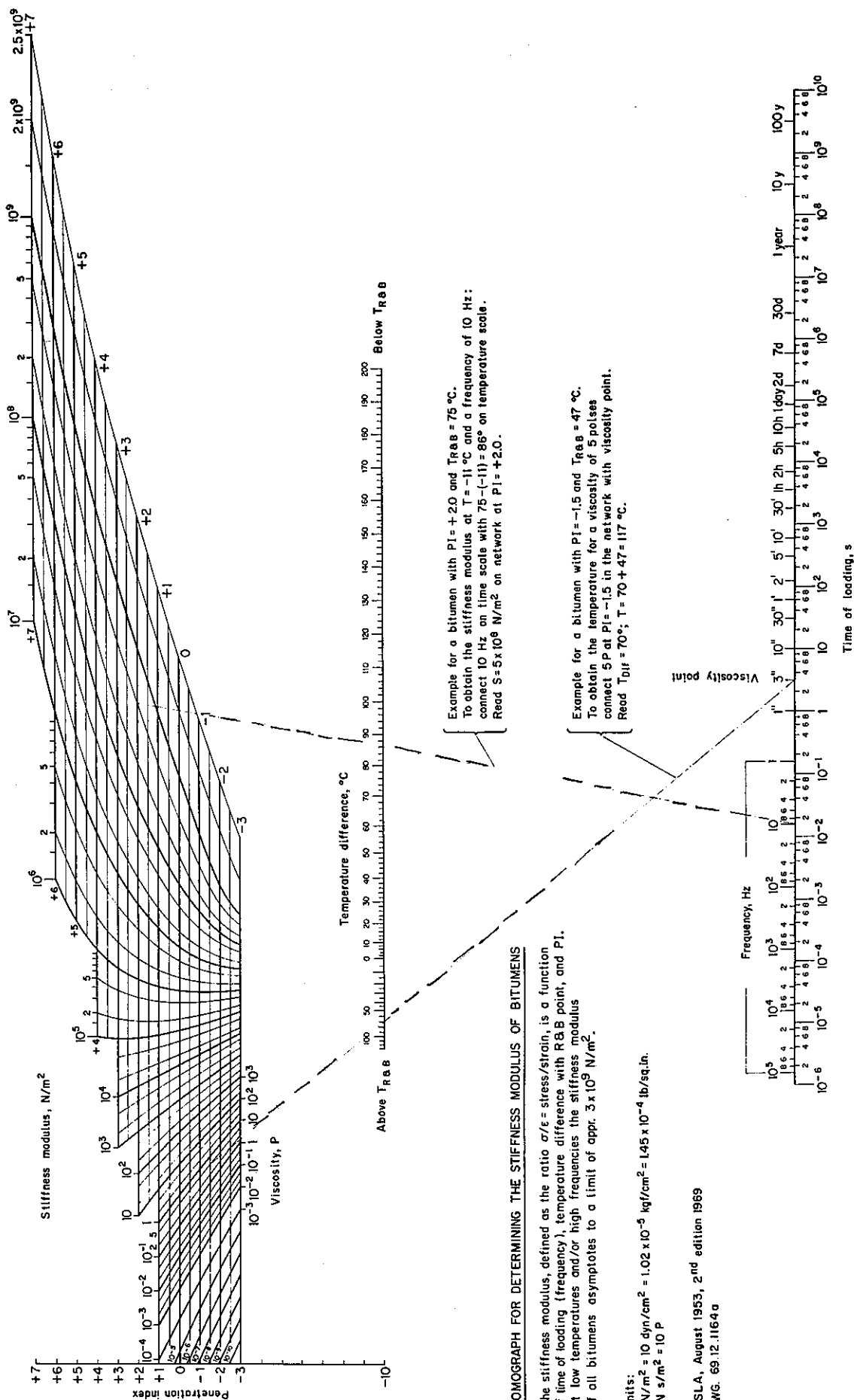


Fig. 27 -- Nomograph for determination of asphalt stiffness. (After Shell)

As noted earlier, it may be desirable to eventually consider the non-linear response of asphalt concrete to load. Dehlen (20) has performed some testing of this type. Results from a complete pattern of stressing are shown in Fig. 28. This figure illustrates the variation of axial strain corresponding to various stress states in triaxial compression. A similar set of results would be required to define the variation of radial strain with stress state.

The procedure described above may not be applicable to define the response of asphalt treated materials containing liquid asphalts or asphalt emulsions during the curing process in situ. Additional testing may be required, testing of the type described for untreated aggregates since these materials in the partially cured state are dependent on the applied stress conditions as seen in Fig. 29.

Other Treated Materials. Stiffness characteristics of lime-treated materials have been investigated by Thompson (37) and Mitchell et al (38). Thompson has presented data indicating a relationship between unconfined compressive strength and modulus of the form:

$$E = A + B \text{ (unconfined compressive strength)}$$

and modular ratios for lime treated to untreated soil in the range 3 to 25.

The investigation of Mitchell et al (38) has been limited to a study of Vicksburg Buckshot clay stabilized with lime and $MgSO_4$. Results of this study as well as those of Thompson indicate that after a reasonable curing period the lime treated material may, for all practical purposes, be considered elastic in response.

Research on stiffness characteristics of cement-treated soils is well summarized in Ref. (10). As with lime treated materials, the response of cement stabilized soils after a reasonable curing period can be considered to be elastic from an engineering standpoint and values up to 3×10^6 psi may be expected. For these materials, Poisson's ratio will vary considerably. However, for cement-treated granular materials, Poisson's ratios will be in the range 0.1 to 0.2 (10).

Methods of Analysis for Stresses and Deformations in Pavement Systems

To estimate the stresses and deformations resulting from moving wheel loads so that the potential for development of fatigue distress can be ascertained, a realistic representation of the pavement structure is required.

At present there are a number of methods of analyses which might be used to reasonably ascertain the response of the pavement structure to moving wheel loads, all of which make use of elastic theory.

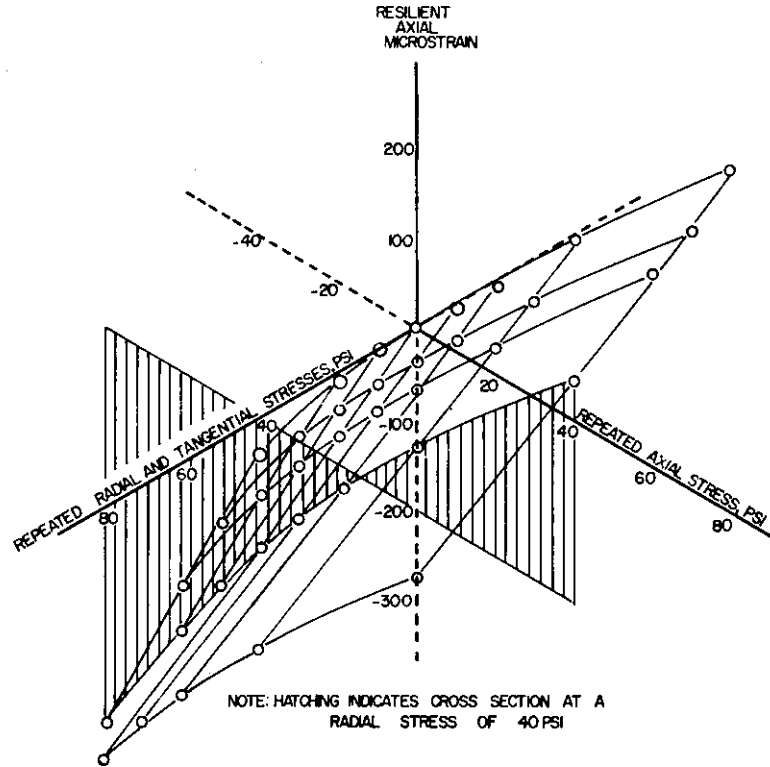


Fig. 28 - Three-dimensional surface-axial strains for various stress states in the triaxial apparatus (asphalt concrete core H2, 70°F).

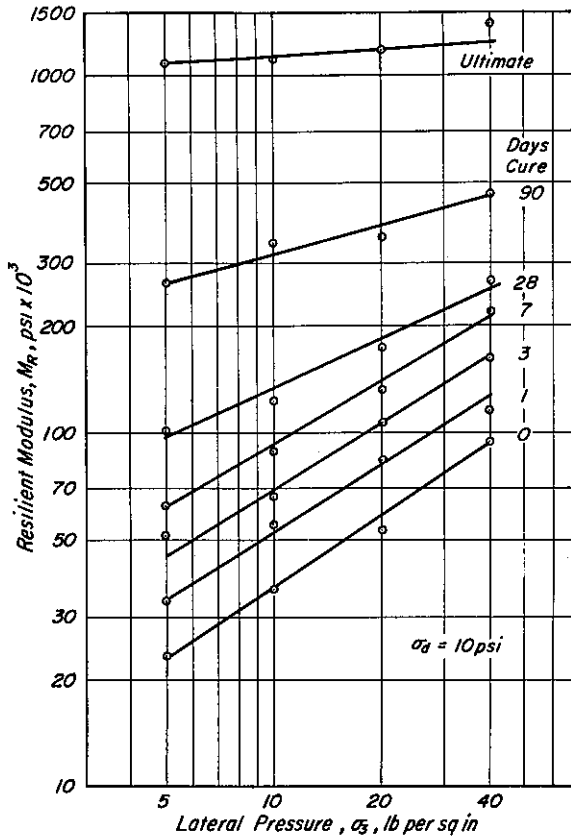


Fig. 29a - Resilient modulus vs. lateral pressure for SM-K treated aggregate at increasing ages.

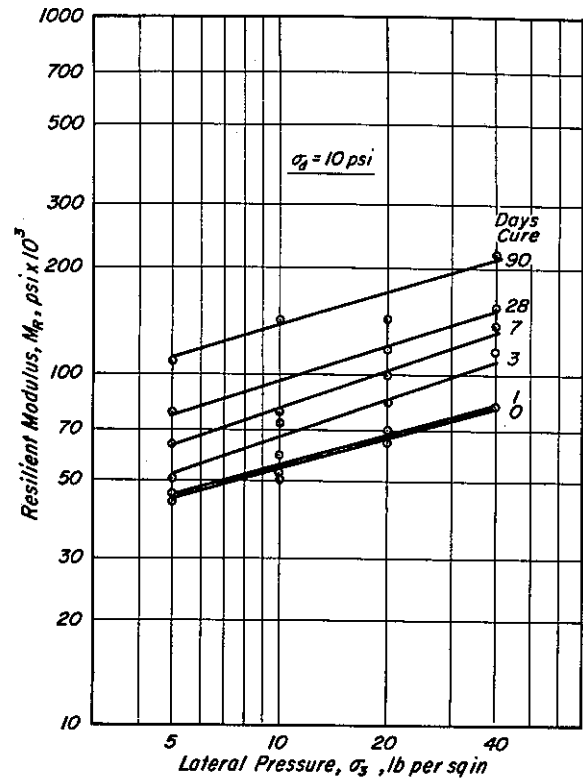


Fig. 29b - Resilient modulus vs. lateral pressure for MC-800 treated aggregate at increasing ages.

The most readily usable method at present treats the pavement as a layered elastic solid with the lowest layer semi-infinite in extent (Fig. 30). Two computer solutions* are available to estimate stresses and deformations in such a system; the one developed by the Chevron Research Company (39) (CHEV 5L) and the other by the Shell Oil Company (40) (BISTRO). The BISTRO program is somewhat more versatile than the CHEV 5L program in that up to 10 layers (versus 5 in the CHEV 5L) can be analyzed, the response to multiple loads is accomplished on the computer, and principle stresses and strains together with their directions at a point are ascertained.

The other approach makes use of the finite element method of analysis. For analysis by this procedure, the body to be analyzed is divided into a set of elements connected at their joints or nodal points, e. g. , cylinder shown in Fig. 31. The continuous variation of stresses and strains in the real system is replaced by an assumed linear variation of displacements, and hence constant stresses and strains within each element. This assumption meets the requirements of compatibility of displacements between elements. For given element geometry and constitutive equation, the stiffness matrix relating displacements and loads at the corners of each of the basic triangular elements is established. The four triangular elements forming one rectangular element are generally combined eliminating the common nodal point. Combination of the element stiffness matrices yields the symmetric banded matrix for the entire structural assembly, which is modified using known displacements at bound axes. Solution of this system of linear equations yield all nodal point displacements, from which the element strains and stresses are computed, the average of the stresses in the four triangular elements giving the best estimate of the stresses at the centroid of the rectangular element.

The element configuration, e. g. , Fig. 32, must be carefully selected to optimize the results. Generally the accuracy is improved by the use of a finer mesh, particularly in areas of rapidly varying stresses, but the greater number of elements increases the computational time and therefore the costs. Dehlen (20) has suggested that an optimum rectangular mesh has finer vertical subdivisions near the surface and in both materials near layer interfaces; and finer radial subdivisions both near the axis and near the edge of the loaded area, e. g. , Fig. 32.

This procedure can be used directly for analyzing systems with non-linear elastic materials by using either an iterative or an incremental technique.

*Referred to as integral transform solutions.

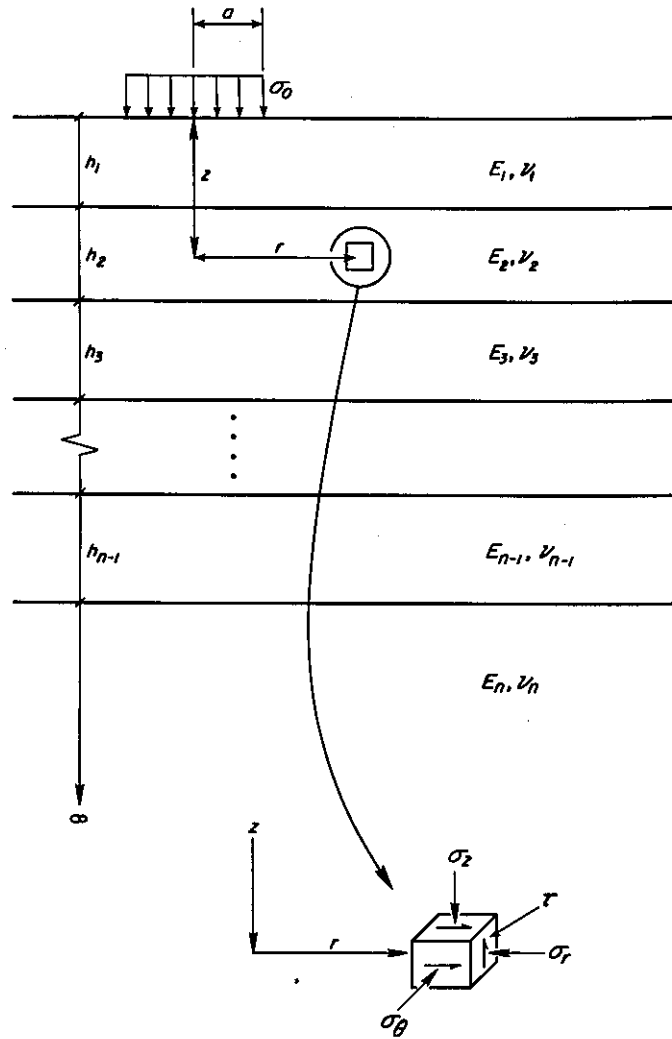


Fig. 30 — Schematic representation of multilayer system.

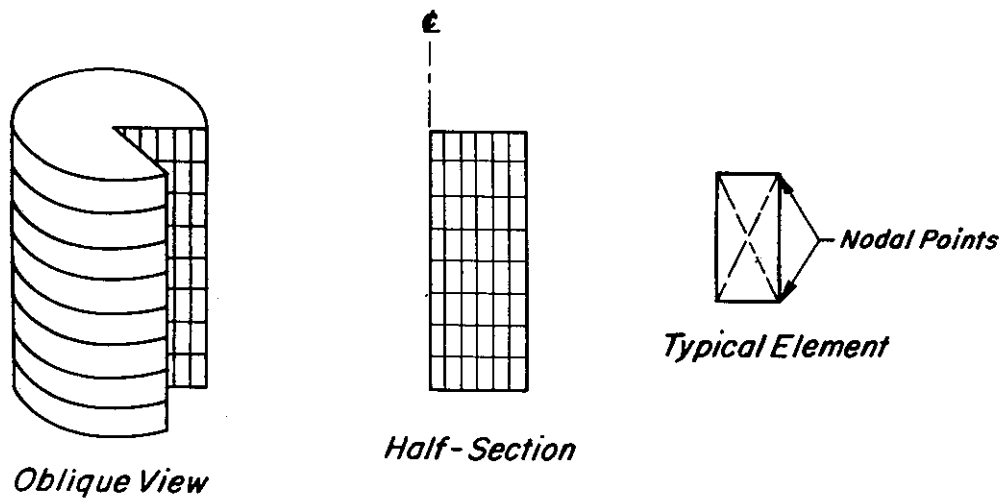


Fig. 31 — Finite element idealization of a cylinder.

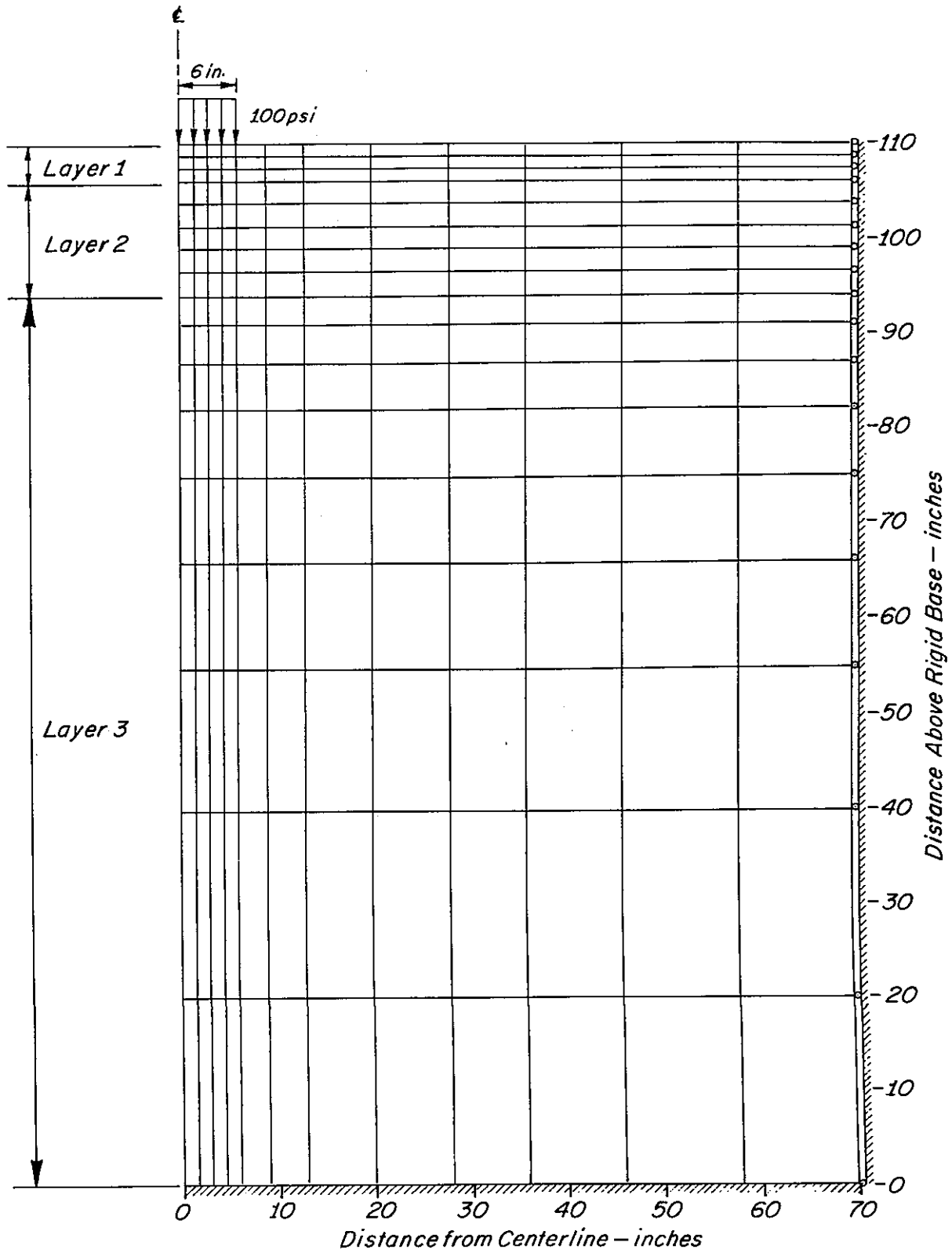


Fig. 32 — Finite element configuration used for analysis of homogeneous and layered systems.

One form of the iterative procedure starts with the computation of gravity stresses for all elements together with a first approximation for the traffic stresses assuming an elementary stress distribution. Equivalent linear stress-strain coefficients (corresponding to secant moduli) are evaluated for the state of stress in each element from the relevant non-linear constitutive relations. The full load is then applied and a linear elastic finite element solution is obtained providing a revised estimate of stresses. These stresses are then used to revise the stress-strain coefficients for each element, and a new stiffness matrix is formed. Iterations are continued until the coefficients used in the solution are compatible with the resulting stresses.

In the incremental method the gravity stresses and corresponding equivalent linear stress-strain coefficients (equivalent to tangent moduli) are evaluated for each element. An increment of load, representing a fraction of the traffic load, is then applied and resulting displacements and stresses computed using a linear finite element procedure. The resulting stresses are added to the gravity stresses; the new stress-strain coefficients evaluated and a new stiffness matrix formed; a further increment applied, and the process repeated until the full load has been applied, and all the incremental displacements and stresses have been summed.

Hicks (30) has modified the above procedure somewhat to include variations in Poisson's ratio with stress (e. g. , Fig. 23).

The finite element procedure is not limited to the axisymmetric case. However, the greatly increased computer storage and the time required has limited developments in this area. Pretorius (10) has utilized the program for a three dimensional prismatic solid developed by Wilson (41) to examine the development of load associated cracking in an asphalt concrete layer over a cement-treated base in the vicinity of a shrinkage crack in the cement-treated layer.

This latter approach is still essentially two-dimensional with the third dimension introduced into the idealization by expressing the load as Fourier series in this direction (sometimes referred to as 2D extended). A finite element discretization is shown in Fig. 33. The structure is solved for every Fourier term necessary to adequately represent the load. The x- and y-displacements vary cosinusoidally and stresses sinusoidally in the z-direction which enables a complete stress solution at any desired z position.

Appendix C contains listings of the various programs which are available.

Fatigue Response

Some measure of the fatigue response of asphalt mixtures and other treated materials (if utilized) in the pavement section is required.

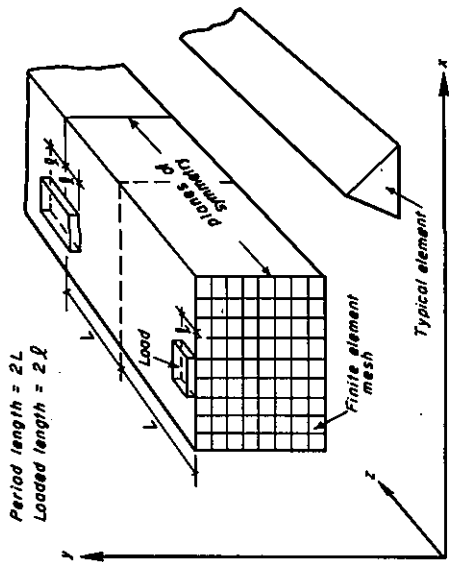


Fig. 33a - Prismatic space finite element representation.

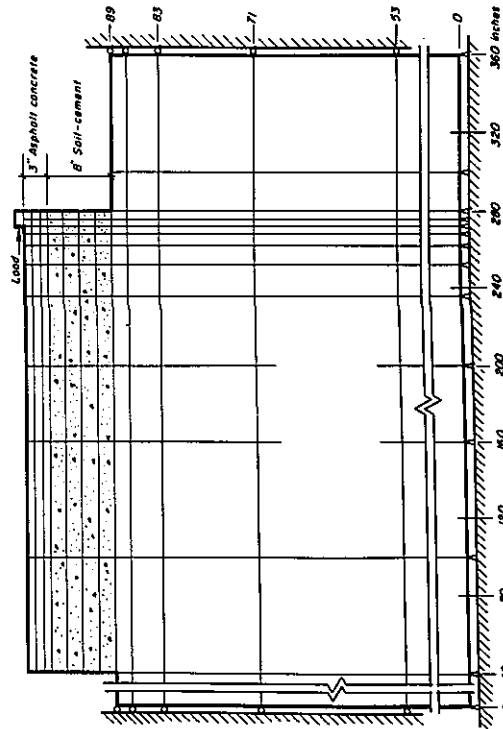


Fig. 33b - Finite element mesh for load at an edge.

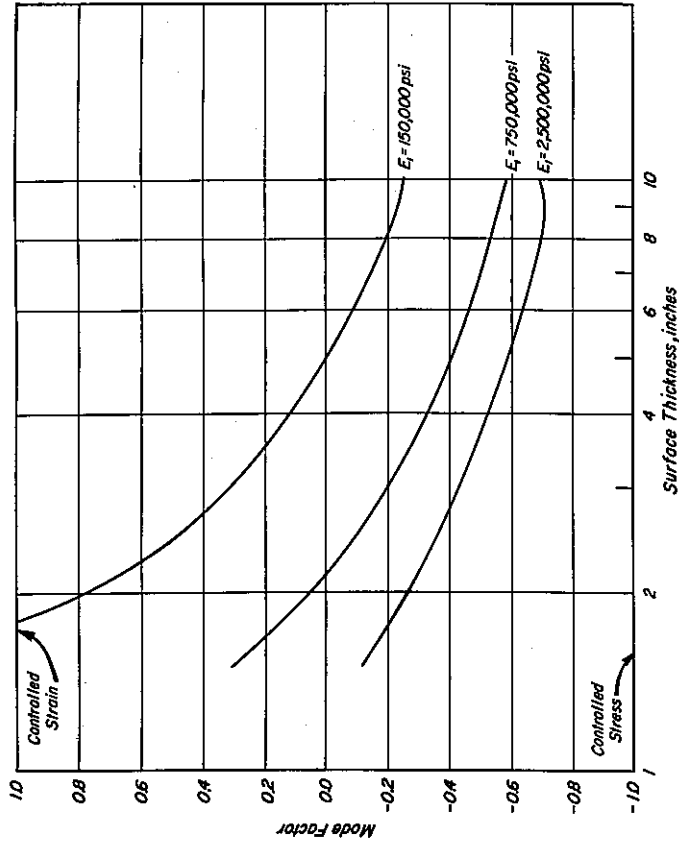


Fig. 34 - Variation of mode factor with surface thickness, support of low stiffness ($E_2 = 10,000$ psi, $E_3 = 4,000$ psi, and $h_1 + h_2 = 28$ in.)

For asphalt concrete mixtures when used in thick sections this response should be measured by means of the controlled-stress mode of loading (42). For comparatively thin asphalt bound layers (≈ 2 in.) the controlled-strain mode of loading is more appropriate. Differentiation between the two modes of loading can be placed on a more quantitative basis by introducing a parameter termed the mode factor (42) and defined as:

$$MF = \frac{|A| - |B|}{|A| + |B|} \dots\dots\dots (11)$$

where::

- MF = mode factor
- A = percentage change in stress due to a stiffness decrease of C percent
- B = percentage change in strain due to a stiffness decrease of C percent
- C = an arbitrary but fixed percentage reduction in stiffness

In the controlled-stress mode of loading, the mode factor would have a value of -1, whereas for the controlled-strain mode of loading the mode factor would assume a value of +1.

From analyses of a series of pavement sections using layered system elastic theory, a typical example of which is shown in Fig. 34, it would appear that the controlled-strain mode of loading will be approached in pavements containing thin (2 in. or less), flexible sections of asphalt concrete as noted above. On the other hand, the controlled-stress mode of loading will only be approached in pavements containing comparatively thick (greater than 6 in.), stiff sections of asphalt concrete.

For the remaining ranges in thickness, some form of loading intermediate between these two modes is appropriate. From an engineering standpoint, however, it should be noted that fatigue response developed in the controlled-stress mode of loading will probably provide the most conservative estimate of fatigue response.

Results of fatigue tests may be plotted either in the form of stress or strain vs. fatigue life, average results of which are shown in Figs. 35 (stress) and 36 (strain).

Available evidence suggests that the fatigue behavior of asphalt concrete such as that illustrated in Fig. 36 can be represented by an equation of the form:

$$N_f = K \left(\frac{1}{\epsilon_{mix}} \right)^n \dots\dots\dots (12)$$

where::

- N_f = stress applications to failure
- ϵ_{mix} = tensile strain repeatedly applied to the mix
- K, n = constants depending on mixture characteristics

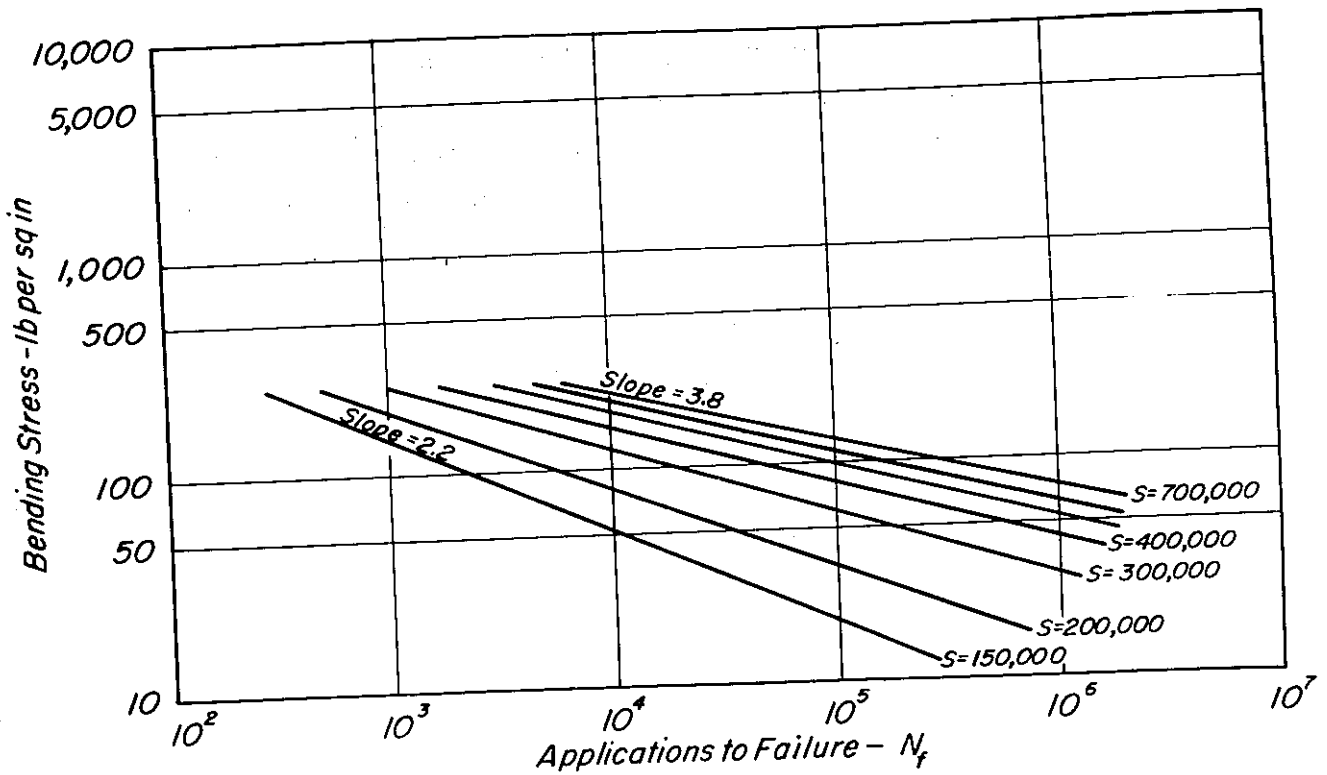


Fig. 35 - Bending stress vs. applications to failure, for mixes of different stiffness - California graded mixes, granite aggregate, 85-100, 60-70, and 40-50 penetration asphalts, 6.0 percent asphalt.

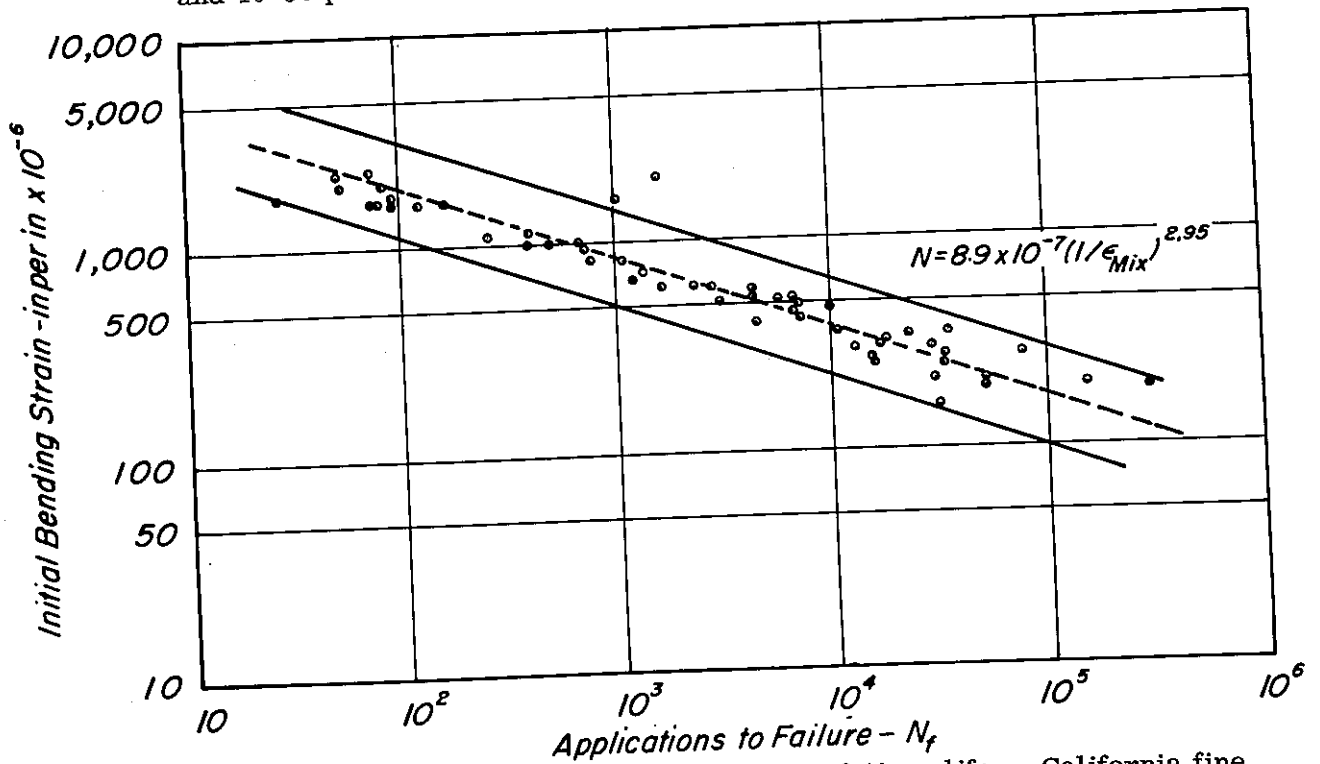


Fig. 36 - Initial mixture bending strain vs. fatigue life - California fine grading, granite aggregate, 85-100 penetration asphalt, 6 percent asphalt.

The coefficient n in the above equation appears to be dependent on mixture stiffness. For the range of stiffnesses encountered in practice, n varies in the range 2 to 6. Data illustrating this point are presented in Fig. 35. Since stiffness of the asphalt bound layer will vary in the road due to temperature variations, one fatigue curve with a particular slope probably will not suffice to estimate damage development. From a design standpoint this should present no difficulty since only a small increase in input to the subsystem of Fig. 2 is required.

In practice, pavements are subjected to a range of loadings; accordingly, a cumulative damage hypothesis is required since fatigue data (defined by equation 12) are usually determined from the results of simple loading tests. One of the simplest of such hypothesis is the linear summation of cycle ratios. This cumulative damage hypothesis states that fatigue failure occurs when

$$\sum_{i=1}^i \frac{n_i}{N_i} = 1 \dots\dots\dots (13)$$

where:

- n_i = number of applications at strain level i
- N_i = number of applications to cause failure in simple loading at strain level i

Equation 13 indicates that fatigue life prediction under compound loading becomes a determination of the time at which this sum reaches unity.

Some measure of the scatter in fatigue test data can also be considered at this time. Pell and Taylor (43) and Kasianchuk (44) have indicated that the distribution function for fatigue lives at a particular stress level can be represented as logarithmic normal:

$$f(y) = \frac{1}{\sigma^i \sqrt{2\pi}} \left\{ \exp \left(- (y - m^i)^2 / z(\sigma^i)^2 \right) \right\} \dots\dots\dots (14)$$

where:

- $f(y)$ = the normal density of Y^{i*}
- Y^i = log of the service of fracture life, N^i
- m^i = mean of Y^i
- σ^i = variance of Y^i

*The superscript, i , refers to a particular strain level.

Results of an reanalysis of data developed by Deacon (45), using this approach are shown in Fig. 37. Comparison between the experimentally determined relationship and that estimated on the basis of a logarithmic normal distribution function indicate the reasonableness of this approach.

Data developed by Pell and Taylor (43) and shown in Figs. 38 and 39 also substantiate such an assumption.

Use of this distribution function permits prediction not only of a mean fracture or service life but also the life corresponding to any desired confidence level.

To substantiate the point that mixture design and pavement design are interrelated, a brief summary of the influence of a number of variables on fatigue response is included in Table 6. Results summarized in this table have been obtained from research reported in a number of references (e. g., 31, 42, 43, 45, 46, 47, 48, 49, 50, and 51).

It would appear that regardless of the type of test (i. e., controlled-stress or controlled-strain) and therefore regardless of the thickness of the asphalt bound layer, as much asphalt as possible should be incorporated in the mixture. As will be seen subsequently, there will be an upper limit to the amount because of stability requirements; this upper limit should be approached, however, in order to increase fatigue resistance.

In addition, adequate compaction of the mixture is required in order to promote improved fatigue resistance. This means that the mixture should be compacted to the design density at the time of construction (e. g., the void content in the compacted mixture should be of the order of 4 percent).

For heavy-duty pavements for highway loading conditions incorporating approximately 6 or more inches of asphalt concrete, it appears that any measures taken to increase the stiffness of the mixture will promote increased fatigue resistance, as long as a reasonably balanced and nonbrittle mixture is maintained. With respect to asphalt selection, therefore, improved performance may be anticipated by specifying a more viscous asphalt. It should be emphasized, however, that proper compaction must be obtained with the harder asphalts. The data also indicate that dense gradations of aggregate are desirable and that rough textured aggregates are more suitable than smooth textured materials.

For light-duty pavements incorporating approximately 2 in. or less of asphalt-bound materials, it appears that the asphalt mixture should be made as flexible as possible. As a means of accomplishing this, the asphalt cement should be relatively soft, such as a 120-150 penetration grade. While little information is available regarding the aggregate gradation to be used in these pavements, it would appear that the fines content should be reduced so that the grading is not as dense as that desired in the thicker sections and the stiffness will be less.

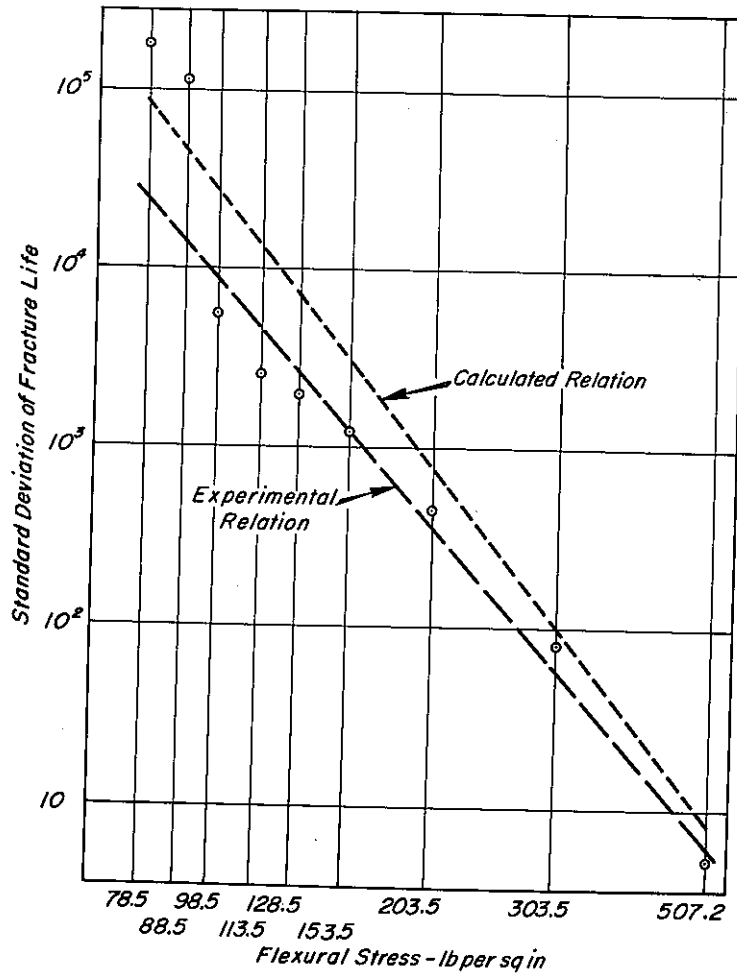


Fig. 37 - Standard deviation of fracture life against stress level.

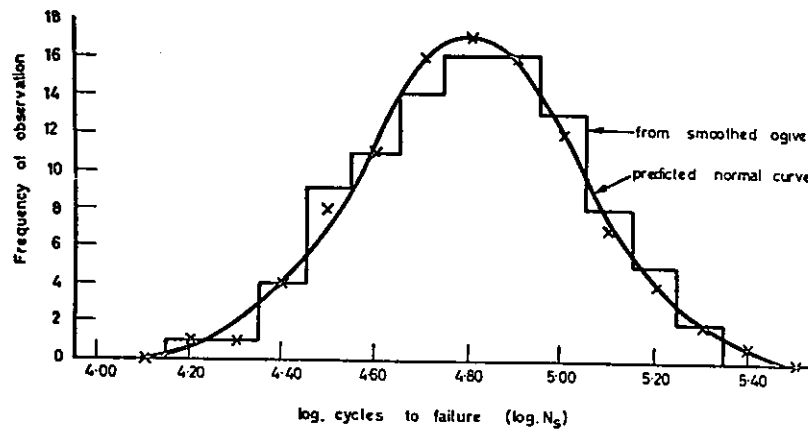


Fig. 38 - Histogram of 100 fatigue test results. (After Pell and Taylor.)

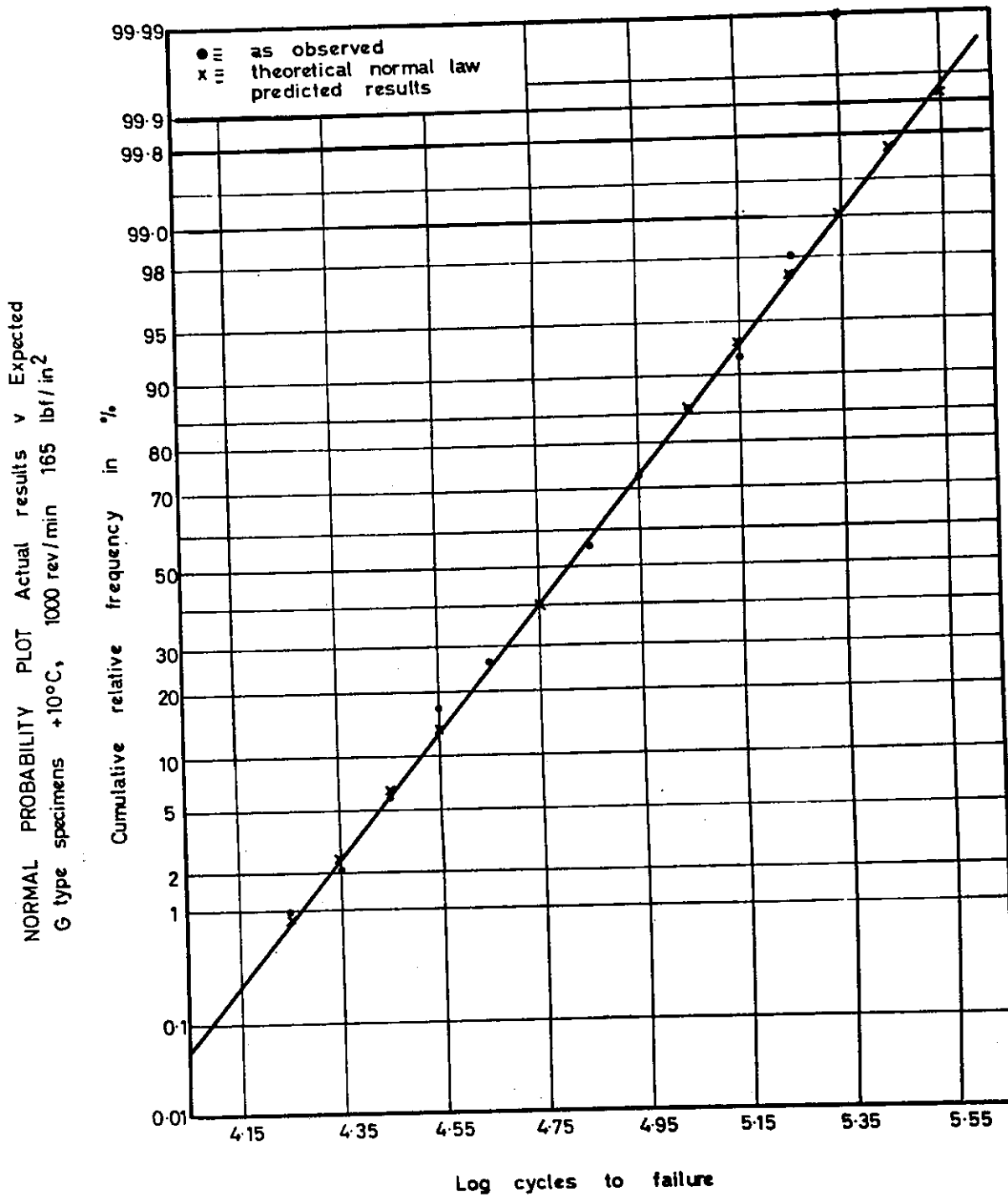


Fig. 39 — Normal probability plot of fatigue results (After Pell and Taylor)

For pavements incorporating from approximately 2 in to 6 in. of asphalt-bound materials, the general guidelines recommended above should be followed: i. e. , the asphalt content should be as large as practical, the mixture should be adequately compacted, and an aggregate should be selected that enables the incorporation of relatively large amounts of asphalt. More specific guidelines must await the extension of current research endeavors.

TABLE 6 — FACTORS AFFECTING THE STIFFNESS AND FATIGUE BEHAVIOR OF ASPHALT CONCRETE MIXTURES

Factor	Change in Factor	Effect of Change in Factor		
		On Stiffness	On Fatigue Life in Controlled-Stress Mode of Test	On Fatigue Life in Controlled-Strain Mode of Test
Asphalt Penetration	decrease	increase	increase	decrease
Asphalt Content	increase	increase ¹	increase ¹	increase ²
Aggregate Type	increase roughness and angularity	increase	increase	decrease
Aggregate Gradation	open to dense gradation	increase	increase	decrease ⁴
Air Void Content	decrease	increase	increase	increase ⁴
Temperature	decrease	increase ³	increase	decrease

¹Reaches optimum at level above that required by stability considerations.

²No significant amount of data; conflicting conditions of increase in stiffness and reduction of strain in asphalt make this speculative.

³Approaches upper limit at temperature below freezing.

⁴No significant amount of data.

While available data for other treated materials are not as extensive as for asphalt concrete mixtures, these data provide some useful design criteria as noted in the succeeding paragraphs.

For cement-treated materials, strain repeatedly applied appears to be an excellent damage determinant as shown in Fig. 40. For soil-cement, the PCA (52) has defined generalized fatigue relationships in terms of a critical radius of curvature (Fig. 41). Comparison of the data in Fig. 40 with that which would be estimated using the PCA method

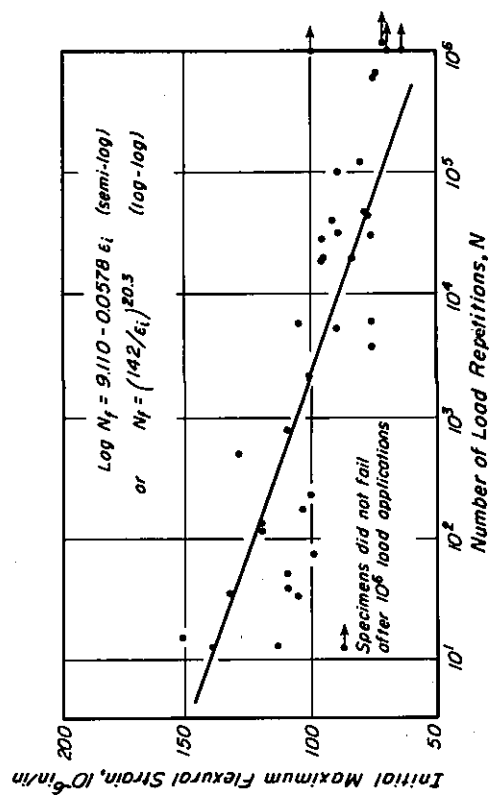


Fig. 40 - Fatigue life of flexural specimens.

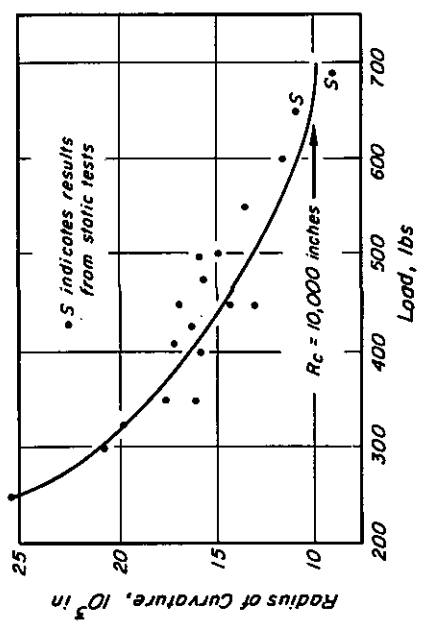


Fig. 41 - Critical radius of curvature.

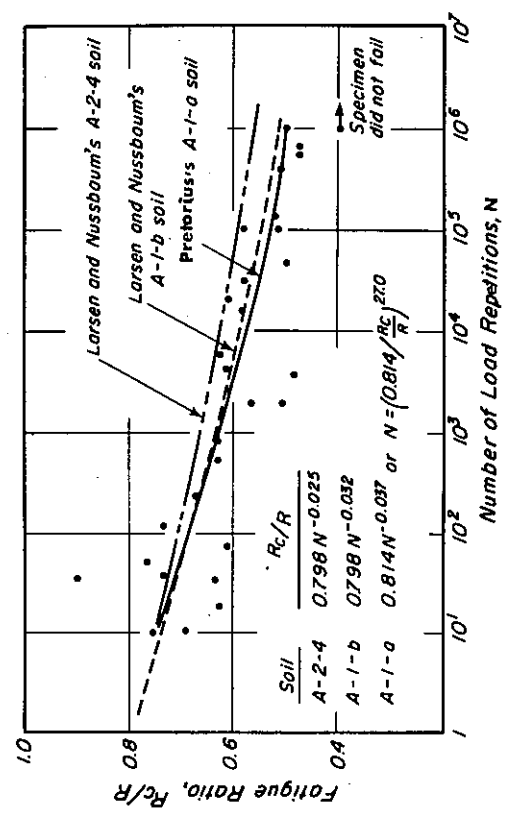


Fig. 42 - Comparison of fatigue results with data presented by Larsen and Nussbaum (1967).

is shown in Fig. 42 with reasonable agreement being indicated. Accordingly it is recommended that for soil cement, at least, the PCA procedure to define a fatigue criterion be utilized at this time. For cement-treated materials not meeting the criteria for soil-cement, no generalized guides are available as yet although considerable research effort is underway (e. g. , 53).

Swanson and Thompson (54) have developed fatigue for a series of lime treated soils. Fig. 43 illustrates a typical fatigue diagram for treated specimens tested after curing for 30 days at 70°F. Fig. 44 contains a summary of a series of tests on a range of treated materials, the results of which are plotted in terms of the ratio of the applied stress to the static flexural strength.

Summary

Using the information presented in this section the steps in the process of design or evaluation using the subsystem of Fig. 2 thus consist of the following:

1. Definition of the seasonal variation in the stiffness of the asphalt concrete together with variations in water content (and/or suction) of the underlying untreated materials.
2. Determination of the expected response of the asphalt concrete layer in the trial design section for the range of wheel loads and particular temperature regime.
3. Prediction of the fatigue life of the trial design under the action of the expected traffic volumes.
4. Evaluation of the trial design with respect to the adequacy of the section in providing the requisite life for fatigue.

If the trial section which has been selected is inadequate or conservative, another trial section is selected and the procedure repeated,

These steps have been programmed for use with a digital computer and the programs are included as an appendix to the report. A design example is presented subsequently to illustrate the application of this procedure to a city-county highway in Contra Costa County, California.

It should be emphasized that the format of Fig. 2 provides the framework for the analyses of existing pavements as well as a procedure for design. Subsequently two in-service pavements will be analyzed following this same format, (1) a state highway near Morro Bay, California and (2) a state highway near Folsom, California.

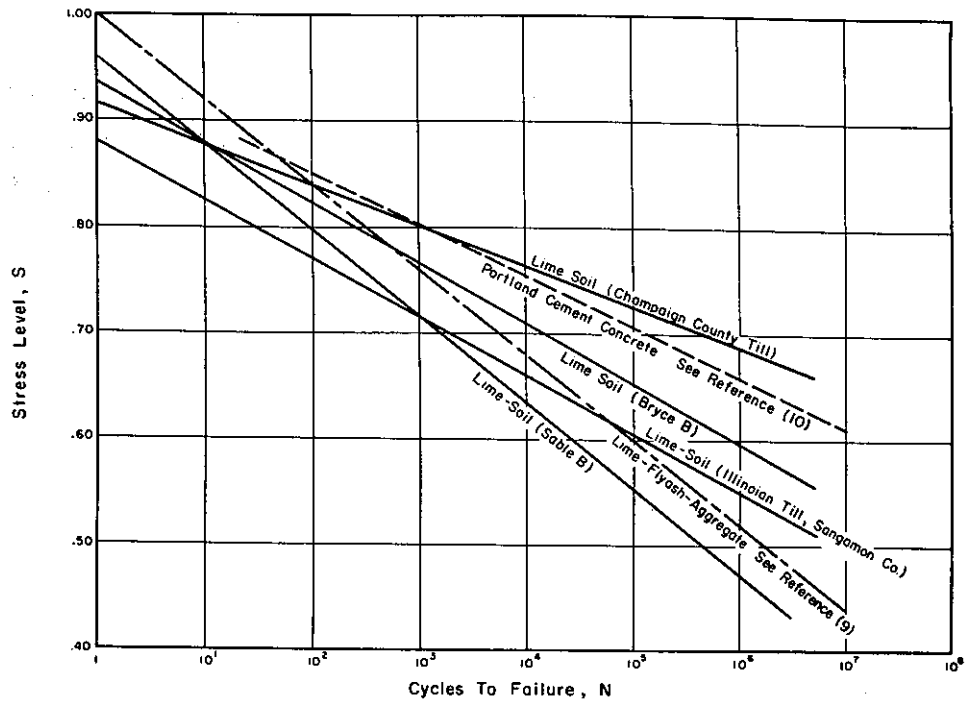


Fig. 44 – Flexural fatigue response curves. (After Swanson and Thompson.)

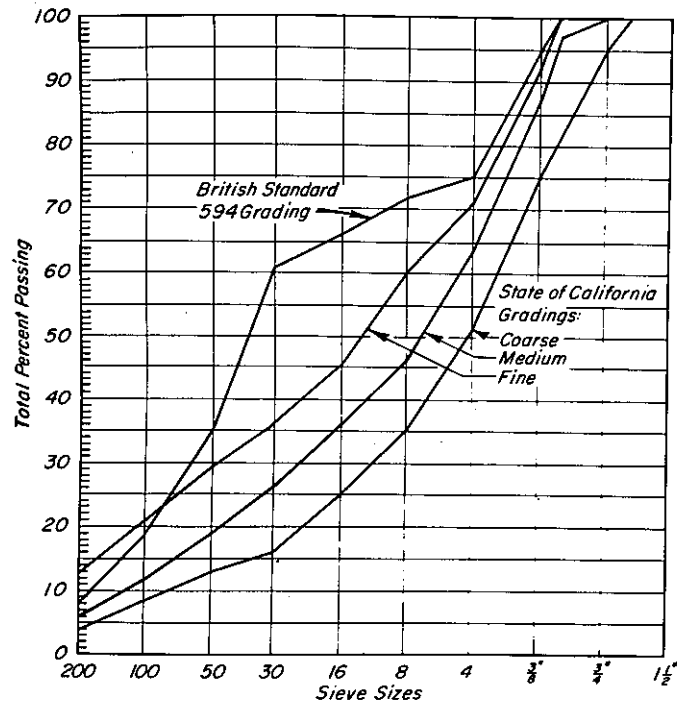


Fig. 45 – Aggregate grading curves, laboratory study.

LABORATORY DETERMINED FATIGUE RESPONSE

While the effects of mixture variables on fatigue response have been summarized in the previous section (Table 6) some of the recommendations included therein are based on studies conducted as part of this investigation. Accordingly this section of the report includes the results of a laboratory investigation to study the effects of mixture variables. Also included are the results of laboratory tests on materials used in the three projects whose performance or design will be discussed subsequently.

Influence of Mixture Variables

Data are presented to illustrate the influence of: mixture stiffness, air void content, aggregate gradation, aggregate type, asphalt content, and asphalt type. Table 7 contains a summary of a number of variables influencing fatigue response. Those considered in this study are shown by asterisk (*) to provide a convenient indication of the relationship of this study to the overall problem.

A summary of the mixture variables is included in Table 8. As seen in this table, four aggregate types*, four aggregate gradations, three grades of asphalt and a range in asphalt contents were examined.

Asphalts. Asphalts used for the laboratory study were supplied by the Chevron Asphalt Company. Properties of the asphalts as received are shown in Table 9. Properties of the asphalts recovered from the various mixtures were also determined; these results are shown in Table 10. In this table, it is interesting to observe that the amount of hardening (for a given grade) is dependent on the aggregate grading, with the largest change occurring in the mix with the largest number of fines.

Aggregates. As noted in Table 8, four different aggregate gradations were utilized. Three of the gradings correspond to State of California specifications for 1/2 in. maximum size aggregate and represent the extreme fine, the extreme course, and the middle of the grading band. A grading corresponding to the British Standard 594 requirement was also utilized to permit comparisons to be made with the results of other investigations (e. g. , Pell (46)). The four gradations are shown in Fig. 45. Other characteristics of these materials are shown in Table 11.

Mixtures. More than 300 individual specimens were tested in this phase of the investigation. Table 12 presents a summary of the air void content data for mixtures in each of the test series.

*The material termed basalt corresponds to the aggregate used in the Ygnacio Valley Road, the design example to be presented subsequently.

TABLE 7 — LABORATORY TEST VARIABLES AFFECTING
FATIGUE BEHAVIOR^a

Load Variables	Mixture and Specimen Variables	Environmental Variables
1. Pattern of stressing	1. Asphalt	1. Temperature
2. Stress level (*)	a. Type (*)	2. Moisture
3. Testing Method	b. Hardness (*)	3. Alteration of material properties during service life (e. g. aging)
a. Load history	2. Aggregate	
(1) Simple loading (*)	a. Type (*)	
(2) Compound loading	b. Gradation (*)	
b. Mode of Loading	3. Specimen	
(1) Controlled-stress (*)	a. Stiffness (*)	
(2) Controlled-strain	b. Air void content (*)	
(3) Intermediate	c. Asphalt content (*)	

a. Adapted from Reference 42.

(*) Variables considered in this investigation.

TABLE 8 — MIXTURE VARIABLES

Aggregate	Asphalt	Asphalt Content (by dry wt. of aggregate)			
		State of Calif., 1/2 in. Max. Grading			British Standard 594
		Coarse	Medium	Fine	
Crushed Basalt	60-70	-	5.3 to 8.7	-	-
Crushed Limestone	85-100	-	4.7	-	-
Crushed Granite	40-50	-	6.0	-	7.9
	60-70	-	6.0	-	-
	85-100	6.0	5.2 and 6.0	6.0	-
Crushed Gravel	85-100	-	4.6	-	-

TABLE 9 — PROPERTIES OF ORIGINAL ASPHALTS

Property	Asphalt Cement Classification		
	40-50	60-70	85-100
Penetration, dmm 100-gr. 5 sec, 77°F	33	67	92
Viscosity, cp 140°F	4.06×10^5	2.22×10^5	-
Viscosity, cs 275°F	375	369	238
Flash Point, PMCT, °F	-	-	460

TABLE 10 — RECOVERED PROPERTIES FOR ASPHALTS
USED IN LABORATORY STUDY

Mix Designation		Original Asphalt Cement	Properties of Recovered Asphalts	
Aggregate Type	Gradation		Penetration, dmm 100 gr., 5 sec, 77°F	Ring and Ball Softening Point, °F
Granite	Coarse	85-100	36	125
Granite	Medium	85-100	37	127
Granite	Fine	85-100	30	129
Granite	Medium	60-70	35	129
Basalt	Medium	60-70	32	136.5
Granite	Medium	40-50	26	132
Granite	British 594	40-50	21	140

TABLE 11 — AGGREGATE CHARACTERISTICS

Test Property	Crushed Granite	Crushed Basalt	Crushed Limestone	Crushed Gravel
LA Abrasion Loss - percent				
After 100 rev.	6	--	5	--
After 500 rev.	24	18	27	--
Cleanness Value - percent	89	--	--	94
Sand Equivalent - percent	--	41	89	89
Oil Equivalent - percent	3.7	--	2.3	2.7
Centrifuge Kerosene Equivalent - percent				
(at surface area of approx. 34 sq. ft. per lb.)	4.0	--	3.3	3.9

TABLE 12 — AIR VOID CONTENTS FOR LABORATORY
PREPARED SPECIMENS

Mix Designation	Asphalt Cement	Asphalt Content Percent	Percent Air Voids		
			Mean	Standard Deviation	Coefficient of Variation
Granite British 594	40-50	7.9	5.38	.69	12.8
Granite, Coarse	85-100	6.0	5.71	.59	10.3
Granite, Fine	85-100	6.0	5.71	.46	8.1
Granite, Medium	85-100	6.0	4.49	.55	12.3
Granite, Medium	60-70	6.0	4.80	.43	9.1
Granite, Medium	40-50	6.0	4.73	.50	10.6
Basalt	60-70	5.7	7.65	.46	6.0
Basalt	60-70	6.2	6.72	.62	9.3
Basalt	60-70	6.7	5.20	.34	6.6
Basalt	60-70	7.7	4.05	.26	6.5
Basalt	60-70	8.7	1.60	.14	8.8
Granite	85-100	5.2	7.06	.73	10.4
Limestone	85-100	4.7	6.40	.55	8.6
Crushed Gravel	85-100	4.6	8.18	.52	6.3

TABLE 13 — COMPARISON OF ASPHALT CONTENTS USED IN TEST SPECIMENS WITH THOSE ESTIMATED ACCORDING TO STATE OF CALIFORNIA METHOD OF MIX DESIGN

Mix Designation	Asphalt Content — Percent (By Dry Wt. Aggregate)					
	85-100		60-70		40-50	
	Actual	Estimated	Actual	Estimated	Actual	Estimated
Granite British 594	-	-	-	-	7.9	6.3
Granite Coarse	6.0	5.5	-	-	-	-
Granite Fine	6.0	5.9	-	-	-	-
Granite Medium	6.0 5.2	5.8	6.0	6.1	6.0	6.6
Limestone	4.7	4.3	-	-	-	-
Crushed Gravel	4.6	4.5	-	-	-	-
Basalt	-	-	5.7 to 8.7	5.9	-	-

Laboratory test specimens were prepared by kneading compaction. Details of the preparation procedure are contained elsewhere (31).

Table 13 illustrates a comparison of the asphalt contents used in the mixtures with those which would be selected for design based on the State of California requirements for a Type B aggregate.

Mixture Variables. A summary of the mixture characteristics which have been investigated are shown in Table 8. At the outset it should be emphasized that the results presented were obtained at 68°F (20°C), thus the effect of temperature on fatigue life is not apparent from this study.

Since variations in air void content and mixture stiffness occurred in every test series, the influence of these variables will be presented first.

Air Voids. The influence of air void content on fatigue response has been reported by Saal and Pell (47), Monismith (21) as well as other investigators (51); results of these investigations indicate, in general, that mixes containing high air void contents exhibit comparatively short fatigue lives.

Fig. 46 illustrates the influence of air void content on fatigue life at 68°F at a stress level of 150 psi for mixes with the granite aggregate and gradings conforming to the B. S. 594, California fine, and California coarse requirements. As with earlier test data, these results emphasize the importance of proper compaction in order to obtain good performance characteristics.

Results of linear regression analyses (fatigue life as the dependent variable) are superimposed on the data in Fig. 46. The regression lines, indicate that a smaller change in void content is required to change the fatigue life by a specific amount for the California graded mixes (4 to 6 percent increase in air voids to reduce the fatigue life by one order of magnitude) than is required for the British Standard mix (10 percent increase to reduce fatigue life by one order of magnitude).

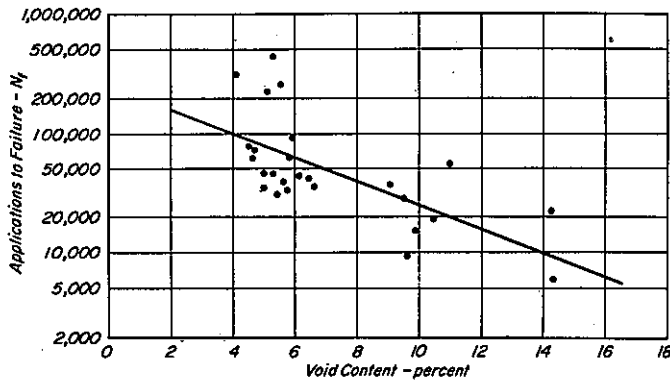
These data suggest that the structure of the voids (i. e. , size, shape, degree of interconnection) as well as their absolute volume is of importance. For example, for mixes with the same absolute volume of voids, the size of the void may be important in that the presence of a very large void will produce a greater reduction in the load carrying solid cross section than several smaller voids which are likely to be scattered throughout the specimen. In addition, stress concentration effects associated with the voids can lead to differences in fatigue lives depending on the shape (and size) of the voids (55).

The difference in fatigue life noted between the British and California graded mixes may thus in part be due to the size and shape of the voids in the two types of mixes since visual examination indicated that the British mix contained smaller size voids than the State of California fine and coarse mixes.

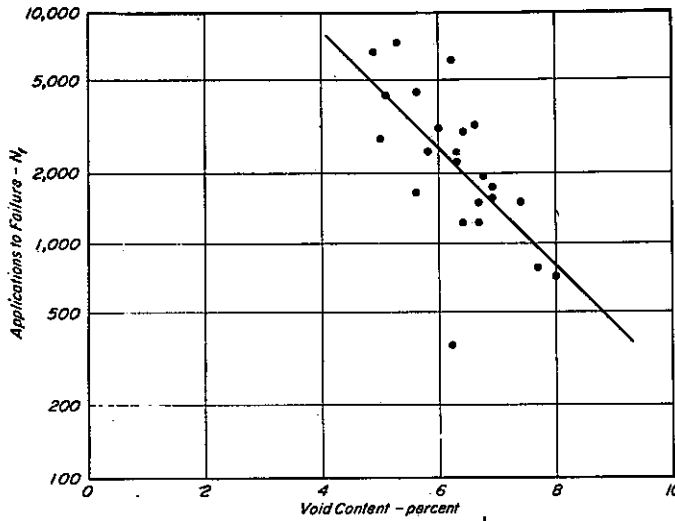
Stiffness. Stiffness as used herein is the relationship between stress and strain measured during the conduct of the flexural fatigue test and is dependent both on time of loading and temperature. In addition, stiffness is dependent upon air void content, aggregate grading, aggregate type, asphalt type and amount, and the stress level at which it is measured.

As has been indicated earlier, stiffness affects the fatigue response of mixtures in the controlled-stress mode of loading; accordingly it is desirable to assess the effects of stiffness on fatigue life and, in turn, the influence of the above-noted mixture characteristics on stiffness and fatigue life.

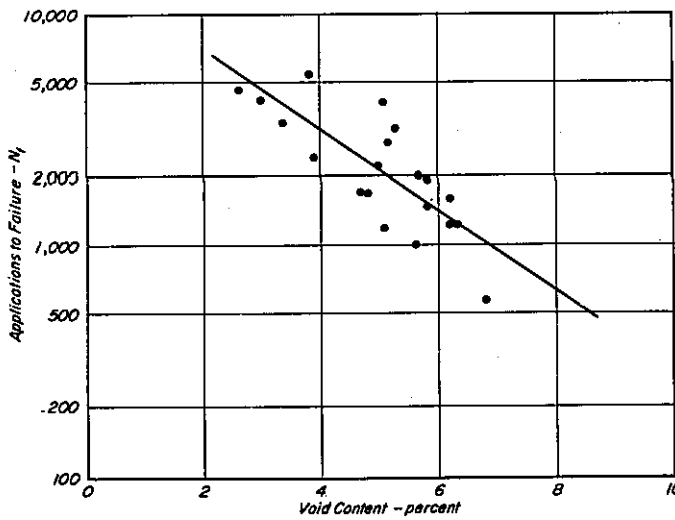
This section will attempt to define only the influence of stiffness on fatigue response. Later sections will indicate the influence of mixture variables both on stiffness and on fatigue behavior.



a. British Standard 594 grading — 79 percent asphalt.



b. California fine grading — 6 percent asphalt.



c. California coarse grading — 6 percent asphalt.

Fig. 46 — The effect of void content on fatigue life.

Data presented by Deacon (45) and Bazin and Saunier (48) indicate that stiffness is reduced with an increase in air void content. Fig. 47 illustrates such trends for the mixes whose fatigue life vs. void content data were presented in Fig. 46. Regression lines drawn through the data show an increase in stiffness with reduction in air void content. Considering the change in void content required to change the fatigue life by one order of magnitude results in changes in stiffness as follows for the three mixes.

<u>Mix</u>	<u>Change in Void Content to Change Fatigue Life by One Order of Magnitude</u>	<u>Change in Stiffness</u>
British Standard	10%	375,000 psi
California Fine	~4%	130,000
California Coarse	6%	130,000

Thus part of the increase in fatigue life in the controlled-stress mode of loading due to decrease in air void content is due to the increase in stiffness resulting from this reduction.

To investigate the influence of stiffness on fatigue life, data from five mixes containing granite aggregate and with the same asphalt content (6 percent) were analyzed. Air void contents ranged from 4 to 6 percent (Table 10) with an average value of about 5.5 percent. The data for all mixes were grouped together at each of the stress levels utilized in the test program and linear regression lines were obtained for stiffness vs. fatigue life (fatigue life as the dependent variable). Fig. 48 illustrates the resulting relationships each of which had the following statistics:

<u>Stress Level, psi</u>	<u>Correlation Coefficient</u>	<u>Standard Error of Estimate</u>
150	.952	.167
100	.916	.227
75	.746	.290

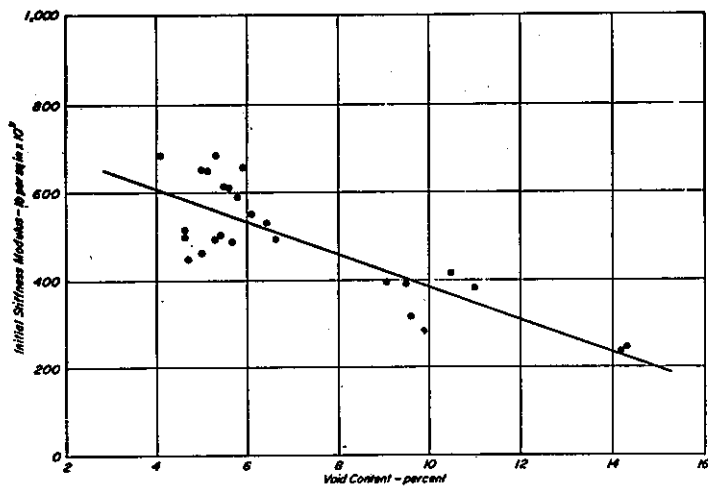
By interpolation from Fig. 48, stress vs. fatigue life relationships were obtained for a range in stiffness of 150,000 psi to 700,000 psi and have already been shown in Fig. 35. In this figure it will be noted that as the stiffness increases, the fatigue life at a particular stress level increases, and the slope of the line changes (in this case from 2.2 to 3.8* for the range of stiffnesses examined).

*The slope is represented by the coefficient n in the following expression:

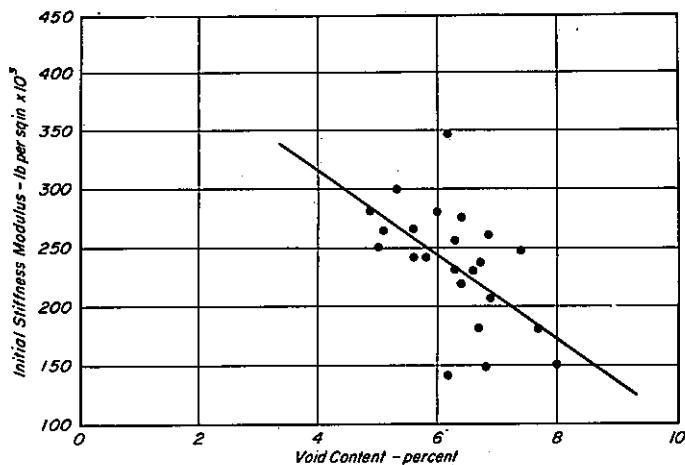
$$N_f = K \left(\frac{1}{\sigma} \right)^n$$

where:

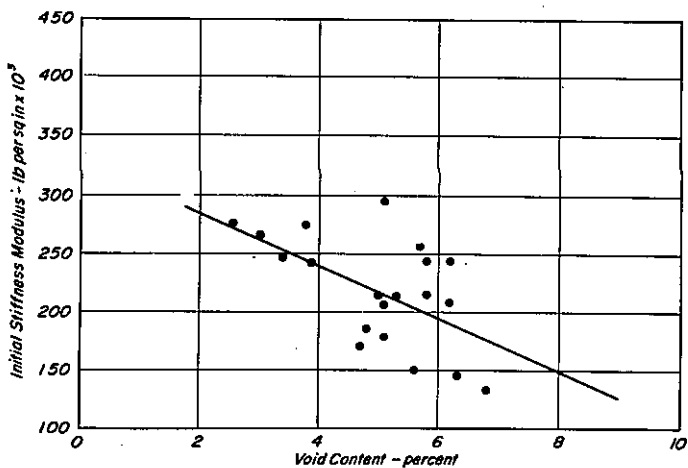
N_f = number of stress applications to failure
 σ = bending stress, repeatedly applied, psi



a. British Standard 594 grading - 7.9 percent asphalt.



b. California fine grading - 6 percent asphalt.



c. California coarse grading - 6 percent asphalt.

Fig. 47 - Relationships between initial stiffness modulus and air void content - granite aggregate.

Strain vs. fatigue life relationships can also be obtained from the data presented in Fig. 48 utilizing the transformation:

$$\epsilon_{\text{mix}} = \sigma_{\text{mix}}/S_{\text{mix}}$$

where:

$$\epsilon_{\text{mix}} = \text{mixture strain - in. per in.}$$

$$\sigma_{\text{mix}} = \text{applied stress - psi}$$

$$S_{\text{mix}} = \text{mixture stiffness - psi}$$

Results of such an analysis are presented in Fig. 49 for stiffnesses ranging from 200,000 to 500,000 psi. For this range in stiffness the data appear to be represented by a single relationship. If a wider range in stiffness is considered, however, a single line may no longer represent the relation between strain and load applications as seen in Fig. 50. It should be noted that the difference in fatigue life due to stiffness differences is not as large as is indicated on the stress vs. fatigue life plot (Fig. 35).

These results appear in line with the suggestion of Pell (46) that mixes for which large numbers of load applications are associated with crack propagation will exhibit steeper fatigue curves than those for which few applications are associated with crack propagation. In the controlled-stress mode of loading, tests performed on mixtures with low stiffness necessitate loading at lower stress levels — which in turn contributes to a slower rate of crack propagation and hence a steeper relationship between stress or strain and applications to failure.

Fig. 48 can also be used to ascertain the variation in fatigue life due to changes in mixture stiffness independent of large variations in air void content.

As shown previously, the fatigue life of the California fine graded mix is increased an order of magnitude at a stress level of 150 psi by decreasing the air voids by approximately 4 percent, (Fig. 46). Assuming that the air void content is reduced from 8 percent to 4 percent, one would expect an increase in stiffness from 180,000 psi to 310,000 psi for the tests performed at 150 psi, (Fig. 47). This change in stiffness increases the fatigue life from 840 to 5,300 applications which is less than one order of magnitude. Correspondingly, the fatigue life of the State of California coarse graded mix will increase by less than an order of magnitude for variation in air void content from 8.5 to 3.0 percent. Thus the change in fatigue life due to variations in air void content cannot wholly be explained by the change in stiffness produced by the same air void variation. Increased air

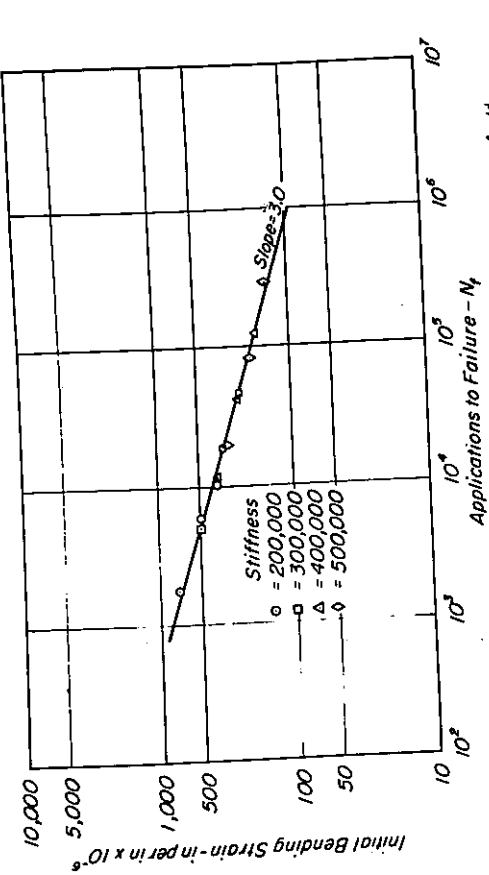


Fig. 49 - Initial bending strain vs. application to failure, for mixes of different stiffness - California graded mixes, granite aggregate, 85-100, 60-70, and 40-50 penetration asphalts, 6.0 percent asphalt.

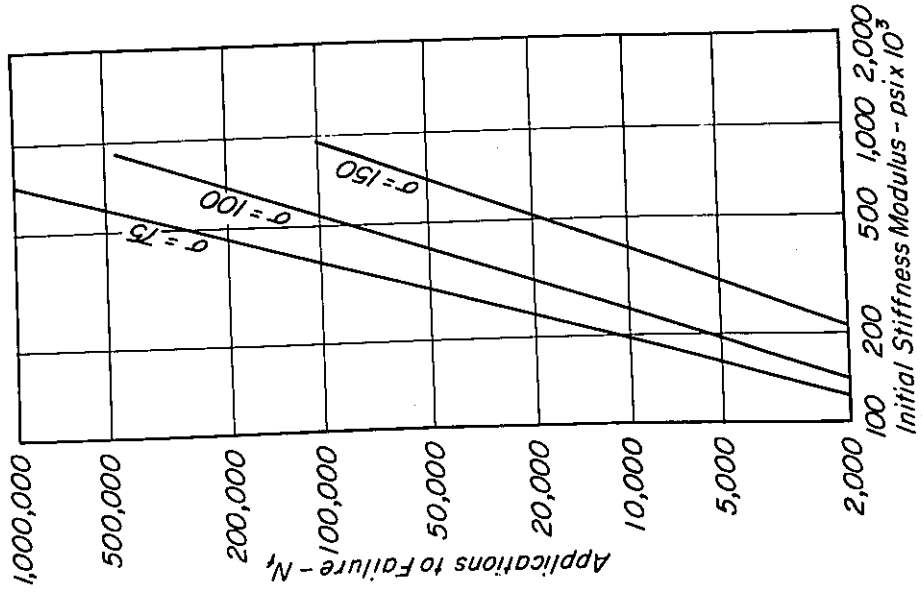


Fig. 48 - Relation between fatigue life and initial stiffness modulus California graded mixes, granite aggregates, 85-100, 60-70, and 40-50 penetration asphalts, 6 percent asphalt content.

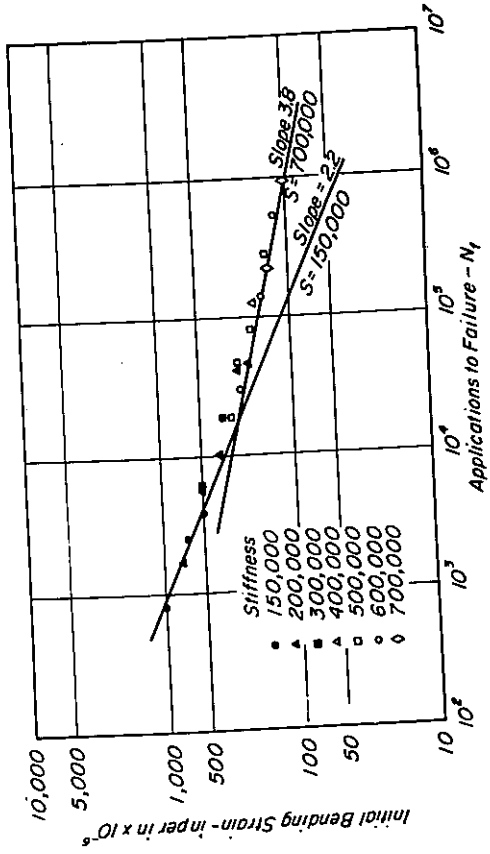


Fig. 50 - Initial bending strain vs. application to failure, for mixes of different stiffness - California graded mixes, granite aggregate, 85-100, 60-70, and 40-50 penetration asphalts, 6.0 percent asphalt.

void content tends to reduce the load carrying cross section of the specimen and to create additional locations for the formation of stress concentrations as noted earlier, thus contributing to a reduction in stiffness and fatigue life.

Aggregate Grading. From an examination of data obtained by Pell (46), Kirk (49), and Bazin and Saunier (48), it would appear that aggregate grading has little effect on fatigue behavior that cannot be explained by differences in asphalt content and air void content of the mixes, at least for tests conducted at temperatures less than approximately 10°C (50°F).

With the results of these investigations as a basis, three State of California 1/2 in. maximum size aggregate gradings were selected representing the extreme fine, the middle, and the extreme coarse portions of the grading band. All mixes were prepared with an asphalt content of 6 percent and the compactive effort was controlled so that air void contents averaged about 5.7 percent for the extreme graded mixtures and 4.5 percent for the medium graded mix. Controlled-stress fatigue tests were conducted at 20°C (68°F).

Individual test results, a linear regression line, and scatter bands representative of two standard deviations or 95 percent of the data for the mixture strain vs. fatigue life relationship are shown on Fig. 51 for the fine mix. Similarly, results for the stress vs. fatigue life relationship are shown in Fig. 52. It should be noted that the fine graded mix was tested over a range in stress from 450 to 75 psi whereas the other two mixes were tested at only three stress levels (150, 100 and 75 psi). Results from the other test series are presented in Tables 14 and 15. Comparisons of the mixture strain vs. fatigue life and stress vs. fatigue life relationships for the three mixes may be found in Figs. 53 and 54.

Differences in fatigue life exist on both the strain vs. fatigue life and stress vs. fatigue life plots for these mixes. Factors which contribute to these differences may be attributed to one or a combination of the following:

1. stiffness
2. air void content
3. inherent scatter in test and data
4. aggregate grading

Since the asphalt content remained constant at 6 percent, it is not considered to be an important factor in explaining these variations.

By examining Figs. 53 and 54, it can be seen that the medium graded mix exhibited a longer fatigue life on both the strain vs. fatigue life and the stress vs. fatigue life plots than the extreme fine and coarse graded mixes.

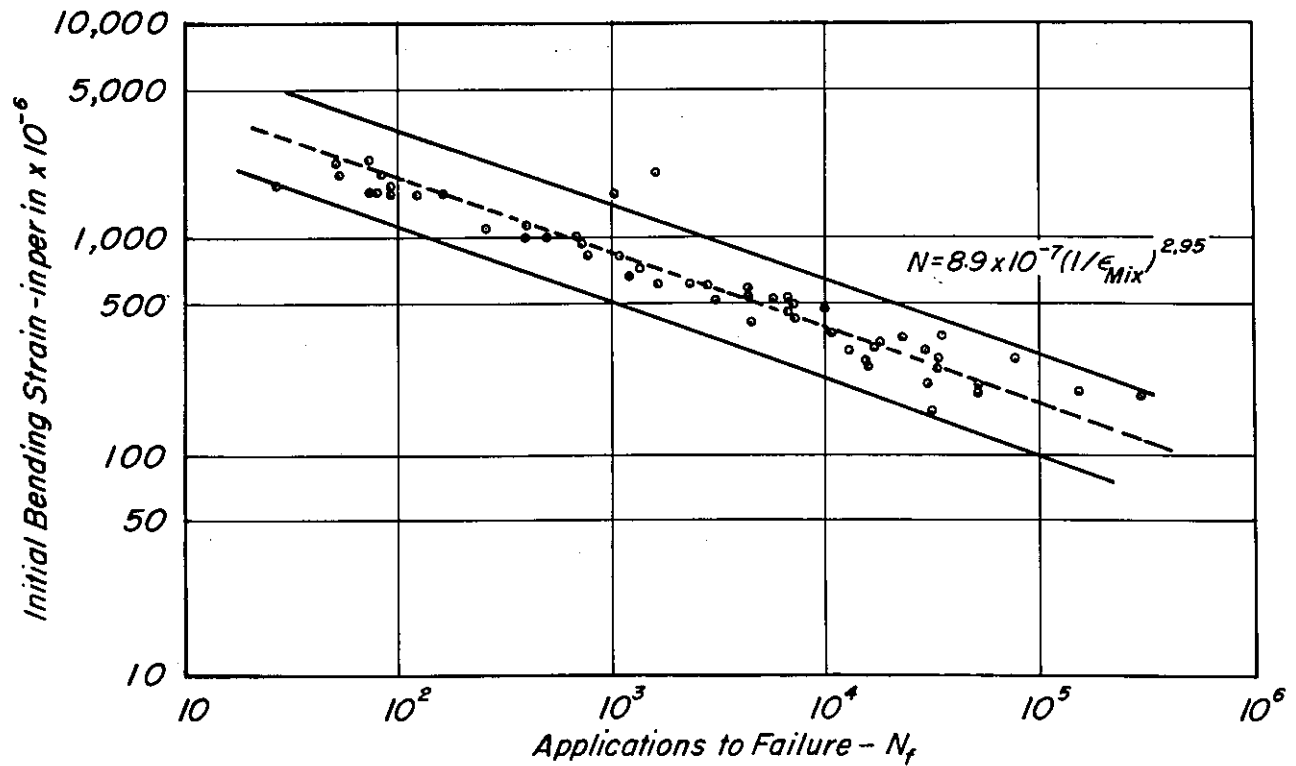


Fig. 51 — Initial mixture bending strain vs. fatigue life — California fine grading, granite aggregate, 85-100 penetration asphalt, 6 percent asphalt.

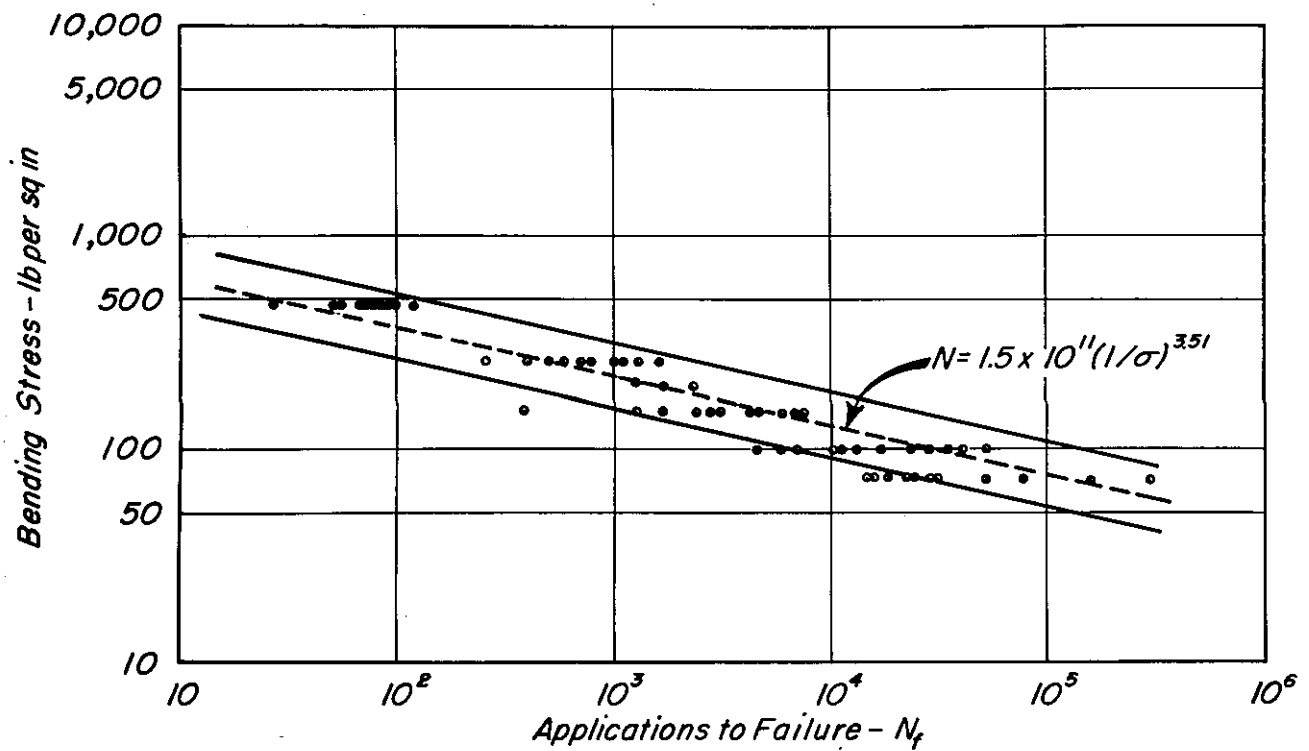


Fig. 52 — Mixture bending stress vs. N_f — California fine grading, granite aggregate, 85-100 penetration asphalt, 6 percent asphalt.

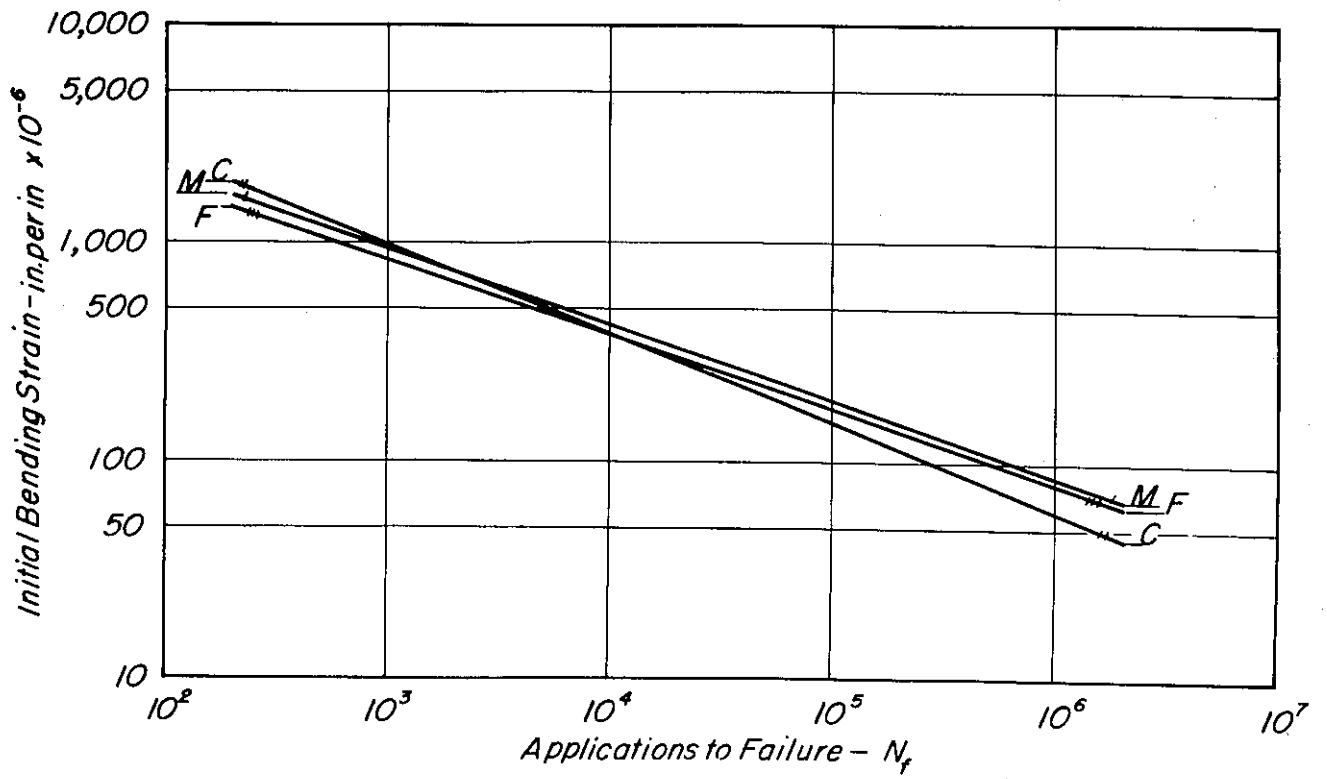


Fig. 53 — Effect of aggregate grading on the initial mixture bending strain vs. N_f plot — granite aggregate, 85-100 penetration asphalt, 6 percent asphalt.

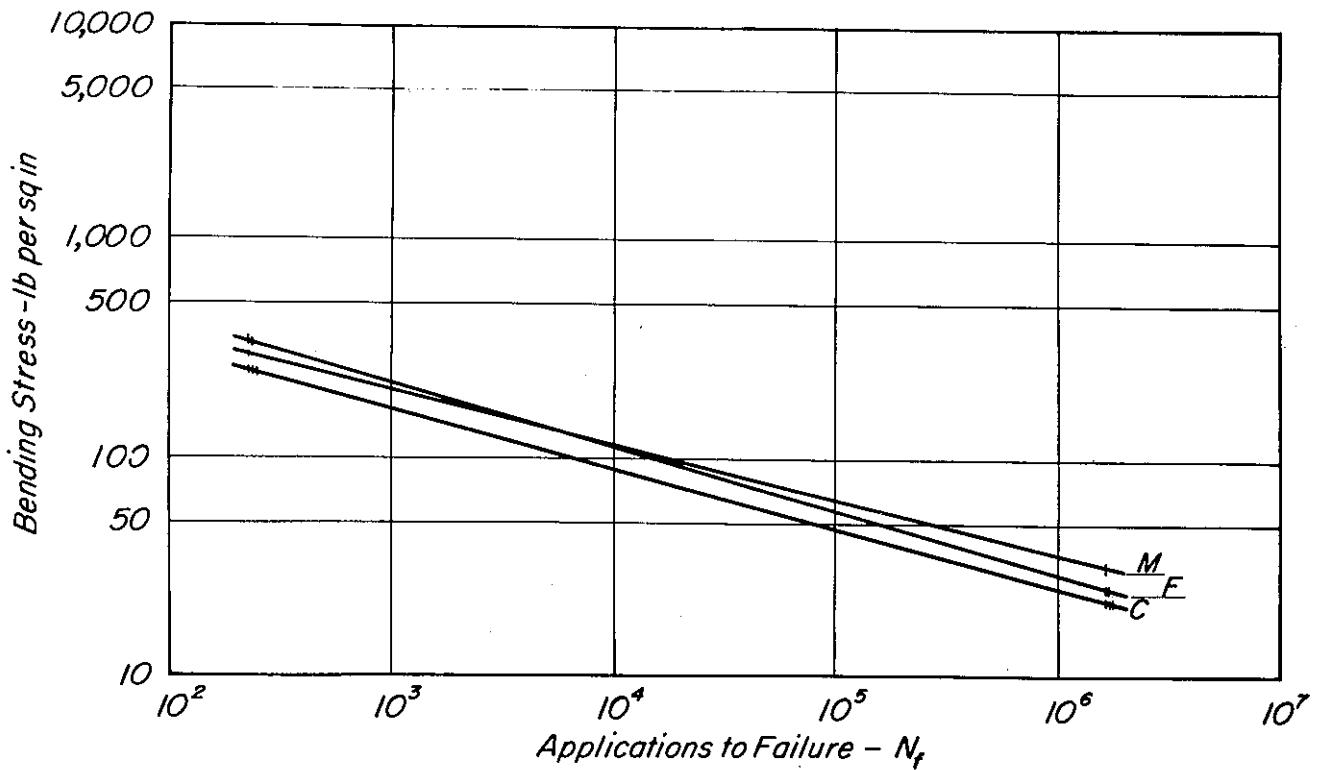


Fig. 54 — Effect of aggregate grading on the mixture bending stress vs. N_f plot — granite aggregate, 85-100 penetration asphalt, 6 percent asphalt.

TABLE 14 — MEAN, STANDARD DEVIATION AND COEFFICIENT OF VARIATION OF STIFFNESS, STRAIN, AIR VOIDS AND FATIGUE LIFE FOR GRANITE AGGREGATE MIXES — LABORATORY STUDY

Mix Identification Grading & Asphalt Penetration	Stress Level psi	No. of Bars	Stiffness		Strain		Percent Air		Fatigue Life			
			Mean $\text{psi} \times 10^3$	Std. Dev. $\text{psi} \times 10^3$	Mean in. per in. $\times 10^{-6}$	Std. Dev. in. per in. $\times 10^{-6}$	Mean C _v	Std. Dev.	Mean	Std. Dev.	C _v	
British Standard 594	175	10	567	90	15.8	46	5.19	.84	16.2	67,385	48,625	72.1
	150	14	565	80	14.2	37	5.42	.67	12.4	104,923	129,188	123.1
40-50 penetration	125	11	578	86	14.8	30	5.50	.58	10.5	175,032	107,347	61.3
	all	35	570	83	14.4		5.38	.69	12.8			
California Coarse Granite Aggregate	150	9	193	37	18.9	153	5.48	.58	10.7	1,605	571	35.5
	100	10	248	64	25.8	94	5.80	.63	10.9	7,885	3,054	38.7
85-100 penetration	75	9	239	45	18.8	48	5.85	.55	9.3	23,017	12,873	55.9
	all	28	228	54	23.8		5.71	.59	10.3			
California Fine Granite Aggregate	450	10	246	32	13.1	272	5.72	.47	8.2	72	25	35.3
	250	10	254	60	23.4	404	5.62	.57	10.1	836	435	52.0
85-100 penetration	150	11	257	52	20.0	163	5.64	.52	9.2	3,800	2,424	63.8
	100	11	284	83	29.3	94	5.82	.28	4.9	19,277	15,271	79.2
75	11	11	317	68	21.3	50	5.73	.49	8.5	72,059	97,541	135.3
	all	53	273	65	23.8		5.71	.46	8.1			
California Medium Granite Aggregate	150	6	258	35	18.6	74	4.60	.38	8.3	3,509	1,274	36.3
	100	6	276	59	21.5	81	4.30	.52	12.1	21,193	8,038	37.9
85-100 penetration	75	7	325	44	13.6	31	4.57	.70	15.5	73,310	56,672	77.3
	all	19	288	53	18.5		4.49	.55	12.2			
California Medium Granite Aggregate	150	9	285	58	20.2	101	4.83	.48	10.2	6,592	4,419	67.0
	100	9	334	66	19.8	61	4.68	.50	10.7	28,812	13,974	48.4
60-70 penetration	75	9	335	30	8.9	20	4.87	.33	6.9	123,936	90,590	73.0
	all	27	318	57	17.8		4.80	.43	9.1			
California Medium Granite Aggregate	175	7	631	117	18.5	49	4.78	.52	10.8	22,944	19,345	84.3
	150	8	655	82	12.5	30	4.55	.53	11.8	42,818	25,383	59.2
40-50 penetration	125	2	590	33	5.5	11	5.55	.07	1.2	58,921	25,704	43.6
	100	6	708	71	10.0	14	4.63	.19	4.2	346,538	197,055	56.8
all	23	656	92	13.9		4.73	.50	10.6				

TABLE 15 — LEAST SQUARES REGRESSION EQUATION AND STATISTICAL QUANTITIES FOR LABORATORY PREPARED FATIGUE STUDIES

N_f = dependent variable

Mix Designation	No. of Bars	Asphalt Penetration for N_f	K_1		Correlation Coefficient	Standard Error of Estimate
			$K_1(1/\epsilon_{mix})^{n_1}$	n_1		
British Standard 594	35	40-50	6.11×10^{-8}	3.383	.789	.230
California Coarse Granite Aggregate	28	85-100	3.20×10^{-5}	2.485	.932	.184
California Fine Granite Aggregate	53	85-100	8.91×10^{-7}	2.952	.950	.326
California Medium Granite Aggregate	19	85-100	2.87×10^{-6}	2.832	.899	.260
California Medium Granite Aggregate	27	60-70	1.12×10^{-7}	3.256	.952	.187
California Medium Granite Aggregate	23	40-50	1.03×10^{-10}	4.010	.962	.150
California Medium Basalt Aggregate	24	60-70	1.34×10^{-7}	3.222	.896	.213

Mix Designation	No. of Bars	Asphalt Penetration for N_f	K_2		Correlation Coefficient	Standard Error of Estimate
			$K_2(1/\sigma_{mix})^{n_2}$	n_2		
British Standard 594	35	40-50	1.36×10^{11}	2.871	.448	.335
California Coarse Granite Aggregate	28	85-100	1.64×10^{11}	3.685	.917	.202
California Fine Granite Aggregate	53	85-100	1.55×10^{11}	3.514	.948	.333
California Medium Granite Aggregate	19	85-100	2.11×10^{12}	4.036	.895	.265
California Medium Granite Aggregate	27	60-70	7.29×10^{12}	4.206	.888	.279
California Medium Granite Aggregate	23	40-50	1.97×10^{15}	4.928	.886	.255
California Medium Basalt Aggregate	24	60-70	6.01×10^{10}	3.238	.872	.235

As previously shown, the greater the stiffness, the flatter the slope of the regression line and the longer the life. The medium mix exhibited the highest stiffness, and therefore would be expected to be in the relative position shown at fatigue lives greater than 10^4 . Increasing stiffness would normally be expected with increasing fine content; however, the medium mix has been compacted at a slightly lower air void content than the fine and coarse mixes, and thus it has approximately the same stiffness as the fine graded mix. By referring to Fig. 47 it will be noted that a reduction of approximately 30,000 to 40,000 psi in the stiffness would be justified if the medium mix contained an average air content of 5.7 percent (as do the coarse and fine mixes) rather than 4.5 percent. With this reduction in stiffness due to air void content, the average stiffness would be as follows:

Coarse graded mix	228,000 psi
Medium graded mix	250,000 psi
Fine graded mix	273,000 psi

No clear-cut trend is noted in the slopes of the lines other than that the coarse graded mix with the lowest stiffness exhibits the steepest slope on both plots.

To compare the slopes of the regression lines on strain-fatigue life plots, the F test was first used to test the null hypothesis that the standard errors of the estimate for the two relations are equal. Appendix D contains tabulated values upon which the decision to reject or accept the appropriate hypothesis was made.

The null hypothesis could not be rejected for an equal-tail test at a level of significance equal to 95 percent and thus we can assume that the standard errors of the estimate for the three possible comparisons are equal (Appendix D).

Since the standard errors of the estimate can be shown to be equal, it is now possible to use the ttest. This test was used to test the null hypothesis that the difference between the slopes of the lines equals zero. In all possible cases this hypothesis could not be rejected for a two-tail test at a level of significance equal to 95 percent. Particular emphasis was placed on the analysis of the fine graded vs. the coarse graded mix since the two mixes represent extreme gradings and in this investigation contained equal average air void contents and asphalt contents. It was felt that if these mixtures could be represented as a single line, then the effect of grading on fatigue life could be considered negligible. From the analyses presented above it seems possible that the three regression lines may be considered to be one at a significance level of 95 percent. With this in mind the data for the three test series were regressed together and the following equation was obtained:

$$N_f = 1.15 \times 10^{-6} (1/\epsilon_{\text{mix}})^{2.92}$$

with a correlation coefficient of .948 and a standard error of the estimate equal to .282. Thus it seems possible that the effect of aggregate grading does not significantly influence the results of fatigue tests when the tests are represented on a plot of mixture strain vs. fatigue life. It should be pointed out that this judgment is based on a mix with three different aggregate gradings, identical asphalt contents and containing air voids that varied over a narrow range.

Slopes of the regression lines on the stress-fatigue life plots were also analyzed. The slope of the lines for the coarse and fine graded mix were first considered. The F test on these two mixes suggested that at a 95 percent significance level the standard error of the estimate for the two relations are not equal. Therefore, the t test could not be used. The comparisons made for the fine mix vs. the medium mix and the coarse mix vs. the medium mix suggest that the slopes of the lines are equal to a level of significance equal to 95 percent.

Since the slopes of the fine mix and coarse mix could not be shown to be equal using the above techniques, a test of the equality of the means of the fatigue lives of the mixes at different stress levels was performed. This test may be applied using independent samples from two populations and assuming that the populations variances are equal. At a stress level of 150 psi the null hypothesis which assumes that the means are equal, must be rejected at a level of significance of 95 percent for a two-tailed test. At stress levels of 100 and 75 psi the above null hypothesis must be accepted or judgment can be reserved since the variance of the fatigue lives becomes large at the lower stress level (Appendix D). Because the variance at these lower stress levels is quite high, there is some doubt whether the mean fatigue lives of the two mixes may be the same. Thus it seems possible that grading may have an effect on the results of fatigue tests when represented on the stress-fatigue life plot.

It can be concluded from the comparison made with the coarse and fine mixes, which represented the extreme fine and coarse California gradations, that the effect of grading on the strain vs. fatigue life relationship is negligible. The differences noted on Fig. 53 can be explained by the scatter noted in the data at a level of significance of 95 percent. The differences noted in the stress-fatigue life relationship cannot be wholly accounted for by the scatter in the data at a significance level of 95 percent. Stiffness differences noted in the mixes probably account for some of the differences in the location of the regression lines for the coarse and fine mixes which have the same mean air void content. The medium mix has a lower air void content and thus its location is somewhat displaced from its ideal location between the coarse and fine mixes.

Aggregate Type. Aggregate type will be used to describe the surface texture, shape and petrographic classification of the aggregate. The effect of aggregate type on fatigue properties of asphalt concrete has not been extensively studied.

Pell (46) has concluded that it has a negligible effect, based on an analysis of fatigue test results on mixes made with two aggregates, gravel and crushed rock, and containing equal amounts of a 40-50 penetration asphalt and identical gradings. Kirk (49) has also described its negligible effect on the fatigue response of asphalt mixes.

Jimenez (50), however, has presented data which suggest that aggregate type is important in that it determines the amount of asphalt that can be incorporated in the mix. His data indicate that rough textured aggregate allows more asphalt to be incorporated into the mix, thus resulting in longer fatigue lives than mixes containing lesser quantities of asphalt necessitated by the smooth textured material.

In this study two test series were used to investigate the influence of aggregate type on the fatigue properties of asphalt concrete. From the first series, fatigue relationships were developed for mixes of the same grading at equal asphalt contents by volume. These mixes contained the 1/2 inch maximum medium graded aggregate and a 60-70 penetration asphalt. Test results at 68°F are summarized in Tables 14, 15, and 16 for these two mixes. Mean regression lines for these test series are presented in Figs. 55 and 56 for the strain vs. fatigue life and stress vs. fatigue life relationships respectively.

As noted in Fig. 55 the strain vs. fatigue life relationships are almost identical although the average air voids of the mixes differ by approximately 2 percent. However, stiffness values of the mixes are almost the same (Tables 14 and 16). It can be shown statistically that the slopes of the two lines are the same at a confidence level of 95 percent (Appendix D). Similarly the slopes of the lines on the stress vs. fatigue life plot can also be shown to have the same value (Appendix D). The difference in air void content in part contributes to the observed differences in the mean lines on the stress vs. fatigue life plot since as noted earlier, high air void contents are associated with short fatigue lives at any particular stress level.

The second series of tests to investigate the influence of aggregate type on fatigue behavior utilized three aggregate types namely granite, limestone and crushed gravel. Mixes prepared with these aggregates contained the same grading, 85-100 penetration asphalt, and asphalt contents based on California stability requirements. Stability-asphalt curves were determined and an asphalt content 0.3 percent less than that predicted for 35 stability was chosen for each of these mixes. The 0.3 percent decrease allows for variation in asphalt content that may occur during construction. Mixes with crushed gravel and limestone had almost identical asphalt contents by weight and

TABLE 16 — MEAN, STANDARD DEVIATION AND COEFFICIENT OF VARIATION OF STIFFNESS, STRAIN, AIR VOIDS AND FATIGUE LIFE FOR BASALT AGGREGATE — LABORATORY PREPARED MIXES

Mix Identification Grading & Asphalt Percent	Stress Level psi	No. of Bars	Stiffness		Strain		Percent Air		Fatigue Life					
			Mean psi x 10 ³	Std. Dev. psi x 10 ³	Mean in. per in. x 10 ⁻⁶	Std. Dev. in. x 10 ⁻⁶	Mean %	Std. Dev.	Mean	Std. Dev.	c _v			
California Medium Basalt Aggregate Type I (5.7%)	150	8	279	51	18.3	553	96	17.4	7.65	.46	6.0	4,878	3,270	67.0
California Medium Basalt Aggregate Type I (6.2%)	150	8	318	27	8.5	475	41	8.6	6.17	.54	8.8	6,645	3,808	57.3
	100	8	284	61	21.5	367	80	21.6	7.00	.45	6.5	21,512	11,562	53.7
	75	8	293	56	19.1	265	51	19.1	7.00	.51	7.3	54,968	16,672	30.3
	all	24	298	50	16.9				6.72	.62	9.3			
California Medium Basalt Aggregate Type I (6.7%)	150	4	380	40	10.5	398	40	10.0	5.20	.34	6.6	19,136	11,160	58.3
California Medium Basalt Aggregate Type I (7.7%)	150	4	301	22	7.2	500	35	7.0	4.05	.26	6.5	14,953	5,985	40.0
California Medium Basalt Aggregate Type I (8.7%)	150	4	190	4	2.2	789	20	2.4	1.60	.14	8.8	9,573	2,215	23.1
California Medium Basalt Aggregate Type II (5.3%)	150	4	223	55	24.5	705	173	24.5	8.77	.54	6.1	2,387	2,285	95.7
California Medium Basalt Aggregate Type II (5.7%)	150	4	278	20	7.2	539	35	6.4	8.10	.28	3.4	3,298	1,582	47.7
California Medium Basalt Aggregate Type II (6.2%)	150	4	277	38	13.8	549	74	13.4	7.20	.64	9.0	4,605	2,426	52.6

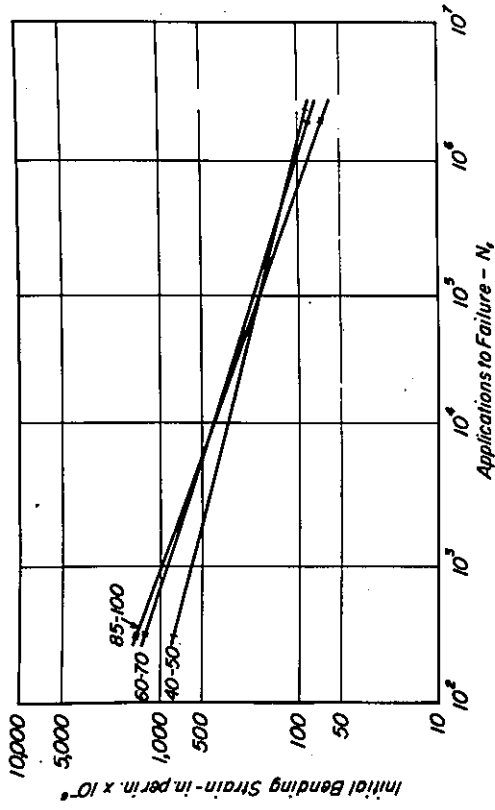


Fig. 57 - Effect of asphalt penetration on the initial mixture bending strain vs. N_f plot - California medium grading, granite aggregate, 6 percent asphalt.

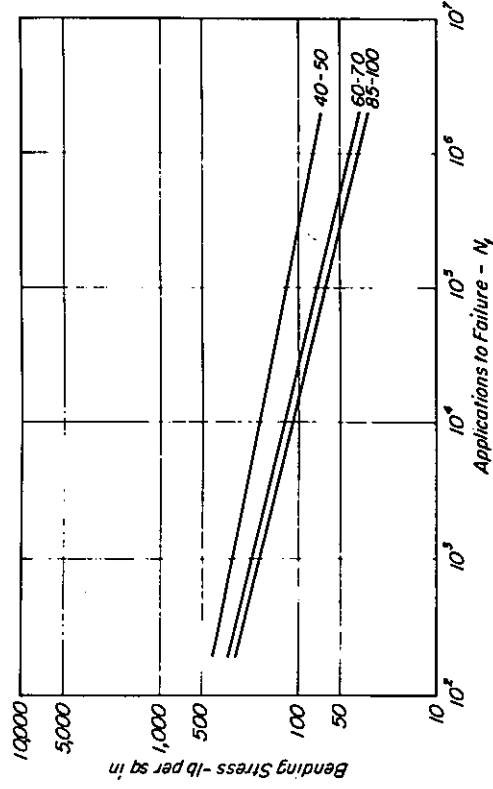


Fig. 58 - Effect of asphalt penetration on the mixture bending stress vs. N_f plot - California medium grading, granite aggregate, 6 percent asphalt.

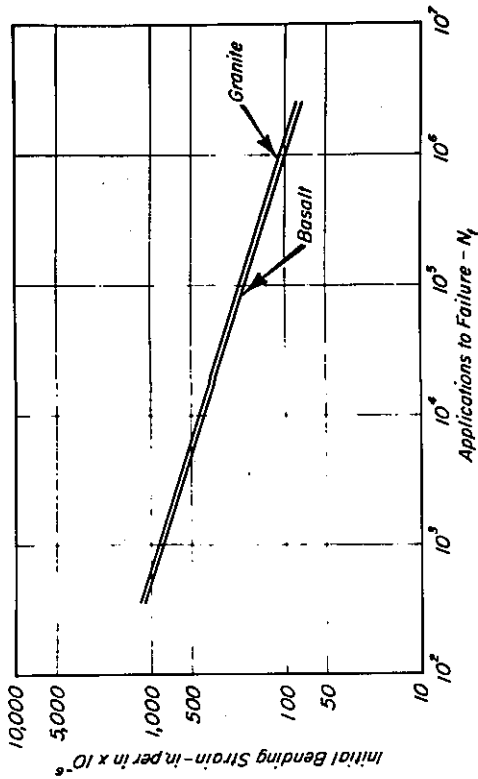


Fig. 55 - Effect of aggregate type on the initial mixture bending strain vs. N_f plot - California grading, 60-70 penetration asphalt.

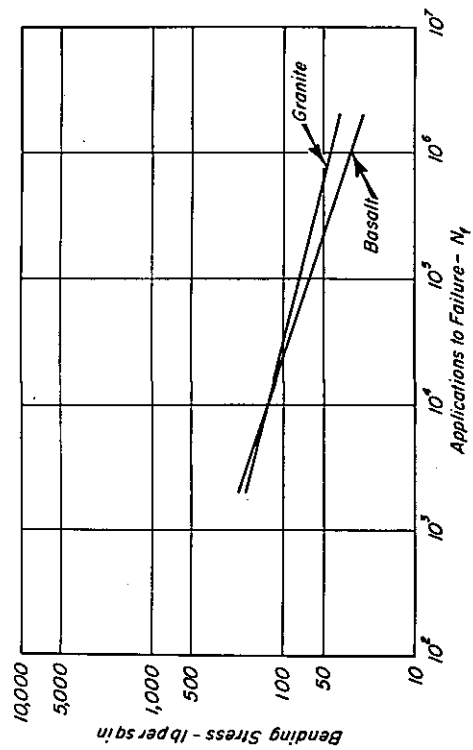


Fig. 56 - Effect of aggregate type on the mixture bending stress vs. N_f plot - California medium grading, 60-70 penetration asphalt.

volume — 4.6 to 4.7 percent respectively — while the granite contained a slightly higher value — 5.2 percent. Average air voids of the mixes varied from 6.4 to 8.2 percent (Table 17) with the limestone mix having the lowest and the gravel the highest air void content. A minimum of eight bars of each aggregate type was tested at a stress level of 75 psi. Resulting fatigue lives and stiffnesses are shown in Table 17.

The same statistical procedure utilized to test the equality of two means was used to test the means of the fatigue lives of these mixes. In the three comparisons possible, the means at a level of significance equal to 95 percent must be considered equal (Appendix D). This result is in part due to the large scatter in the data. The same procedure was used to test mean values of stiffness. When comparing the granite and limestone with the crushed gravel mixes, the mean could not be considered to be the same. Thus it was possible that the crushed gravel which produced mixes with higher stiffnesses would also produce mixes with somewhat higher fatigue lives as is evident from the data (Table 17).

Comparisons between the limestone and crushed gravel mixes can ignore the effect of asphalt content, since both have approximately the same amount by volume. Furthermore, the influence of air voids tends to contradict the observed behavior both for stiffness and fatigue life. The higher air voids in the crushed gravel mix suggest that the stiffness and fatigue life should both be lower; however, the reverse is evident. On the basis of this study it seems possible that different aggregates, as manifested by various surface textures and shapes may influence the stress-fatigue life relationship to a certain degree. These results agree with that presented by Jimenez and discussed earlier. The limestone, which has a smoother surface texture as measured by the C. K. E. and Oil Equivalent Tests (Table 11), has a lower fatigue life than the rougher textured crushed gravel when comparisons are made at equal asphalt contents.

The apparent short fatigue life associated with the granite mix cannot be justified on the basis of air voids or asphalt content. The granite mix has a higher asphalt content and lower air voids, both of which should contribute to a longer fatigue life. Moreover, the granite mixes have a higher stiffness than the crushed gravel mix. Since both mixes were made with the same asphalt and were mixed and compacted using the same procedure, the differences noted were therefore probably due to the structure of the air voids.

Results for these test series indicate that aggregate type probably has little effect on the strain vs. fatigue life relationship, while the stress vs. fatigue life behavior may be influenced by the aggregate type. The degree of this influence, however, has not been well defined.

TABLE 17 -- MEAN, STANDARD DEVIATION AND COEFFICIENT OF VARIATION OF STIFFNESS, STRAIN, AIR VOIDS, AND FATIGUE LIFE FOR LABORATORY PREPARED MIXES -- GRANITE, LIMESTONE AND CRUSHED GRAVEL AGGREGATES

Mix Identification Grading & Asphalt Percent	Stress Level psi	No. of Bars	Stiffness		Strain		Percent Air		Fatigue Life					
			Mean psi x 10 ³	Std. Dev. C _v psi x 10 ³	Mean in. per in. x 10 ⁻⁶	Std. Dev. C _v in. per in. x 10 ⁻⁶	Mean C _v	Std. Dev. C _v	Mean C _v	Std. Dev. C _v				
California Medium Granite Aggregate 5.2%	75	8	289	25	8.7	262	24	9.1	7.06	.73	10.4	19,925	13,231	66.4
California Medium Limestone Aggregate 4.7%	75	8	293	50	17.0	261	39	14.7	6.40	.55	8.6	23,556	15,361	65.2
California Medium Crushed Gravel 4.6%	75	9	371	48	12.9	206	30	14.3	8.20	.52	±6.3	42,474	30,924	72.8

Asphalt Type. Pell (46) has presented results of controlled-stress fatigue tests on mixes containing identical aggregate gradings and asphalt contents but differing in the type of asphalt. One mix contained a 40-50 pen. asphalt cement, whereas the other contained a 90-100 pen. asphalt cement. The tests were performed at 0°C (32°F) and the stress vs. fatigue life relationships varied in both relative position and slope of the lines. The softer material exhibited a slightly steeper slope than the harder material and also a lower fatigue life at the same stress level. When the results are plotted on a strain vs. fatigue life plot, only a small difference was observed in the relative position of the fatigue lives and the mixes made with 40-50 penetration exhibited a slightly flatter slope than those mixes made with 90-100 penetration material. From these data Pell concluded that "the grade of bitumen appears to effect the fatigue life mainly though its influence on the slope of the fatigue line."

Jimenez (50) has shown that as the penetration of the asphalt decreases or as the viscosity increases, a greater number of applications of load is required to produce failure. This finding is in line with the fact that increased viscosity or lower penetration should increase the stiffness of the mixture which in turn should increase the fatigue life at a particular stress level, (Fig. 35). Heukelom and Klomp (35) have also suggested that at a particular stress level the number of load applications to failure will increase as the stiffness increases.

Bazin and Saunier (48) have shown that stiffness is dependent upon the penetration and temperature susceptibility characteristics of the asphalt. They have also shown that the relative position and slope of the strain vs. applications to failure curve is dependent upon the bitumen used.

Vallerga, et al, (51) from an investigation of the effect of asphalt aging on fatigue properties, have shown that harder asphalts produce mixes which exhibit longer fatigue lives at a particular stress level thus producing a series of curves on the stress vs. fatigue life plot. However, to a first approximation, the same relationship between strain and fatigue life is obtained regardless of penetration.

With the above mentioned trend in mind, a granite aggregate graded to meet the State of California half-inch medium requirements was mixed with three different penetration grade asphalts namely 85-100, 60-70, and 40-50, in order that the influence of asphalt type could be studied. Asphalt content was held constant at 6 percent by dry weight of aggregate so that the influence of asphalt content could be eliminated. Mean air void contents varied from 4.5 to 4.8 percent and thus can be considered to have negligible influence on the fatigue relationships. The medium graded mix containing the 85-100 penetration grade asphalt cement was also used to study the influence of aggregate gradation on fatigue behavior.

Mean fatigue relationships for the three mixes are presented in Figs. 57 and 58. Detailed data are included in Tables 14 and 15.

Since the air void content and asphalt content are approximately equal for these three mixes, the difference in stiffness and fatigue life can be attributed to the differences in the type of asphalt cements. Table 14 indicates that the stiffness increases with decreasing penetration, with the 40-50 penetration mix exhibiting an average stiffness of 656,000 psi. The mixes containing the 85-100 and 60-70 penetrations material have stiffnesses which average 288,000 psi and 318,000 psi respectively, which can be shown to statistically have equal mean values at a level of significance of 95 percent.

Stiffness differences can be used to explain the location and slopes of the mean regression lines for the stress vs. fatigue life relationships shown on Fig. 58. The mix containing the hardest asphalt, and thus having the highest stiffness, has the longest fatigue life and the flattest slope. The mixtures containing the 85-100 and 60-70 penetration asphalts also show the effect of stiffness; but since the stiffness values of both mixes are approximately equal, the differences relative to both slope and location are small.

Although the mean regression lines for the strain vs. fatigue life relationship are somewhat confusing, the stiffness values can be used to explain the trends noted. At fatigue lives in excess of approximately 10^6 repetitions, the relative positions of the lines are as expected. The mix with the highest stiffness exhibits the longest fatigue life and the flattest slope, while the mix with the lowest stiffness has the shortest fatigue life and steepest slope. The slopes of the mixes made with 85-100 and 60-70 penetration asphalts can be shown to be statistically equal at a level of significance of 95 percent, while comparisons between the 85-100 and 40-50, and 60-70 and 40-50 penetration mixes cannot be shown to be equal at this level of significance. This would suggest that the harder asphalts tend to have flatter slopes which cannot be explained by variations in air voids and scatter in the data, but rather by the rheological properties of the asphalt as reflected in the stiffness of the mix.

Since the slope of the regression line of the mixture made with 85-100 and 60-70 penetration asphalt can be considered equal, a regression line was fit to the combined data of these two mixes. The equation of the line is:

$$N_f = 4.07 \times 10^{-7} (1/\epsilon_{\text{mix}})^{3.09}$$

with a correlation coefficient of .929 and standard error of the estimate equal to .220.

It has been suggested that the results of the fatigue tests for mixes with equal asphalt contents made with the same aggregate and asphalt type may be represented as a single line on a log-log plot of strain vs. fatigue life regardless of the aggregate grading.

Similarly, the results of fatigue tests for mixes with equal asphalt contents made with the same aggregate and aggregate grading but with different types of asphalt can also be represented as a single line, providing the mixture stiffnesses do not vary to a large degree. Since the above conclusions were based on two test series, both of which contained the same aggregates and asphalt content, it seems reasonable that, regardless of the aggregate grading and the type of asphalt and provided large variation in stiffness does not occur, the results may be represented as a single regression line on a log-log plot of strain vs. fatigue life. Although the slopes of the lines, developed for the California coarse graded mix and the California medium graded mix with a 60-70 penetration asphalt, cannot be shown to be statistically equal (Appendix D), a regression line was, nevertheless, fit to the results of the tests used to investigate the effect of grading (coarse, fine, and medium mixes) and the mixes used to study the effect of asphalt type (with the exception of the 40-50 penetration asphalt mixes). The resulting equation:

$$N_f = 6.28 \times 10^{-7} (1/\epsilon_{\text{mix}})^{3.01}$$

with a correlation coefficient of 0.952 and a standard error of the estimate equal to .270 suggests that the data may be represented by a single regression line to a first approximation. It should be reemphasized that this equation was developed from data for mixes with the same asphalt content (6 percent by dry weight of aggregate) and the same aggregate with average mixture stiffnesses ranging from 228,000 to 318,000 psi.

A regression equation was also fit to the results of the above test series and the mix containing the 40-50 penetration asphalt cement. This line can be described by the equation:

$$N_f = 7.91 \times 10^{-7} (1/\epsilon_{\text{mix}})^{2.98}$$

The correlation coefficient had a value of 0.956 while the standard error of the estimate equaled 0.263. This equation, however, is largely influenced by the abundance of tests conducted on relatively low stiffness mixes.

Asphalt Content. Pell (46) and Jimenez (50) have studied the effect of asphalt content on fatigue life. Both investigators present convincing data which show that a specific asphalt content exists for optimum fatigue behavior. However, Jimenez indicates that the optimum asphalt content is a function of the type of aggregate used.

To investigate the effect of asphalt content on fatigue behavior, a basalt aggregate from two different manufacturers but the same geological formation was graded to meet the California 1/2 inch maximum medium specification and mixed with a 60-70 penetration asphalt cement. Asphalt contents varied from 5.3 to 8.7 percent by dry weight of aggregate.

Tests were performed at a stress level of 150 psi. Average values of stiffness, strain, air voids, and fatigue life for the various asphalt contents are shown in Table 16.

Results of these tests suggest that a maximum fatigue life at a stress level of 150 psi will occur at an asphalt content of 6.7 percent (Fig. 59). Fig. 60 indicates that maximum fatigue life occurs at the asphalt content resulting in the highest stiffness. Thus as previously suggested by Pell and Jimenez, a peak asphalt content exists for optimum fatigue life; and as shown in Fig. 60, this peak asphalt content also produces the mixture with the highest stiffness. It is interesting to note that the location in terms of asphalt content cannot be predicted from use of the nomograph developed by Heukelom and Klomp (35), since the nomograph will give values of decreasing stiffness with increasing asphalt content (Fig. 61).

As noted above, the optimum asphalt content based on fatigue behavior would be selected at 6.7 percent; however, as seen in Table 13, this is about 0.8 percent above the asphalt content that would be selected on the basis of stability requirements.

As shown previously, fatigue tests at two different asphalt contents have been performed on the medium graded granite aggregate. Tests at an asphalt content of 5.2 percent (representative of an asphalt content based on stability requirements) result in an average fatigue life of 19,925 repetitions at a stress level of 75 psi; while the results in the mix with 6.0 percent asphalt show an average fatigue life of 73,310 at the same stress level. These two sets of results emphasize that the optimum asphalt content based on stability requirements for this rough textured aggregate is lower than that required for best fatigue results.

Increased use of thick sections of asphalt concrete in pavements will allow for the selection of the asphalt content to be based on two criteria. The upper portion of the asphalt section may be based on stability requirements whereas the remaining portion of the section may be designed for asphalt contents which result in optimum fatigue behavior (44). Thus it will become important to perform fatigue tests which identify the peak asphalt content necessary for optimum fatigue response for a certain mix. It will then be necessary to describe a mixture strain vs. fatigue life relationship for a mix of the chosen asphalt content so that damage due to fatigue may be precluded.

The above test series used to study the effect of asphalt content on fatigue life also illustrates the steps required to select an asphalt content to optimize fatigue response. These test results together with relationships developed by Pell (46) may be used to develop the necessary mixture strain vs. fatigue life relationship which is a necessary part of this design procedure.

Pell has suggested that the influence of a variation in asphalt content may be taken into account by using the following expressions:

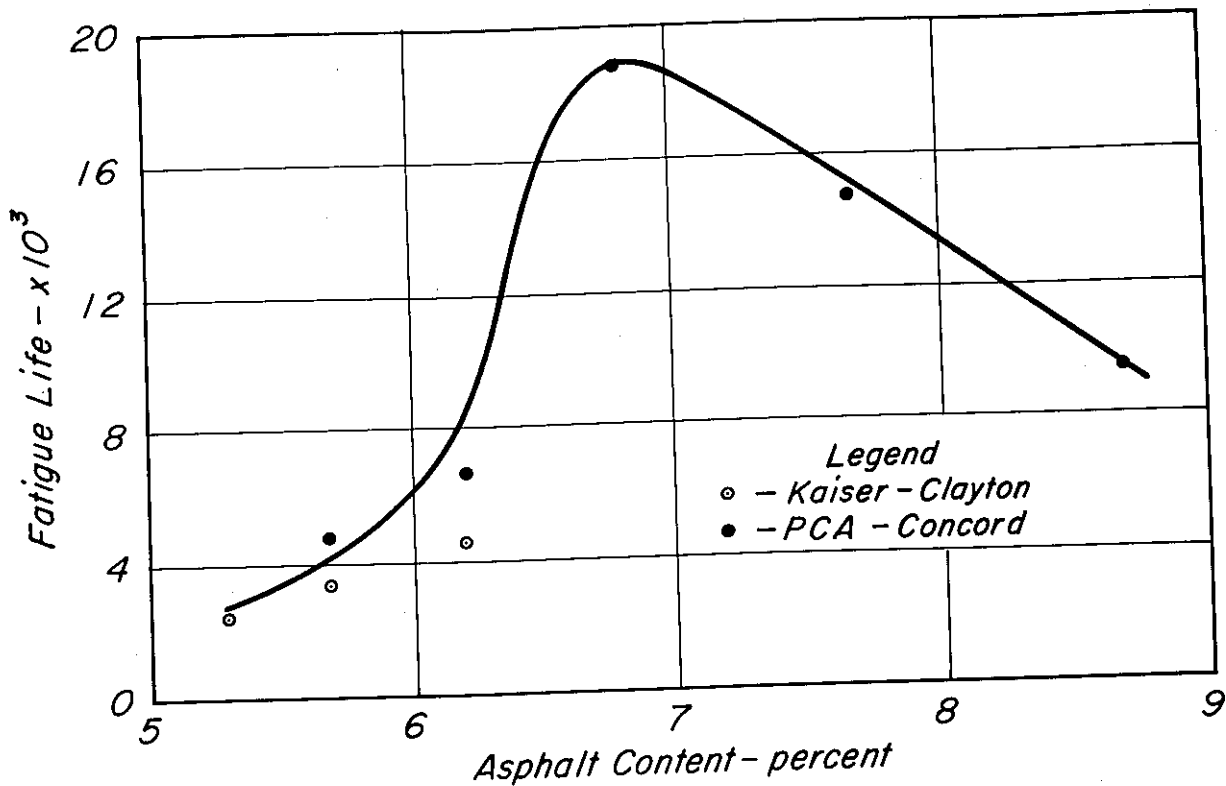


Fig. 59 - Effect of asphalt content on fatigue life - California medium grading, basalt aggregate, 60-70 penetration asphalt.

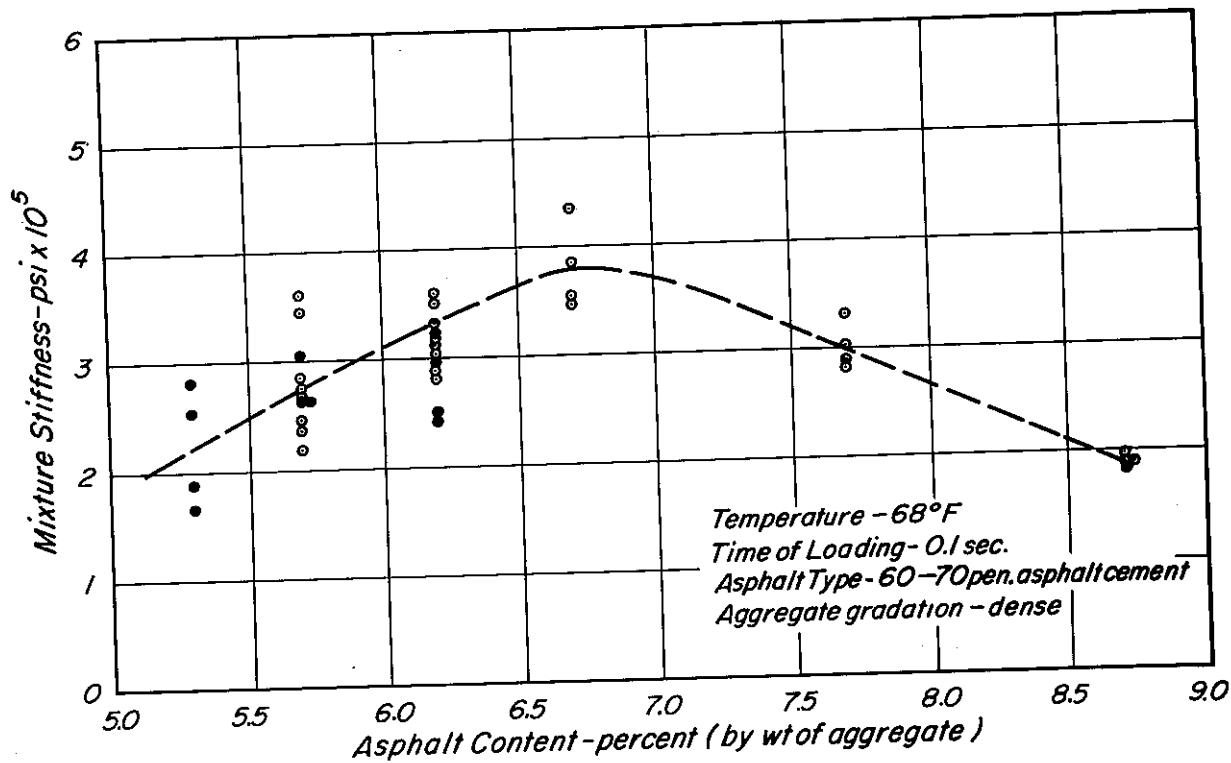


Fig. 60 - Relationship between initial stiffness modulus and asphalt content - California medium grading, basalt aggregate, 60-70 penetration asphalt.

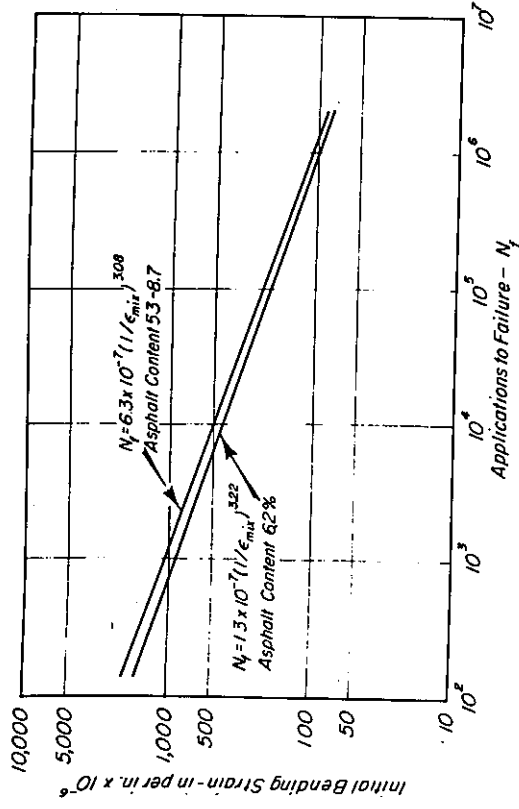


Fig. 63 - Comparison of calculated and measured fatigue behavior - California medium grading, basalt aggregate 60-70 penetration asphalt, 5.3-8.7 percent asphalt.

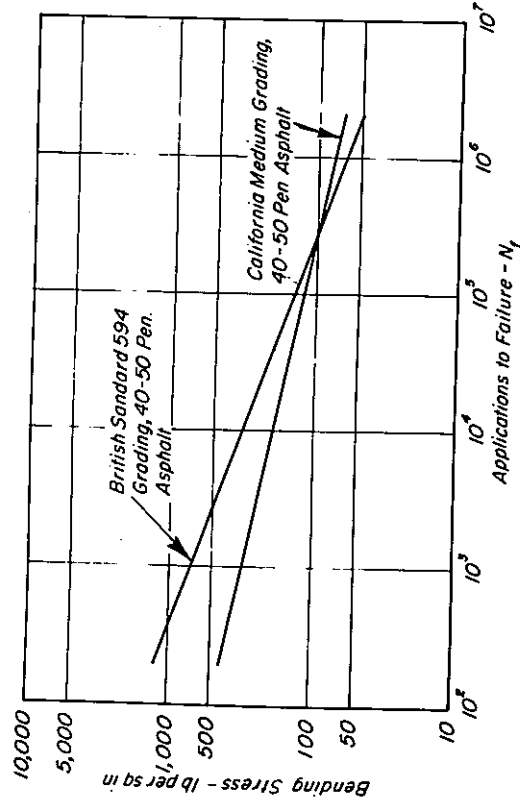


Fig. 64 - Comparison of fatigue results from British standard 594 graded mix and California medium graded mix - mixture bending stress vs. N_f.

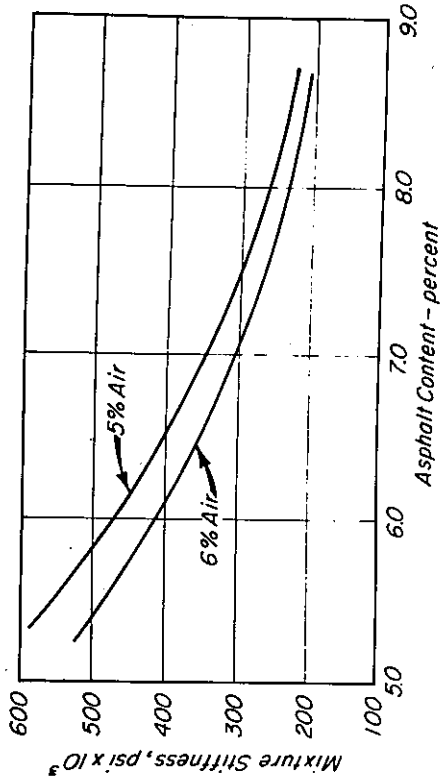


Fig. 61 - Estimated mixture stiffness from properties of recovered asphalt.

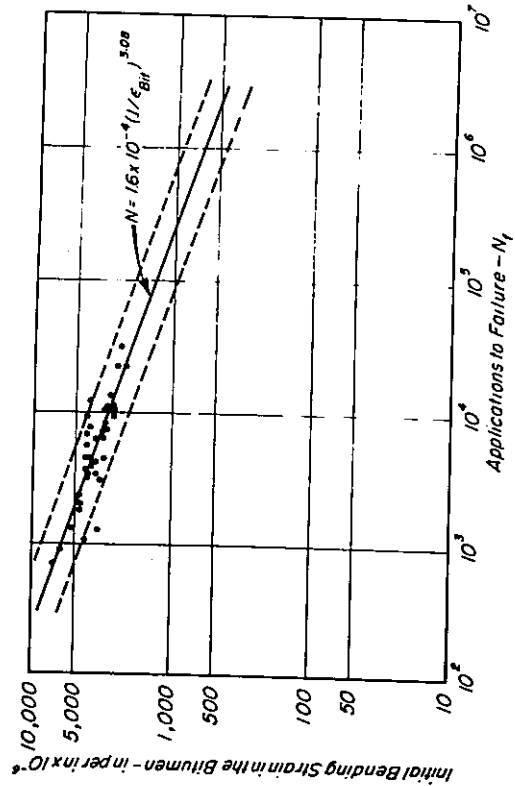


Fig. 62 - Initial bitumen bending strain vs. fatigue life - California medium grading, basalt aggregate, 60-70 penetration asphalt, 5.3-8.7 percent asphalt.

$$N_f = K_3 (1/\epsilon_{bit})^{n_1} \dots \dots \dots (15)$$

where:

K_3 = constant

ϵ_{bit} = tensile strain in the bitumen, in. per in.

The strain in the bitumen may be obtained by using the following equation:

$$\epsilon_{bit} = \frac{\epsilon_{mix}}{\alpha B_v} \dots \dots \dots (16)$$

where:

α = factor depending on amount of filler or voids present in the mix, or both

B_b = $1 - C_v$; volume concentration of bitumen

C_v = volume concentration of aggregate

Thus assuming $\alpha=1$ and using appropriate values of B_v for the various asphalt contents, the bitumen strain may be calculated from the measured mixture strain. Computed values of bitumen strain have been plotted versus fatigue life and the results are shown on Fig. 62 together with the mean regression line (determined with the fatigue life as the dependent variable). The resulting regression equation

$$N_f = 1.6 \times 10^{-4} (1/\epsilon_{bit})^{3.08} \dots \dots \dots (17)$$

is of the same form as equation 15 and may be converted into a mixture strain vs. fatigue life equation

$$N_f = K_1 (1/\epsilon_{mix})^{n_1} \dots \dots \dots (18)$$

by the following technique for any selected asphalt content.

Substituting equation 16 into equation 15 results in the following relationship:

$$N_f = K_3 \left(\frac{\alpha B_v}{\epsilon_{mix}} \right)^{n_1} \dots \dots \dots (19)$$

Rearranging equation 19 gives

$$N_f = K_3 (\alpha B_v)^{n_1} \left(\frac{1}{\epsilon_{mix}} \right)^{n_1} \dots \dots \dots (20)$$

and thus

$$N_f = K_1 \left(\frac{1}{\epsilon_{mix}} \right)^{n_1} \dots \dots \dots (18)$$

with

$$K_1 = K_3 (\alpha B_v)^{n_1} \dots \dots \dots (21)$$

As an example, an asphalt content of 6.2 percent has been selected for the mix containing the basalt aggregate; this asphalt content results in a value of B_v equal to 0.147. Using the above techniques with α again equal to one, the following equation results

$$N_f = 6.32 \times 10^{-7} (1/\epsilon_{\text{mix}})^{3.08}$$

Development of the above relationship has been dependent upon the assumption that bitumen strain may be calculated from $N_f = 7.91 \times 10^{-7} (1/\epsilon_{\text{mix}})^{2.91}$ with α equal to one, together with the assumption that fatigue behavior may be represented as a straight line on a log-log plot both in terms of mixture strain and bitumen strain vs. fatigue life. It seems reasonable to assume that both the fatigue life vs. bitumen and fatigue life vs. mixture strain relationships are linear on a log-log plot; therefore, to check the validity of the assumptions necessary to calculate bitumen strain from mixture strain, an additional series made with the same aggregate, aggregate grading, and asphalt type with a 6.2 percent asphalt content was tested. As seen in Fig. 63 the resulting relationship from tests performed on samples with 6.2 percent asphalt.

$$N_f = 1.34 \times 10^{-7} (1/\epsilon_{\text{mix}})^{3.22}$$

agrees well with the above equation which in turn was based on tests performed with asphalt contents ranging from 5.3 to 8.7 percent.

Thus the above procedure appears to allow the designer to perform tests over a range of asphalt content so that an optimum asphalt content may be selected to minimize fatigue distress. As shown, the longest fatigue life occurs at an asphalt content where maximum stiffness occurs. Furthermore, these same tests may in turn be used to predict the mixture strain vs. fatigue life relationship for any selected asphalt content. It should also be noted that the maximum stiffness while producing optimum fatigue behavior also reduces somewhat the strain in the pavement due to wheel load (44).

Comparison of British and American Mixes

A mix conforming to the British specifications was prepared and tested. The mixture gradation and asphalt content conformed insofar as possible to that used by Pell (46) for a test series for which extensive data were available. In this investigation a crushed granite aggregate and a 33 pen. asphalt were used for the mixes whereas Pell's data were obtained for a mixture containing a crushed gravel and limestone filler with a 43 pen. asphalt.

A comparison of the data are shown in Fig. 64. Individual data points appear to be scattered among each other; however, regression lines (with fatigue life as the dependent variable) result in two distinct lines with slopes of 6.05 and 3.38 for the crushed gravel (Pell) and crushed granite (University of California) mixes respectively.

In general, results of tests performed by Pell have shown slopes of the order of 5 or 6, while tests conducted for this study have resulted in slopes of approximately 3.0. Several possible reasons for this discrepancy exist and will be discussed at this time.

Pell's tests were performed utilizing rotating cantilever loading system while tests at the University of California made use of a four-point bending machine. Thus Pell's specimens were subjected to reversal of extreme fiber stress and strain while specimens tested with the flexural apparatus did not undergo this reversal.

Pell determined the slopes of the fatigue diagrams from the average of two linear regressions, one regression considering fatigue life as the dependent variable while the second regression considering fatigue life as the independent variable. Regression lines for this study have been determined only by assuming fatigue life to be the dependent variable. Linear regression lines with fatigue life equal to the independent variable resulted in flatter slopes than lines with fatigue life equal to the dependent variable for the results of all mixes included in this report. Accordingly Pell's averaging technique would result in a slightly flatter slope.

Pell's strain vs. fatigue life results were obtained by using the nomograph stiffness (35) which, as he has noted, may be in error by factor of two. Thus the slope of the stress vs. fatigue life and strain vs. fatigue life plot will be identical for the results of a particular mix at a single temperature. Table 15 shows in general that regression lines obtained from stress vs. fatigue life data result in flatter slopes; hence if the nomograph stiffnesses were used for these mixes to obtain the strain vs. fatigue life relationships, the slopes for these lines would also be flatter.

The nomograph stiffness makes no provision for stiffness to be stress dependent; however, measured stiffness used in test series reported incorporates the dependence of mixture stiffness on stress. Pell (46) has suggested that if stiffness is considered to be a function of the applied stress magnitude, the resulting strain vs. fatigue life line will be slightly steeper for controlled-stress tests than if the assumption was made that stiffness has no dependency upon applied stress magnitude. Furthermore, Deacon (45) has shown that the stress vs. fatigue life plot and the strain vs. fatigue life plot cannot be simultaneously linear if the stiffness is dependent upon the applied stress magnitude. However, it has been assumed that both stress vs. fatigue life and strain vs. fatigue life plots are linear on the log-log representation.

The role of stiffness and slope is not clear. Pell suggests that a mix tested at different temperatures will result in a single line on the strain vs. fatigue life plot; however, he suggests that a steeper slope may result for mixes made with soft asphalts with low stiffness values and thus longer crack propagation times. Tests performed at different temperatures result in specimens of varying stiffnesses being tested. As suggested previously, tests at higher temperatures because of lower mixture stiffness may result in fatigue lines with steeper slopes. Since the majority of Pell's tests were performed at 10°C (50°F) and since the tests performed in this investigation were at a higher temperature it does not seem unreasonable that a steeper slope of the fatigue diagram would be obtained for the granite aggregate mix.

It is interesting to note that the results of Bazin and Saunier, which were apparently regressed with fatigue life as the dependent variable, also exhibit slopes near 3.0 for dense graded mixes made with the softer asphalts.

Using a statistical test (Appendix D), the null hypothesis that the slope of the regression lines for the studies reported herein are equal to 5 must be rejected at the significance level of 95. Thus the slopes of the lines resulting from tests performed in this study are not of the order of 5.0 to 6.0 as has been suggested by Pell. These differences moreover do not appear unreasonable in the light of the discussion presented herein.

Figs. 65 and 66 show comparisons of the fatigue relationships for the California medium graded granite mix made with a 40-50 penetration asphalt and the granite mix graded according to the British requirements and tested in this laboratory. The British mix has a mean stiffness of 570,000 psi and an average air void content of 5.4 percent while the California mix has a stiffness of 656,000 psi and an air void content of 4.7 percent. However, the British mix, even with its lower stiffness and higher air void content, provides a longer fatigue life at strain levels expected in pavements. Part of the observed difference may be due to the lower asphalt content for the California mix. As suggested before, however, the structure of the air voids may also be an important factor leading to part of the difference in fatigue life observed between these two mixes.

It would appear that the British designed mix utilizing a harder asphalt and a larger asphalt content tends to give better fatigue response than a comparable American mix. While the effect of grading is not clearly defined; the British grading appears to produce an air void structure which does not influence the fatigue behavior of these mixes to the same degree as for the American dense graded mixes.

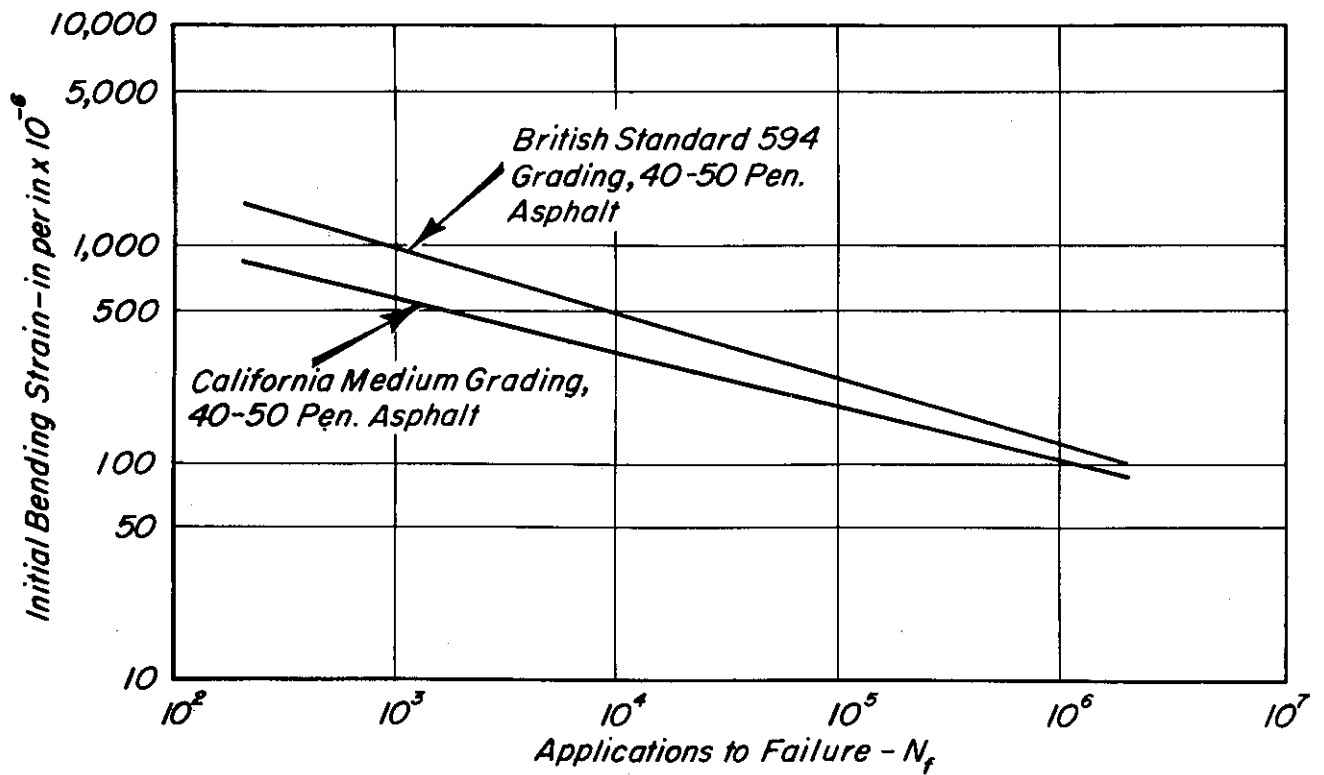


Fig. 65 – Comparison of fatigue results from British Standard 594 graded mix and California medium graded mix – initial mixture bending vs. fatigue life.

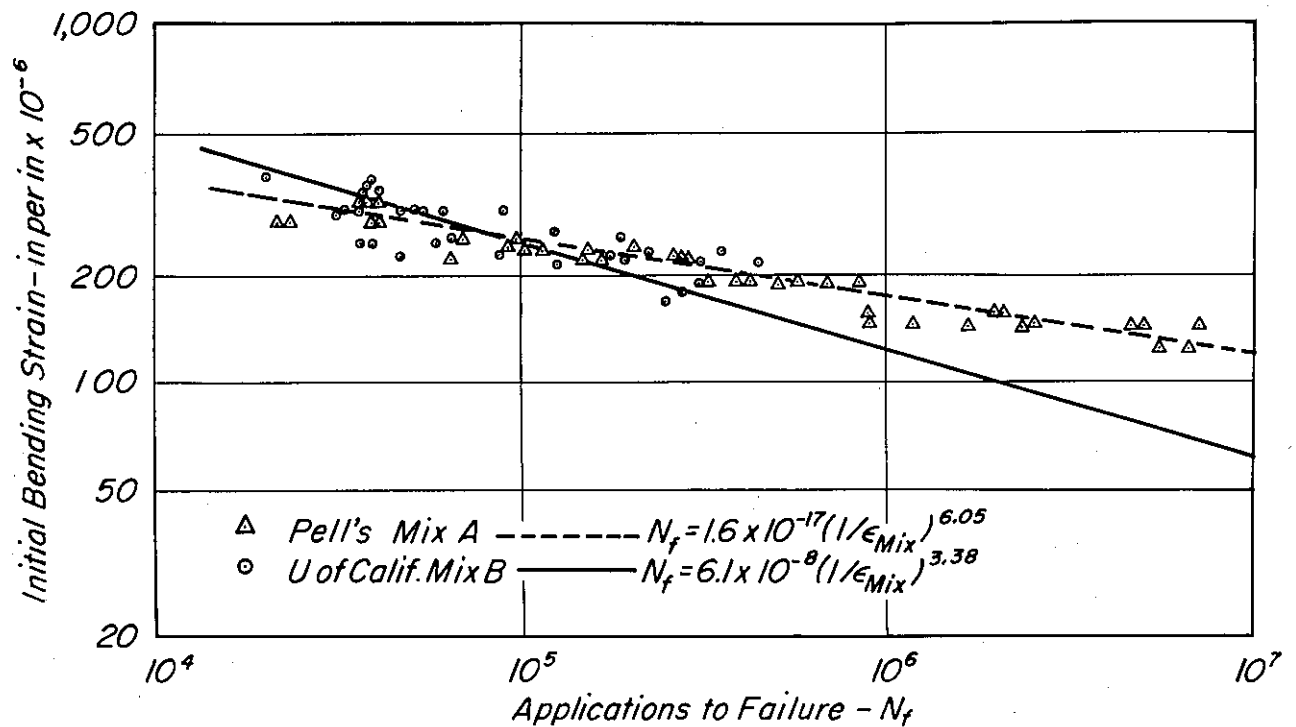


Fig. 66 – Comparison of individual test results of Pell's mix A and the British Standard 594 graded mix tested in the University of California laboratory.

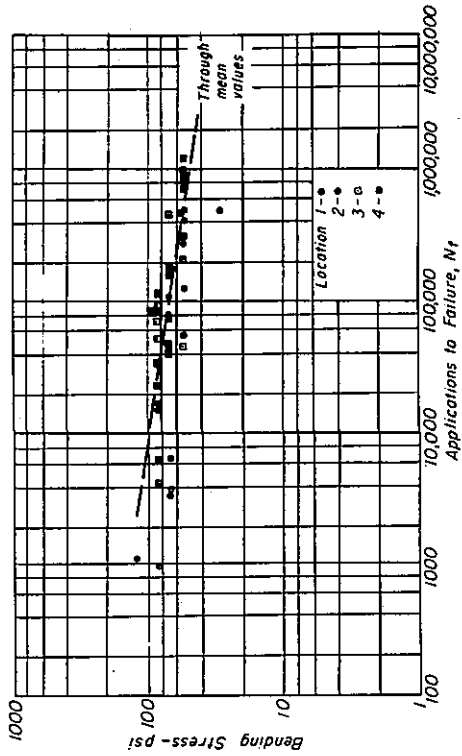


Fig. 67 - Controlled-stress tests, Morro Bay pavement; December 1965 sampling; temperature - 68°F; field specimens.

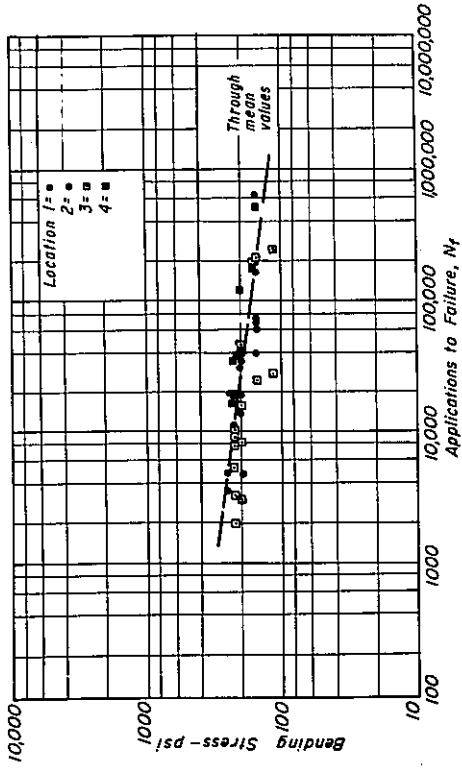


Fig. 68 - Controlled-stress tests, Morro Bay pavement; December 1965 sampling; temperature - 40°F; field specimens.

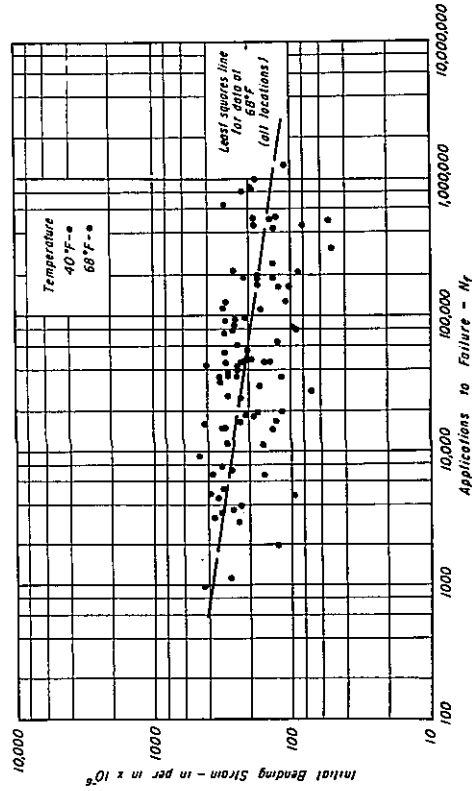


Fig. 69 - Strain vs. applications for Morro Bay pavement; pavement specimens; field sampling, December 1965.

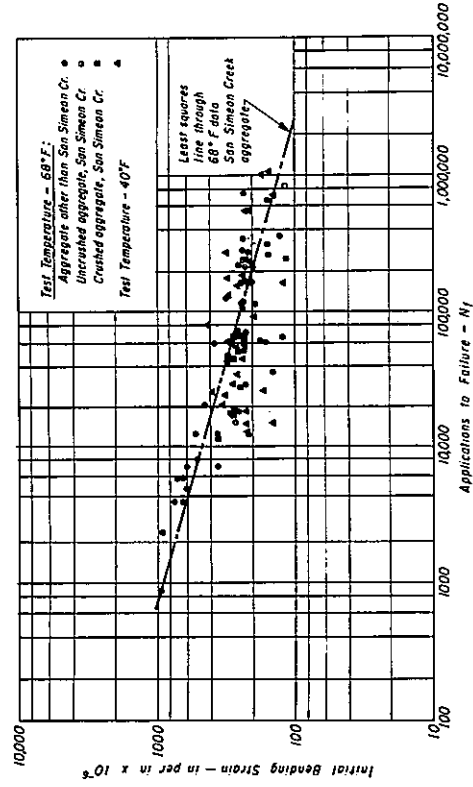


Fig. 70 - Initial strain vs. cycles to failure, controlled-stress tests on laboratory prepared specimens.

Tests on Materials from In-Service Projects

Three projects, as noted earlier, will be discussed in the section concerned with the use of the subsystem in practice. Fatigue characteristics of the asphalt concrete for the city-county highway (Ygnacio Valley Road) has already been presented in the previous section — i. e. , tests on the mixture containing the basalt aggregate. Accordingly only the data from the Morro Bay and Folsom projects will be included therein.

Morro Bay Project (V-SLO-56C,D). Appendix E contains a brief description of the pavement cross-section as well as providing an indication of the sampling locations for testing.

Both controlled-stress and controlled-strain fatigue tests were performed on specimens obtained from pavement samples and on laboratory prepared specimens composed of essentially the same materials as used in the original construction.

Controlled-Stress Tests. Details of the controlled-stress tests have been discussed in Report TE 66-6 (31); hence only a summary of the test results will be presented in this section.

Fig. 67 illustrates the stress vs. applications to failure relationship for tests performed at 68⁰F on specimens obtained from the December 1965 sampling. While it had been indicated in Report TE 66-6 that there may be some differences between locations 1 and 3 and 2 and 4, only the mean line through all of the data points has been drawn in this figure.

Similarly, in Fig. 68 the results for tests at 40⁰F are shown. Again, the curve shown in the figure is that through the mean values at each stress level.

During these fatigue tests, flexural stiffnesses were measured; mean values from these tests are summarized in Table 18. From the measured stiffness values, an initial strain was computed for each of the specimens. The resulting relationship between computed initial strain and applications to failure is shown in Fig. 69.

In Fig. 69, only the least squares line through the 68⁰F data has been shown, since as has been indicated earlier, there was considerably more scatter in the data at 40⁰F as compared to that at 68⁰F.

Controlled-stress fatigue tests were also performed on laboratory prepared specimens of the materials used in the pavement construction. Tests were conducted on specimens prepared from aggregates obtained from three sources, namely: Arroyo De La Cruz, San Simeon Creek, and Toro Creek. In Fig. 70 are presented the results of computed strain vs. applications to failure for all the laboratory prepared specimens.

From additional study of the job records it would appear that only the specimens containing the San Simeon Creek aggregate should be considered. Accordingly the least squares

line of best fit shown in Fig. 70 has been developed only from the data for the San Simeon Creek aggregate. Moreover, as with the data for the field specimens, only the 68°F data have been utilized. Comparison of this line with that for field specimens shown in Fig. 69 would indicate that it has a steeper slope and is displaced to the right (larger number of applications to failure at a particular strain level).

Controlled-Strain Tests. In addition to the controlled-stress fatigue tests, controlled-strain tests were also performed on laboratory prepared specimens of the mixtures.

These tests were performed in the same equipment as used in the controlled-stress tests. However, to maintain a particular strain (deflection) level, it was necessary to continually monitor the test and to adjust the load.

Since the specimens did not completely fracture as in the controlled-stress tests, it was necessary to define a service life in terms of changes in mix response to load. In this instance the reduction in stiffness with load repetitions was utilized. A typical relationship between stiffness and number of stress applications is shown in Fig. 71.

From such a relationship, service lives corresponding to a 25 percent and a 50 percent reduction in stiffness were selected as being representative of conditions with a small amount and extensive crack propagation. Both criteria are shown in Fig. 72 for tests at 68°F.

TABLE 18 — SUMMARY OF TEST RESULTS FOR ASPHALT CONCRETE
SAMPLED NEAR MORRO BAY, CALIFORNIA IN DECEMBER, 1965

Location	Number of Samples	Mean Stiffness (psi)	Standard Deviation	Coeff. of Variation percent
<u>Tests at 68°F</u>				
1	9	345,000	138,000	39.8
2	11	333,000	108,000	32.4
3	10	341,000	105,000	30.7
4	14	335,000	115,000	34.3
Grand Mean	44	338,000	112,000	33.1
<u>Tests at 40°F</u>				
1	4	1,130,000	715,000	63.2
2	14	943,000	396,000	42.0
3	16	965,000	400,000	41.4
4	9	1,235,000	506,000	40.9
Grand Mean	43	1,030,000	453,000	43.9

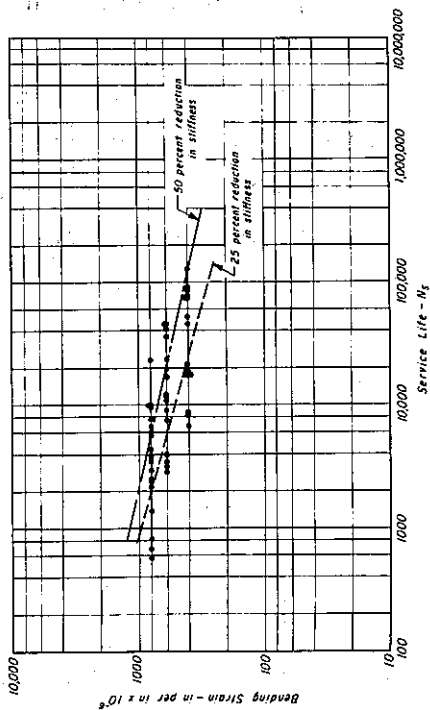


Fig. 71 - Stiffness vs. stress applications, controlled-strain test at 400×10^{-6} in. per in.

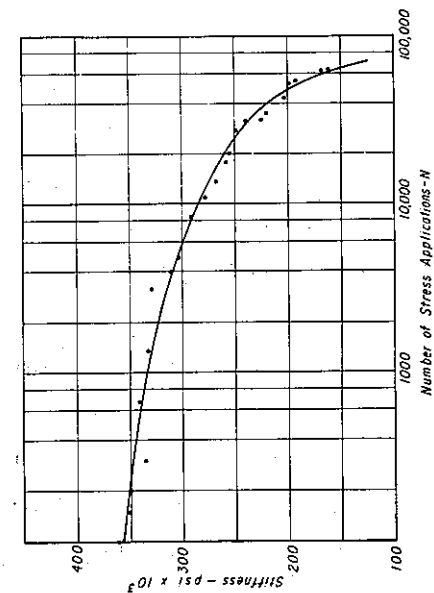


Fig. 72 - Controlled-strain fatigue tests on laboratory prepared specimens - 68°F .

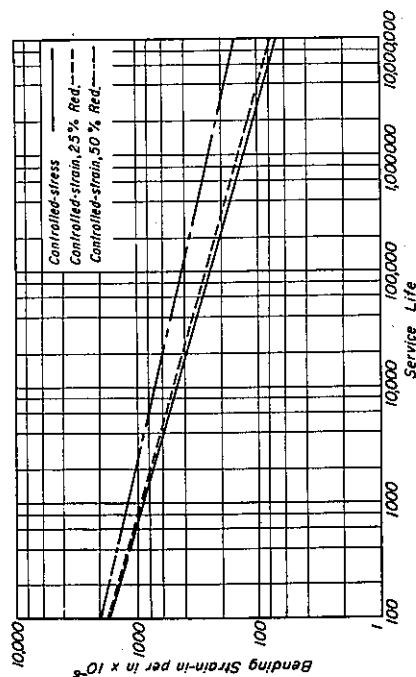


Fig. 73 - Comparison of controlled-stress and controlled-strain tests on laboratory prepared specimens of the Morro Bay pavement; 68°F .

The least squares lines for both the controlled-stress tests (Fig. 70) and controlled-strain tests (Fig. 72) are compared in Fig. 73. It will be noted that the relationship based on a 25 percent reduction in stiffness compares very favorably with that obtained from the controlled-stress tests and would thus suggest that this particular criterion includes little crack propagation time.

In the analysis of pavement service life to be presented in a subsequent section, the controlled-strain fatigue curve corresponding to a 50 percent reduction in stiffness was selected as being representative of the pavement section. This selection was based on the discussion presented earlier regarding the applicability of controlled-stress and controlled-strain tests depending on the thickness of the asphalt concrete surfacing (in this case, 2.5 inches).

The equation for the curve of strain vs. applications corresponding to a 50 percent reduction in stiffness is:

$$N_s = 2.78 \times 10^{-7} \left(\frac{1}{\epsilon}\right)^{3.38} \dots \dots \dots (22)$$

~~Folsom Project (03-SAC, ED-507)~~. A description of this project is included in Appendix E. As noted therein the portion of the project for study included a test section in which an experimental asphalt as well as a conventional paving asphalt were utilized. In the subsequent paragraph Locations 3 and 4 correspond to sections containing the experimental asphalt while Locations 1 and 2 refer to those with the control material.

Asphalts. Properties of the asphalts used in the actual pavement are shown in Table 19. the experimental asphalt was supplied by the Chevron Asphalt Company to conform to the proposed 1965 State of California specification (56) the limits of which are also shown in the table. The control asphalt, conforming to current standard specification requirements of the Division of Highways for an asphalt cement was supplied by the Shell Oil Company of Martinez; results of tests associated with the proposed specification on this material are also shown in Table 19.

Neither asphalt had been obtained in sufficient quantity to permit fabrication of a large number of beam samples for fatigue testing and it was thus necessary to obtain additional asphalt samples for the laboratory specimens. The Chevron Asphalt Company blended an asphalt to conform as close as possible to that used in the field project and the Shell Oil Company supplied an asphalt from their current production believed to be similar to that used in the field. Test results on these materials are also presented in Table 19. From a comparison of the results of the tests, it can be concluded that the materials are reasonably similar.

TABLE 19 — PHYSICAL PROPERTIES OF ASPHALT CEMENTS —
FOLSOM PROJECT

Test	Spec. Requirements	Shell		Chevron Experimental	
		As Used In-service	Lab. Specs.	As Used In-service	Lab. Specs.
Flash Point, P. M. C. T. °F	475 min.	455	455	500	485
Penetration of Original sample at 77°F - dmm	-	93	84	75	81
Stain Number of Original Sample. Maximum after 120 hrs at 140°F — 50 psi	10	6	4	6	4
Rolling Thin Film Test 325°F, 75 min.					
Viscosity, Residue 140°F, poises	4000-6000	3829	4459	4060	4174
279°F, centistokes	425-800	466	477	467	486
Ductility, Residue, 77° - cm	75 min.	100+	100+	100+	100+
Durability Test Viscosity of Residue after Durability Test, 77°F Shear Rate 0.05 sec ⁻¹ megapoises	25 max.	45	52	26	32.3
Shear Rate 0.01 sec ⁻¹ megapoises	60 max.	160	125	45	56
Micro-ductility of Residue, 1/2 cm per min. - mm	10 min.	4	4	21	8
Solubility, CCl ₄ original Sample — percent	99 min.	99.9	99.9	99.9	99.9

TABLE 20 — PROPERTIES OF RECOVERED ASPHALTS

	Penn @ 77°F dmm	Ring and Ball Soft Pt. - °F
Chevron - Immediately after field mixing ^a	54	126
Shell - Immediately after field mixing ^a	54	124
Field Base - Location 1 ^b	31	135
Field Base - Location 2 ^b	28	138
Field Surface - Location 1 ^b	38	132
Location 2 ^b	26	141
Location 3 ^b	28	135
Location 4 ^b	28	132
Location 4 ^b	21	140
Chevron - Laboratory prepared	28	134
Shell - Laboratory prepared	37	132

- a. Samples obtained immediately after plant mixing.
b. Samples obtained 2.25 years after construction.

In addition to properties of the original asphalts, properties of recovered materials were determined by the Materials and Research Department. These test results are shown in Table 20 for both the field and laboratory specimens.

Aggregates. The aggregate used in both the surface and base were obtained from the American River near Fair Oaks, California. Test results obtained by the Materials and Research Department for specific index properties of the material are shown in Table 21.

Average grading curves determined from project reports are shown in Fig. 74 for the surface course and in Fig. 75 for the base course. Corresponding specification limits are also shown in the figures. These average grading curves served as the basis for the preparation of the laboratory beam specimens for fatigue testing.

Mixtures. Stiffness and air void characteristics of the field specimens are shown in Table 22 for the surface course mixtures from the four locations. In general it will be noted that the stiffness values for the specimens from the experimental sections (locations 3 and 4) are higher than those from the control sections (locations 1 and 2). Results for the base course mixtures are shown in Table 24. The base course was prepared with the Shell asphalt

Project reports indicated that the surface course exhibited an average asphalt content of 4.9 percent (by weight of aggregate) and the base course an average value of 4.2 percent. The average asphalt content of 4.9 percent was used for the preparation of the laboratory specimens. Results of stiffness and air void determinations for those specimens are shown in Table 23 and compared with the field specimens in Table 24.

Stiffnesses for the various specimens were estimated from the properties of the recovered asphalts (Table 20). These estimated stiffnesses have been compared with the measured values in Table 25. In general it will be noted that measured and computed stiffnesses are in reasonable agreement.

Fatigue Test Results. Controlled stress fatigue tests were performed on beam specimens sawed from the field samples and both controlled-stress and controlled-strain tests were performed on laboratory prepared beam specimens using the equipment described in earlier reports (e.g. 31). Tests on the field specimens were conducted only at a temperature of 68°F whereas tests on the laboratory prepared specimens were performed at 68°F, and 83°F.

1. Field Surface Course. Results of the fatigue tests on specimens from the four sampling locations are shown in Figs. 76 through 79. A summary of the results at various stress levels is included in Table 26. Least squares regression relationships were determined from test results for samples from each location. In addition, the

TABLE 21 — AGGREGATE CHARACTERISTICS,
FOLSOM (FAIR OAKS)

Specific Gravity	
Fine	2.85
Coarse	2.88
Sand Equivalent,	
Surface course material	89
Cleanness Value,	
Surface course material	94
L. A. Abrasion (500 Revolutions)	
Surface course material	18

TABLE 22 — MIXTURE PROPERTIES — FIELD SPECIMENS
FOLSOM PROJECT, SURFACE COURSE

Location	No. of Specimens	Air Void Content - percent			Stiffness - $\text{psi} \times 10^3$, at 68°F, 0.1 sec. loading			
		Mean	Std. Dev.	c_v	Stress	Mean	Std. Dev.	c_v
1 (Shell)	8	8.1	0.6	7.1	75	338	89	26.2
	8	7.9	0.3	4.3	100	336	49	14.7
	7	8.0	0.4	5.3	125	335	52	15.4
	7	8.0	0.5	5.8	150	351	104	29.7
	30	8.0	0.4	5.5	-	340	73	21.5
2 (Shell)	6	8.0	1.2	15.2	75	500	44	8.8
	7	8.7	0.4	4.5	100	394	93	23.5
	6	8.4	0.3	3.7	125	313	88	28.2
	7	8.4	0.4	4.6	150	353	96	27.2
	26	8.4	0.7	7.9	-	389	105	26.7
3 (Chevron)	6	7.9	0.8	10.3	75	489	130	26.4
	7	7.3	0.8	10.9	100	609	132	21.6
	7	7.7	0.8	10.9	125	415	81	19.4
	6	7.4	0.8	11.0	150	484	145	30.0
	26	7.6	0.8	10.7	-	500	137	27.3
4 (Chevron)	8	6.3	0.6	9.3	75	611	283	46.2
	7	6.6	0.4	6.4	100	464	117	25.1
	6	6.5	0.3	4.3	125	479	44	9.2
	5	6.4	0.6	8.9	150	434	30	6.8
	26	6.4	0.5	7.4	-	507	177	34.9

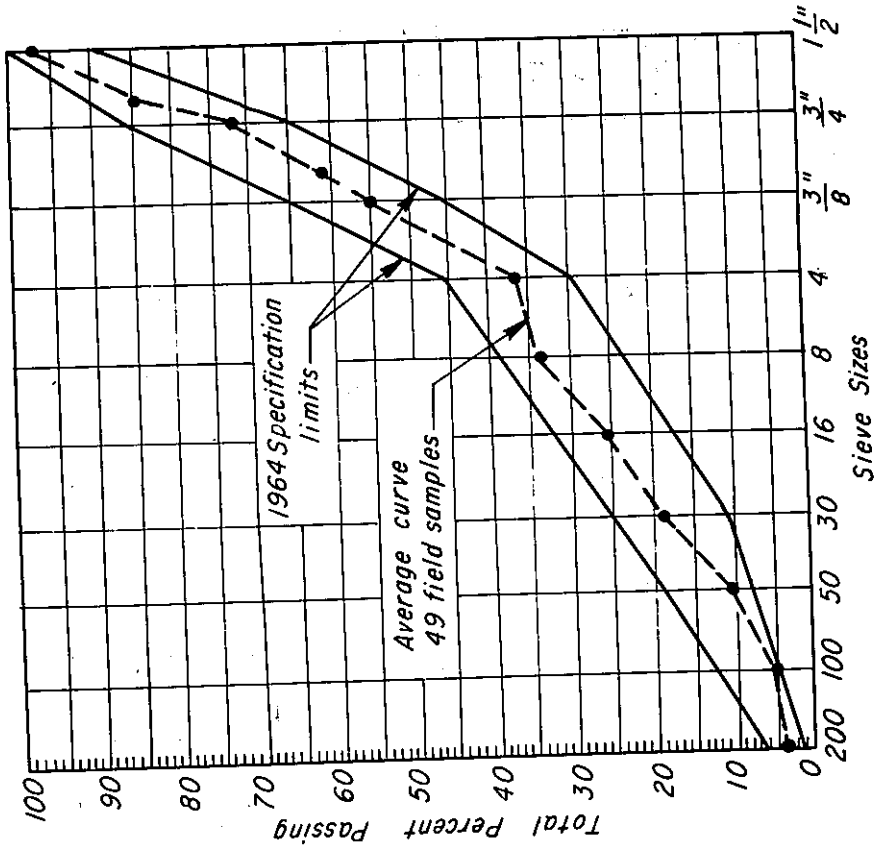


Fig. 74 - Aggregate grading curves asphalt concrete surface course - Folsom project.

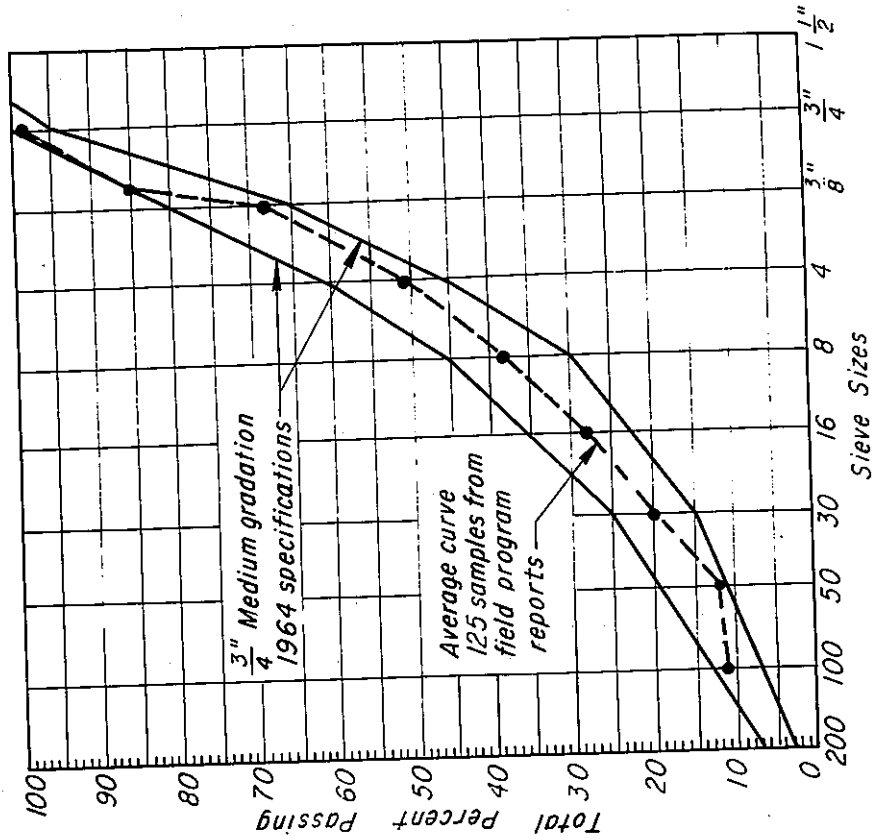


Fig. 75 - Aggregate grading curves asphalt concrete base course - Folsom project.

TABLE 23 — MIXTURE PROPERTIES — LABORATORY PREPARED SPECIMENS, FOLSOM PROJECT, SURFACE COURSE

Material	Temp. °F	Stress psi	No. of Spec.	Air Void Content- percent			Stiffness - psi × 10 ³ 0.1 sec. loading			
				Mean	Std. Dev.	c _v	Mean	Std. Dev.	c _v	
Shell	40	300	10	6.3	0.56	.09	998	188	.19	
	40	250	10	6.9	0.68	.10	925	138	.15	
	40	150	10	6.6	0.89	.14	1,120	200	.14	
	40	120	7	6.6	1.17	.18	1,856	604	.33	
	40	-	37	6.6	0.82	.12	1,192	447	.38	
	68	100	10	7.2	0.89	.13	113	40	.36	
	68	75	10	6.9	0.84	.12	169	53	.31	
	68	50	10	6.9	1.01	.15	171	34	.20	
	68	40	9	6.3	0.51	.08	208	38	.18	
	68	30	10	7.2	0.72	.10	211	40	.19	
	68	-	49	6.9	0.85	.12	173	53	.31	
	83	100	9	7.6	0.57	.08	38	13	.37	
	83	75	10	7.2	0.75	.10	54	16	.29	
	83	50	10	6.8	0.79	.12	77	13	.17	
	83	30	6	6.5	0.88	.14	91	22	.24	
	83	-	35	7.1	0.82	.12	62	25	.41	
	Chevron	40	300	10	6.9	0.31	.05	1,140	152	.13
		40	250	10	7.7	0.83	.11	1,260	178	.14
		40	150	10	7.3	0.58	.08	1,270	191	.16
		40	-	30	7.3	0.67	.09	1,220	179	.15
68		150	15	7.0	0.75	.11	160	58	.36	
68		100	15	7.4	0.90	.12	223	78	.35	
68		75	16	7.4	0.83	.11	292	89	.31	
68		-	46	7.3	0.83	.11	226	93	.41	
Strain in/in × 10 ⁶										
Shell		68	1000	9	5.9	1.05	.18	115	23	.20
Strain	68	700	9	6.2	0.49	.08	154	23	.15	
Controlled	68	500	9	6.7	0.74	.11	170	36	.21	
	68	-	27	6.3	0.82	.13	146	36	.25	

TABLE 24 — COMPARISON OF FIELD AND LABORATORY
PREPARED SPECIMENS

	No. of Specimens	Air Void Content - percent			Stiffness - $\text{psi} \times 10^3$ * at 68°F, 0.1 sec. loading		
		Mean	Std. Dev.	c_v	Mean	Std. Dev.	c_v
Field-Surface (Locations 1 & 2)	56	8.2	0.6	7.2	362	92	25.3
Shell - Laboratory	30	7.0	0.9	13.0	151	50	33.0
Field-Surface (Locations 3 & 4)	52	7.0	0.9	12.4	503	157	31.1
Chevron - Laboratory	46	7.3	0.8	11.0	226	93	41.0
Field-Base (Locations 1, 2, 3, & 4)	103	8.0	0.8	10.4	425	105	24.8

*Determined after 200 stress applications in fatigue testing device.

TABLE 25 — COMPARISON OF COMPUTED AND
MEASURED MIXTURE STIFFNESS

	No. of Specimens	Stiffness $\times 10^5$ psi	
		Measured	Computed
Field Surface - Location 1	30	3.40 (0.73) ^a	2.60 ^b
Field Surface - Location 2	26	3.89 (1.05)	3.66 ^b
Field Surface - Location 3	26	5.00 (1.37)	4.82 ^c
Field Surface - Location 4	26	5.07 (1.77)	4.18 ^c
Shell - Laboratory, 40°F	30	10.40 (2.05)	11.30 ^c
Shell - Laboratory, 68°F	30	1.51 (0.50)	2.84 ^c
Chevron - Laboratory, 40°F	30	12.20 (1.79)	14.10 ^d
Chevron - Laboratory, 68°F	30	2.58 (0.97)	3.65 ^d

a. Standard deviation shown in parenthesis.

b. Based on $c_v = 0.861$ and Air Void Content = 8.2%

c. Based on $c_v = 0.861$ and Air Void Content = 7.0%

d. Based on $c_v = 0.861$ and Air Void Content = 7.3%

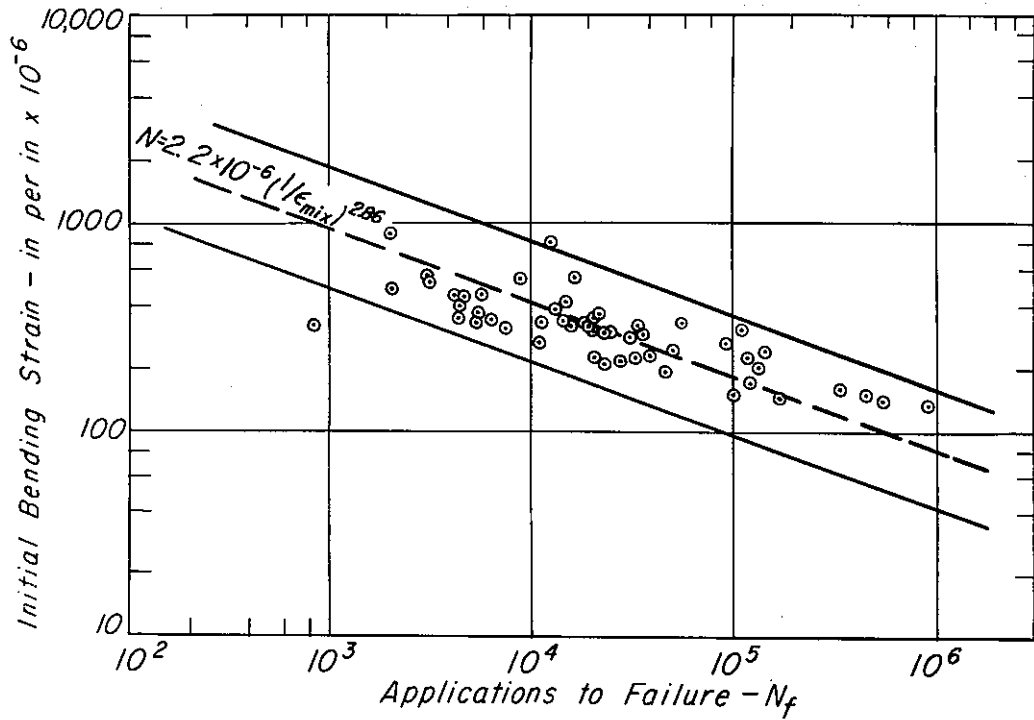


Fig. 76 - Initial mixture bending strain vs. applications to failure, controlled-stress tests on field specimens from locations 1 and 2, Folsom project; temperature of test - 68°F.

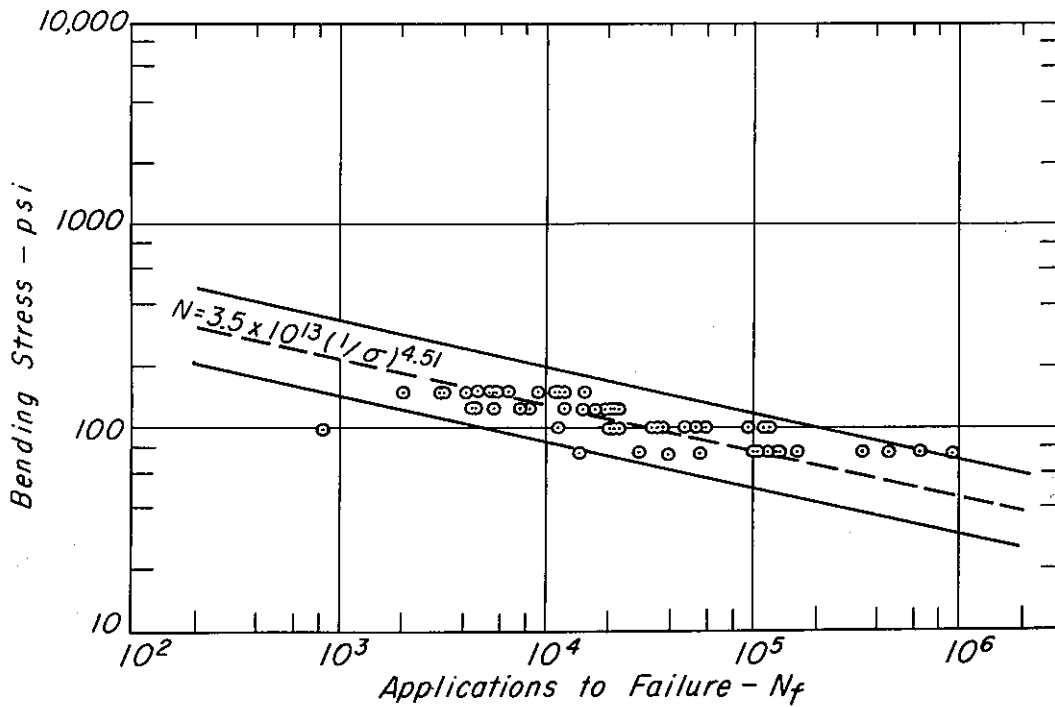


Fig. 77 - Mixture bending stress vs. applications to failure, controlled-stress tests on field specimens from locations 1 and 2, Folsom project; temperature of test - 68°F.

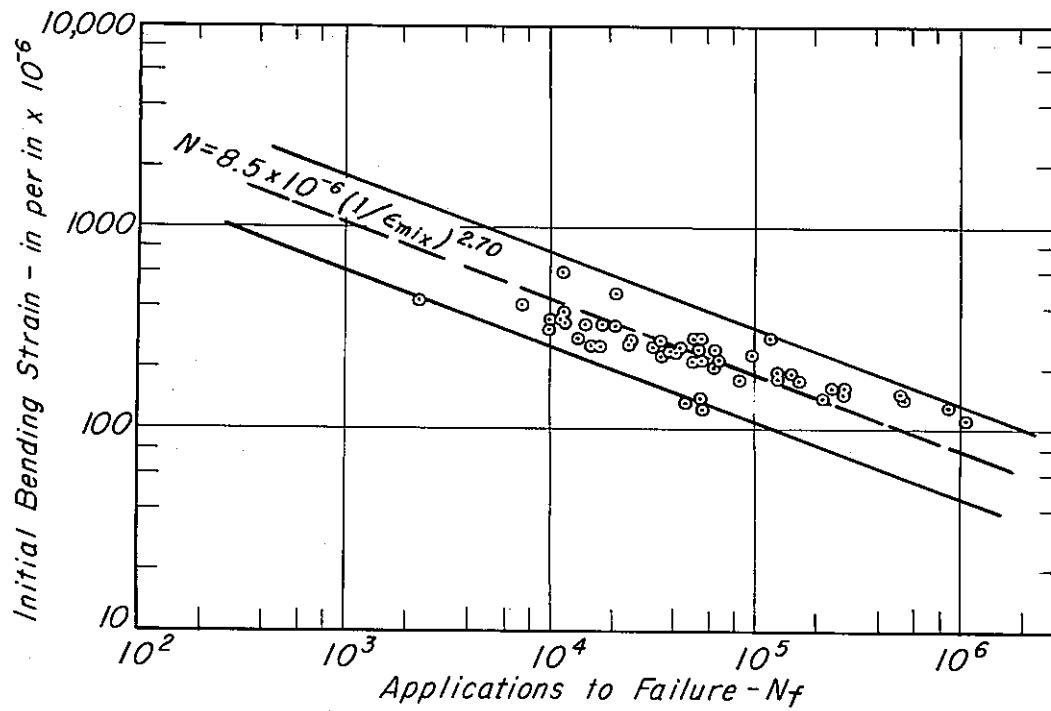


Fig. 78 - Initial mixture bending strain vs. applications to failure, controlled-stress tests on field specimens from locations 3 and 4, Folsom project; temperature of test - 68°F.

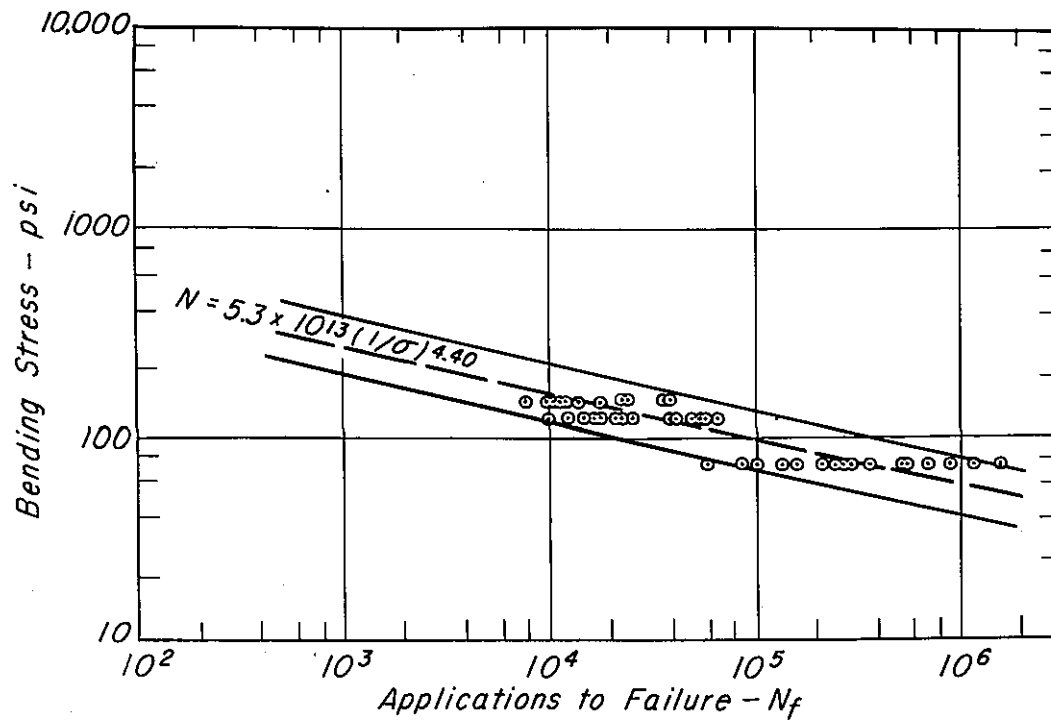


Fig. 79 - Mixture bending stress vs. applications to failure, controlled-stress tests on field specimens from locations 3 and 4, Folsom project; temperature of test - 68°F.

TABLE 26 — FATIGUE DATA* — FOLSOM FIELD SURFACE COURSE

Location	Stress psi	Number of Specimens	Fatigue Life - N_f		
			Mean	Standard Deviation	C_v
1	75	8	123,590	146,203	118.2
	100	8	45,033	46,135	102.4
	125	7	14,462	7,619	52.6
	150	7	5,933	3,186	53.7
	all	30			
2	75	6	375,088	325,611	86.8
	100	7	50,256	24,338	48.4
	125	6	11,893	5,760	48.4
	150	7	8,254	5,482	66.4
	all	26			
3	75	5	427,796	455,786	106.5
	100	7	120,240	75,304	62.6
	125	7	32,347	19,652	60.7
	150	6	21,575	12,556	58.1
	all	26			
4	75	8	517,847	462,993	89.4
	100	7	69,130	39,897	57.7
	125	6	33,078	20,035	60.5
	150	5	14,826	5,429	36.6
	all	26			
1 & 2	75	14	231,375	263,620	113.5
	100	15	47,470	36,405	76.6
	125	13	13,276	6,680	50.3
	150	14	7,093	4,472	63.0
	all	56			
3 & 4	75	14	479,254	444,371	92.7
	100	13	94,685	63,680	67.2
	125	13	32,684	18,507	58.0
	150	11	18,507	10,151	54.8
	all	51			
all locations	75	28	355,314	379,754	106.8
	100	29	70,264	55,875	79.5
	125	26	22,980	17,099	74.4
	150	25	12,115	9,338	77.0
	all	108			

*Test temperature - 68°F

results from locations 1 and 2 and locations 3 and 4 were grouped together since they contained the same asphalt types and the air void contents were approximately the same (Table 22).

Fatigue data together with the results of the regression analyses are presented in Figs. 76 and 77 for locations 1 and 2 and in Figs. 78 and 79 for locations 3 and 4. The scatter bands shown in these figures represent \pm two standard errors of the estimate (encompassing 95 percent of the data).

Comparison of the mean regression lines for mixes from locations 1 and 2 and locations 3 and 4 are shown in Figs. 80 and 81. As seen in Fig. 80 the strain vs. fatigue life relationships are approximately the same. Considering the data from the four locations together, the following regression equation was obtained:

$$N_f = 3.58 \times 10^{-6} \left(\frac{1}{\epsilon_{\text{mix}}} \right)^{2.80}$$

with a correlation coefficient and standard error of the estimate of the same order as the individual sets of data as seen in Table 28.

Properties of the recovered asphalts (presented in Table 20) indicate that both mixes exhibited about the same stiffness immediately after placement. Data presented in Table 24 indicate, however, that the samples obtained for fatigue testing 2-1/4 years later exhibit a difference in stiffness, with mixes containing the experimental asphalt exhibiting higher stiffness than those with control material. This difference in stiffness is reflected in the difference in locations of the stress vs. fatigue life relationships shown in Fig. 81.

2. Field Base Course. The base course contained only the Shell asphalt and mixes from all four locations exhibited about the same air void content (Table 27), accordingly all of the data were grouped together.

Results of fatigue tests on specimens sawed from the field samples are presented in Figs. 82 and 83. As noted in Fig. 75 the maximum size of the aggregate in the base course was 1-1/2 in. It is likely, therefore, that a considerable portion of the cross section of a number of the beam specimens (1-1/2 in. \times 1-1/2 in.) was occupied by the aggregate. This could contribute to the scatter in data noted in Figs. 82 and 83.* Moreover regression analyses performed on the data were not

*Similar problems were noted in tests on the base course from the Gonzales project. (31).

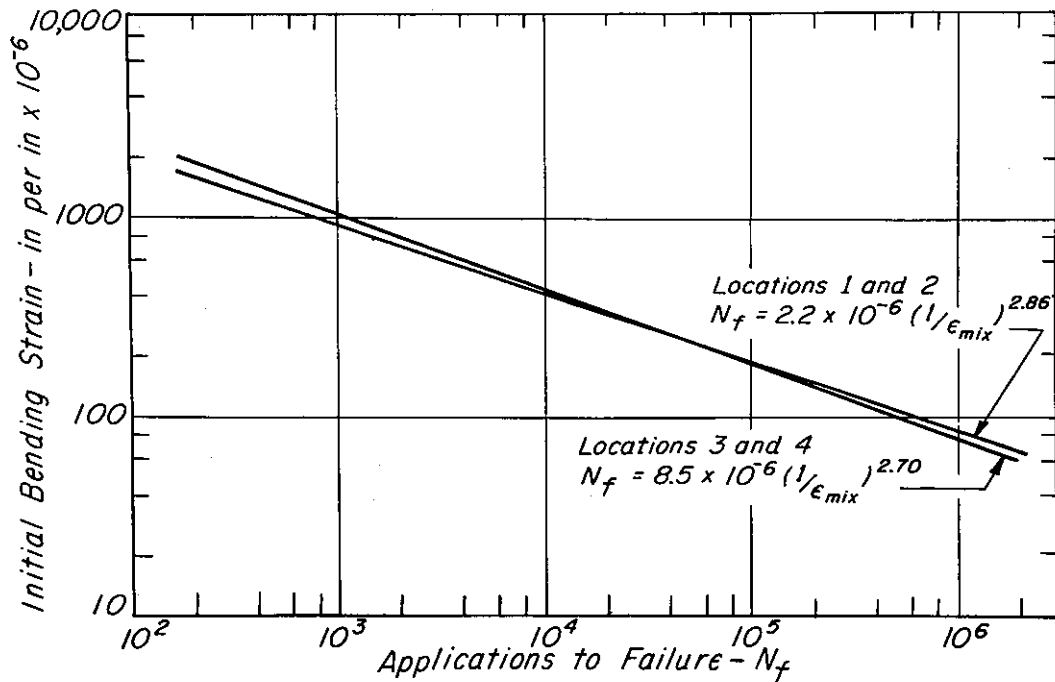


Fig. 80 - Comparison of fatigue test results (ϵ vs. N_f) for field specimens obtained from locations 1 and 2 and locations 3 and 4, Folsom project.

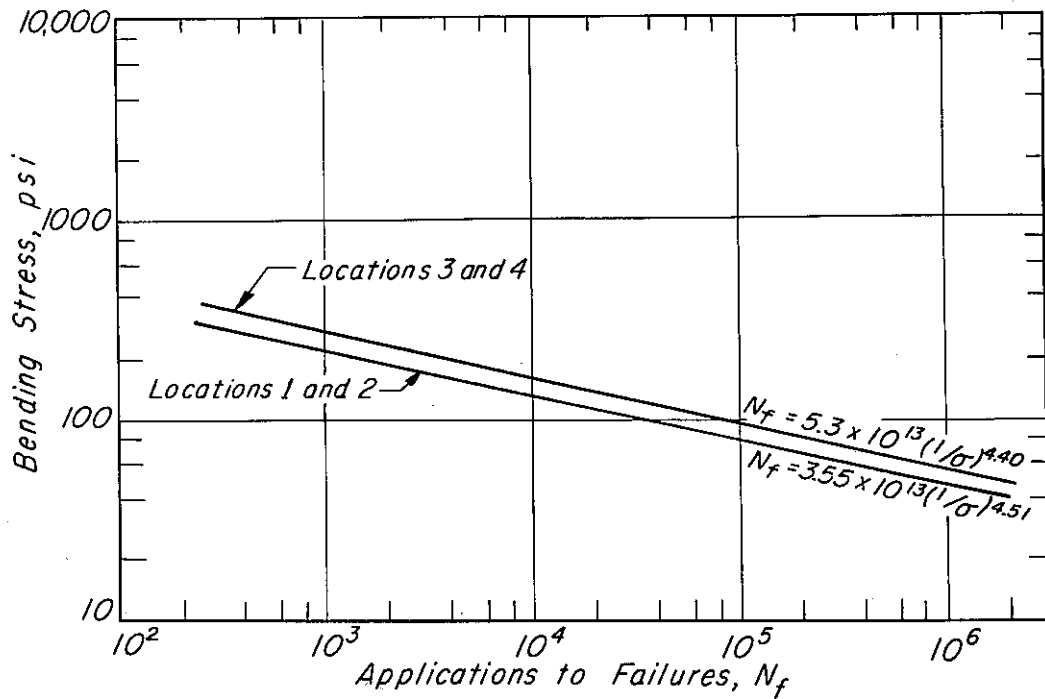


Fig. 81 - Comparison of fatigue test results (σ vs. N_f) for field specimens obtained from locations 1 and 2 and locations 3 and 4, Folsom project.

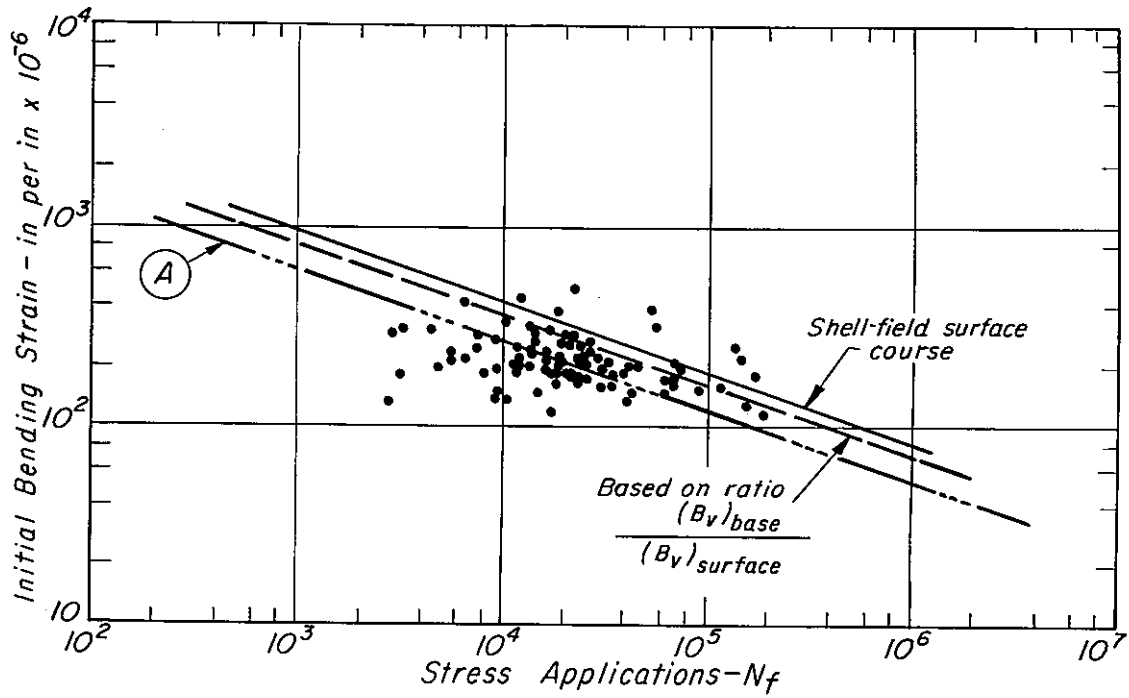


Fig. 82 - Mixture bending stress vs. applications to failure, field specimens - asphalt concrete base course, Folsom project; temperature of test - 68°F.

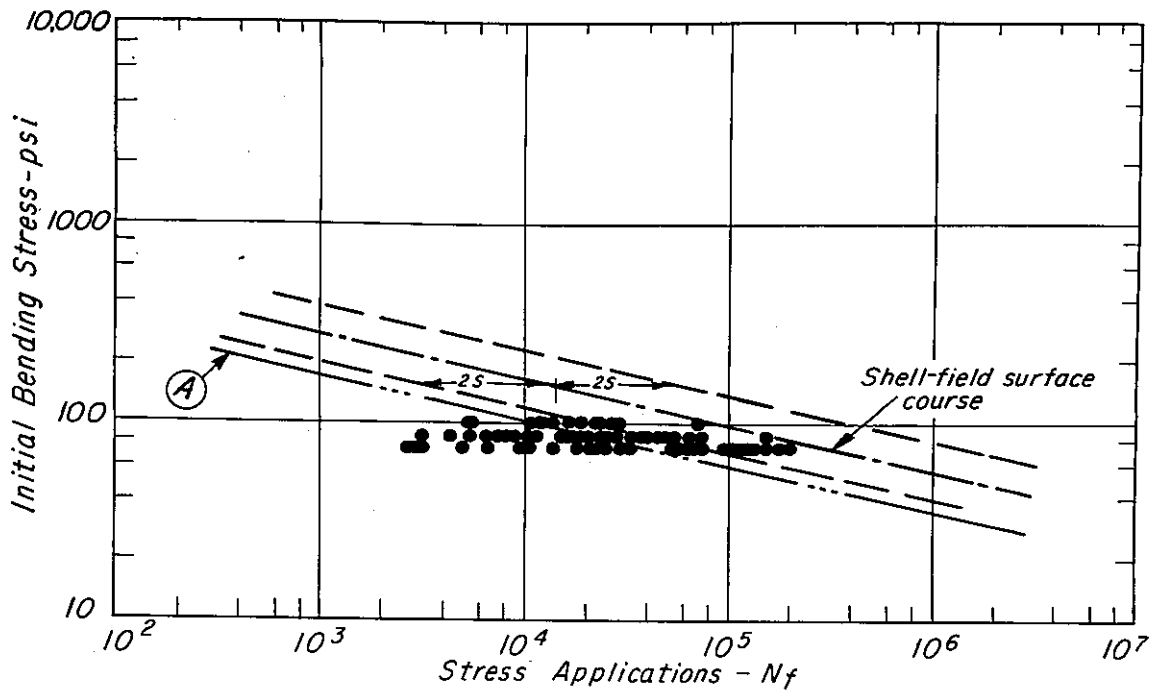


Fig. 83 - Initial bending strain vs. applications to failure, field specimens - asphalt concrete base course, Folsom project; temperature of test - 68°F.

TABLE 27 — FATIGUE DATA* — FOLSOM FIELD BASE COURSE

Location	Stress -psi	Number of Specimens	Fatigue Life - N_f		
			Mean	Standard Deviation	c_v
1	75	7	99,165	72,229	72.8
	85	8	44,063	47,786	108.4
	100	7	21,382	8,070	37.7
	all	22			
2	75	7	50,288	50,043	99.5
	85	8	20,366	17,865	87.7
	100	8	23,211	20,156	86.6
	all	23			
3	75	7	56,385	34,714	61.5
	85	8	29,375	15,304	52.1
	100	9	17,326	4,329	24.9
	all				
4	75	12	24,140	31,586	130.8
	85	11	23,692	18,147	76.5
	100	11	15,623	6,557	41.9
	all	34			
all locations	75	33	52,441	52,905	100.8
	85	35	28,887	27,586	95.4
	100	35	18,947	11,043	58.2
	all				

*Test temperature — 68°F

TABLE 28 - RESULTS OF REGRESSION ANALYSES ON FATIGUE DATA OBTAINED FOR FIELD SURFACE AND LABORATORY SPECIMENS

Mix Designation	No. of Specimens	Temp. of F	$N_f = K_1(1/\epsilon_{mix})^{n_1}$			$N_f = K_2(1/\sigma_{mix})^{n_2}$			Mean Stiffness $\times 10^{-3}$		
			K_1	n_1	Corr. Coef.	Stand. Err. of the Estimate	K_2	n_2		Corr. Coef.	Stand. Err. of the Estimate
Field Specimens											
Surface -											
Location 1	30	68	1.09×10^{-7}	3.22	0.744	0.416	6.97×10^{11}	3.72	0.697	0.447	340.
" 2	26	68	1.26×10^{-5}	2.65	0.837	0.388	5.96×10^{15}	5.54	0.905	0.302	389.
" 3	26	68	4.56×10^{-5}	2.56	0.820	0.324	9.07×10^{12}	4.02	0.805	0.336	500.
" 4	26	68	1.60×10^{-5}	2.89	0.874	0.307	3.11×10^{14}	4.79	0.887	0.291	507.
" 1 & 2	56	68	2.21×10^{-6}	2.86	0.794	0.410	3.55×10^{13}	4.51	0.783	0.410	362.
" 3 & 4	52	68	8.52×10^{-6}	2.70	0.848	0.312	5.22×10^{13}	4.40	0.848	0.311	503.
" All	108	68	3.58×10^{-6}	2.80	0.839	0.358	5.59×10^{13}	4.51	0.775	0.415	430.
Laboratory Specimens											
Stress Controlled											
Shell	35	83	6.38×10^{-6}	2.90	0.969	0.274	4.03×10^{13}	5.71	0.960	0.307	69.
	50	68	3.70×10^{-8}	3.45	0.937	0.395	5.97×10^{13}	5.32	0.899	0.495	173.
	30	40	5.20×10^{-11}	4.08	0.950	0.260	1.16×10^{18}	5.71	0.921	0.320	1,037.
Chevron	46	68	9.67×10^{-7}	2.97	0.960	0.242	3.97×10^{14}	5.36	0.804	0.502	226.
	30	40	8.35×10^{-12}	4.17	0.920	0.290	1.55×10^{16}	4.97	0.896	0.324	1,222.
Strain Controlled											
*(1) Shell	27	68	3.06×10^{-6}	2.90	0.807	0.271	4.80×10^8	2.52	0.564	0.380	
(2)	27	68	7.64×10^{-8}	3.51	0.804	0.331	1.43×10^{10}	3.11	0.578	0.454	146.
(3)	27	68	1.64×10^{-8}	3.78	0.878	0.263	5.53×10^9	2.81	0.531	0.465	
(4)	27	68	1.70×10^{-9}	4.07	0.897	0.256	1.36×10^{10}	3.04	0.543	0.487	

*(1) -Ns defined for 25 percent decrease in stiffness

(2) -Ns defined for 40 percent decrease in stiffness

(3) -Ns defined for 50 percent decrease in stiffness

(4) Ns defined for 25 percent decrease in stiffness at high strains; 50 percent at low

considered meaningful. Accordingly, the regression equations developed for the surface course mixes containing the Shell asphalt (locations 1 and 2) are shown in both figures. On the strain vs. fatigue relationship, Fig. 83, an additional line is shown which represents an adjusted curve recognizing the difference in asphalt content of the base as compared to the surface (4.2 percent vs. 4.9 percent). Even with the adjustment for asphalt content (the basis for which has been discussed earlier) it is apparent that the fatigue response of the base course as measured on the $1-1/2 \times 1-1/2$ in. specimens is somewhat poorer than that of the surface course. Some judgment will be required, however, in selecting a relationship for analysis of the structural pavement section recognizing the influence of the large aggregate on fatigue response.

To attempt to develop relationships which could be used for analyses of the response of the pavement structure to load, best fit lines were obtained for data in Figs. 82 and 83 (N_f as the dependent variable) which had the same slopes as those for the surface course mixes, a procedure somewhat different than that normally used. These curves have been indicated by the symbol (A) in both figures.

Laboratory Prepared Surface Course. Fatigue data for the laboratory prepared specimens are presented in Figs. 84 and 85 for the mixture containing the Shell asphalt and in Figs. 86 and 87 for the mixture with the Chevron asphalt. Results of regression analyses are shown on the figures and are summarized in Table 28 for comparison with the data obtained from the field specimens.

Since the void contents of both the field and laboratory prepared specimens are about the same, the strain vs. fatigue life relationships at 68°F have been plotted together in Fig. 88. With the exception of the relationship for the Shell laboratory prepared specimens, the various regression lines agree reasonably well. These data can thus serve as the basis for the prediction of the potential for pavement cracking resulting from repetitive traffic loading to be discussed subsequently.

As with the Morro Bay project controlled-strain tests were also performed at 68°F on laboratory prepared specimens (specimens with Shell asphalt). Results are summarized in Table 28 and are compared with the controlled stress test data in Fig. 89. In this figure it will be noted that depending on the distress criteria selected, different results will be obtained as compared to the controlled-stress tests indicating different periods of time associated with crack propagation depending on the amount of damage considered.

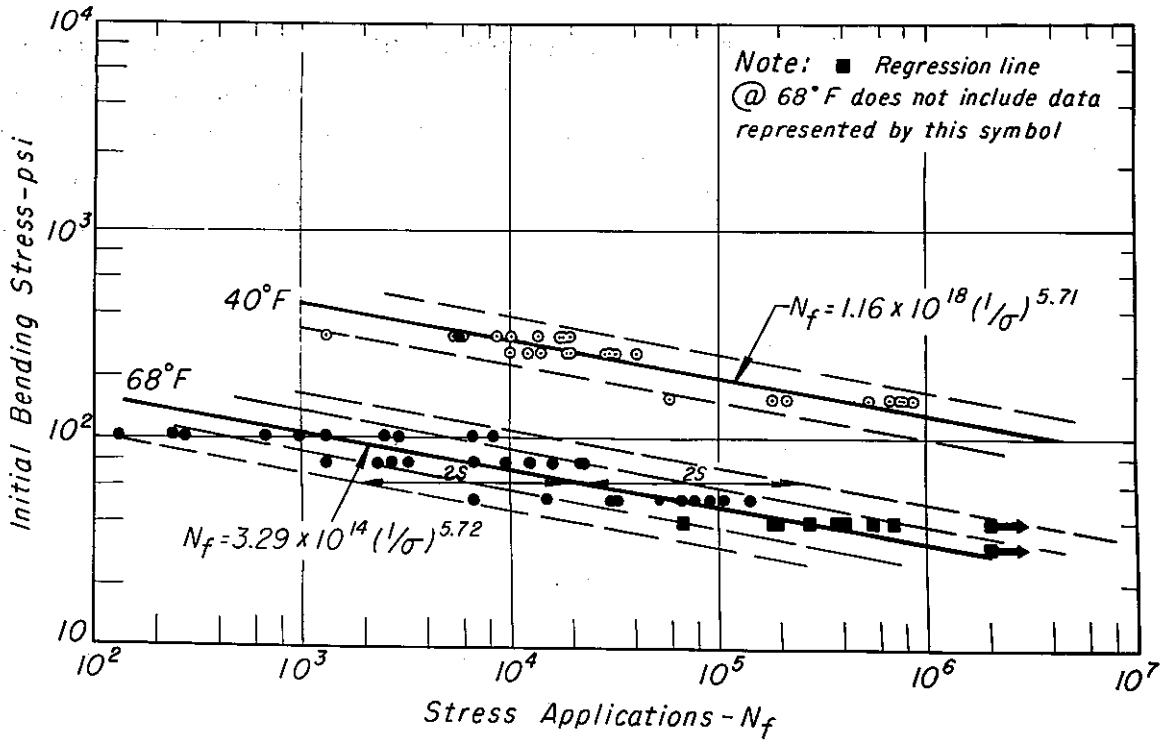


Fig. 84 - Mixture bending stress vs. applications to failure, laboratory prepared specimens of surface course containing Shell asphalt, Folsom project.

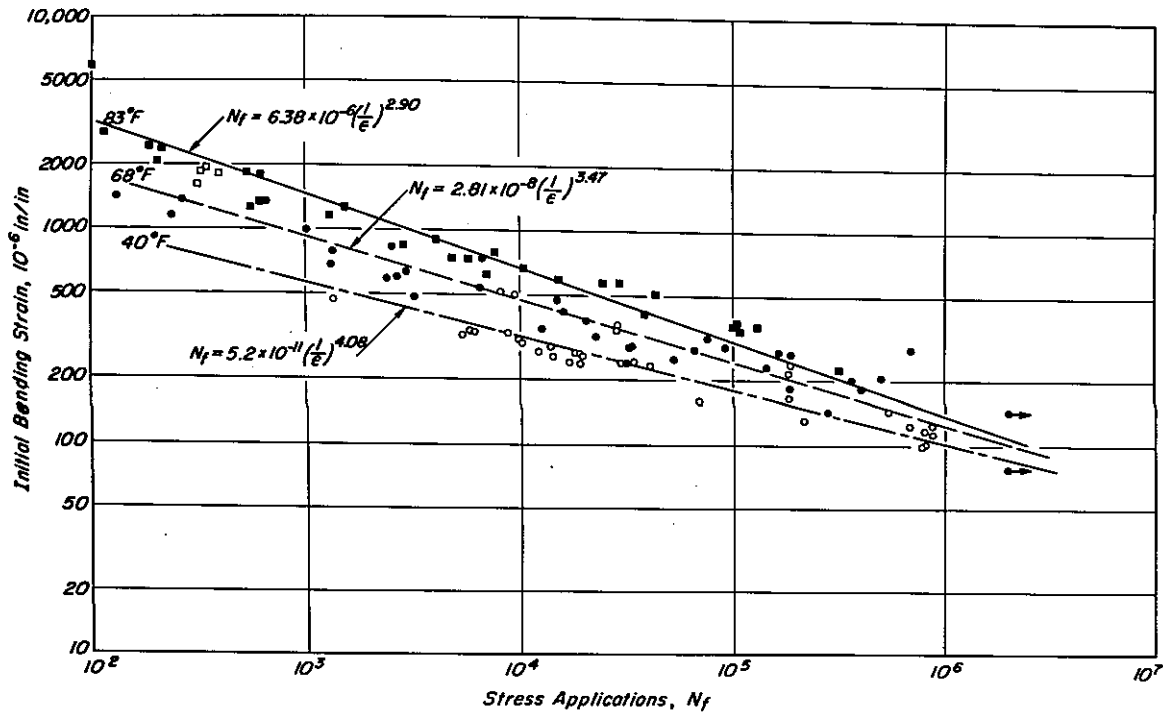


Fig. 85 - Initial bending strain vs. applications to failure - laboratory prepared surface course containing Shell asphalt, Folsom project.

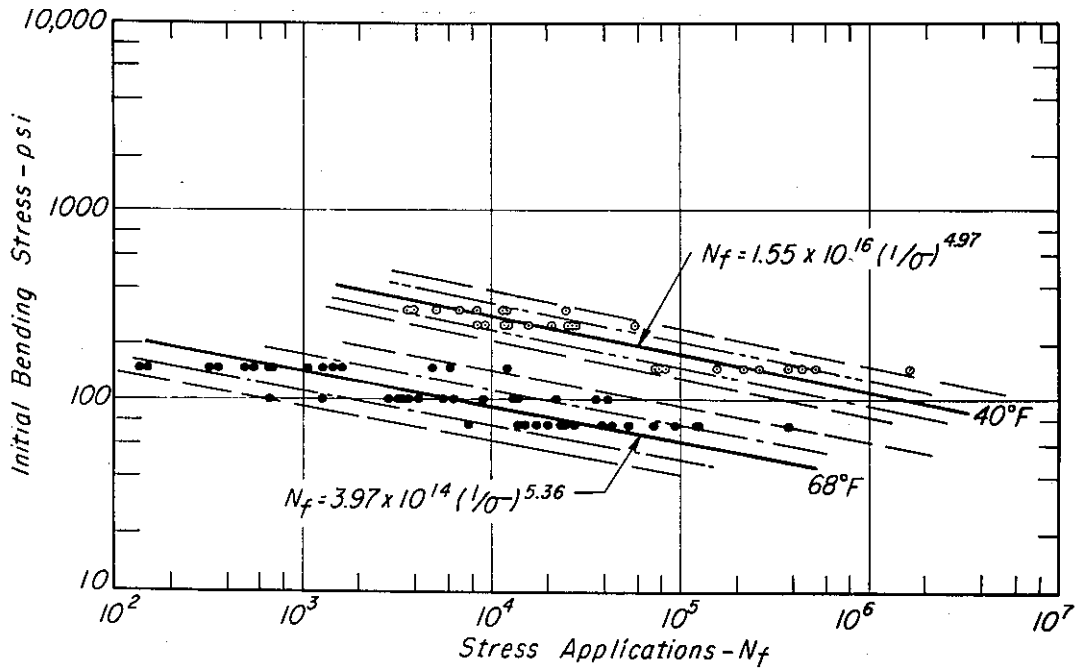


Fig. 86 - Mixture bending stress vs. applications to failure, laboratory prepared specimens of surface course containing Chevron asphalt, Folsom project.

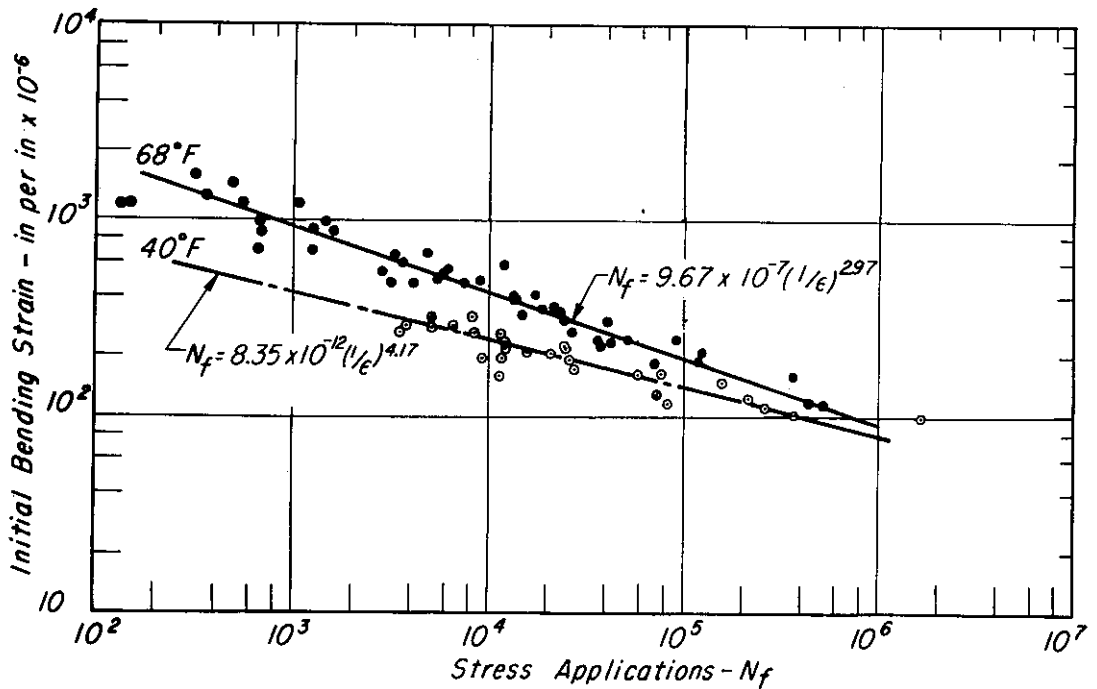


Fig. 87 - Initial bending strain vs. applications to failure, laboratory prepared specimens of surface course containing Chevron asphalt, Folsom project.

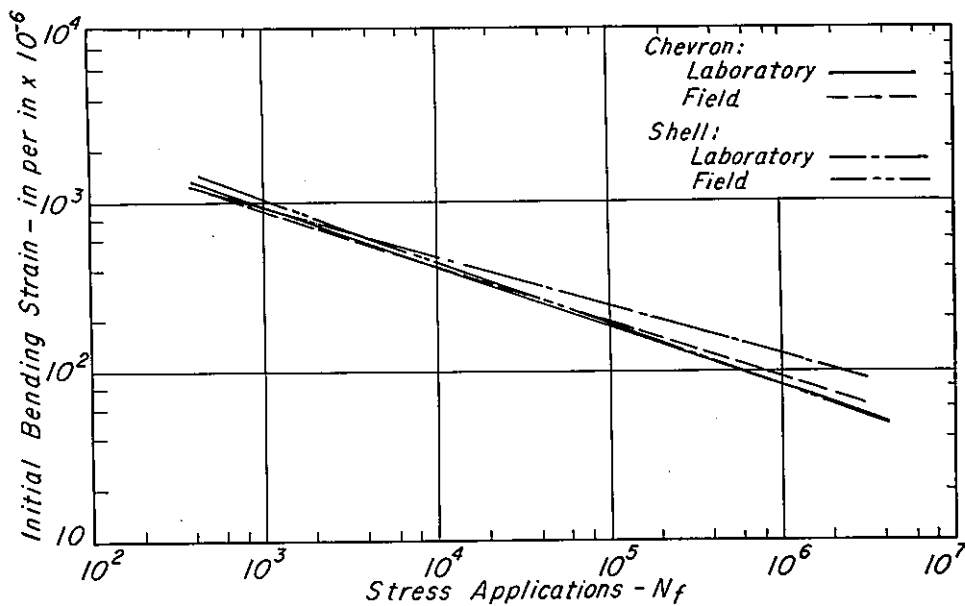


Fig. 88 – Comparison of fatigue response of field and laboratory prepared specimens, Folsom project.

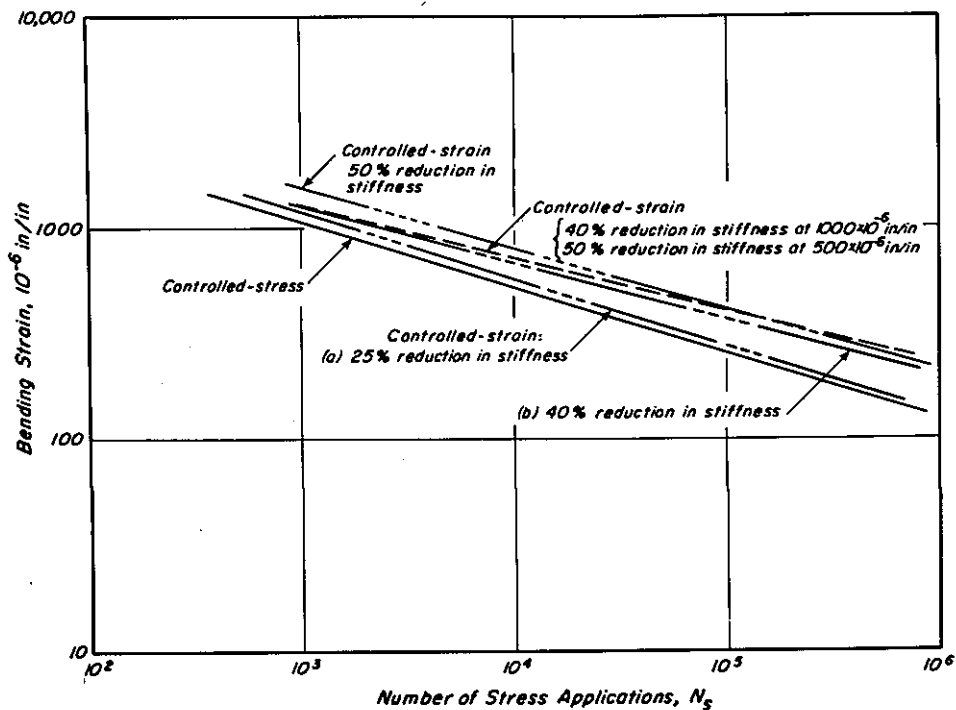


Fig. 89 – Controlled-strain fatigue relationships based on estimates of service lives corresponding to different mixture stiffness reductions; 68°F , Folsom mixture.

DESIGN CONSIDERATIONS

In an attempt to utilize the fatigue data developed to date to permit incorporation of this factor in the design process, relatively simply, results of a series of fatigue tests on California type mixtures have been analyzed within a framework originally suggested by Heukelom and Klomp (35) and briefly described in an earlier report (31).

The previous section contains a summary of the various statistical comparisons made with the data. For convenience these have been summarized in Part I of Table 29 for individual mixes and for various combinations in Part II of the same table.

It was shown in the previous section that a regression line fit to the data for mixes A, B, C, and D and F of Table 29 resulted in the equation (Table 29)

$$N_f = 6.28 \times 10^{-7} \left(\frac{1}{\epsilon_{\text{mix}}} \right)^{3.01}$$

which is applicable for mixes with stiffnesses of the order of 300,000 psi. Thus it is possible that relationships for California type mixes might be developed in terms of stiffness to permit the development of a generalized (or simplified) approach to the definition of fatigue response. The concept was further checked by combining all of the 68°F data reported in Ref. 57 to obtain the relationship:

$$N_f = 2.92 \times 10^{-6} \left(\frac{1}{\epsilon_{\text{mix}}} \right)^{2.81}$$

with a correlation coefficient of 0.928 and a standard error of the estimate of 0.290.

Summary plots of the various analyses are presented in Figs. 90 and 91. In Fig. 90 the affect of mixture stiffness on slope is apparent. In this instance the mixture prepared with the granite aggregate and the 40-50 penetration material (656,000 psi) has a distinctly flatter slope than the curves representing the less stiff mixes (approximately 300,000 psi - Table 29). This difference is also illustrated in Fig. 91 which contains a comparison between the regression line for all California mixes at 68°F and those developed for the Folsom project laboratory prepared specimens containing the Chevron asphalt, at 68°F and 40°F. The reasonable agreement between the regression lines at 68°F lends support to the idea that a generalized fatigue diagram might be developed for California type mixes recognizing the dependence of the location of the relationship between strain and cycles to failure on stiffness.

In Report TE 68-8 (58) it was suggested that the laboratory determined curves may be somewhat conservative and that as the stiffness of the mix decreases the slope of the

TABLE 29 - MIXTURE CHARACTERISTICS

Mix Identification Grading and Asphalt Penetration	No. of Speci- mens	Asphalt Content percent	Stiffness at 68°F, 0.1 sec. loading		Percent Air		$N_f = K_1^{1/n_1} / \epsilon_{mix}^{n_1}$	Standard Error of Estimate					
			Mean $\text{psi} \times 10^3$	Std. Dev. $\times 10^3$	Mean	Std. Dev.			K_1	n_1 Corr. Coef.			
<u>Part I - Individual Mix Text Results</u>													
California Coarse A Granite 85-100 penetration	28	6.0	228	54	23.8	23.8	5.7	0.6	10.3	3.20×10^{-5}	2.485	0.932	0.184
California Fine B Granite 85-100	53	6.0	273	65	23.8	23.8	5.7	0.5	8.1	8.91×10^{-7}	2.952	0.950	0.326
California Medium C Granite 85-100 penetration	19	6.0	288	53	18.5	18.5	4.5	0.6	12.2	2.87×10^{-6}	2.832	0.899	0.260
California Medium D Granite 60-70 penetration	27	6.0	318	57	17.8	17.8	4.8	0.4	9.1	1.12×10^{-7}	3.256	0.952	0.187
California Medium E Granite 40-50 penetration	23	6.0	656	92	13.9	13.9	4.7	0.5	10.6	1.03×10^{-10}	4.010	0.962	0.150
California Medium F Basalt 60-70 penetration	24	6.2	298	50	16.9	16.9	6.7	0.6	9.3	1.34×10^{-7}	3.222	0.896	0.213
<u>Part II - Combined Results</u>													
California Coarse, Medium, Fine Granite 85-100 penetration (A + B + C)	100	6.0	-	-	-	-	-	-	-	1.15×10^{-6}	2.920	0.948	0.282
California Medium Granite 60-70, 85-100 pen. (C + D)	46	6.0	-	-	-	-	-	-	-	4.07×10^{-7}	3.090	0.929	0.222
Mixes A, B, C, D, and F	-	-	-	-	-	-	-	-	-	6.28×10^{-7}	3.010	0.952	0.220
All California Mixes (Reference (57))	-	-	-	-	-	-	-	-	-	2.92×10^{-6}	2.810	0.928	0.290

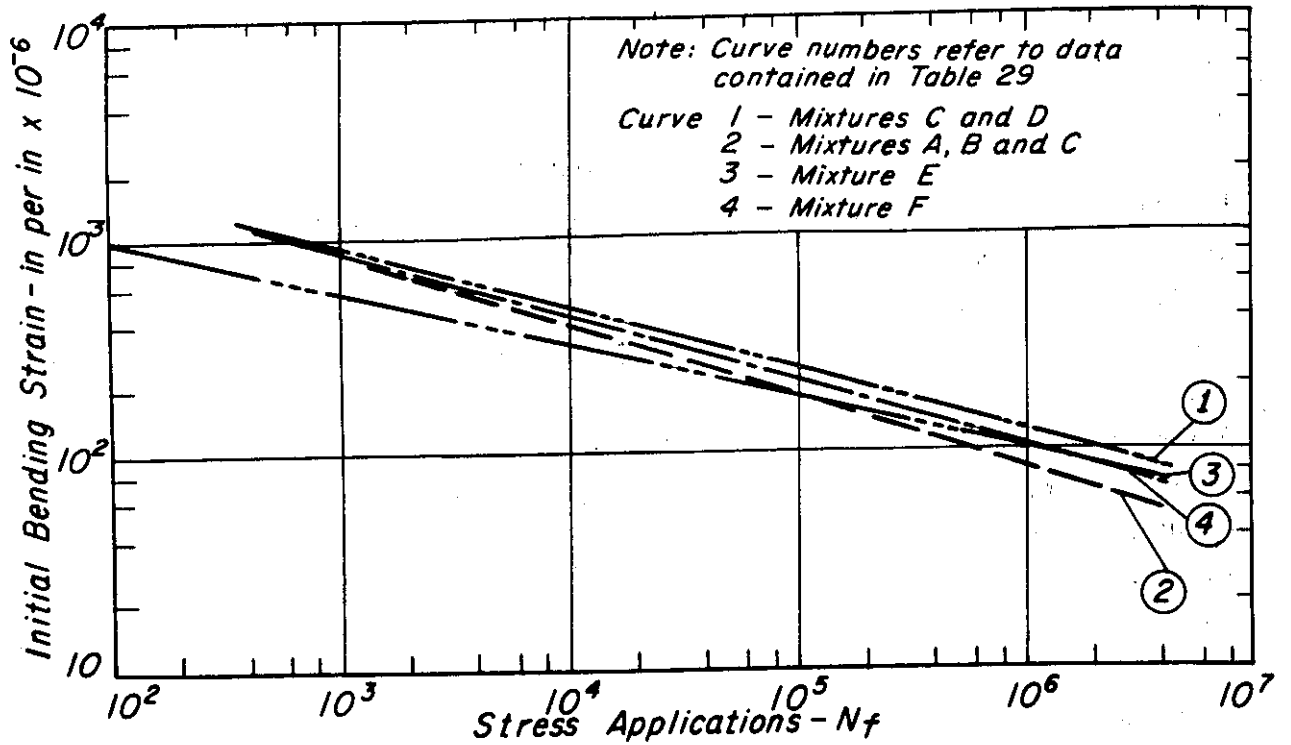


Fig. 90 - Initial bending strain vs. applications to failure at 68°F, laboratory prepared specimens.

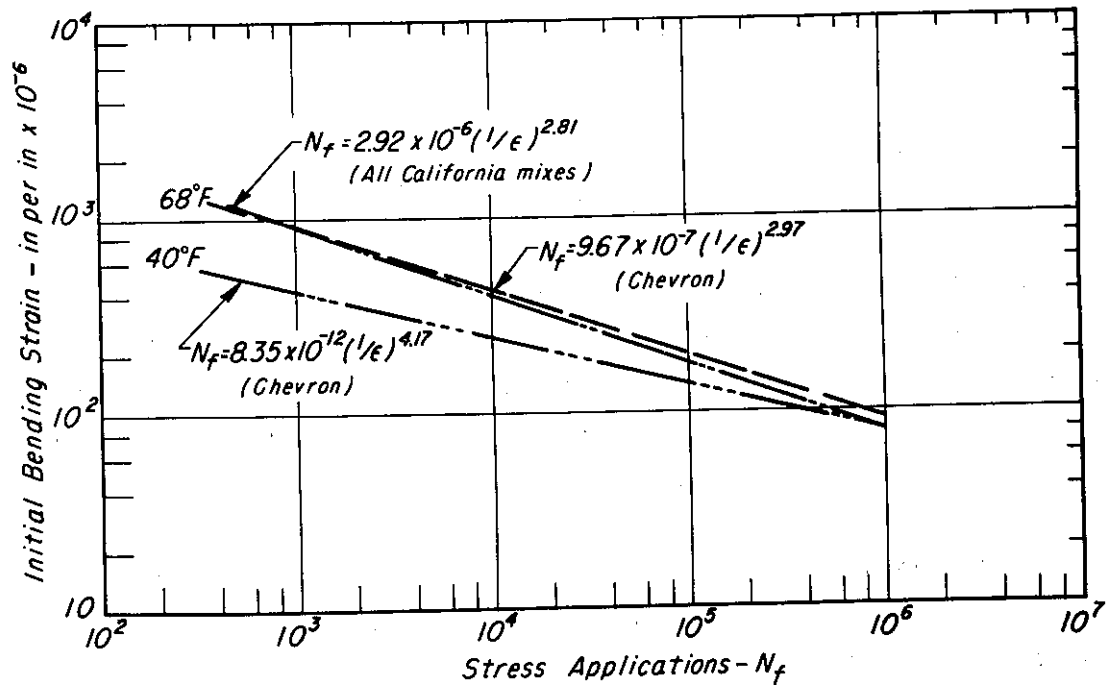


Fig. 91 - Comparison of fatigue response of laboratory prepared specimens from Folsom project containing Chevron asphalt with regression analysis for data from all California-type mixes tested.

ϵ_{mix} vs. N_f relationship becomes steeper due to the increase in time (or cycles) required for cracks to propagate once they have been initiated. The figure illustrating this point schematically is shown in Fig. 92. Such a hypothesis appears well documented by the data presented in this section. Accordingly the data presented herein will form the basis for the development of a generalized fatigue diagram which eventually could become a part of the fatigue subsystem of Fig. 2.

Utilizing the fatigue curves for the Chevron material (Fig. 87) and assuming that limiting slopes of the fatigue curves (ϵ_{mix} vs. N_f) will be 2 and 6 for mixture stiffnesses of 1.0×10^4 psi and 4.0×10^6 psi respectively, a generalized diagram relating cycles to failure to stiffness, stress, and strain is presented in Fig. 93. Since the mixture containing the Chevron asphalt was tested at an air void content of approximately 7 percent the diagram may thus be considered a fatigue diagram at this void content. For purposes of comparison, other fatigue data (presented in this report) based on tests on both laboratory and field specimens are also shown in this figure. While some scatter is evident the relationship appears reasonable.

To ascertain the effect of void content on fatigue response, data presented in Fig. 46 could be utilized. Relationships between fatigue life and void content are shown in Fig. 94 for both the coarse and fine mixes. While there is some difference between the two mixes, the average curve shown in this figure provides at least an initial basis to consider the effect of void content on fatigue life.

A more generally applicable diagram for design purposes would be one similar in form to Fig. 93 but based on a void content of 5 percent. Such a diagram is shown in Fig. 95 based on available fatigue data from mixes with void contents in this range. The data presented in Fig. 93 have been corrected utilizing the relationship of Fig. 94 and are also shown in this figure for comparison.

The diagram for Fig. 95 probably represents a conservative estimate of the response of mixes in the pavement structure since the data used to develop the relationship are based on controlled-stress tests. Moreover it must be remembered that the data used to develop the figure are based on mix designs conforming to the State of California procedure (59). Should lower asphalt contents be utilized, a correction to the fatigue relationship should be made in accordance with the procedure illustrated in Fig. 83 for the base course mix on the Folsom project.

One could also develop a more generalized approach using the results of controlled-strain tests (e. g. , Fig. 73) as well as the results of the controlled stress tests shown on Fig. 95. This necessitates determining the results of a series of controlled-strain tests over a range in temperatures and defining a family of curves similar to those shown in Fig. 95.

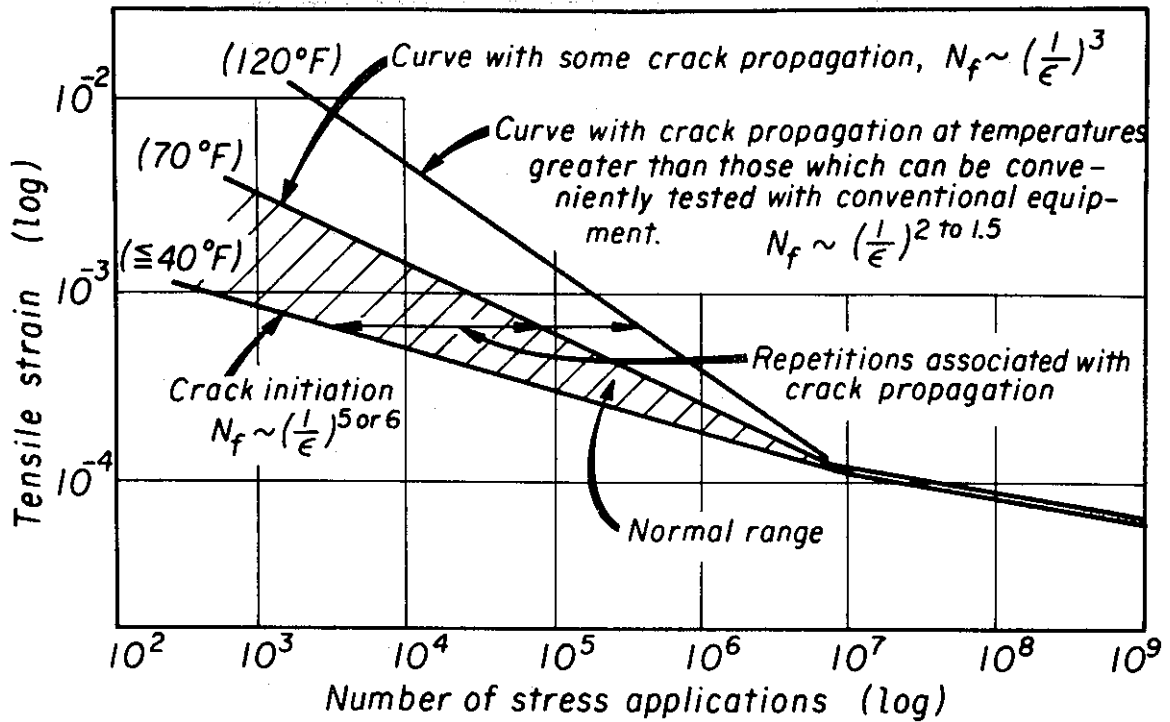


Fig. 92 – Influence of temperature (or mixture stiffness) on the strain vs. stress applications relationship for asphalt concrete.

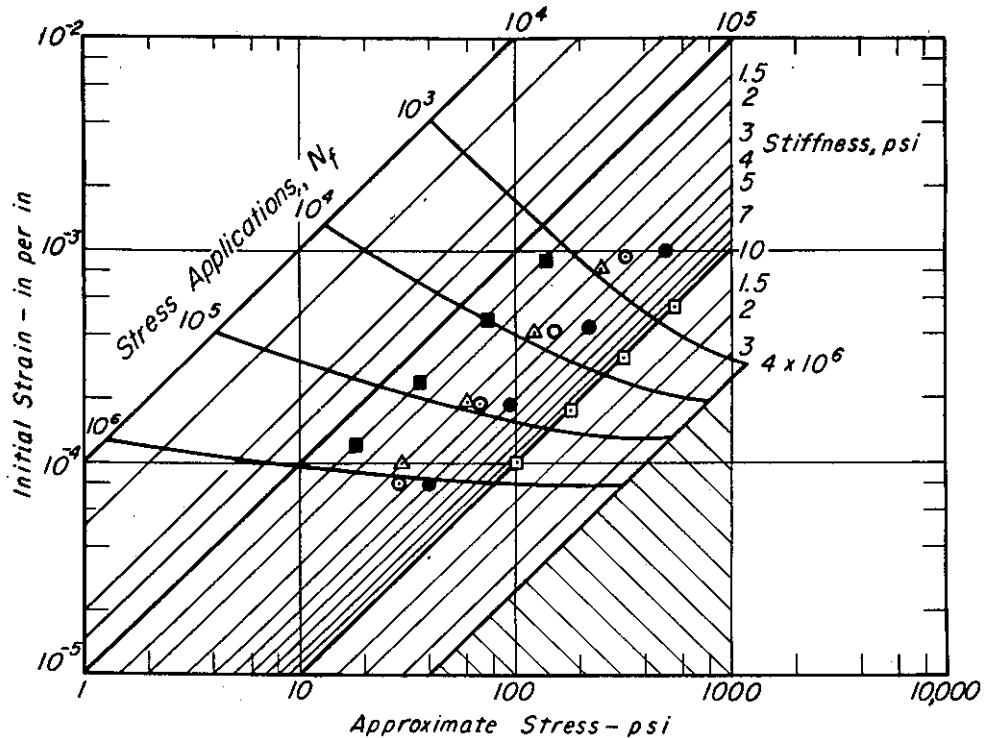


Fig. 93 – Relationship between stress, strain, stiffness, and fatigue life, California type mixtures; approximate void content – 7 percent.

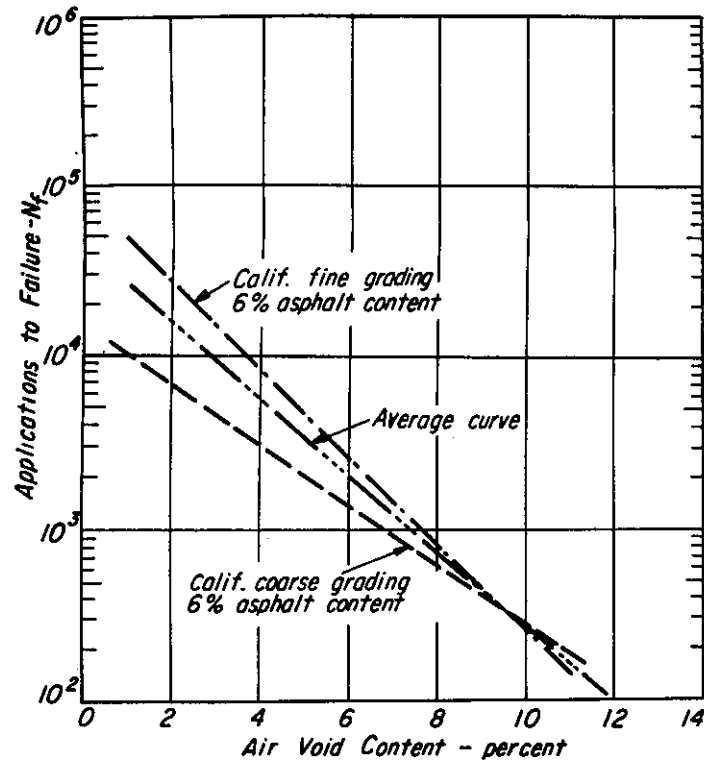


Fig. 94 - Effect of air void content on fatigue life, granite aggregate; stress level - 150 psi.

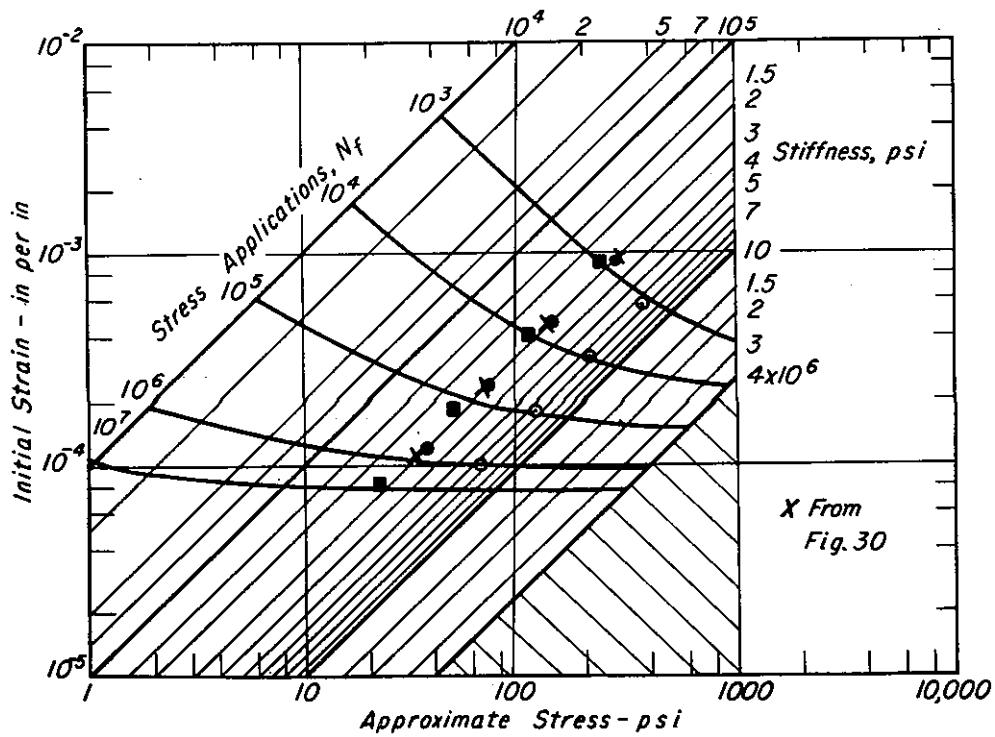


Fig. 95 - Relationship between stress, strain, stiffness, and fatigue life, California type mixtures; approximate void content - 5 percent.

At a particular temperature (or stiffness) one could then plot the curves corresponding to both the controlled-stress and controlled-strain tests which should define the limits of response of the mixture to load. By determining the mode-factor associated with the load and stiffness, we would then define the appropriate fatigue curve to use between the two limits by interpolation. This procedure is illustrated schematically in Fig. 96. and has been used in the performance estimate for the Folsom project.

While such a procedure is more complex it may be required to provide realistic estimates of service lives for pavements in the intermediate thickness range.

For thick asphalt bound layers on the other hand the chart of Fig. 95 should provide a reasonable (conservative) estimate of service life as noted earlier.

The reasonableness of the values in the low strain range would appear to be confirmed by data developed by other investigations which has been summarized in Appendix F. For example it will be noted that at least 75 percent of the data exhibit strains of 100×10^{-6} in. per in. at 10^6 stress applications.

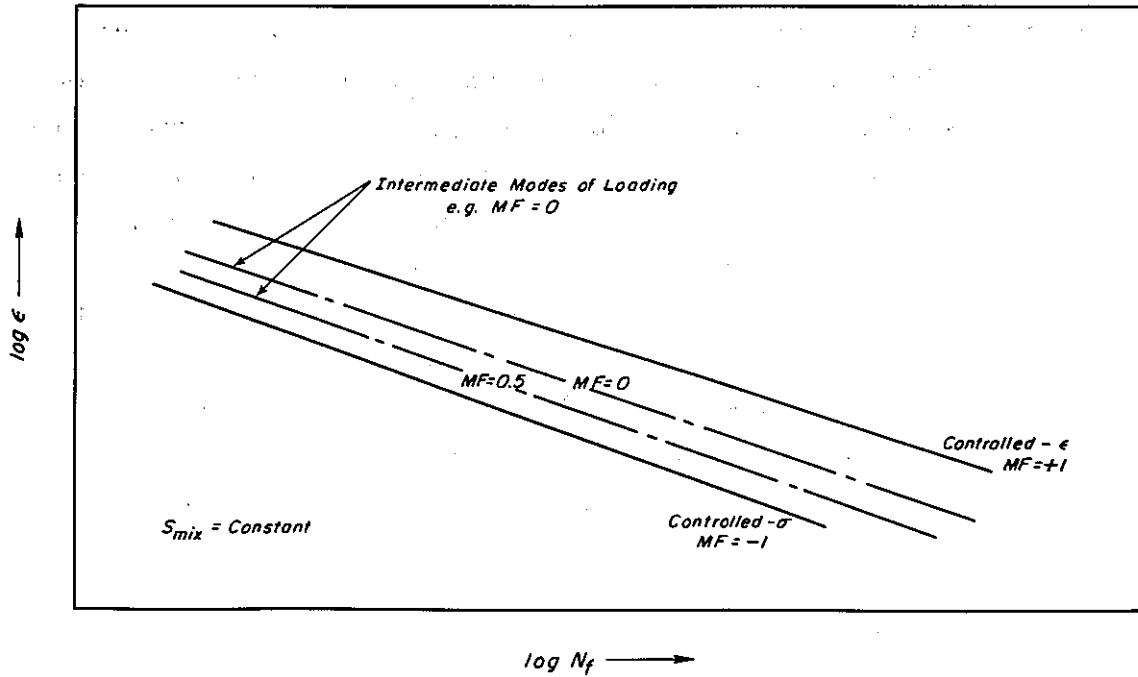


Fig. 96 – Development of fatigue curves for intermediate modes of loading at particular value for mixture stiffness, S.

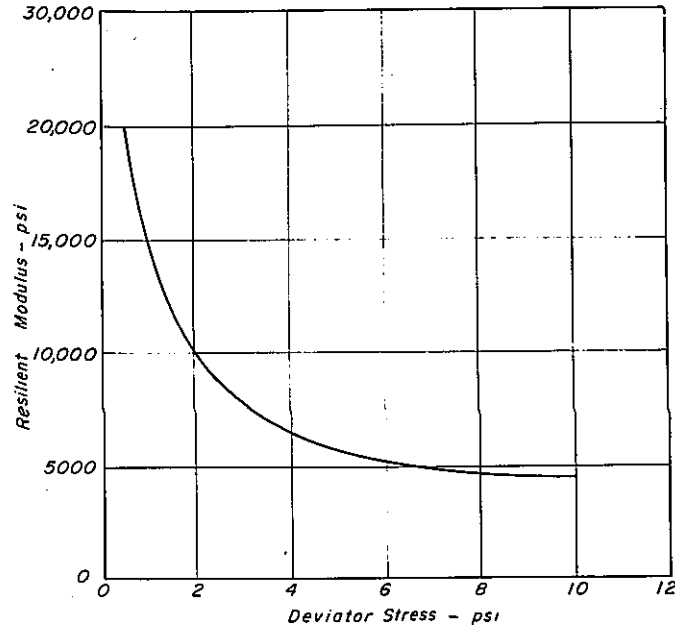


Fig. 97 – Resilient modulus vs. deviator stress – subgrade, Morro Bay.

APPLICATIONS OF FATIGUE SUBSYSTEM IN PRACTICE

As noted earlier the fatigue subsystem provides the framework for the analyses of existing pavements or for the design of new pavements to preclude this mode of distress. In the existing pavement category, two in-service pavements in the State highway system have been analyzed, one near Morro Bay, California, and the other near Folsom, California. For the design example a city-county highway in Contra Costa County will be considered. In each example the material will be presented following the format of Fig. 2.

Prediction of Service Life — Morro Bay Pavement

Field Testing and Sampling. Traveling Deflectometer deflection data were obtained by the California Division of Highways on March 10, 1964 on sections of State Sign Route 1 near Morro Bay, California (Designation V-SLO-56-C,D). Measurements were made using a 15,000 lb axle load and 90 psi inflation pressure in the test truck tires and the results are summarized in Table 30.

TABLE 30 — DEFLECTION SURVEY RESULTS*

Location	Mean Deflection in.	Std.- Dev.	Eightieth Percentile Deflection	Near Sample Location No.
STA 620-630, NBTL-IWT	.0229	.0042		
NBTL-OWT	.0268	.0052	.0312	Loc. 1
NBPL-LWT	.0197	.0023	.0216	Loc. 2
NBPL-RWT	.0223	.0032		
STA 102-92, SBTL-IWT	.0156	.0024		
SBTL-OWT	.0163	.0020		
SBPL-LWT	.0160	.0013		
SBPL-RWT	.0165	.0020	.0181	Loc. 3
STA 715-725, NBTL-IWT	.0159	.0009		
NBTL-OWT	.0197	.0013	.0208	Loc. 4
For all data	.0192	.00452	.023	

*March 1964

Samples of the materials in the pavement section were taken on December 14 to 16, 1965 and in-place densities and water contents were determined at this time. Table 31 indicates the deflections that were measured at the locations from which these samples were taken.

TABLE 31 -- TRAVELING DEFLECTOMETER DEFLECTIONS
AT SAMPLE LOCATIONS**

Sample Location Number	Location	Traveling Deflectometer Deflection, in.
1	STA. 625+00, NBTL-RWT*	0.035
2	STA. 626+00, NBPL-RWT	0.030
3	STA. 100+00, SBPL-RWT	0.013
4	STA. 718+00, NBTL-RWT	0.017
	Mean deflection at sample locations	0.024

* In direction of travel

**March 1964

TABLE 32 -- IN SITU PHYSICAL PROPERTIES AND
STRUCTURAL SECTION*

Layer	Thickness ft	Unit Weight (lb. per cu. ft)	Water Content percent	Dry Density (lb. per cu. ft)	Degree of Saturation percent
Open-Graded Asphalt Concrete	0.06		No included in structural section		
Type B Asphalt Concrete	0.21	139.7			
Class 2 Aggregate Base	0.67	129.5	10.4	117.2	78.
Class 2 Aggregate Subbase	1.00	132.6	11.7	118.6	83.
Subgrade Soil			See Table 29, Report TE 66-6		

*December 1965

Table 32 shows the mean values of the in situ physical properties of the materials in the pavement. Also included in this table are the thicknesses of the various layers, as supplied by the Division of Highways.

Laboratory Test Results

Subgrade Soil. Results of repeated load tests on undisturbed samples of the subgrade soil are contained in Fig. 97. The curve shown in this figure represents the mean line drawn through the data points. This material exhibits a modulus which is dependent on the applied stress, with the stress dependence being most marked in the low stress range.

Untreated Aggregate Subbase. Resilient modulus determinations of the subbase material were made using laboratory prepared specimens. Mean density, water content, and degree of saturation are shown in the accompanying tabulations for the specimens tested.

	<u>Mean</u>	<u>Standard Deviation</u>	<u>Coefficient of Variation-percent</u>
Dry density, lb per cu ft	117.0	4.6	3.9
Water content, percent	9.7	0.55	5.7
Degree of saturation, percent	60.0	9.5	15.6

From a comparison of this data with that presented in Table 32 for the in situ measurements, it will be noted that the dry densities are about the same, but that the degree of saturation of the laboratory prepared specimens is less than that for the field samples.

The resilient modulus — sum of principal stresses relationship,

$$M_R = 2900 (\theta)^{0.47}$$

shown in Fig. 98 has a correlation coefficient of 0.884.

Untreated Aggregate Base. Repeated load tests were performed on laboratory prepared specimens of the aggregate base course material. Density, water content, and degree of saturation data for these specimens were as follows:

	<u>Mean</u>	<u>Standard Deviation</u>	<u>Coefficient of Variation-percent</u>
Dry density, lb per cu ft	113.2	1.45	1.2
Moisture content, percent	8.55	0.59	6.8
Degree of saturation, percent	52.8	3.6	6.8

It will be noted that the average dry density for the laboratory prepared specimens is somewhat less than the average reported for the in-place density measurements (Table 32); in addition the average water content for these specimens was somewhat less than that measured in-place.

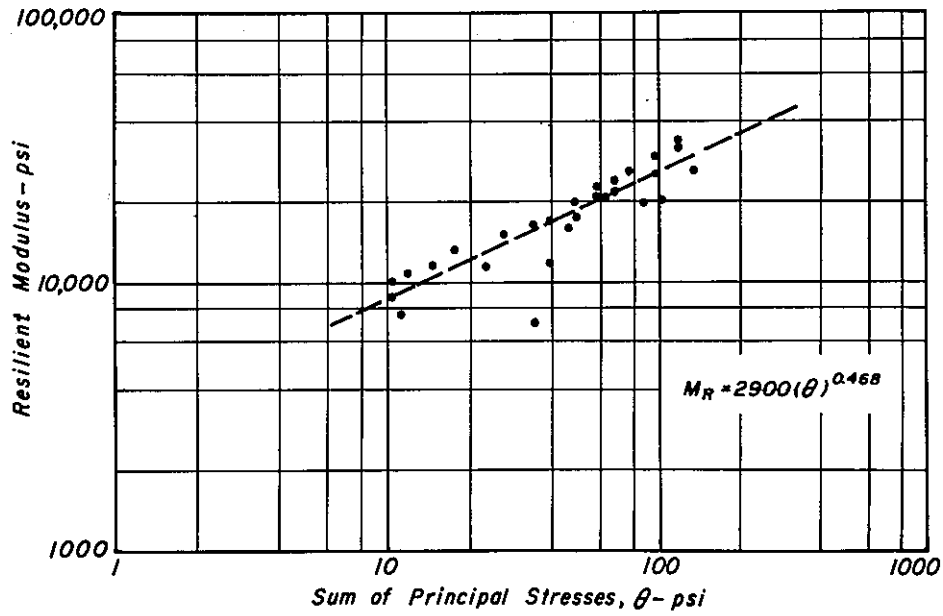


Fig. 98 - Resilient modulus vs. sum of principal stresses - subbase, Morro Bay.

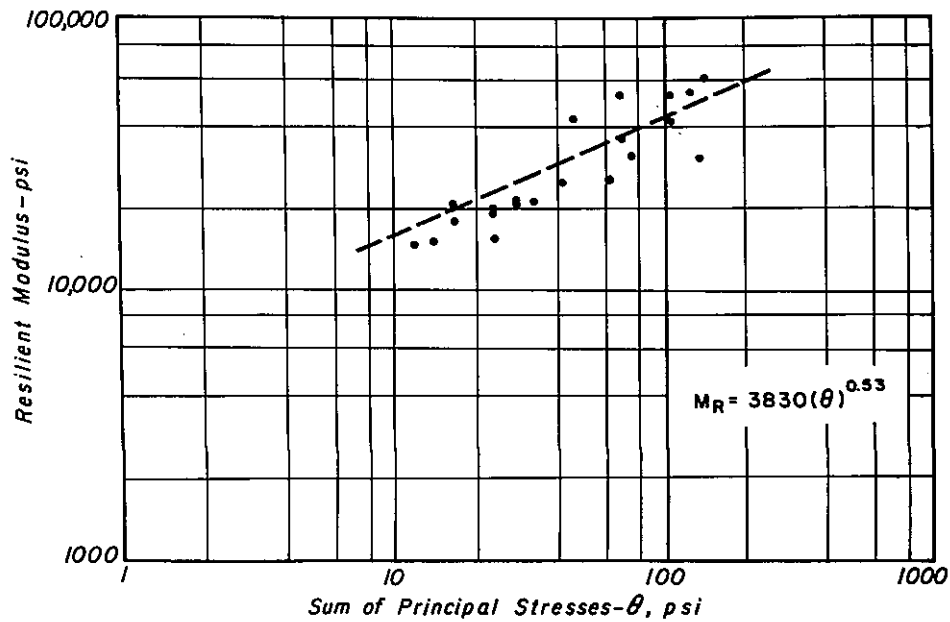


Fig. 99 - Resilient modulus vs. sum of principal stresses - base, Morro Bay.

Fig. 99 shows the relationship obtained between the resilient modulus and the sum of the principal stresses. The equation:

$$M_R = 3830 (\theta)^{0.53}$$

has a correlation coefficient of 0.907.

Asphalt Concrete Surface. Stiffness data for asphalt concrete specimens obtained from pavement samples have already been presented in Table 18. These values were determined from deflection measurements made at the start of the fatigue testing (after 200 stress repetitions) and determined from the relationship:

$$S(t, T) = K \cdot \frac{P}{I \cdot \Delta}$$

where:

- S(t, T) = flexural stiffness at a particular time of loading and temperature
- K = constant depending on loading geometry
- P = applied load
- I = moment of inertial of beam cross section
- Δ = measured center deflection of beam (at 200 stress repetitions)

Both controlled-stress and controlled-strain fatigue tests were performed on specimens obtained from pavement samples and on laboratory prepared specimens composed of essentially the same materials as used in the original construction. To define the potential for distress, however, the controlled-strain test results were selected (42).

From controlled-strain tests on laboratory prepared specimens of the paving mixture, service lives corresponding to a 50 percent reduction in stiffness were selected as being representative of the behavior of the pavement section. The equation for the curve of strain vs. applications corresponding to this reduction in stiffness is:

$$N_s = 2.78 \cdot 10^{-7} \left(\frac{1}{\epsilon}\right)^{3.38} \dots \dots \dots (22)$$

with a correlation coefficient of 0.87 and a standard error of the estimate of 0.248.

Traffic Data

To obtain traffic information for the Morro Bay Project, it was necessary to combine data from a series of sources.

The following data were abstracted from the annual traffic census of the State of California Division of Highways for a station located near the end of the freeway at Cayucos:

<u>Year</u>	<u>Year</u>	<u>Annual ADT</u>
1963	1963	4700
1964	1964	5900
1965	1965	6100

The ADT used in the following calculations is 5600 which is the mean for the years 1963-65. Additional traffic data were provided by the Materials and Research Department as shown below:

1963 Vehicle Census

Average Daily Traffic — Morro Bay

All Vehicles	3400
Trucks and Buses	282
Percent Trucks and Buses	8.3
Buses	0
2-Axle	120
3-Axle	32
4-Axle* or More	282

*77 percent are 5-axle

For the purposes of the calculations, the number of trucks in each class has been increased proportionally so as to conform to the average ADT of 5600 actually measured.

In order to obtain the appropriate number of applications of each axle load, the following assumptions have been made:

1. 50 percent of the ADT moves in each direction.
2. 100 percent of the commercial vehicles travel in the right lane of the divided highway. This assumption would appear reasonable since Taragin (6) has shown that about 90 percent of commercial traffic travels in the right lane at low traffic volumes.
3. Each vehicle stresses the same point in the traffic lane, i. e. , every vehicle tracks the same wheel path. This assumption is somewhat conservative as seen earlier.

The axle load distribution was obtained from the statewide W-4 loadometer surveys (All Main U & R) for the years 1961-66. On the basis of this data and the assumptions made above, the monthly axle load applications shown in Table 33 were determined and used in the fatigue calculations.

TABLE 33 — MONTHLY AXLE LOAD DISTRIBUTION,
MORRO BAY PAVEMENT

Axle Load Group kips	Axle Load kips	Number per Month
Under 3	3	245
3 - 7	5	4409
7 - 8	7.5	1236
8 - 12	10	2899
12 - 16	14	1344
16 - 18	17	1565
18 - 20	19	282
20 - 22	21	15.0
22 - 24	23	5.4
24 - 26	25	33.6
26 - 30	28	3.8
30 - 35	32.5	0.1

The daily variation was assumed to conform to a typical pattern exhibited in California interstate general purpose routes and shown in Fig. 100.

Prediction of Service Life

Using the format shown in Fig. 2 together with the data presented in this section it is possible to make an estimate of the service life for the Morro Bay pavement considering the fatigue mode of distress.

As indicated in Report No. TE 67-4 (60), the reasonableness of the procedure has been checked against deflections as measured by the Traveling Deflectometer.

Material Properties. In addition to the material properties, summaries of which have been presented earlier, i. e.

1. Subgrade soil Fig. 97
2. Untreated aggregate subbase Fig. 98
3. Untreated aggregate base Fig. 99
4. Asphalt concrete (stiffness) Table 18*

*The time of loading employed in the tests, the result of which are shown in Table 18, was 0.1 sec. To obtain stiffnesses corresponding to moving traffic, (0.015 sec. - representative of truck speeds of about 30 mph), the Shell procedure was utilized. However, the estimations were influenced by the measured data shown in Table 18.

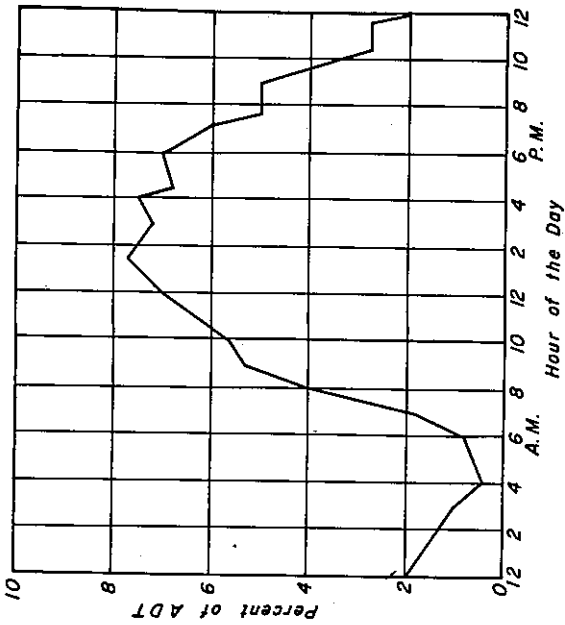


Fig. 100 - Hourly traffic variation, California General Purpose Interstate Route.

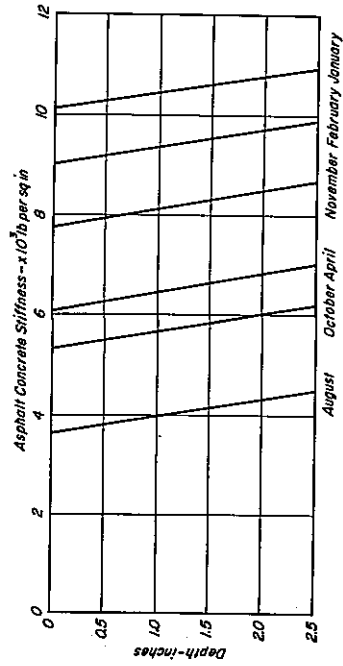
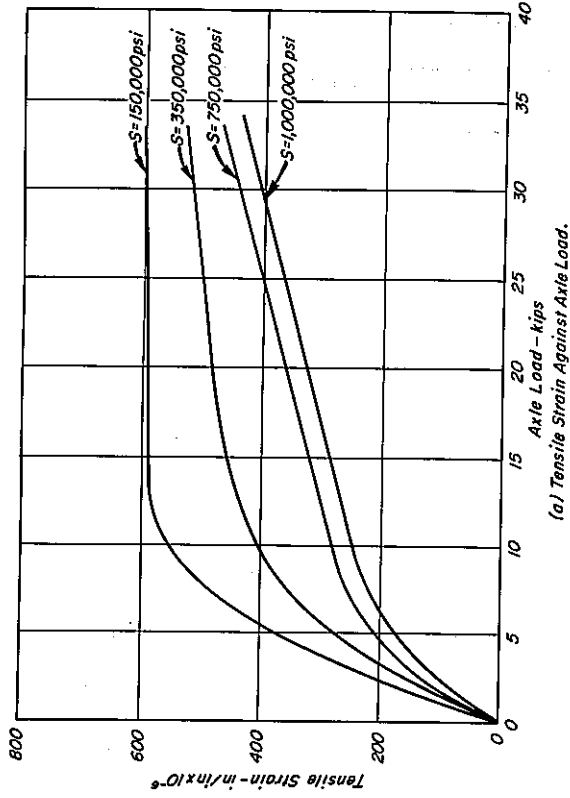
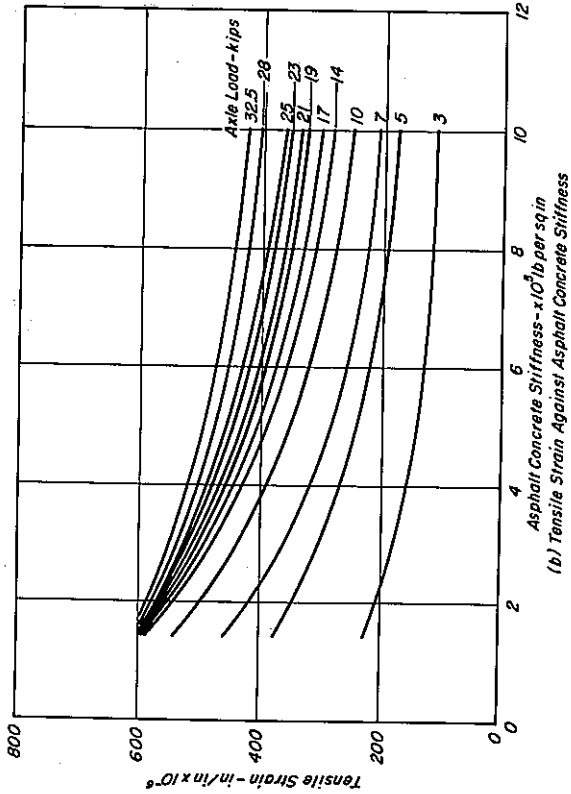


Fig. 102 - Traffic weighted mean stiffness profiles in several months, Morro Bay pavement.



(a) Tensile Strain Against Axle Load.



(b) Tensile Strain Against Asphalt Concrete Stiffness

Fig. 101 - Results of structural analysis of Morro Bay pavement showing maximum tensile strain at bottom of the asphalt concrete layer.

TABLE 34 — WEATHER RECORD DATA FOR MORRO BAY, CALIFORNIA

Month	Avg. Air Temp.	Daily Air Temp. Range	Avg. Wind Velocity	Solar Insol.*	Sky Cover
Jan.	51.0	24.	6.7	269	6.1
Feb.	52.0	23.	7.2	350	5.8
Mar.	54.0	23.	8.3	482	5.6
Apr.	56.0	22.	8.0	569	5.1
May	57.0	21.	8.3	631	4.8
June	58.0	20.	7.9	692	3.7
July	60.0	19.	6.5	681	3.0
Aug.	60.0	19.	6.2	612	3.4
Sept.	60.0	23.	5.9	520	3.1
Oct.	59.0	26.	6.2	413	4.1
Nov.	55.0	28.5	6.6	309	5.2
Dec.	50.0	25.	6.4	251	6.1

*Langley's per day.

TABLE 35 — TRAFFIC WEIGHTED MEAN STIFFNESSES FOR 2.5 INCH ASPHALT CONCRETE LAYER AT MORRO BAY

Month	Stiffness, psi
Jan.	1,053,000
Feb.	947,000
Mar.	799,000
Apr.	655,000
May	580,000
June	457,000
July	362,000
Aug.	406,000
Sept.	437,000
Oct.	577,000
Nov.	822,000
Dec.	1,094,000

1. The tensile strain against stiffness curves for each axle load group (Fig. 101) were stored.
2. The tensile strain under each wheel load magnitude was obtained from the appropriate relationship by a numerical interpolation procedure at the stiffness value representing the month under consideration.
3. The fatigue life that would be expected under simple loading at that strain level was determined from the fatigue curve developed for the material. At the same time, the fatigue life corresponding to a 90 percent confidence level was obtained making use of the assumption of a log normal distribution of fatigue life at any strain level.
4. The cycle ratio for each of the strain levels (axle load groups) was formed using the number of applications per month of each axle load group (n_i) shown in Table 33 and the fatigue life at each strain level determined above (N_i).
5. The sum of the cycle ratios per month was taken and the process repeated for consecutive months until first, the sum at the 90 percent confidence level reached unity, and then, the sum at the mean level reached unity.
6. The fatigue life predictions at the two levels of confidence were taken as the times at which these values were obtained.

Using the data presented herein, the shortest probable fatigue life, at a 90 percent level, was calculated to be 0.8 years. The mean fatigue life of the Morro Bay pavement was predicted to be 1.8 years.

Discussion

Assuming that this pavement was opened to traffic on the completion date of the paving contract in October, 1963, some distress should have been evident at the time of the first sampling in December, 1965. This was not the case. A second sampling of the pavement in August, 1967 did, however, show some effects of the onset of fatigue. Fig. 103 shows the crack pattern observed on the underside of the asphalt concrete slab specimens recovered at one of the sample locations at this time.

The condition of these samples conforms to that which would be anticipated after some fatigue damage has occurred. The cracks, as suggested by the location of the maximum strain values, were initiated at the bottom of the asphalt concrete and have progressed upward in the layer, but have not yet reached the surface of the pavement. This condition is approximately the same as that which was observed in the laboratory fatigue tests in the controlled-strain mode of loading, when they had attained their service lives, as de-

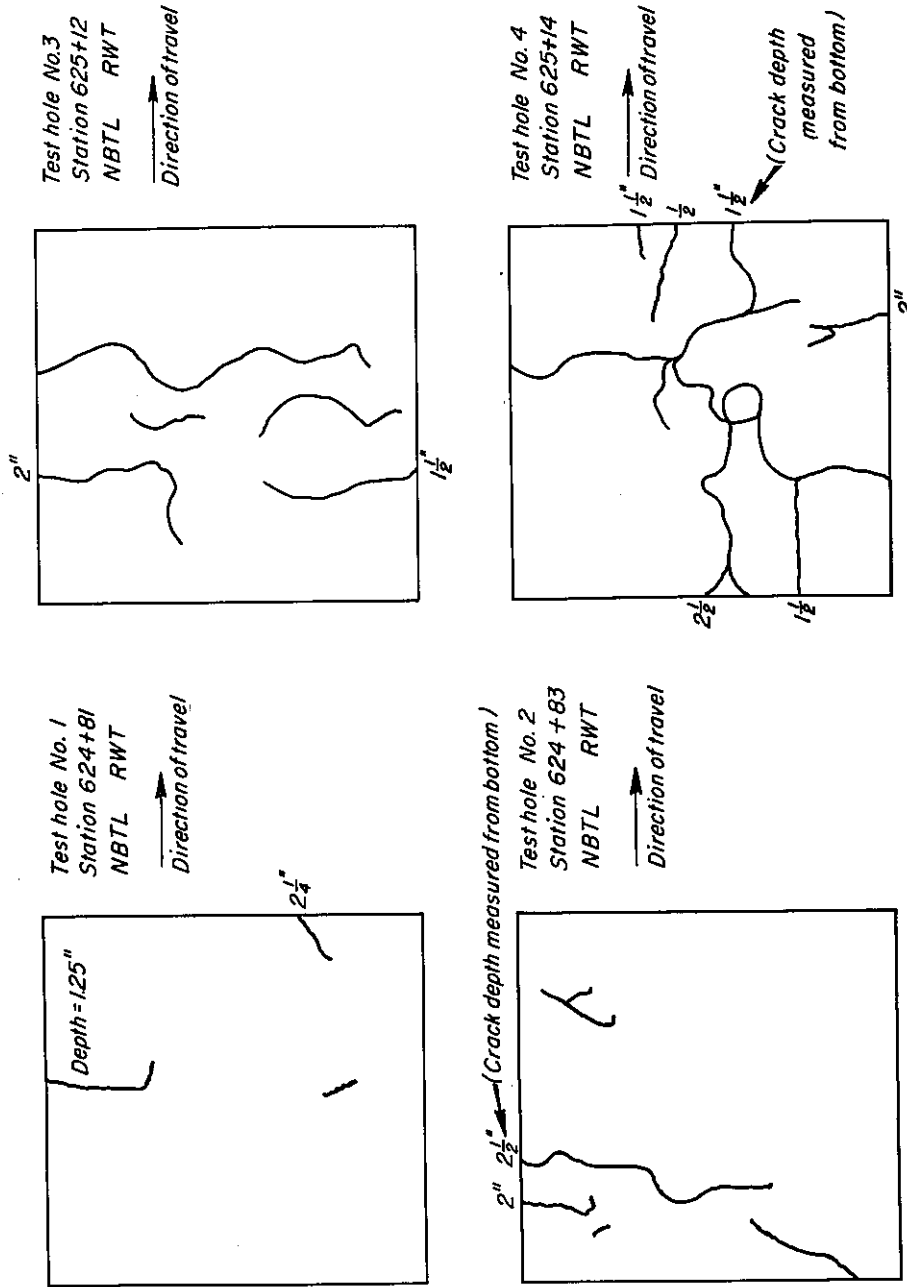


Fig. 103 — Crack patterns on bottom of slabs obtained in vicinity of Sta. 625+00.

fined by a 50 percent reduction in stiffness. In both the laboratory and field situations, then, the effects of this level of fatigue damage is visible only near the location of the maximum repeated strain. It should also be noted that the visible manifestation of this level of damage in the actual pavement will be effectively masked by the thin, open-graded (flexible) surface course overlying the asphalt concrete in the Morro Bay pavement.

Some confidence in the use of the fatigue subsystem is provided by the condition of these samples. Although the predicted life is shorter than that which has actually been experienced in the pavement studied, the type of distress shown does conform to that which is anticipated. The conservative nature of the prediction is to be expected on the basis of the discussion of the method, but several features of this particular analysis deserve comment as contributors to the discrepancy between the predicted and the observed performance.

One probable cause of the difference lies in the use of a wheel load distribution based on the results of statewide loadometer surveys for the fatigue life simulation. While the use of such data is suggested for the design situation in which no other information is available, a survey of the traffic actually using the facility is preferred when analyzing an in-service pavement such as Morro Bay. Considering the nature of this highway and the area which it serves, it is probable that the statewide data overestimate the proportion of heavy wheel loads to which the actual pavement is subjected, resulting, in turn, in an overestimate of the calculated rate of damage accumulation. (Note: a similar comment could also be made with respect to the design analysis, emphasizing the necessity of accurate traffic predictions.)

A second reason for the difference between predicted and actual behavior is the use of an average condition for the degree of saturation of both the base and subbase materials. Although it is probable that conditions more severe than those assumed for this estimate have occurred during the life of the pavement, it is equally probable that less severe conditions could be assumed for longer time periods within the year. Insufficient field data, however, were available to account for this probability. This point also emphasizes the importance of properly defining the conditions of the paving materials in order to make a reasonable assessment of the response of the pavement to load. Since the computer is being utilized it would involve only a small amount of additional input to consider the influence of moisture on the resilient response of granular materials and, in effect, would merely require the stipulation of a family of curves rather than a single curve.

Finally, the difference between estimated and observed performance may also be at-

tributed to the use of one laboratory determined fatigue curve rather than the family of curves illustrated schematically in Fig. 96.

Prediction of Service Life - Folsom Project (03-SAC, Ed-50)

Materials Characterization. Sampling locations (Appendix E) and results of fatigue tests on the asphalt concrete have already been described for the Folsom project.

Granular base and subbase materials were obtained at the same locations to determine in-place densities and water contents as well as gradations. Additional samples for laboratory test specimen preparation were obtained from the Pacific Coast Aggregates plant at Fair Oaks, California.

Subgrade samples were also obtained from the four test locations for in situ densities, water contents and gradations.

Subgrade Soil. Subgrade soils at locations 1 and 2 (control section) were described as a combination of weathered slate, lava conglomerate and silty clay and at locations 3 and 4 (experimental section) as dredger tailings, red silty clay and cemented cobbles*. Afterberg limits for the materials are:

<u>Location</u>	<u>Liquid Limit</u>	<u>Plastic Limit</u>	<u>PI</u>	<u>Unified Classification</u>
1	33	20	13	CL
3	25	19	6	CL
4	30	29	1	ML

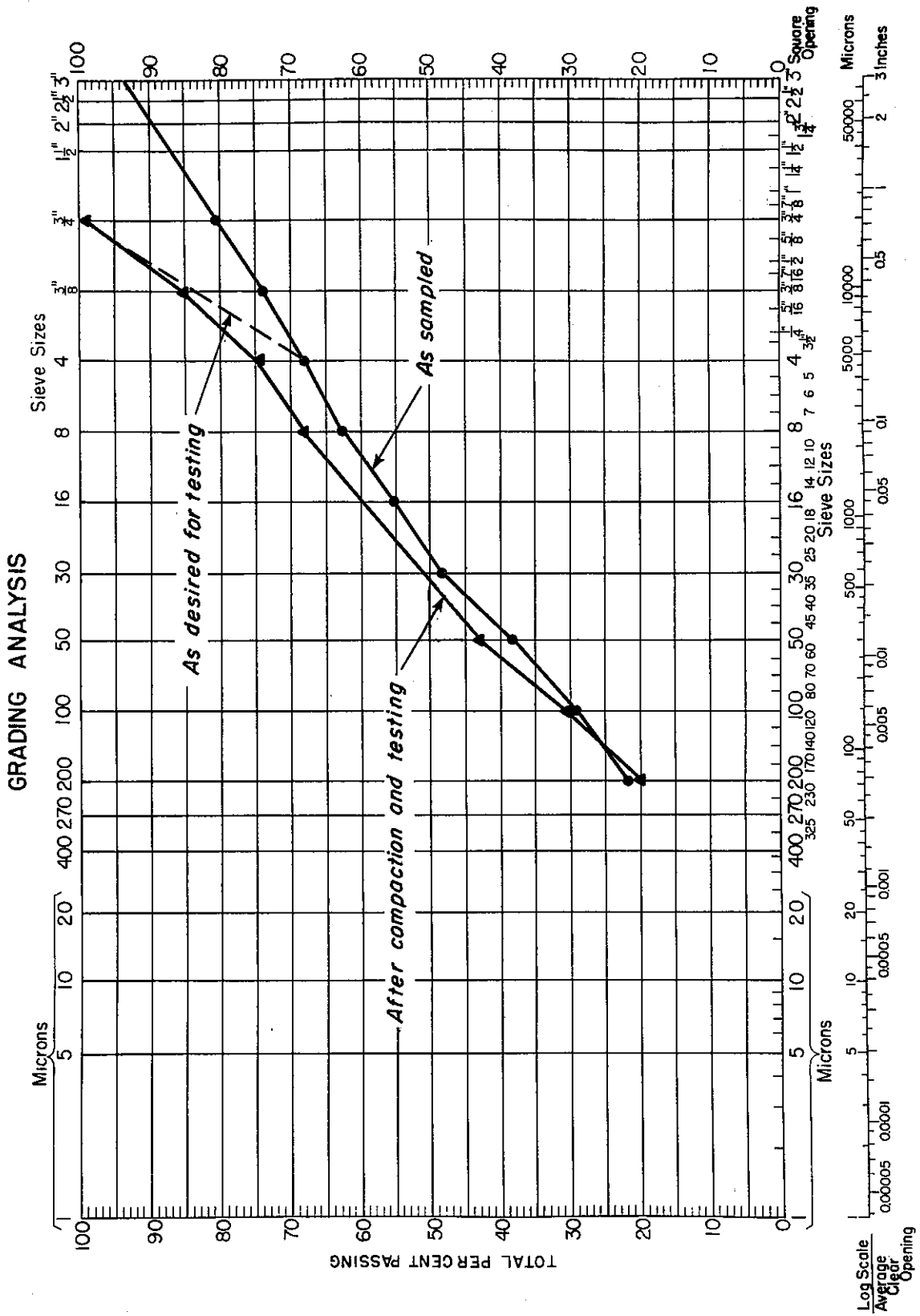
A typical grading curve for the materials is shown in Fig. 104.

Samples for laboratory resilience testing were prepared by separating the soil into three size fractions: passing No. 4 sieve, 3/4 in. by No. 4, and retained on 3/4 in. sieve. To attempt to duplicate the field conditions, in the laboratory specimen the weight of material passing the No. 4 sieve equaled that of the field samples, while material greater than 3/4 in. was wasted and replaced with an equivalent weight of 3/4 in. by No. 4 material.

The modified material was then compacted by kneading compaction into 4 in. diameter by 8 in. high specimens and a series were prepared to cover the range of dry densities and water contents observed in the field sampling program.

Repeated load tests were conducted utilizing a constant cell pressure (σ_3) of three psi and a repeated deviator stress ranging from one to five psi applied at a frequency of 20 repetitions per minute and with a duration of 0.1 sec. Resilient moduli were ascertained

*Descriptions supplied by staff of Materials and Research Department, July, 1967.



from recoverable deformations measured over the center 4 in. of the specimens with dual LVDT's clamped to the membrane surrounding each specimen after 1000 stress repetitions.

From the tests (Table 36) isolines of resilient moduli could be developed in manner similar to that illustrated earlier in Fig. 15. A typical result is shown in Fig. 105 for a repeated deviator stress of two psi. By developing such relationships for a range in deviator stresses a modulus vs. deviator stress relationship could thus be defined for any specified water content and dry density.

TABLE 36 — SUMMARY OF REPEATED LOAD TEST RESULTS FOR
SUBGRADE SOIL, FOLSOM PROJECT*

Site	Test No.	Dry Density lbs/cu ft	Water Content Percent	Resilient Modulus psi $\times 10^{-3}$			Poisson Ratio at $\sigma_d = 3$ psi
				Deviator Stress - σ_d			
				1 psi	2 psi	3 psi	
1	1	133.0	9.6	2.5	1.9	2.2	-
	2	132.2	9.7	7.8	5.2	4.2	0.43
	3	128.2	10.1	1.5	1.7	2.1	0.45
	4	127.4	7.3	2.0	2.6	2.2	-
2	1	134.1	9.8	-	14.0	14.0	-
	1	137.4	8.6	16.0	7.6	9.0	0.58
3	2	122.8	9.1	15.2	14.3	13.9	0.49
	4	139.0	5.8	63.8	54.0	46.8	0.33
	5	136.2	6.3	95.0	56.0	47.6	-
	6	138.4	7.6	63.8	56.1	55.4	0.42
4	1	130.7	9.3	15.9	19.7	12.4	-
	2	130.5	9.8	5.4	6.1	6.4	0.52
	3	130.6	9.4	8.3	6.4	7.2	-0.50

*Confining pressure = 3 psi except for test site 2 material where confining pressure = 2 psi.

Subbase. The subbase material is a well-rounded gravel conforming to the State of California specifications for a Class 1 aggregate subbase (61). Apparent specific gravities of the coarse and fine materials are 2.83 and 2.72 respectively.

Prior to specimen preparation, all material was separated into individual size fractions by dry sieving and material retained on the 3/4-in. sieve was wasted. The grading for the test specimens is shown in Fig. 106; for comparison the average grading of

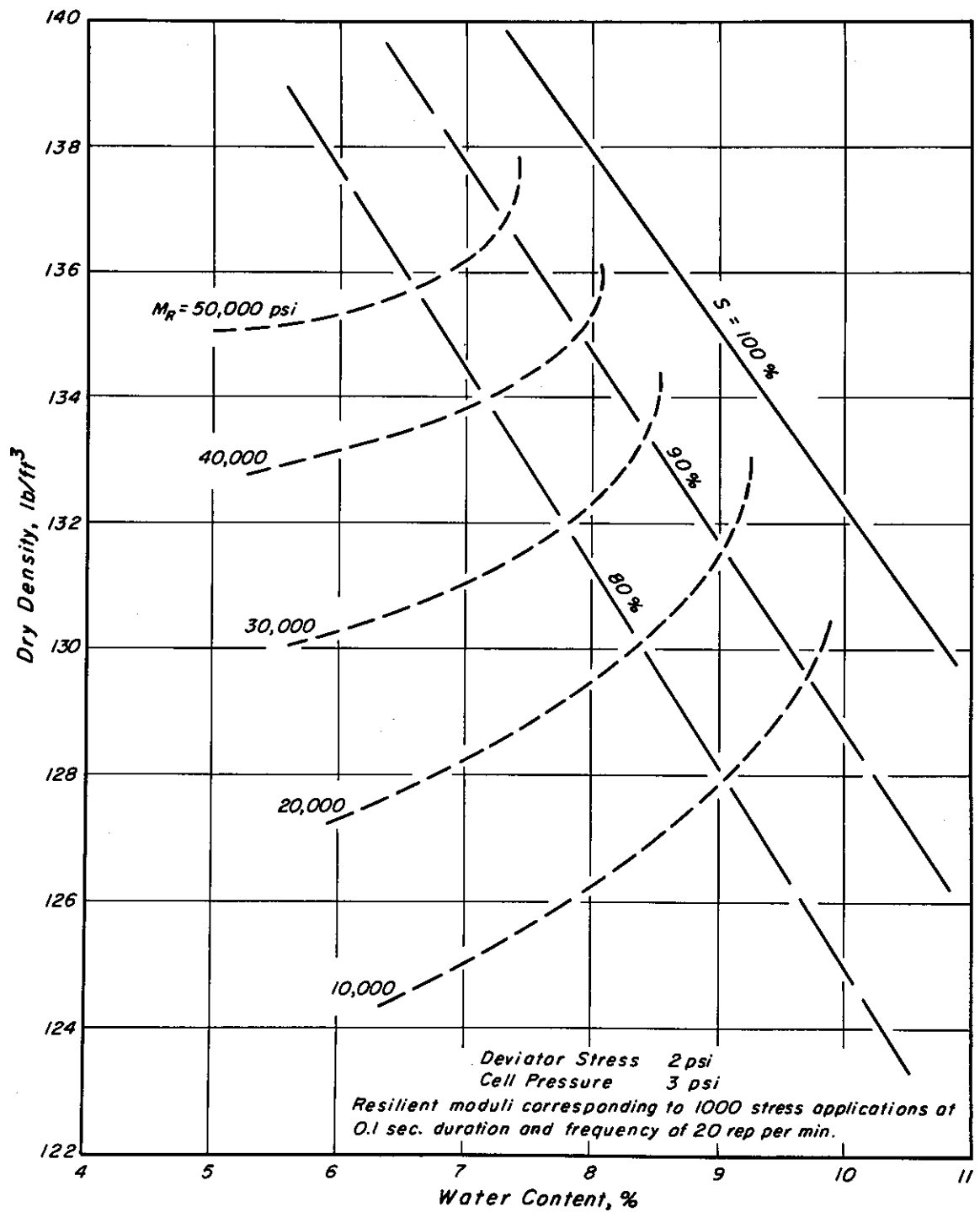


Fig. 105 - Water content - dry density - resilient modulus relationship for Folsom project subgrade soil.

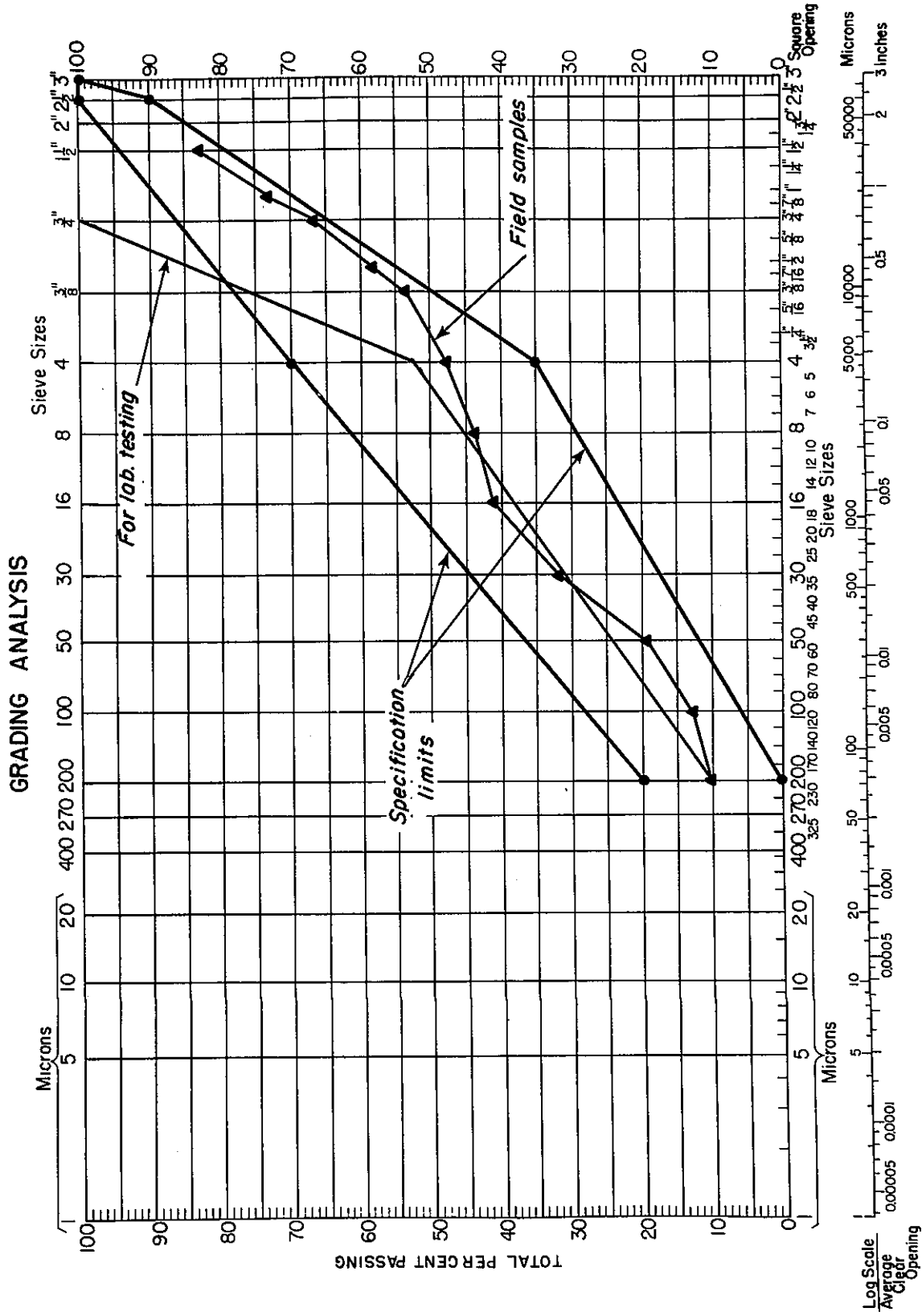


Fig. 106 — Grading curves for field and laboratory samples; subbase material, Folsom project.

the field samples is also shown. It will be noted that the percent by weight passing the No. 4 sieve for the laboratory specimens was maintained the same as that for the field samples. While the plus 3/4-in. material was replaced by an equivalent weight of 3/4 in. by No. 4 material.

Specimens for the repeated load triaxial compression tests were prepared by vibratory compaction at water contents representative of those existing in the roadway at the time of sampling and to densities corrected from field values to account for the modified grading.

The compacted specimens were subjected to a range of repeatedly applied deviator stresses and a range in static cell pressures (σ_3). Results of these tests are presented in Appendix E.

Both axial and circumferential deformations were measured with LVDT's clamped to the central portion of the specimen. Resilient modulus and resilient Poisson's ratio were determined after 200 axial stress repetitions at a particular state of stress for a particular specimen. To minimize the effects of stress history, generally each specimen was first subjected to 200 stress repetitions at an intermediate stress ratio followed by tests over a range in stress ratios from low to high, then in reverse (30).

Linear regression analyses of the logarithm of modulus vs the sum of principal (total) stresses were obtained for each of the nine test series (Appendix E), and for all of the data together. While the results for individual series were generally good (correlation coefficients greater than 0.85) the results for all data together were somewhat poorer reflecting the influence of variations in density and water content.

For the pavement analysis the equation based on all data:

$$M_R = 7730 (\theta)^{0.46}$$

has been utilized (correlation coefficient of 0.68).

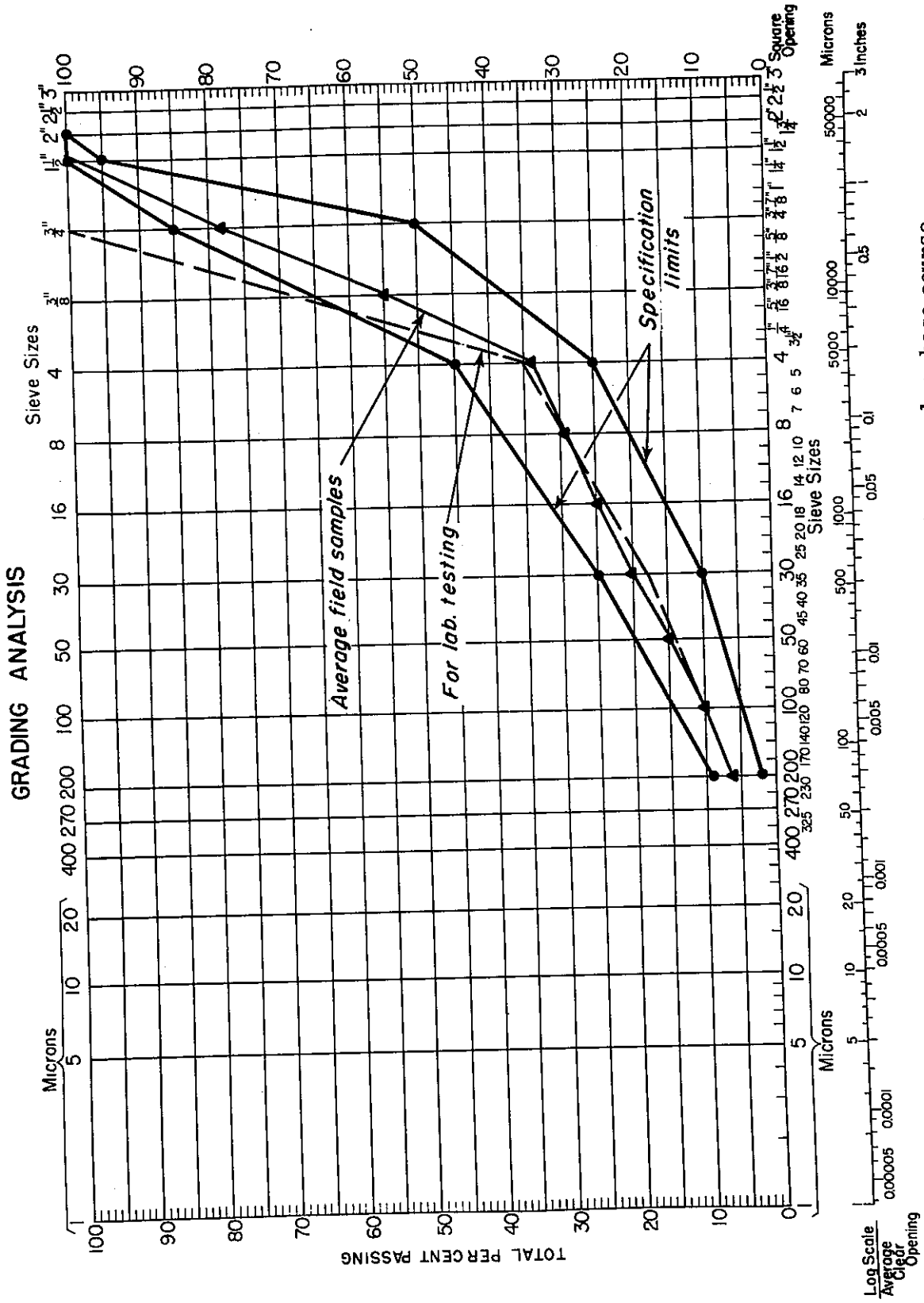
The dependence of Poisson's ratio on stress was also ascertained and the following relationship has been used in the pavement analysis.

$$\nu = 0.13 + 0.05 (\sigma_1 / \sigma_3)$$

Base. The base material is a crushed gravel conforming to the State of California specification for a class 2 aggregate base (61). Apparent specific gravities of the coarse and fine fractions are 2.83 and 2.72 respectively. Fig. 107 contains the grading curves for both the field and laboratory samples.

Resilient moduli were determined in the same manner as for the subbase material and a linear regression using all the test data (Appendix E) resulted in the following relationship:

$$M_R = 3470 (\theta)^{0.65}$$



with a correlation coefficient of 0.96 indicating less scatter than for subbase data.

For Poisson's ratio the relationship:

$$\nu = 0.16 + 0.08 (\sigma_1/\sigma_3)$$

was established.

Asphalt Concrete Surface. Stiffness characteristics of the asphalt concrete from the pavement specimens were determined at only one temperature — 68°F and one time of loading — 0.1 sec. (Table 22). To define the stiffness over the range of temperatures encountered in the field and for a range in times-of-loading, use was made of the Shell procedure together with the following recovered asphalt properties for both base and surface courses (control section):

<u>Location</u>	<u>Course</u>	<u>Pen. at 77°F</u> <u>- dmm</u>	<u>R & B Softening</u> <u>Pt - °F</u>
1	Surface	38	132
1	Base	31	135
2	Surface	26	141
2	Base	28	138

The resulting relationships between mixture stiffness and temperature for times of loading of 0.02 sec. (fast moving traffic) and 0.1 sec. (slow traffic) are shown in Fig. 108.

Poisson's ratio was assumed to vary from 0.30 to 0.35 for the temperature range encountered.

In addition, to estimate the stiffness in situ as a function of temperature using Barber's solution, the asphalt concrete was assumed to have the following thermal characteristics:

Thermal conductivity	- 0.70 BTU ft/ft ² , °F, hr
Specific heat	- 0.22 BTU/lb, °F
Surface coefficient	- 0.85

Analysis of Pavement Response to Load. Fig. 109 illustrates the pavement section as well as the material characteristics and other variables considered in the analysis. For convenience the 7 in. asphalt concrete section was considered as one layer.

As seen in Fig. 109 the stiffness of the asphalt concrete and the resilient properties of the subgrade were considered to be the primary variables affecting the deflection of the pavement under load. The CHEV 5L (w/iteration) program developed by Kasianchuk (44) was used. Since the program only considers a variable modulus in the

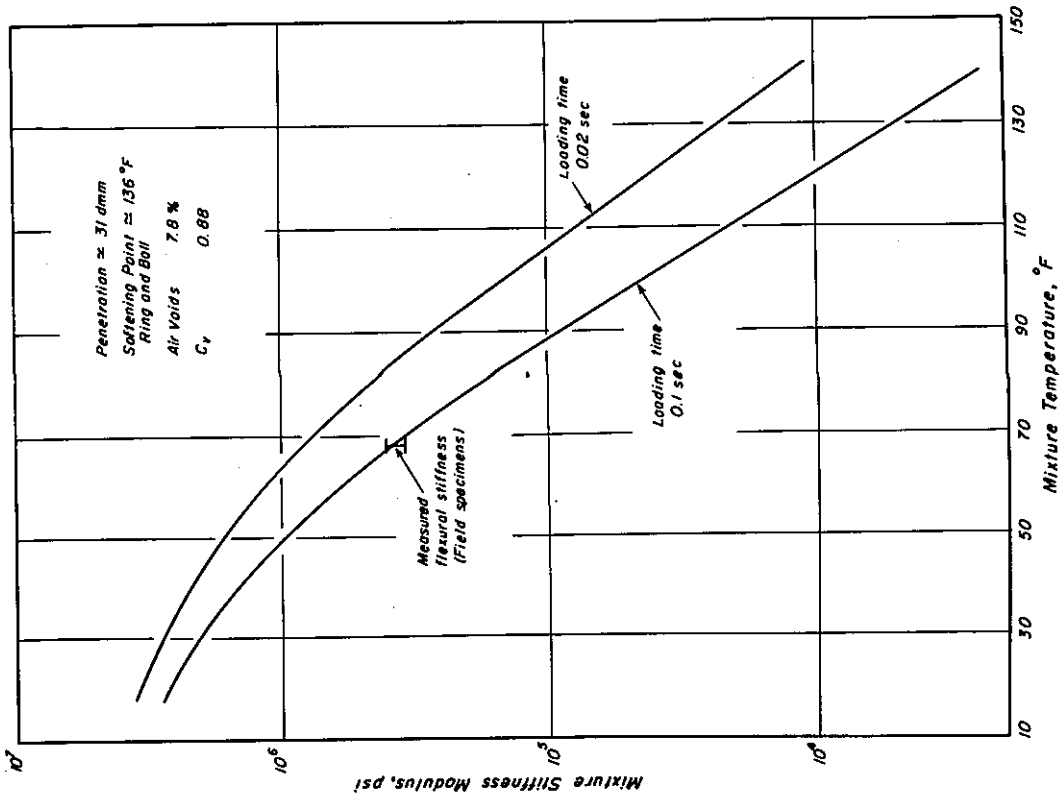


Fig. 108 - Computed relationships between mixture stiffness and temperature - asphalt concrete, Folsom project.

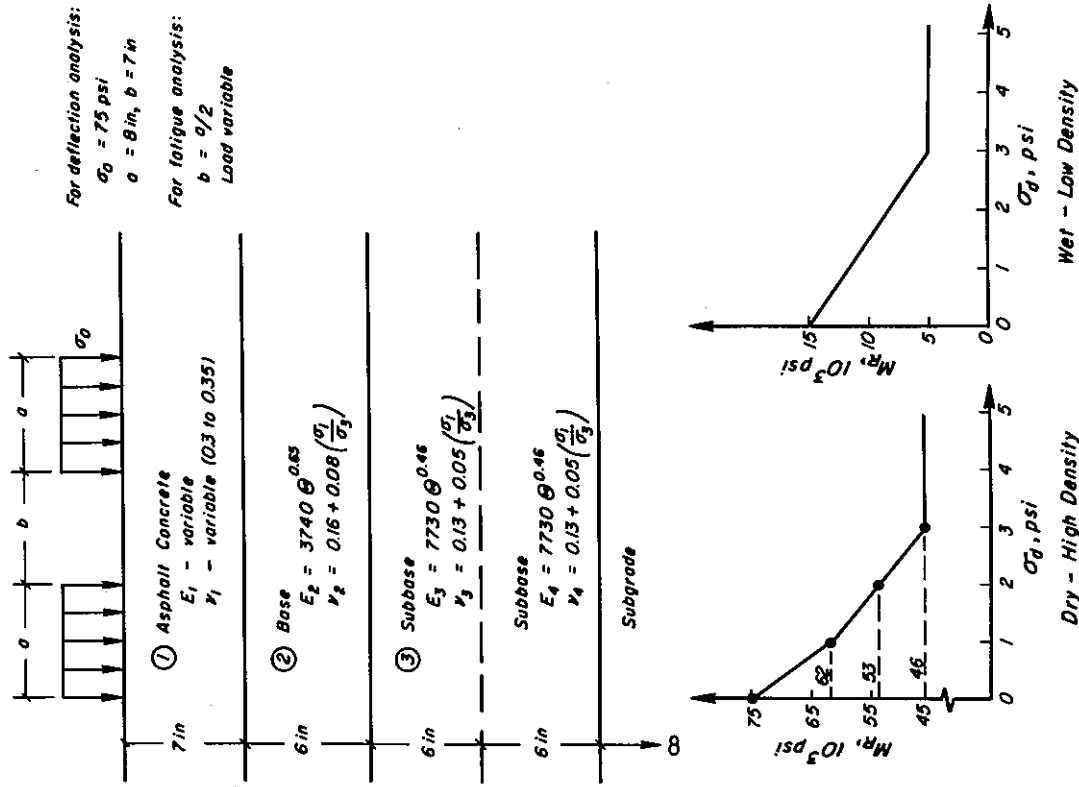


Fig. 109 - Pavement section used in analysis.

granular layers, manual iteration was also required to account for the variability in Poisson's ratio.

Deflections computed by this process are shown in Fig. 110 as a function of the asphalt concrete stiffness. Included are the deflections measured in January 1968. For the temperature conditions at the time of measurement (air temperature - 48°F, surface temperature - 53°F), the asphalt concrete stiffness was estimated to be about 1×10^6 psi (time of loading of 0.1 sec.).

Comparison of the measured deflections with computed values indicates that the dry, high density subgrade condition is most representative of the in situ situation. Hence these subgrade properties have been used in the estimate of fatigue life determined on the next section.

During this analysis it was observed that the vertical stresses at the subgrade surface were of sufficient magnitude (at least 3 psi) so that the modulus could be considered constant. This simplifying assumption has been used in all subsequent calculations.

Estimate of Service Life (Fatigue Analysis). The procedure followed to estimate the potential for fatigue distress in this project differed from that reported in the previous section for the Morro Bay project and might be considered as a "second iteration" in the attempt to realistically consider the effects of traffic and environment as well as the fatigue characteristics of the asphalt concrete.

Traffic. Data from the Perkins (Sac-50-R11-0) recording station, located near the test section, was obtained from the California Division of Highways. Average daily traffic for 1970 was reported to be as follows:

<u>Classification</u>	<u>ADT - 1970</u>
All vehicles	25,000
Trucks	14,000 (100%)
2 axle	800 (57%)
3 axle	100 (7%)
4 axle	100 (7%)
5 or more axles	400 (29%)

The Folsom project was placed in service either in late 1965 or early 1966. Since traffic data are not available for this earlier period, the 1970 data was reduced at a rate of 3 percent per year to obtain the 1966 ADT. Resulting estimates are:

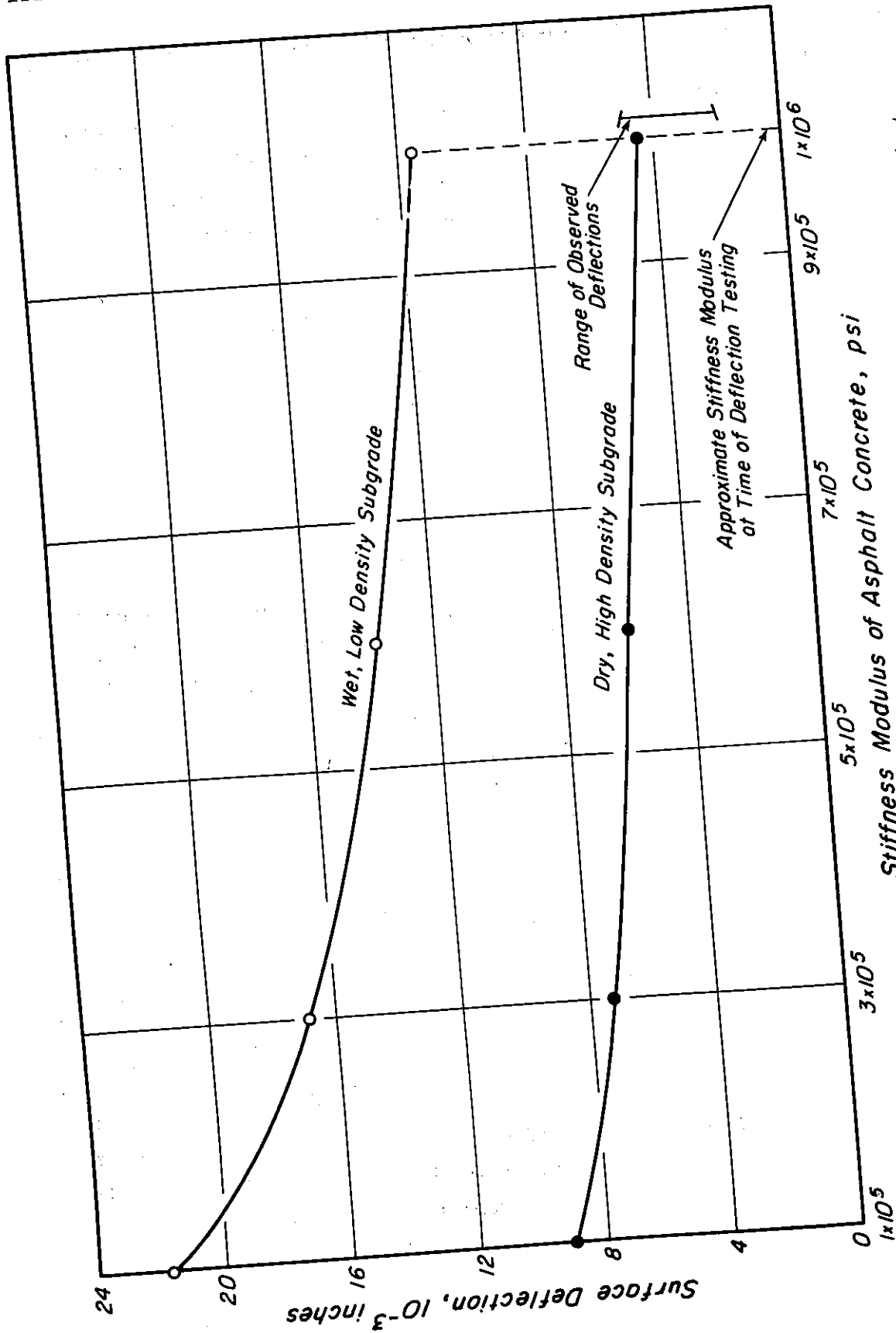


Fig. 110 - Comparison of computed and observed pavement deflections, Folsom project.

<u>Classification</u>	<u>ADT - 1966</u>	<u>(estimated)</u>
Trucks	1242	(100%)
2 axle	708	(57%)
3 axle	87	(7%)
4 axle	87	(7%)
5 axle	223	(18%)
6 axle	137	(11%)

To estimate the truck traffic distribution throughout the day in hourly increments, the average annual statewide data presented in Table 37 was utilized. This data exhibits a smaller proportion of traffic in the midafternoon than was reported earlier and used in the Morro Bay analysis.

TABLE 37 — ANNUAL AVERAGE DAILY TRUCK TRAFFIC
STATEWIDE SURVEY - 1967

	Hour	Percent Traffic		Hour	Percent Traffic
	12-1	2.8		12-1	5.2
	1-2	2.7		1-2	5.6
	2-3	2.9		2-3	5.7
	3-4	3.1		3-4	5.7
	4-5	3.5		4-5	5.4
am	5-6	4.1	pm	5-6	4.5
	6-7	4.2		6-7	3.8
	7-8	4.3		7-8	3.5
	8-9	4.8		8-9	3.3
	9-10	5.0		9-10	3.2
	10-11	5.2		10-11	3.3
	11-12	5.2		11-12	3.0

To relate axle load groups (12 in this analysis) to operations in each classification, the monthly wheel load factors shown in Table 38 were utilized. This is the same procedure described earlier; however, the data in Table 38 are the result of a more recent survey by the California Division of Highways.

Additional assumptions included:

1. Truck operations are equally divided directionally.

TABLE 38 — MONTHLY WHEEL LOAD FACTORS BASED ON
W-4 LOADOMETER STUDIES - CALIFORNIA 1966-1968

Axle Load (kips)	2-Axle	3-Axle	4-Axle	5-Axle	6 or more Axles
Under 3	4.126	0.161	1.034	0.511	1.450
3-7	17.786	16.425	20.904	19.658	21.740
7-8	2.083	6.342	7.498	6.785	8.172
8-12	3.816	12.814	18.334	16.777	32.766
12-16	1.503	6.955	8.203	16.669	19.998
16-18	0.537	1.927	3.322	12.947	4.459
18-20	0.142	0.340	0.627	1.934	0.585
20-22	0.004	0.033	0.101	0.058	0.724
22-24	0.003	0.004	-	0.027	0.227
24-26	-	-	-	0.006	0.204
26-30	-	-	0.009	0.011	0.399
30-35	-	-	-	-	-

- 85 percent of the operations in each direction occur in the lane adjacent to the shoulder (design lane).
- Truck operating speeds correspond to a time of loading of 0.02 sec. in the asphalt concrete.

Analytically the traffic variables were related as follows:

$$AHT_{ij} = ADTT \cdot \frac{A_j}{100} \cdot \frac{HT_i}{100}$$

where:

ADTT = Average daily truck traffic, one direction in design lane.

A_j = percentage of truck traffic of class j (2 axle, 3 axle, etc; tabulation p.143)

HT_i = percentage of truck traffic in the hourly interval i (Table 37).

AHT_{ij} = number of operations of class j in hour i (daily)

and

$$AXLD_{ik} = \sum_{j=1}^S (AHT_{ij} \cdot WLF_{kj})$$

where:

WLF_{kj} = wheel load factors to relate axle class j to axle load group k (Table 38).

$AXLD_{ik}$ = is a matrix of the number of axle loads of group k in each hour i (on a monthly basis)

The $AXLD_{ik}$ values were expanded to an annual basis by incorporating climatic information as described in the following section.

Relation of Climatic Data to Asphalt Concrete Stiffness. Stiffness moduli for the asphalt concrete layer were estimated using the computer solution described earlier. The climatic data utilized for the Folsom area, Table 39, was obtained from records of the Sacramento airport, the nearest location to the test site for which long time records were available. The other information required to determine the effect of temperature on stiffness have been presented in the section describing the asphalt concrete.

TABLE 39 — CLIMATIC DATA — FOLSOM PROJECT*

Month	Average Air Temperature	Daily Air Temp. Range	Avg. Wind Velocity	Solar Insol.	Sky Cover
Jan.	45.2	16.0	8.7	182.0	7.1
Feb.	49.2	18.8	8.7	287.0	5.9
Mar.	53.4	22.8	9.7	426.0	5.5
Apr.	58.4	26.1	9.3	547.0	4.6
May	69.0	28.5	9.8	642.0	3.9
June	70.5	32.1	10.5	701.0	2.0
July	75.4	36.0	9.7	685.0	0.9
Aug.	74.1	35.6	9.7	621.0	1.3
Sept.	71.6	33.2	8.3	506.0	1.7
Oct.	63.5	28.2	7.4	374.0	3.2
Nov.	52.9	22.6	6.8	248.0	5.4
Dec.	46.4	16.5	7.4	157.0	6.9

*Data for Sacramento airport.

In the analysis, the computer solution developed by Kasianchuk was modified to include determination of additional means of temperature and stiffness modulus as shown in Fig. 111 and as follows.

The computer program permits determination of the temperature (T_i) and stiffness (S_i) at the beginning and end of each hour of the day (25 values per day) at each specified depth, d_i .

If w_i is defined as:

$$w_i = \left(\frac{d_i - d_{i-1}}{2} \right) + \left(\frac{d_{i+1} - d_i}{2} \right)$$

(w_i and w_n must be adjusted for the boundaries)

then w_i is the increment of total depth which each T_i and S_i represent.

Means of temperature and stiffness can then be determined:

$$T_{\text{mean}} = \left(\sum_{i=1}^n t_i \cdot w_i \right) / D$$

$$S_{\text{mean}} = \left(\sum_{i=1}^n S_i \cdot w_i \right) / D$$

Twenty-five such values are computed for each day.

By averaging the values for the beginning and end of each hour, a representative value of the stiffness of the asphalt concrete during the hourly increment is obtained. Since the rate of change of stiffness in any mass of asphalt concrete is not large, this averaging was considered to be a reasonable estimate of the mean stiffness during the one hour interval.

Use of the mean stiffness also permits the full depth of asphalt concrete to be represented by a single modulus. While there are some advantages to this simplification (as compared to a characterization of the asphalt concrete as two or more layers), use of the single value has some limitations. For example, a system consisting of soft/stiff layers versus one of stiff/soft layers, both with the same mean, do not exhibit the same stresses and deformations. However, for the approximately sinusoidal distribution of temperature with time used in the analyses, where the heating period is nearly balanced with the cooling period, differences tend to be compensated.

The computations resulted in $24 \times 12 = 288$ values of stiffness modulus to represent the daily and seasonal variation of stiffness modulus. These values were then grouped and the frequency matrix shown in Table 40 prepared. The frequencies shown in this

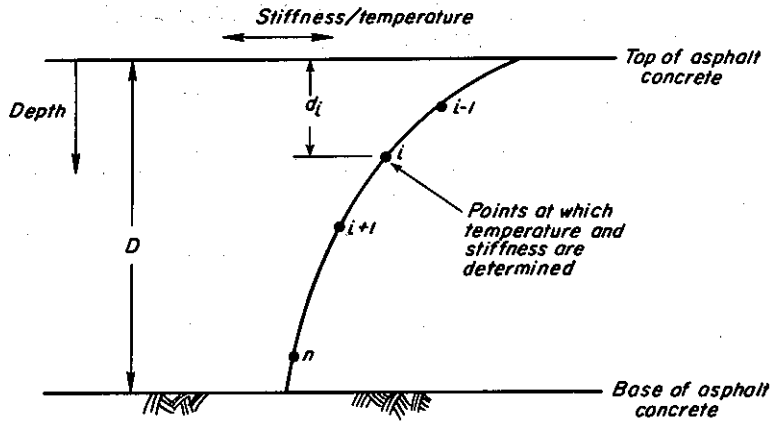


Fig. 111 — Notation for stiffness and temperature determinations.

Fig. 112 — Relation between bending strain on the underside of the asphalt layer and axle load for a range in stiffnesses — Folsom project pavement.

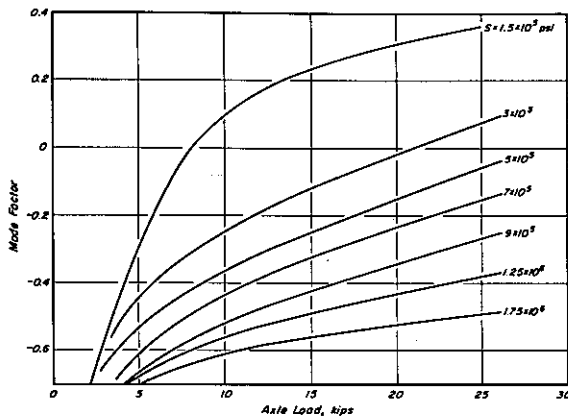
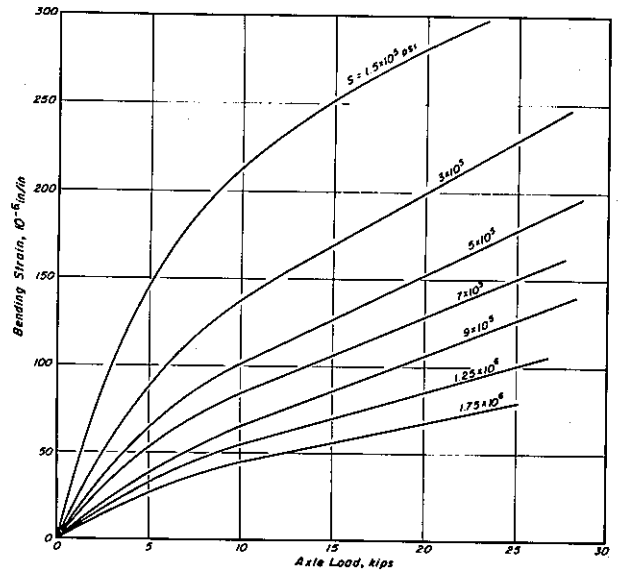


Fig. 113 — Mode factors for the Folsom project pavement as a function of asphalt concrete stiffness and axle load.

TABLE 40 — FREQUENCY OF OCCURRENCE OF PAVEMENT STIFFNESS -
FOLSOM PROJECT PAVEMENT ANALYSIS

Time	Stiffness Group, psi						
	$1.5-2 \times 10^6$	$10^6-1.5 \times 10^6$	$8 \times 10^5-10^6$	$6 \times 10^5-8 \times 10^5$	$4 \times 10^5-6 \times 10^5$	$2 \times 10^5-4 \times 10^5$	$1-2 \times 10^5$
	Midpoint Stiffness, psi						
	1.75×10^6	1.25×10^6	9×10^5	7×10^5	5×10^5	3×10^5	1.5×10^5
12-1	3	3	1	1	3	1	-
1-2	3	3	2	2	2	-	-
2-3	3	3	2	2	2	-	-
3-4	4	2	2	2	2	-	-
4-5	4	2	2	2	2	-	-
5-6	4	2	2	2	2	-	-
6-7	4	2	2	2	2	-	-
7-8	3	3	2	2	2	-	-
8-9	3	3	2	2	2	-	-
9-10	3	3	2	1	2	1	-
10-11	3	2	2	1	3	1	-
11-noon	3	2	1	2	2	2	-
12-1	2	3	1	2	1	3	-
1-2	2	3	-	2	1	3	1
2-3	2	3	-	2	1	3	1
3-4	2	3	-	1	2	2	2
4-5	2	2	1	1	2	2	2
5-6	2	3	-	1	2	1	3
6-7	2	3	-	1	2	1	3
7-8	2	3	-	2	1	2	2
8-9	2	3	-	2	1	2	2
9-10	2	3	1	2	-	4	-
10-11	2	3	1	2	2	2	-
11-12	3	1	2	1	2	2	-

table are the number of months that a given interval of one hour had a mean stiffness in the group shown.

If these frequencies are designated f_{il} , then traffic and stiffness can be related by

$$ADL_{lk} = \sum_{i=1}^{24} (f_{il} \times AXLD_{ik})$$

where:

ADL_{lk} is the annual number of applications of axle load group k to the pavement when the stiffness occurs in stiffness group l

Stress and Deformation Computations. Stresses and deformations at the base of the asphalt concrete were determined using the multi-layer linear elastic solution described previously for a range of axle loads and asphalt concrete stiffnesses.

Results of these computations are shown in Fig. 112 in the form of strain versus axle load with isolines of constant stiffness. Thus the strain corresponding to each of the 11 axle load groups and each of the seven stiffness groups can be obtained.

Fatigue Characteristics of Asphalt Concrete. Fatigue data for the mixtures used in the project, obtained by testing specimens recovered from the road and by testing laboratory prepared specimens have been presented in a previous section (e. g. , Figs. 80-88) and provide a basis for selecting the appropriate data to be used in the performance estimate.

As noted in the section on design considerations, when pavements are in an intermediate range of thickness, consideration should be given to the mode factor (Fig. 96).

For the Folsom pavement, with a 7 in. asphalt concrete layer, stiffnesses were estimated to range from about 100,000 psi to about 2,000,000 psi and it is probable that an intermediate mode of loading (as defined by the mode factor) would be appropriate. To determine this condition (or conditions), mode factors were computed for a range in asphalt concrete stiffnesses and loads as shown in Fig. 113. As seen in this figure, computed values ranged from about -0.7 to +0.4 depending on the wheel load and mix stiffness.

As noted earlier strain vs. fatigue life relationships for intermediate modes of loading will lie between the limits defined by the controlled-stress and controlled-strain modes of loading (Fig. 96). For this analysis, it was assumed that an intermediate mode could be defined by a direct interpolation between the limiting relationships; e. g. , the strain-fatigue life relationship corresponding to a mode factor of zero would lie midway between the two curves.

TABLE 41 - FOLLOU PROJECT - FATIGUE LIFE MATRIX*
 TABLE 41 - FOLLOU PROJECT - FATIGUE LIFE MATRIX*

Axle Load Stiffness	1:5		5		7.5		10		14		17		19		21		23		25		28	
	1	2	3	4	5	6	7	8	9	10	11	12	13	14	15	16	17	18	19	20	21	22
1.75x10 ⁶	ε	9	26	45	54	61	65	70	75	78	86											
	MF	-1	-0.8	-0.65	-0.55	-0.55	-0.55	-0.5	-0.5	-0.5	-0.5											
	N _f	10 ⁹⁹	10 ⁹⁹	10 ⁹⁹	10 ⁹⁹	10 ⁹⁹	10 ⁹⁹	10 ⁹⁹	3.3x10 ⁶	2.5x10 ⁶	2.1x10 ⁶	1.4x10 ⁶										
1.25x10 ⁶	ε	11	33	46	55	66	76	82	88	94	108											
	MF	-1	-0.7	-0.6	-0.55	-0.50	-0.50	-0.45	-0.45	-0.4	-0.35											
	N _f	10 ⁹⁹	10 ⁹⁹	10 ⁹⁹	10 ⁹⁹	10 ⁹⁹	2.8x10 ⁶	1.95x10 ⁶	1.5x10 ⁶	1.1x10 ⁶	8.8x10 ⁵	6.4x10 ⁵										
9x10 ⁵	ε	13	39	54	65	81	93	102	110	118	138											
	MF	-1	-0.65	-0.6	-0.50	-0.45	-0.4	-0.35	-0.35	-0.3	-0.2											
	N _f	10 ⁹⁹	10 ⁹⁹	10 ⁹⁹	10 ⁹⁹	2.75x10 ⁶	1.7x10 ⁶	1.2x10 ⁶	7.6x10 ⁵	6.2x10 ⁵	5.0x10 ⁵	3.6x10 ⁵										
7x10 ⁵	ε	18	53	71	84	101	115	124	132	141	163											
	MF	-1	-0.6	-0.5	-0.45	-0.35	-0.3	-0.25	-0.2	-0.2	-0.1											
	N _f	10 ⁹⁹	10 ⁹⁹	6.5x10 ⁶	3.6x10 ⁶	1.8x10 ⁶	1.15x10 ⁶	8.4x10 ⁵	6.8x10 ⁵	5.4x10 ⁵	4.3x10 ⁵	3.2x10 ⁵										
5x10 ⁵	ε	23	64	86	102	122	136	148	158	168	194											
	MF	-1	-0.5	-0.45	-0.35	-0.3	-0.2	-0.2	-0.15	-0.1	-0.05											
	N _f	10 ⁹⁹	10 ⁹⁹	4.5x10 ⁶	2.7x10 ⁶	1.45x10 ⁶	1.0x10 ⁶	7.1x10 ⁵	5.8x10 ⁵	4.9x10 ⁵	4.0x10 ⁵	2.8x10 ⁵										
3x10 ⁵	ε	30	87	116	138	163	180	194	206	218	250											
	MF	-1	-0.4	-0.3	-0.25	-0.15	-0.1	-0.05	0.0	0.05	0.1											
	N _f	10 ⁹⁹	7x10 ⁶	2.4x10 ⁶	1.4x10 ⁶	9.5x10 ⁵	6x10 ⁶	5.2x10 ⁵	4.4x10 ⁵	3.9x10 ⁵	2.7x10 ⁵											
1.5x10 ⁵	ε	54	146	165	212	246	264	275	285	295	318											
	MF	-1	-0.3	0.0	0.1	0.2	0.3	0.3	0.3	0.35	0.4											
	N _f	10 ⁹⁹	1.6x10 ⁶	9.5x10 ⁵	7.2x10 ⁵	3.8x10 ⁵	3.3x10 ⁵	2.9x10 ⁵	2.4x10 ⁵	2.2x10 ⁵	2.0x10 ⁵	2.2x10 ⁵										

ε = in. per in. x 10⁶

* Shell Laboratory Data, N_f = ∞ at ε < 70 x 10⁻⁶ in. per in.

To obtain some measure of the difference, controlled-strain tests were performed at 68°F (as noted earlier); Fig. 89 provides some indication of this difference in response. The selected curve is based on a 40 percent reduction in stiffness at high strains and on 50 percent reduction at low strains. This particular curve has been plotted together with the actual test data in Fig. 114.

Comparison of the controlled-stress and controlled-strain data (68°F) are shown in Fig. 115. Lines representing the intermediate modes are also shown. The data are based on specimens whose stiffnesses were in the range 160,000 to 170,000 psi. To cover the range in stiffnesses anticipated some adjustment was necessary in the data and a series of relationships like that shown in Fig. 115 are required to cover the range of stiffness expected in-service.

For example, for a stiffness of 150,000 psi (the lowest value used in the analysis) the controlled-stress relationship was steepened slightly and the controlled-strain relationship made flatter. Similar adjustments were also made for other stiffnesses. At stiffnesses greater than 700,000 psi the controlled-stress and controlled-strain lines were assumed to coincide (this decision being based on the experience of other investigators (e. g. 46)).

Fatigue Life Prediction. Data necessary to complete the fatigue analysis was set up in the form shown in Table 41. The strain corresponding to each stiffness modulus and axle load group was obtained from Fig. 112. A mode factor was then obtained from Fig. 113. The number of repetitions to failure for the strain level and mode factor could then be obtained from a series of charts of the form of Fig. 115. These repetitions were designated $ENNF_{\ell k}$, where ℓ is the stiffness group and k is the axle load group. Then

$$\sum_{\ell} \sum_k (APL_{\ell k} / ENNF_{\ell k}) = \text{Annual Damage}$$

Traffic values were then incremented by an expansion factor (3 percent) and the process repeated until the total damage was equal to one.

Fatigue life predictions were made using three sets of strain-repetitions to failure relationships. The relationships and the predicted fatigue life were as follows:

1. Fatigue life was based on tests of laboratory results using the control asphalt, that is the test data described in the previous section. Individual estimated lines were linearly extrapolated to the full range of strain computed. This data resulted in a predicted fatigue life of 9.5 years.

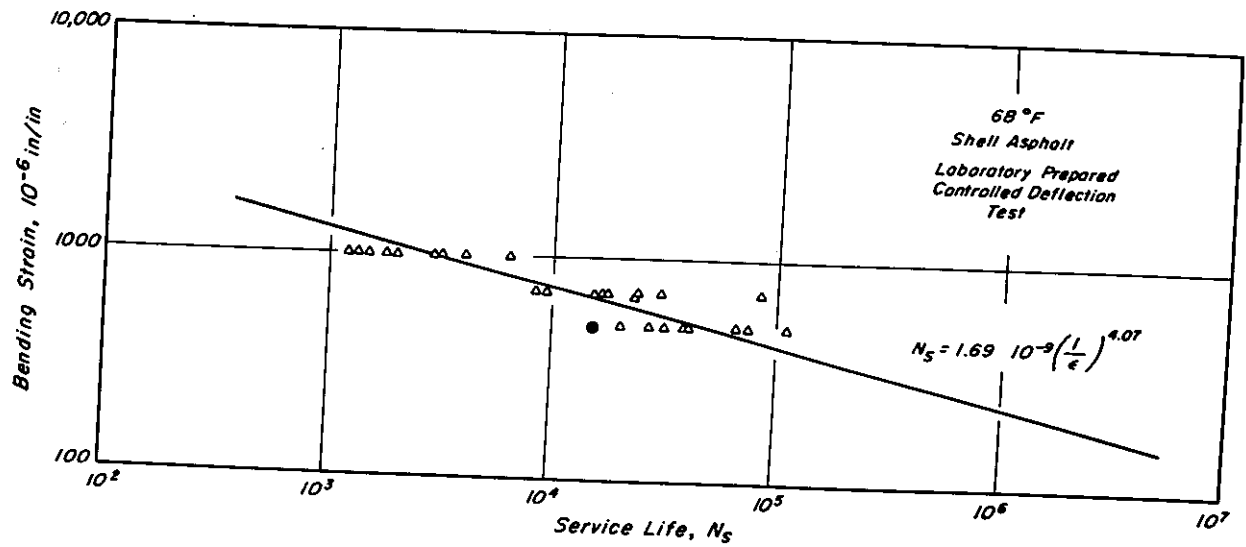


Fig. 114 - Initial bending strain vs. service life in controlled-strain (deflection) tests on laboratory prepared specimens with Shell asphalt; 68°F.

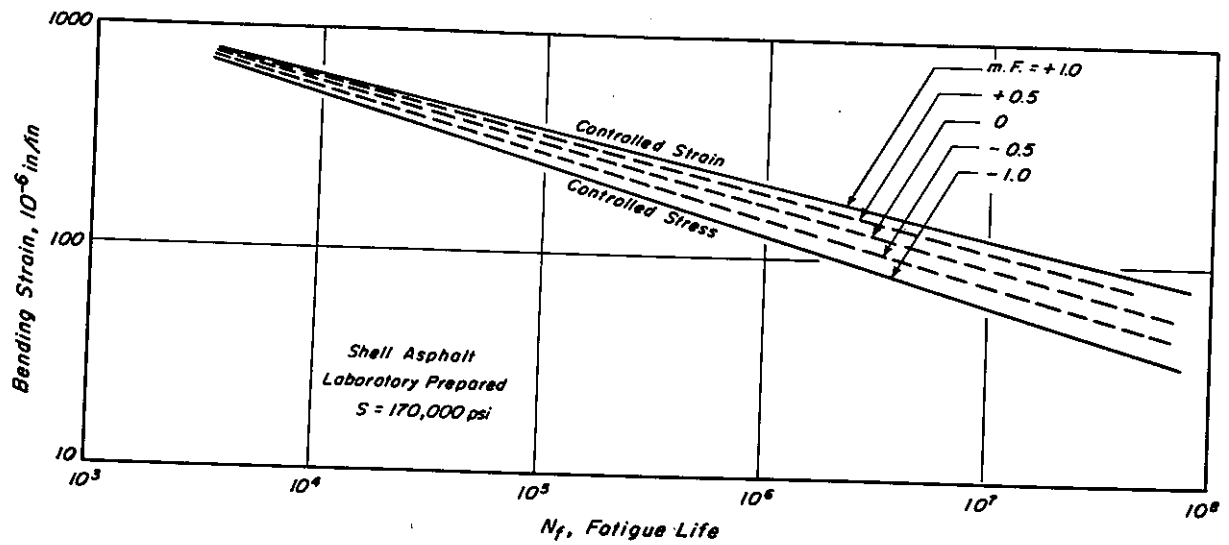


Fig. 115 - Fatigue curves for Folsom project asphalt concrete including those for a series of intermediate modes-of-loading.

2. Same data as (1) except that the assumption was made that strains less than 70×10^{-6} in. per in. caused no fatigue damage (Fig. 95). The purpose of this calculation was to estimate the cumulative effect which the large number of small loads have on the fatigue life estimate. This data resulted in a predicted fatigue life of 12 years.
3. A set of relationships were estimated from results of tests on specimens obtained from the field surface course layer. Strain less than 70×10^{-6} in. per in. were again excluded. This data resulted in a predicted fatigue life of 6 years.

Discussion. In this example the California Division of Highways had designed the pavement to exhibit a 10 year life. Using the measured traffic data for 1970 with reasonable extrapolations to both the initial and later stages of its service life, the pavement can be expected to perform reasonably from a fatigue standpoint. That is, based on the mean fatigue data, a service life in the range 9 to 12 years appears feasible.

The fact that a longer (and reasonable) life was obtained recognizing the changed loading conditions (as compared to the Morro Bay example for which only one fatigue curve was used) suggests that one fatigue curve may not be suitable for design purposes. Rather, families of curves (e. g. , Fig. 95) with results based both on controlled-stress and controlled-strain loading may be required, particularly for pavements with asphalt-bound layers 6 in. in thickness or less.

Design Example — Ygnacio Valley Road, Contra Costa County

To illustrate the applicability of the subsystem for design, an example will be presented illustrating the design of the structural section for the widened portion of the Ygnacio Valley Road between Walnut Avenue and Oak Grove Road in the City of Walnut Creek and the unincorporated areas of Contra Costa County, California. The proposed reconstruction includes the overlay of the existing two-lane pavement plus the widening of the facility to four lanes by the addition of new 12-ft wide traffic lanes on each side of the present roadway all of which was to be designed for a 10-year life.

A full depth asphalt concrete section was considered for the new construction involved with the widening, primarily to alleviate the problems that would be encountered if excavation were required for a thicker structural section. Since the surface grade elevation is fixed by the existing roadway, a conventional structural section could be accommodated only by excavating into the silty clay subgrade soil whose water content increased with depth. It was the previous experience of the Materials Division of the Public Works Department of Contra Costa County that both excavation and compaction

difficulties would be met in this situation. A thinner all-asphalt concrete section would not require this excavation, and the anticipated construction problems could be avoided.

A second factor, not considered during the selection of the design section, but nevertheless important to the design deliberations, is the possibility of the occurrence of saturated base conditions were a conventional section constructed. The reconstruction contemplated the use of a landscaped median strip which would be irrigated. Because of the flat topography of the area and the characteristics of the subgrade soil, it is possible that any water reaching the base from the irrigation operation would remain in the section unless expensive drainage facilities were provided.

A third factor influencing the decision was the development of capabilities for the placement of asphalt concrete in thick lifts (greater than 4 in. compacted at one time) and the attendant economies in construction.

Two design procedures have been utilized. The first is based on a single fatigue curve and the use of the traffic weighted stiffness concept for a 10 year design and for a specific traffic estimate. The second is for a range in traffic, the more generalized fatigue consideration (Fig. 95), and for a 20 year design period. The first is described in the following paragraphs while the second is included as Appendix G.

Traffic. Estimated traffic to be served by the facility for a 10-year period is shown in Table 42.

Several other features of the traffic on the new facility were also estimated on the basis of available information. Since it was known that a major source of truck traffic on this road would be two quarries providing aggregate for construction in the surrounding areas, some consideration was given to the operations in these quarries to obtain the daily and seasonal variations in traffic. This led to the assumption that the daily variation for a California Interstate general purpose route would adequately represent the anticipated pattern. The seasonal variation expected was one in which higher traffic volumes would be handled during the summer months, and to include this expectation, the monthly traffic numbers shown in Table 42 were proportioned accordingly. The values were increased to 1.2 times those shown in the months May to September, inclusive, and reduced to 0.8 times those shown in the months November to March, inclusive.

Materials Characterization. For the asphalt concrete mix variation in stiffness with depth and throughout the year is illustrated in Fig. 116. This stiffness was determined at a time of loading of 0.015 sec. (which would correspond to vehicles moving in the speed range to 30 to 40 mph) and for the environmental data of Table 43.

TABLE 42 — ESTIMATED AXLE LOAD DISTRIBUTION
YGNACIO VALLEY ROAD

Axle Load Group kips	Axle Load kips	Number per Month
Under 3	3	515.1
3 - 7	5	7,924.6
7 - 8	7.5	1,955.7
8 - 12	10	4,174.5
12 - 16	14	1,816.6
16 - 18	17	1,913.4
18 - 20	19	348.2
20 - 22	21	18.4
22 - 24	23	5.9
24 - 26	25	1.6
26 - 30	28	0.8
30 - 35	32.5	0.1

TABLE 43 — WEATHER DATA USED IN THE SIMULATION OF PAVEMENT
TEMPERATURES, YGNACIO VALLEY ROAD

Month	Avg. Air Temp. °F	Daily Range °F	Avg. Wind Velocity mph	Solar Insolation Langleys per Day	Sky Cover (Sunrise to Sunset)
Jan.	46	18	6.2	182	7.0
Feb.	48	21	7.0	287	6.0
Mar.	52	23	8.8	426	5.5
Apr.	59.5	26	9.3	547	4.8
May	61.5	28	9.9	642	3.8
June	66	31	9.8	701	2.0
July	69	33	9.1	685	0.9
Aug.	72	33	8.9	621	1.1
Sept.	66.5	31	7.7	506	1.4
Oct.	62.5	27	6.6	374	3.3
Nov.	54	21	5.8	248	5.3
Dec.	44.5	13.5	5.8	157	7.2

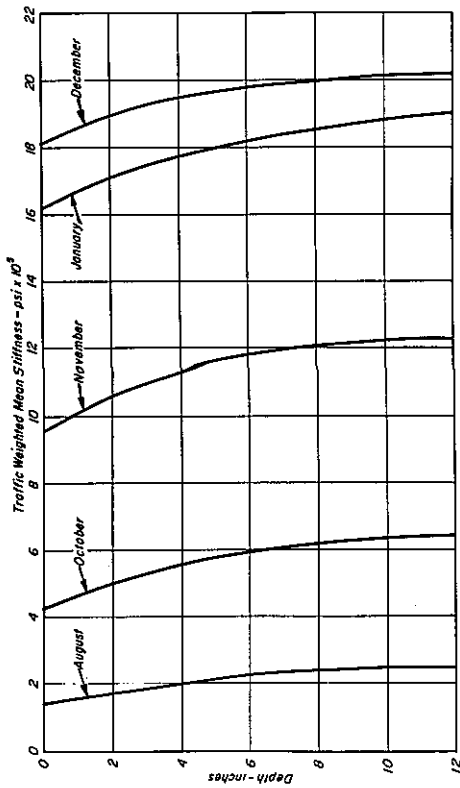


Fig. 116a - Traffic weighted mean stiffness of asphalt concrete vs. depth for various months during the year.

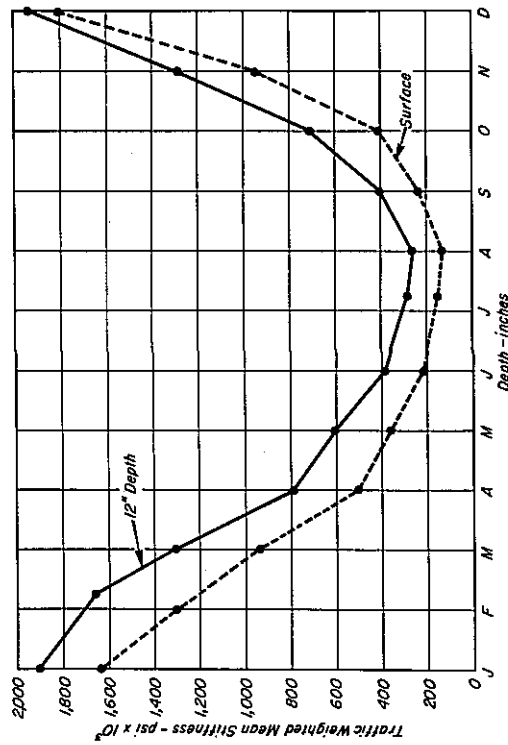


Fig. 116b - Variation of traffic weighted mean stiffness of asphalt concrete throughout the year, both at surface and 12 in. depth.

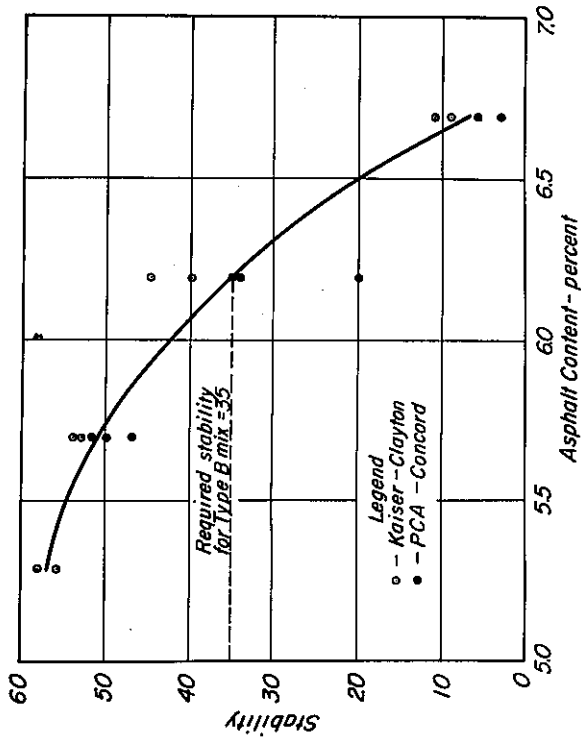


Fig. 117 - Results of stabilometer tests, Ygnacio Valley Road.

Special consideration was given to the design of the asphalt concrete mixture to be used in this pavement to provide a compromise between the stability requirements and requirements for best fatigue resistance.

A mixture was first designed using the standard stabilometer procedure of the State of California (59) by the Materials Division of Contra Costa County. The results of the tests are shown in Fig. 117. Although tests were performed on mixes fabricated using aggregates from each of the two major sources in the area, the results were treated as one set of data, these aggregates being almost identical in terms of petrography, surface texture, and shape throughout the range of sizes. A 60-70 penetration grade asphalt cement supplied by the Chevron Asphalt Company was incorporated in the design mixture to take advantage of the higher stiffness and consequent longer fatigue life that it would afford in this situation. Fig. 117 shows that the asphalt content which satisfies the stability requirement for Type B mixes (i. e. , Stability 35 at 140°F) is 6.2 percent. In line with standard California practice, this value is reduced by 0.3 percent to allow for expected field variation, and the design asphalt content is quoted as 5.9 percent.

At the same time, fatigue test specimens were prepared in the laboratory, containing the same aggregates and with asphalt contents ranging from 5.3 to 8.7 percent. Controlled-stress fatigue tests were performed on these specimens. Data have already been presented for these mixes in a previous section. Fig. 59 shows the mean fatigue lives determined in these tests at a stress level of 150 psi and indicates that the best fatigue performance would be provided by a mixture containing an asphalt content of 6.7 percent.

The elements of the necessary compromise can be seen by comparing the two mixture designs, i. e. , 5.9 percent vs. 6.7 percent. The selection of the optimum design, however, takes some other facts into consideration. The stability requirement is based on the necessity of providing adequate resistance to deformation at the highest temperatures to be experienced by the pavement. This criterion, in general, places a maximum on the amount of asphalt that can be incorporated into the mixture. Consideration of the pavement temperature simulation, however, indicates that the lower portion of a full depth asphalt concrete section will not attain the high maximum temperatures experienced at the surface. Higher asphalt contents can then be tolerated in the lower portion without sacrificing the stability of the layer.

Increase in the asphalt content of a mixture will also provide additional benefits in terms of increased ease of compaction and increased resistance to weathering. Thus, the decision to suggest a higher asphalt content for the mixture to be used in the lower portion of the layer is based on additional criteria to that which would provide the best resistance to fatigue.

On these grounds it was recommended that the uppermost three inches of the section be produced of an asphalt concrete containing 5.9 percent asphalt while the lower portion of the layer contain 6.2 percent.

Analysis and Design. Temperature simulation for this pavement using the data presented in Table 43 indicated that the highest monthly averages would be experienced in August. Such temperatures would result in the least stiff asphalt concrete section in this month. Using typical properties of the materials under these conditions, strains were calculated for 8, 12, and 16 in. thick layers of asphalt concrete under a 9 kip wheel load with dual tires using the iterative procedure to insure compatibility of the vertical compressive stresses at the subgrade and the modulus of the subgrade (Fig. 14). The following summary indicates the levels of strains obtained in these calculations.

Thickness in.	Subgrade Vertical Compressive Strain in. per in. $\times 10^{-4}$	Asphalt Concrete Tensile Strain in. per in. $\times 10^{-6}$
8	5.72	350
12	2.94	167
16	1.90	99

The vertical compressive strain at the subgrade level should be kept below about 6.5×10^{-4} in. per in. according to the Shell criteria for 10^6 repetitions of an 18 kip axle load. From the above summary it can be seen that each of the trial thicknesses provides sufficient thickness to achieve this level during the month when the mixture stiffness is at a minimum.

The fatigue behavior of the asphalt concrete is assumed to be controlled by the horizontal tensile strain on the underside of the asphalt bound layer. A strain level of about 150×10^{-6} in. per in. was considered to be a reasonable maximum value based on previous experience, e. g. , data presented in earlier sections. The value of strain for the 12-in. thickness as seen in the summary above is sufficiently close to this value. Accordingly this thickness was selected for more detailed analysis.

The asphalt concrete layer was represented for the purposes of the layered elastic system calculations as three 4-in. layers whose monthly variations in stiffness values are shown in Table 44.

The complete structural analysis of this pavement is greatly simplified by the fact that the tensile strain in the asphalt concrete can be represented as a linear function of wheel load magnitude for any given condition of asphalt concrete stiffness. In this pavement the only layer whose modulus is a function of stress level and hence, wheel

TABLE 44 — TRAFFIC WEIGHTED MEAN STIFFNESS VARIATION
YGNACIO VALLEY ROAD - (10^3 psi)

Month	Depth, inches		
	0-4	4-8	8-12
Jan.	1,720	1,840	1,890
Feb.	1,410	1,570	1,640
Mar.	1,030	1,250	1,280
April	580	700	770
May	430	535	600
June	245	316	365
July	175	230	270
Aug.	162	210	244
Sept.	267	342	389
Oct.	480	580	636
Nov.	1,030	1,170	1,225
Dec.	1,880	1,980	2,020

load, is the subgrade soil and the variation in stress level in this material is greatly attenuated by the action of the 12-in. asphalt concrete layer. This leads to only small variation in the subgrade modulus with changes in the wheel load, especially when compared with the constant values of stiffness of the asphalt concrete layers in any given month. The number of individual representations of the pavement for the purposes of calculation of the tensile strain in the asphalt concrete need not be compounded by the number of wheel load magnitudes being considered.

The results of the calculation of the tensile strain in the asphalt concrete for the August traffic weighted mean stiffness values are shown in Fig. 118. These calculations were performed taking into account the variation of the subgrade modulus with stress level using the iterative method. It can be seen from this figure that the results may be represented in terms of the slope of the line relating the tensile strain in the asphalt concrete to the axle load magnitude. This slope has been termed the normalized strain, B , such that

$$\epsilon = BW$$

where:

- ϵ = the tensile strain in the asphalt concrete
- W = the axle load magnitude
- B = the normalized strain which is a function of the stiffness of the asphalt concrete in the month under consideration.

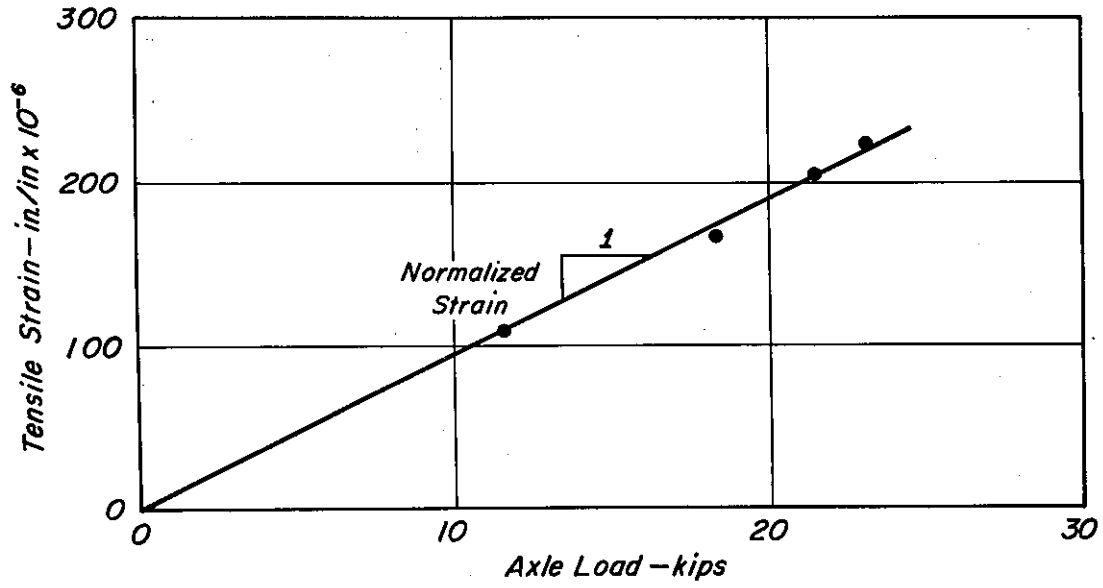


Fig. 118 – Tensile strain against axle load, Ygnacio Valley Road, August.

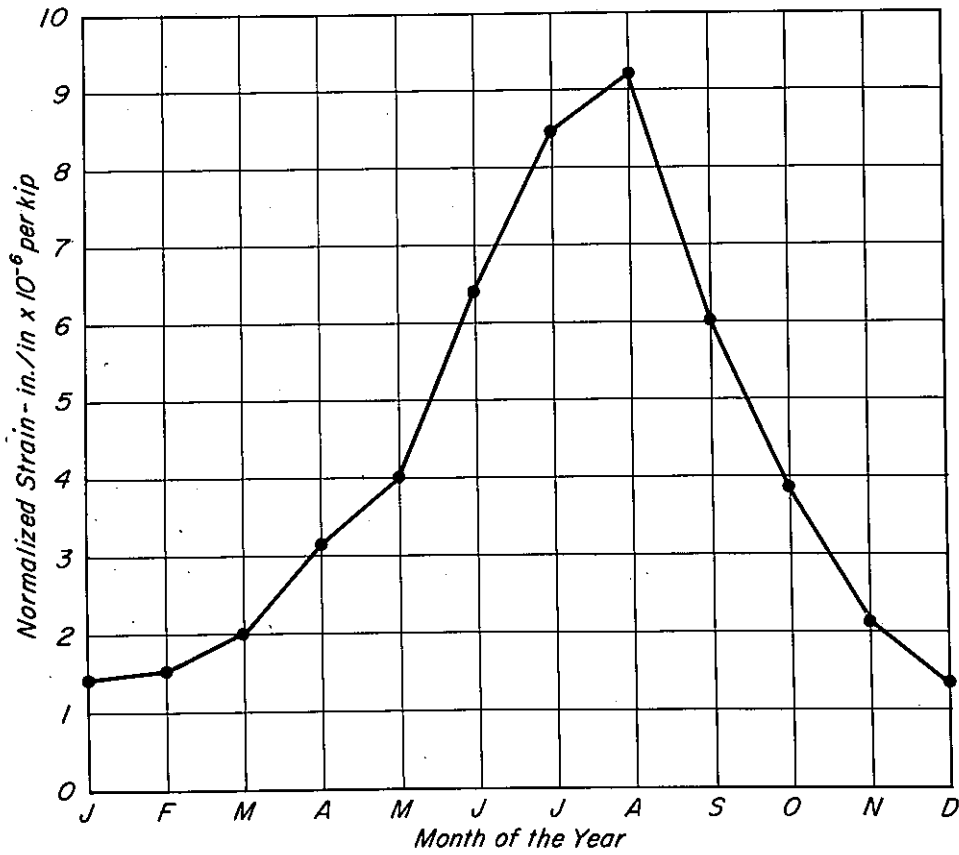


Fig. 119 – Seasonal variation in normalized strain, Ygnacio Valley Road.

Fig. 119 shows the results of the structural analysis calculations for the Ygnacio Valley Road pavement presented in terms of normalized strain.

It should be noted that this simplification is not generally applicable, especially where untreated granular materials are included in the structural section.

Utilizing the fatigue data represented by the lower curve of Fig. 63 together with the strain data and the linear summation of cycle ratios it was estimated that the 12 in. thick layer resting directly on the subgrade would be suitable for the required 10-year period (actually for the mean fatigue curve about 12 years). In addition, assuming a log-normal distribution for the fatigue behavior, it was estimated that the shortest fatigue life at a 90 percent confidence level was about 7 years.

The reasonableness of the recommended 12-inch asphalt concrete layer can be seen by comparing it with thicknesses indicated by use of other design methods:

State of California A (5)	19.3 inches
Asphalt Institute (62)	13 inches
Shell Design Method (63)	11 inches
AASHO Interim Guide (64)	9.5 inches

At this point it should be emphasized, however, that an advantage of this design subsystem, as compared to existing procedures, is that it permits detailed consideration of the particular set of conditions under which the pavement is expected to perform since fatigue life is predicted as a function of anticipated traffic, subgrade and asphalt concrete material properties, environmental variables, and their expected interaction at a specific location.

Summary

In this section the subsystem of Fig. 2 has been applied to the analyses of existing pavements and to the design of a new section. This proposed method permits incorporation of realistic material properties into the design process within the framework of elastic layer theory to define the potential for cracking of the pavement structure under repetitive traffic loading. The subsystem has been shown for conventional materials and traffic to reasonably predict in-service performance and for design purposes to result in thicknesses which are quite reasonable, based in comparisons with other existing design methods. This particular subsystem would appear to have some advantages, however, when compared to existing procedures in that it can be extended to consider loading conditions and material characteristics for which experience is not now available. Moreover, as other subsystems to consider additional distress modes become

available, this subsystem can be incorporated within the general systems framework shown in Fig. 1 since a specific mode of distress has been delineated.

DIRECT TENSION (FRACTURE) TESTING-RELATIONSHIP TO FATIGUE

If the fatigue factor is to be considered in specifications for asphalt concrete it is necessary to have some control or specification requirements for the response of mixtures to load, even though one has available a diagram for design purposes such as that illustrated in Fig. 95.

Fatigue testing is relatively costly and time-consuming and does not appear (at least at this stage in time) amenable to performance on a routine basis. Accordingly, some simplified procedure would appear desirable. In this regard direct tensile fracture testing offers a potentially useful and simple way to bring the fatigue factor into the materials control process.

Methods by which fatigue and fracture can be interrelated have already been presented by Heukelom (65), Jimenez (66), Majidzadeh, et al (67), and Salam (68). Some effort in this investigation has been devoted to tensile testing of asphalt concrete mixtures comparable specimens of which had also been subjected to fatigue testing. The relationship of these results to fatigue will be briefly discussed. In addition, the results of the investigation by Salam (68) will also be briefly summarized to illustrate in a quantitative manner one approach by which fracture data can be used to predict fatigue response.

Equipment and Procedures

Specimens for the tension testing program were sawed into 4.5 in. lengths from the 1.5 in. \times 1.5 in. bars normally used for fatigue testing. These specimens were bonded to aluminum end caps 2.25 in. in diameter with an epoxy resin to permit tensile forces to be applied.

The testing system is shown in Fig. 120. Universal joints were used to reduce the effect of eccentricity that might have existed in aligning the piston with the top-loading rod. Dual LVDT's minimized the effect of bending of the specimen on the measured deformation.

An electro-hydraulic closed-loop testing system was used to control the piston movement. This permitted a constant rate of deformation of the piston to be obtained. Due to deformation in the loading frame, universal joints, and loading rods, the specimen deformation was not linear with time (Fig. 121); however, the specimen load vs. time relationship was linear (Fig. 122). If a true constant rate-of-deformation test is to be performed on materials such as asphalt concrete, feedback to the electro-hydraulic load unit must be from the specimen deformation and not from the piston deformation as was the case in this study.

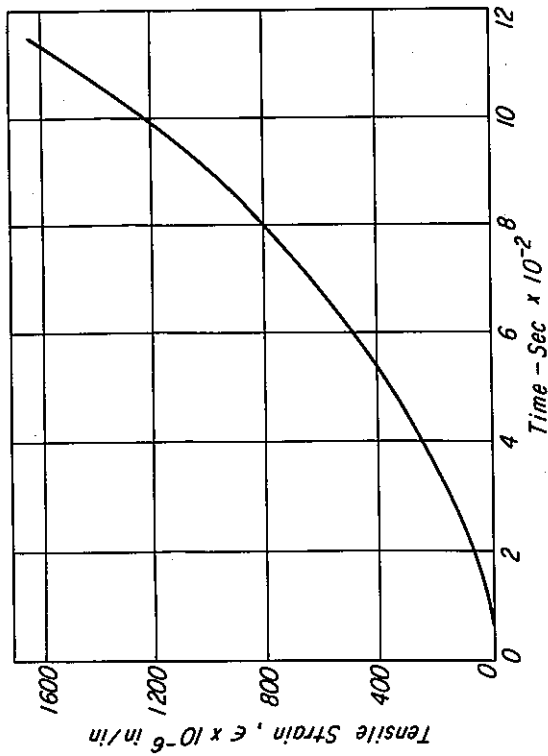


Fig. 121 - Relationship between tensile strain and time, direct tension test.

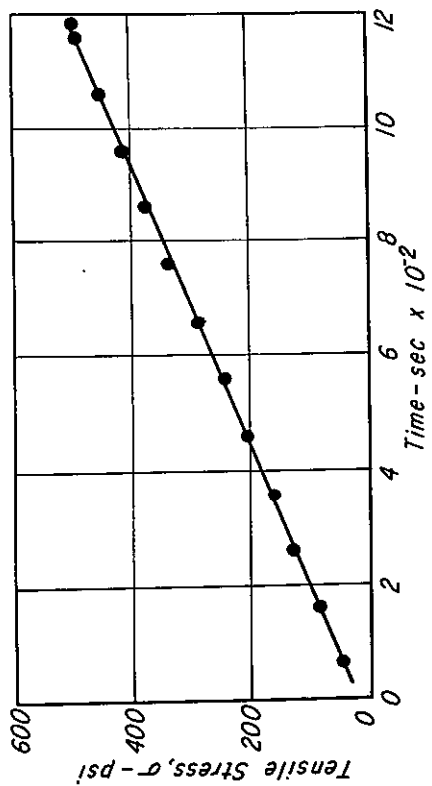


Fig. 122 - Relationship between tensile stress and time, direct tension test.

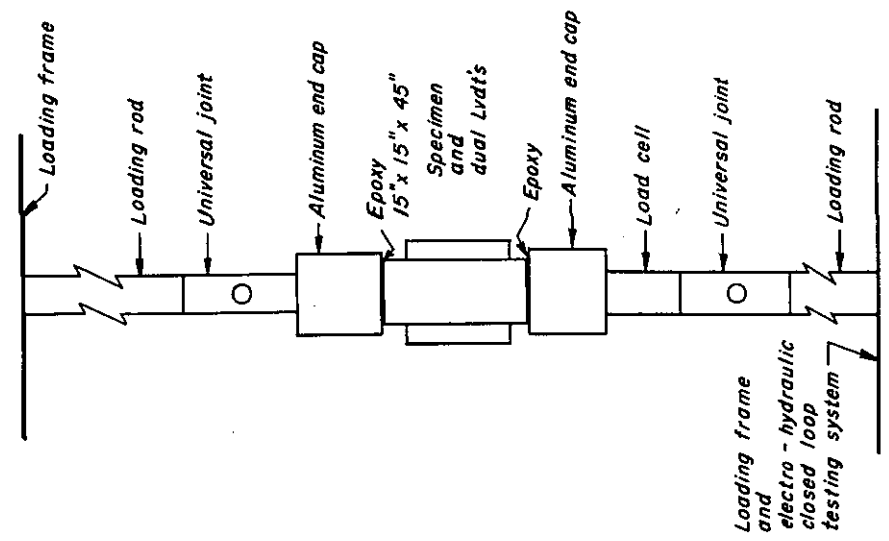


Fig. 120 - Direct tension testing apparatus.

The loading system was programmed so that fracture could be obtained in about 0.1 sec.*, a time selected to correspond to the time of loading used in fatigue tests on the same mixtures. Since some variation could be expected, both stress vs. time and strain vs. time relationships were represented as linear regression lines on log-log plots. Fig. 123 illustrates a typical strain vs. time and the corresponding stress vs. strain relationships. For tests on mixtures associated with this study only a temperature of 68°F was utilized. In the tests conducted by Salam temperatures ranged from -20°F to +68°F.

Test Results - Field Specimens

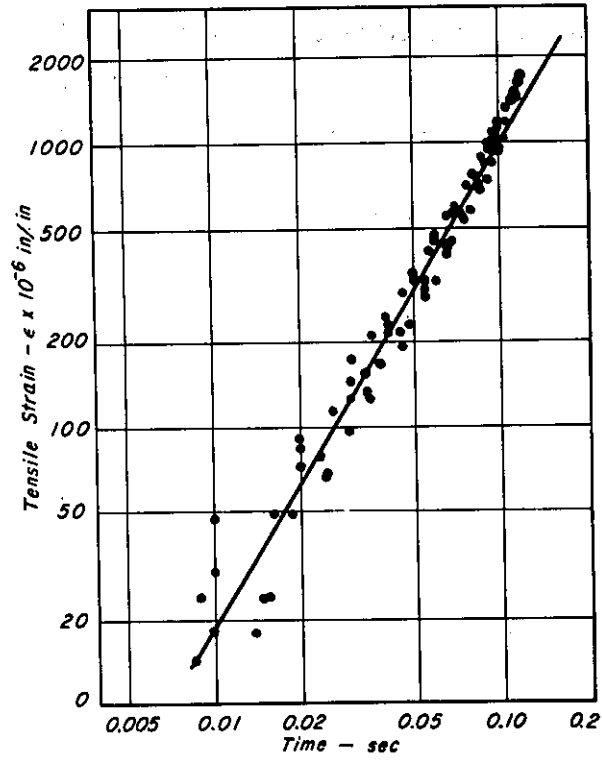
Direct tension tests have been performed on specimens obtained from pavement samples from: Gonzales By-Pass, Morro Bay, Folsom, and the San Diego Test Road (29). Detailed results are presented in Ref. 57 and only the results of Morro Bay and Folsom are included in this report.

In testing field specimens it must be recognized that the material has been subjected to repeated traffic loading prior to testing which may, in turn, influence the results of the tension testing (when compared to the results for unloaded specimens). To assess the probable effect of prior loading, a laboratory prepared mix containing the granite aggregate with a medium gradation was tested in tension both before and after fatigue testing. Stress vs. strain characteristics for both the unloaded and fatigue mixtures are shown in Fig. 124. From the data it is evident that a mix subjected to prior testing exhibits a slightly lower strength and strain at break.

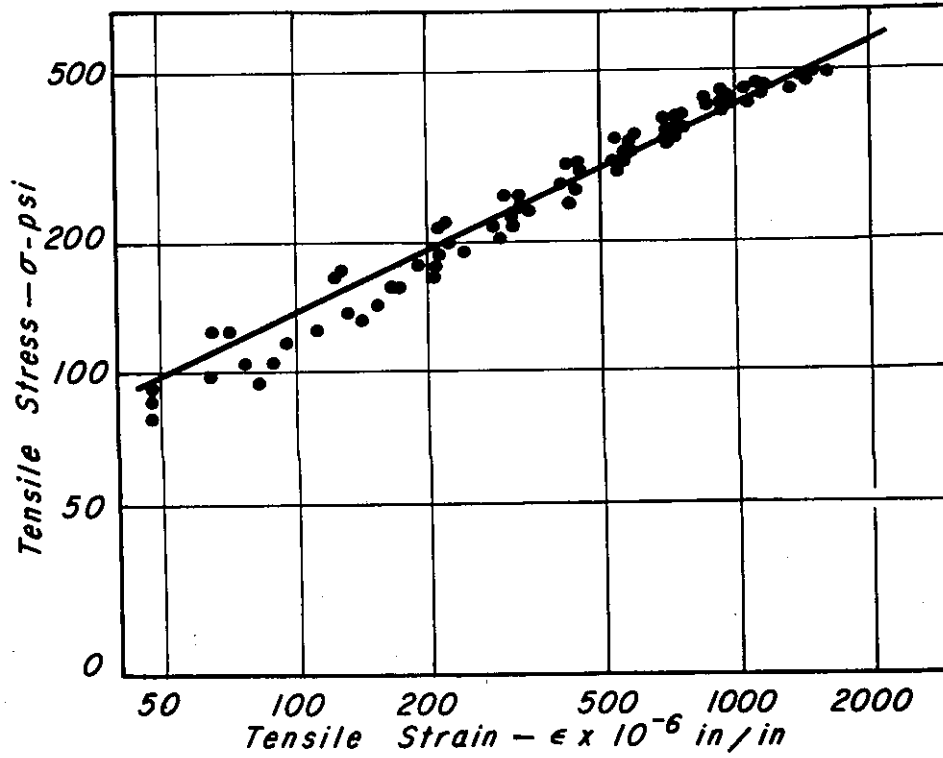
A summary of mix data reported in this section is contained in Table 45.

Morro Bay. Samples were obtained from the Morro Bay pavement in December 1965 and August 1967. Average results of tests from the two sampling periods are shown in Fig. 125. These data indicate that the pavement has been damaged — strength reduction 430 psi to 280 psi and strain-at-break reduction 990×10^{-6} in. per in. to 670×10^{-6} in. per in. Mixture stiffness, on the other hand, has changed only slightly 4.40×10^5 psi in December 1965 vs. 4.20×10^5 in August 1967. Stiffnesses determined from flexure tests and reported in TE 67-4 differed only slightly also. Interestingly, little difference in fatigue response was observed between the 1965 and 1967 samplings, the reason for this also having been discussed in TE 67-4. The data presented in Fig. 125 suggest, however, that damage development may be directly assessed in tension tests.

*For the data obtained by Salam (68), the time of loading was approximately 0.5 sec.



a. Strain vs. time.



b. Stress vs. strain.

Fig. 123 — Typical results of direct tension tests.

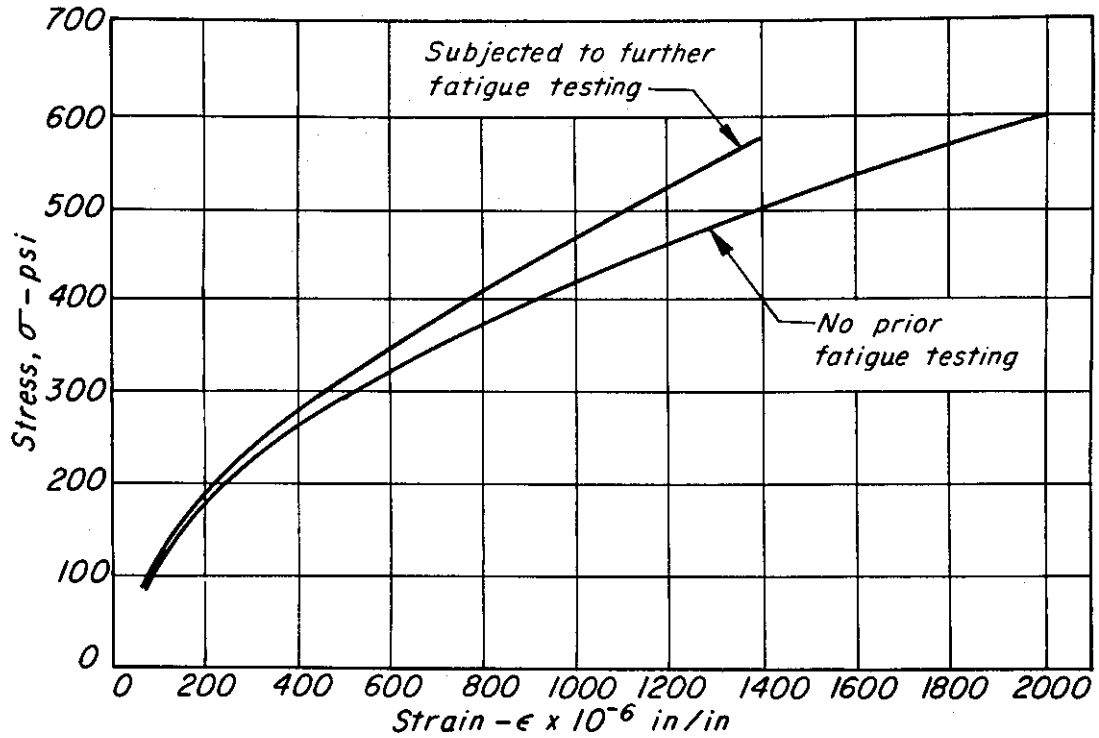


Fig. 124 - Comparison of stress vs. strain characteristics of mixtures in direct tension test with and without prior fatigue testing; California medium graded mixture, granite aggregate, 85-100 pen. asphalt cement, asphalt content - 6 percent.

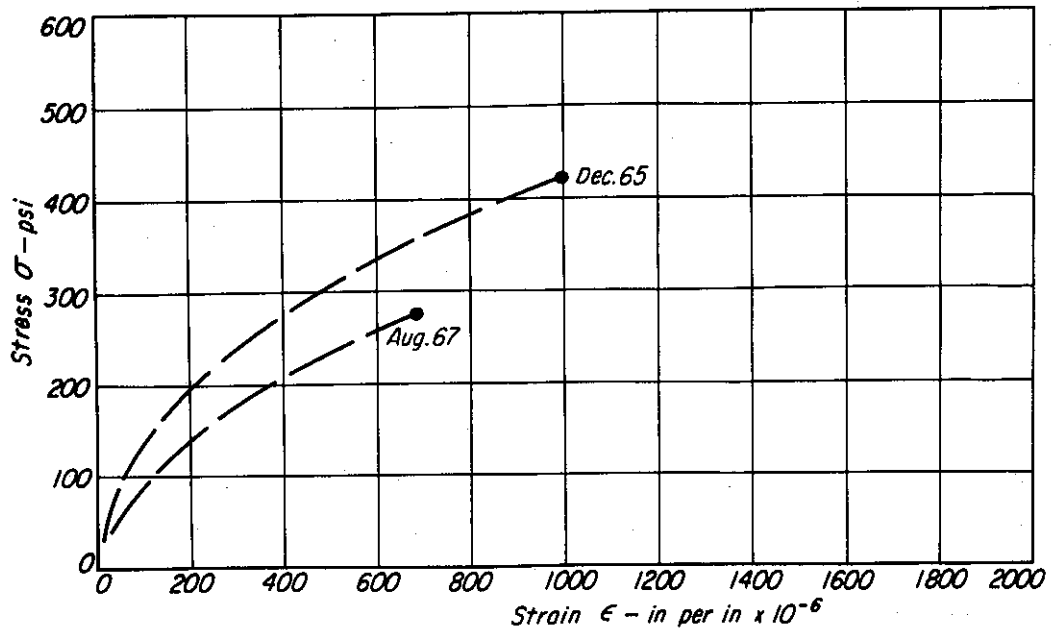


Fig. 125 - Comparison of direct tension test results for specimens from field samples of the Morro Bay pavement obtained in December 1965 and August 1967.

TABLE 45 — DIRECT TENSION TEST RESULTS

Mix Designation	Asphalt Pen.	No. of Tests	Stress at Break psi	Strain at Break $\times 10^{-6}$ in./in.	Stiffness at Break $\times 10^3$ psi	Air			Time to Break Range, sec.
						Mean	Std. Dev.	Coef. of Var.	
Morro Bay, Dec., '65	85-100	7	433	986	439	8.41	.43	5.0	.092-.118
Morro Bay Aug., '67	85-100	8	279	667	418	8.53	.53	6.1	.089-.145
Folsom, Shell	85-100	8	441	1031	428	8.69	.26	3.0	.087-.119
Folsom, Chevron	85-100	7	469	774	606	7.04	1.20	17.0	.092-.128
Medium graded granite mix subjected to prior fatigue testing	85-100	7	592	1404	422	4.23	.62	14.5	.089-.124

Folsom. Comparisons of the results of tests on specimens from the two sections of the Folsom project are shown in Fig. 126. It will be noted that the strengths of the mixes are essentially the same but that the strain at break is larger for the mixture containing the Shell asphalt.

Stiffness at break for the mix containing the Chevron asphalt (6.05×10^5 psi) is larger than that for the mix with the Shell asphalt (4.27×10^5 psi) and is of the same order of magnitude as that measured in flexure (Table 22). From an examination of the shapes of the stress vs. strain curves it would be expected that the stiffness near break is less than that obtained by dividing the stress at break by the strain at break. However, it will be noted that the stiffness values determined in this way are ordered the same as those obtained from the limiting values.

Summary. Results from the Morro Bay project obtained from samples taken at different times indicate that damage due to repeated loading may be reflected in stress-strain response in direct tension even though fatigue tests do not show such differences.

Test results from the Folsom project indicate that stiffnesses measured in direct tension on field specimens are about the same as those measured in flexure.

Both results are considered to be significant. Since the tension test is relatively simple to perform, it affords the opportunity for quickly estimating stiffness and has the potential to follow the development of damage in the asphalt concrete in the field through a planned program of testing.

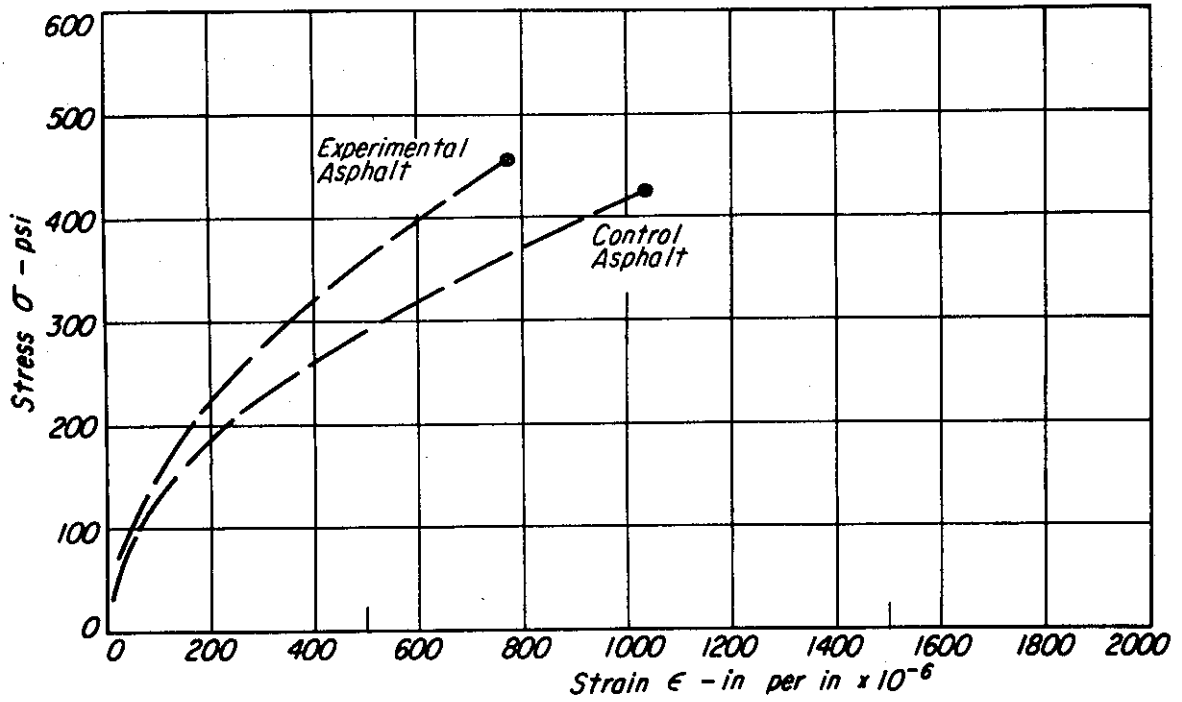


Fig. 126 — Comparison of direct tension test results for specimens obtained from field samples of the folsom project.

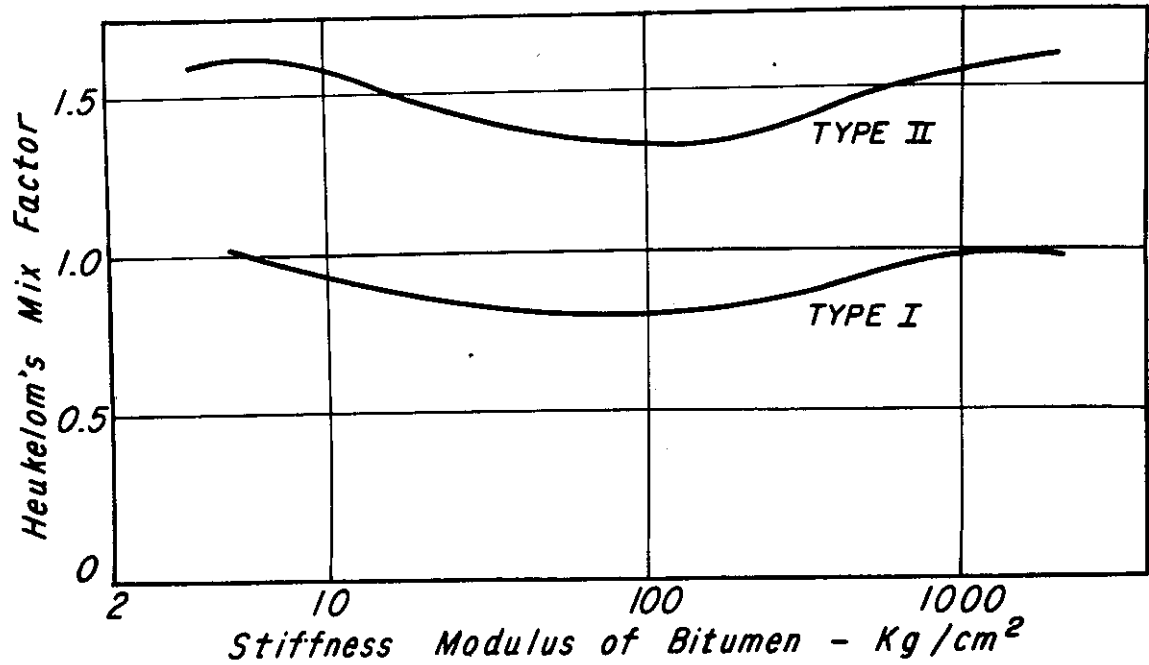


Fig. 127 — Relationship between the mix factor as defined by Heukelom and asphalt stiffness.

These factors coupled with the possibility that there may exist a relationship between fatigue and fracture has prompted a more extensive investigation utilizing laboratory prepared specimens the fatigue results of which have been presented earlier in the report (Table 14).

Relationships Between Fatigue Response and Tensile Strength

As noted earlier a number of investigators have attempted to relate fatigue response and fracture (or tensile) data (65, 66, 67).

± Heukelom (65) has presented data indicating a relationship between the fracture characteristics of pure asphalts and their fatigue characteristics. He obtained a definitive relationship between the deformation energy in fatigue and that in simple bending as well as the stiffness of asphalt and observed cycles to failure in repetitive loading, i. e.

$$\left[\frac{Q_{d \text{ fatigue}}}{Q_{d \text{ bending}}} \right] = \frac{S_{\text{asp}}}{E - S_{\text{asp}}} \cdot \frac{40}{\sqrt{N_f}}$$

where:

$Q_{d \text{ fatigue}}$ = deformation energy, fatigue loading

$Q_{d \text{ bending}}$ = deformation energy, simple bending

E = limiting value of S_{asp} as $t \rightarrow 0$

Jimenez (66) has suggested that the intercept on the stress axis of the stress vs. fatigue life relationship at one repetition of load is related to the tensile properties of the mix as measured by a modified cohesiometer test and that it may thus be possible to assure fatigue resistance by means of suitably specified cohesiometer value.

More recently Majidzadeh, et al (67) have indicated a procedure whereby the fatigue relationship may be defined from simple fracture tests using experimental and analytical procedures adapted from the field of fracture mechanics. Using such a procedure Salam (64) has developed data to be presented subsequently which indicates that such an approach is promising though not quite ready for general use as yet.

Recognizing the difficulties associated with the latter procedure, particularly, an attempt has been made to relate fatigue and fracture for a number of the mixtures utilized in this investigation. The various techniques are described in detail in Ref. 57 and only one method will be discussed herein to illustrate the type of information which may be required to accomplish the prediction.

Use of asphalt strain as developed by Pell (46) was indicated earlier to be a useful way to examine the effect of asphalt content on fatigue response. This same concept may be useful in permitting the development of generalized fatigue data simply by performing fracture tests on a particular mix and on representative samples of the asphalt contained therein.

Pell has indicated that the fatigue life of a mix may be related to the strain in the asphalt by the expression:

$$N_f = K_3 (1/\epsilon_{asp})^{n_1} \dots \dots \dots (23)$$

where:

ϵ_{asp} = asphalt strain

The asphalt strain can in turn be determined from:

$$\epsilon_{asp} = \frac{\epsilon_{mix}}{\alpha B_v} \dots \dots \dots (24)$$

where:

ϵ_{mix} = mixture strain

α = factor dependent on the volume concentration of aggregate, C_v , and type of aggregate

B_v = volume concentration of asphalt, $(1 - C_v)$.

Appendix H contains the development of the following equation:

$$\epsilon_{mix} = M \frac{S_{asp}}{S_{mix}} \epsilon_{bit} \dots \dots \dots (25)$$

where:

M = mix factor, defined as the ratio of the fracture stress in the mix (σ_{mix}) to the fracture strength of the asphalt in the mix (σ_{asp}).

Combining equations 24 and 25 it is possible to develop an expression which permits estimates of the value α to be obtained from the results of fracture tests as shown by the following equation:

$$\alpha = \frac{M}{B_v} \frac{S_{asp}}{S_{mix}} \dots \dots \dots (26)$$

Thus α is a function of variables which must be obtained from a knowledge of mixture proportions and physical properties, and the recovered properties of the asphalt used in the mixture. Heukelom's mix factor "M" may be obtained from Fig. 127 using the stiffness of the recovered asphalt. The volume concentration of the asphalt may be computed for a specific mixture and the ratio of the stiffness of the asphalt to that of the mix can be estimated by the procedure developed by Shell.

Fig. 128 shows the variation in α that may exist for a Type I mixture containing asphalts which range in stiffness from 100 to 1,000 kg per cm², and containing various asphalt contents as reflected in the value of B_v at an air void content of 5 percent.

This figure indicates that an increase in volume concentration of asphalt of the order of .06 to .08 is required to change α by a factor of two. A 3 to 4 percent change in asphalt content by weight is required to change the volume concentration of the asphalt by such a large amount. Thus for changes in asphalt contents by weight of the order of one percent, a change of approximately .01 occurs in the value of α . Accordingly, this factor appears little affected by variations in asphalt contents which normally occur due to construction variations.

The value of α becomes larger with increase in asphalt stiffness as shown in Fig. 128. A change in α by a factor of two may result if the stiffness of asphalt changes from 100 kg per cm² (85-100 penetration asphalt cement*) to 600 kg per cm² (40-50 penetration asphalt cement*).

The effect of aggregate grading and aggregate type cannot readily be assessed by use of these figures. If the same asphalt content and asphalt penetration are used for different gradings, this figure suggests that α will be unchanged by the different gradings. Similarly if different aggregates are mixed with the same asphalt and at the same asphalt content, α will remain unchanged. However, different aggregate types and grading usually require various amounts of asphalt and thus those aggregates which contain higher asphalt contents will tend to have higher values of α .

As shown in Fig. 129, air void content also influences the value of α . The larger the percent air voids, the greater is the value of α as indicated in this figure. This trend of increasing α with increasing air void content is due to the resulting lower stiffness of the mix at high air void contents (indicated by equation (26)).

Values of α have been calculated by the above procedure for the mixtures used in this investigation and are shown in Table 46. Similarly values of α have been calcu-

*Time of loading 0.1 sec. temperature 68°F.

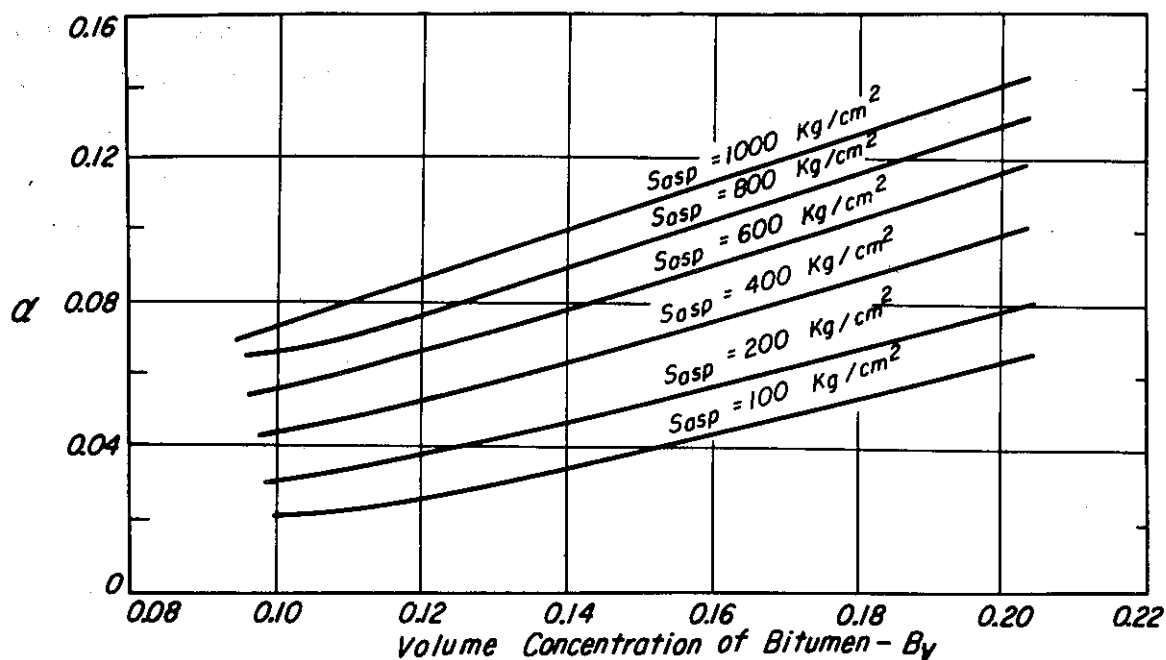


Fig. 128 — Relationship between the factor α and asphalt content for a range in asphalt stiffness.

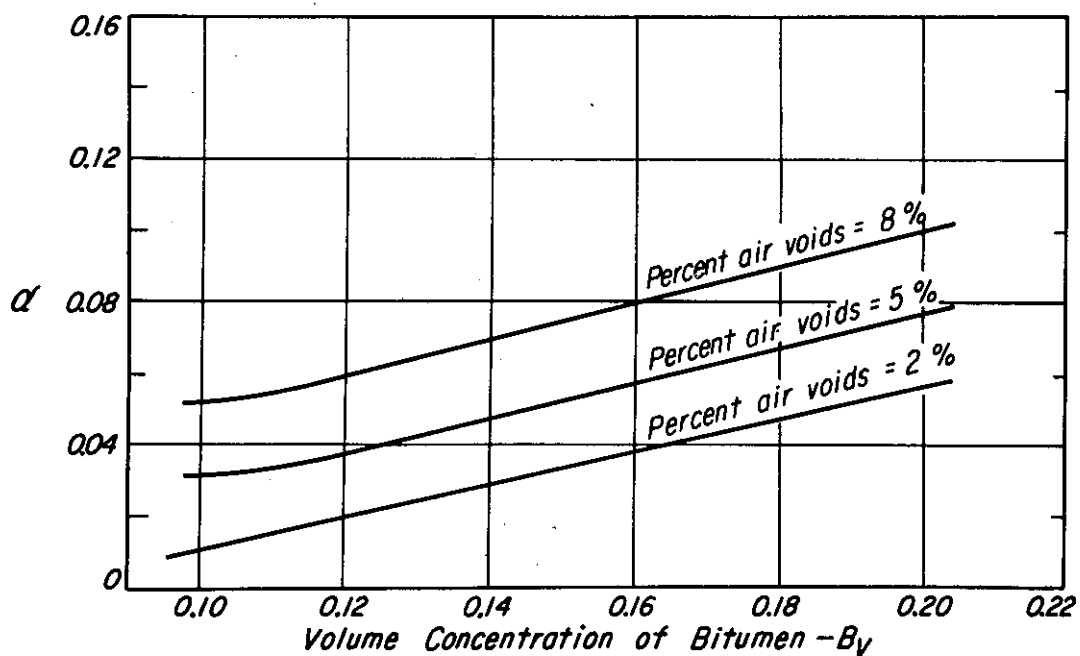


Fig. 129 — Relationship between the factor α and volume concentration of asphalt for a range in air void contents.

lated using the measured strength and stiffness values of the mixes as determined from direct tension tests. The measured values of α are also shown in Table 46.

Measured values of α obtained for the basalt aggregate mixes indicate that little variation exists with changes in asphalt content. Moreover, α is affected by aggregate gradation as noted for the granite aggregate with the finer the gradation, the higher the values of α .

TABLE 46 — COMPARISON OF THE CALCULATED AND MEASURED VALUE OF α

Mixture Identification			α Calculated ⁽¹⁾	α Measured ⁽²⁾
Designation	Asphalt Penetration	Asphalt Percent		
Granite Coarse	85-100	6.0	.056	.054
Granite Fine	85-100	6.0	.069	.088
Granite Medium	85-100	6.0	.046	.068
Granite Medium	60-70	6.0	.048	.065
Granite Medium	40-50	6.0	.056	.022
Basalt	60-70	5.7	.066	.042
Basalt	60-70	6.7	.057	.033
Basalt	60-70	8.7	.062	.042
Granite	85-100	5.2	.058	.035

- (1) Calculated from nomograph solutions.
- (2) Measured from tension test results.

Values of bitumen strain have been calculated using equation (24) with appropriate measured values for α . Ideally, bitumen strain-fatigue life data for all mixes studied should fall about a single regression line described by equation (23).

This equation can then be transformed into the more familiar equation relating mixture strain and fatigue life

$$N_f = K_1 (1/\epsilon_{mix})^{n_1} \dots \dots \dots (27)$$

by substituting equation (24) and the relationship

$$\dots \dots \dots (28)$$

$$K_1 = K_3 (\alpha B_v)^{n_1} \dots \dots \dots (28)$$

into equation (23).

Thus if a relationship between bitumen strain and fatigue life can be obtained for all possible asphalt concrete mixes and if a value of α can be determined for the particular mixture for which the engineer is concerned, an appropriate mixture strain-fatigue life relationship may be calculated which may, in turn, be used for design of asphalt concrete pavements to preclude failure due to fatigue.

Some attempt has been made to examine a limited amount of available fatigue data within this framework, data representative of a number of mixtures conforming to the State of California mix design criteria. With the aid of equation (24) bitumen strains were estimated (Table 47) and are plotted vs. applications to failure in Fig. 130. In these figures it will be noted that no unique relationship between asphalt strain and fatigue life exists for the mixes studied, at least based on the available evidence. Accordingly, the use of the procedure described herein to predict fatigue results from fracture tests must await the results of additional investigations to indicate its potential usefulness in mixture design. *

A portion of the difficulty may be associated with the manner in which the factor α is determined. In Fig. 128 and Table 46 it will be noted that α is dependent upon the stiffness of the asphalt. Since α varies only within a narrow range and the stiffness nomograph is valid within a factor of 2, it would appear useful to measure the fracture strength and stiffness of the asphalt rather than estimate it from the nomograph in order to permit a more realistic value of α to be ascertained.

Relationship Between Fatigue and Fracture Data

An alternative approach to prediction of fatigue response is that based on fracture mechanics as suggested by Majidzadeh (67). In this regard it should be noted that the development of fatigue can be divided into three phases, namely: (1) crack initiation, (2) stable crack growth, and (3) unstable crack propagation. It might be argued that crack initiation takes place only during a small fraction of the total fatigue life of a particular material whereas stable crack growth occupies a large portion. It is for this phase that quantitative models based on fracture characteristics have been proposed and one such "law" will be used to predict the measured fatigue response obtained in this investigation.

*The data shown in Fig. 130 based on computed values of α , indicate much less scatter than these based on the measured values.

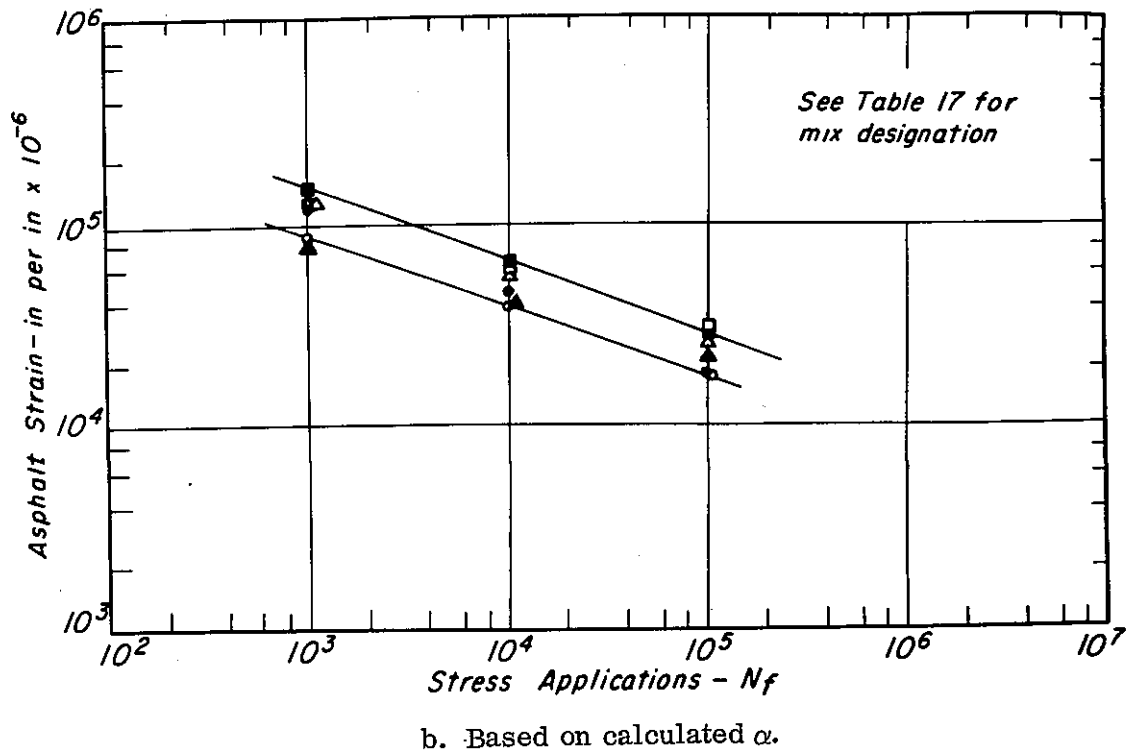
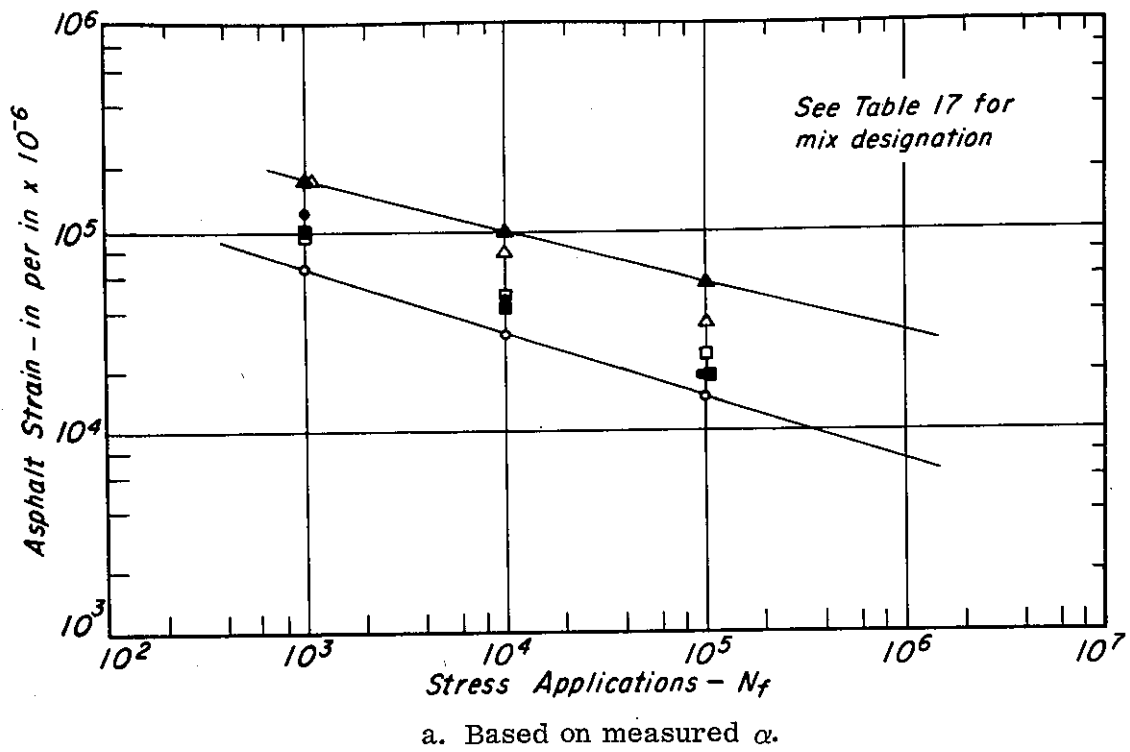


Fig. 130 — Calculated asphalt strain, ϵ_{asp} vs. stress applications.

TABLE 47 -- ESTIMATED VALUES OF BITUMEN STRAIN, ϵ_{asp} , FROM FATIGUE TEST RESULTS

Mix Designation	Asphalt Cement	Asphalt Content-percent	M	B_v	S_{asp} kg per cm ²	S_{mix} psix10 ³	α		ϵ_{mix} in. per in. $\times 10^{-6}$ Corresponding to N_f of		ϵ_{asp} in. per in. $\times 10^{-6}$ Corresponding to N_f of			
							Calc.	Meas.	10 ³ rep	10 ⁴ rep	10 ⁵ rep	10 ³ rep	10 ⁴ rep	10 ⁵ rep
California Coarse Granite Aggr	85-100	6.0	0.725	0.144	225	301	0.056	0.054	998	370	150	126,000 123,000	47,500 45,800	19,200 18,600
California Fine Granite Aggr	85-100	6.0	0.945	0.144	347	369	0.069	0.088	860	400	180	68,000 86,000	31,500 40,000	14,200 18,000
California Medium Granite Aggr	85-100	6.0	0.905	0.144	224	294	0.046	0.068	996	430	190	104,000 151,000	44,000 65,200	19,400 28,800
California Medium Granite Aggr	40-50	6.0	0.862	0.144	306	1,210	0.048	0.065	900	440	230	96,000 130,000	48,000 63,800	24,500 33,300
California Medium Field Specimens	85-100	4.9	0.662	0.121	235	428	0.056	0.022	590	330	185	185,000 73,000	103,000 40,800	58,000 22,800
							0.059	0.043	960	420	190	185,000 133,000	81,000 58,300	36,500 26,400

* Measured α used for this computation.
 ** Calculated α used for this computation.

Analysis of Crack Propagation. Utilizing principles of fracture mechanics it can be shown that (69):

$$G = \frac{1}{2} F^2 \frac{dJ}{da}$$

where:

- a = crack length
- G = energy rate (energy released per unit crack increment, da)
- F = force
- J = compliance (elastic deformation/force)

According to this expression the energy released due to an increment of crack growth is only a function of the applied load and the rate of change of the compliance with respect to crack length. The value of G does not depend upon the loading conditions (provided that the strains are linear). The value of dJ/da can be determined from a compliance calibration determined by measuring J for various values of crack lengths.

The above equation may be rewritten as:

$$\frac{dJ}{da} = \frac{2G}{F^2} = \frac{2(1 - \nu^2)}{E} \cdot \frac{K^2}{F^2}$$

illustrating that K, the stress intensity factor can be determined if the compliance calibration is known.

For this investigation two types of compliance calibration were determined — one based on deflection measurements, the other from crack opening displacements. Both are briefly described in Appendix I.

By obtaining similar relationships during repeated flexural loading it is possible to relate crack size to the number of load applications. Typical curves are shown in Fig. 131 for specimens with various initial notch depths.

A quantitative relationship for crack growth utilizing the stress intensity factor may be formulated as (70):

$$\frac{da}{dN} = A K_1^n$$

A and n being constants related to the specific test.

The value of $\frac{da}{dN}$ can be obtained by differentiation of the differentiation of the a/h vs. N curves (e. g. , Fig. 131) already established and the load P is known for each specimen permitting the stress intensity factor to be obtained for any crack size a.

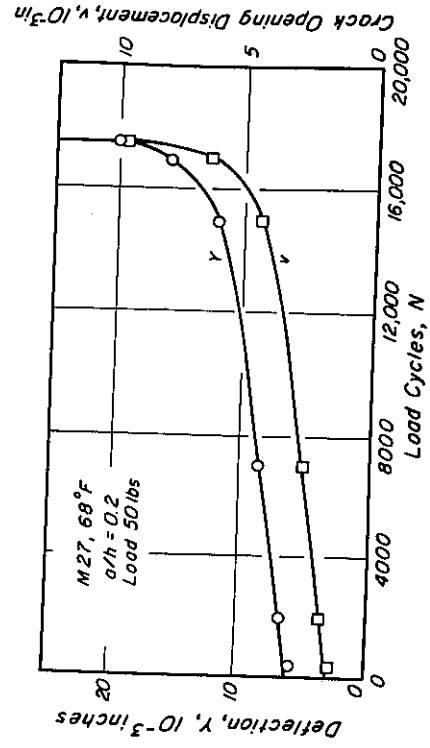
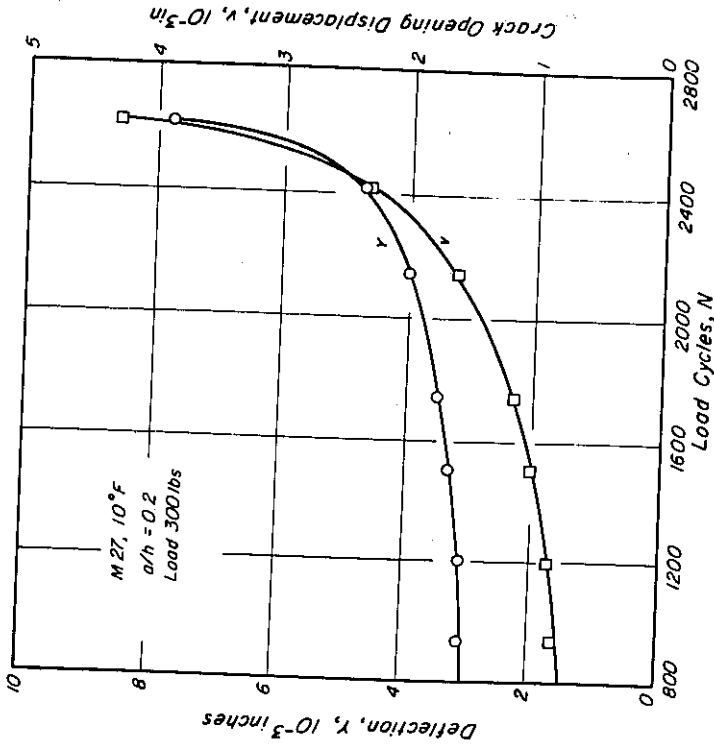


Fig. 133 - Relative resolution of deflection and C. O. D. measurements at 10° and 68°F.

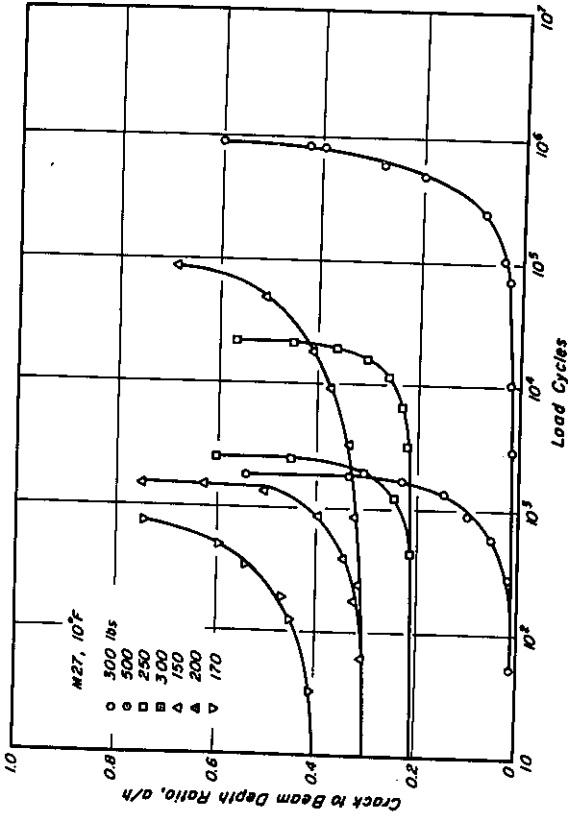


Fig. 131 - Variation of crack length with fatigue load cycles at 10°F.

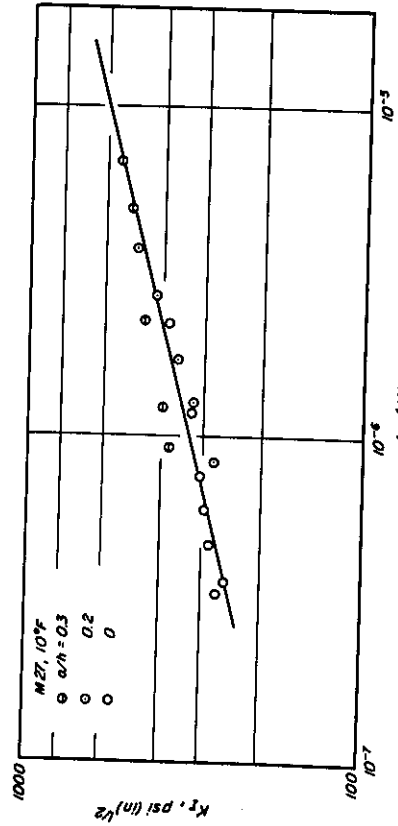


Fig. 132 - Fatigue crack growth rate as a function of K_I , 10°F.

A log-log plot of $\frac{da}{dN}$ vs. K_I is shown in Fig. 132 which can be represented by the following relationship:

$$\frac{da}{dN} = 7.9 \times 10^{-7} K_I^{3.8}$$

Using the same expression, Majidzadeh (67) obtained the following coefficients for sand asphalt and asphalt concrete for beams subjected to three-point loading:

<u>Material</u>	<u>A</u>	<u>n</u>
Sand Asphalt, 23°F 1" x 1" x 12" beams	5×10^{-3}	4
Sand Asphalt, 78.5°F 1" x 3" x 8"	3.5×10^{-7}	3.05
Sand Asphalt, 78°F 2" x 3" x 8"	1.41×10^{-8}	3.05
Asphalt Concrete, 41°F 2" x 3" x 14"	1.5×10^{-8}	3.35
Asphalt Concrete, 78.5°F 2" x 3" x 14"	1.6×10^{-6}	2.25

It should be noted that the sensitivity of fatigue life to the stress intensity factor decreases with decreasing stiffness for at least two reasons:

1. The relative resolution of the deflection and C. O. D. measurements is illustrated in Fig. 133 for notched specimens; at 10°F C. O. D. is more sensitive to N than deflection, while at 68°F the resolution was virtually the same.
2. Available data indicate that the exponent n is larger at low temperatures than at higher ones.

Prediction of Fatigue Life. As noted earlier prediction of fatigue life is based on the assumption that the most significant portion is associated with stable crack growth between some initial crack length a_0 and a critical length a_c which terminates the fatigue life and is determined by K_{IC} .

An incremental procedure, based on the relation

$$\frac{da}{dN} = A K_I^n$$

has been used herein to predict fatigue life. The incremental growth of a crack may be expressed as an average rate:

The number of load repetitions resulting in an increment of crack growth Δa would then be:

$$\frac{\Delta a}{\Delta N} = \frac{[AK^n]_a + [AK^n]_{a+\Delta a}}{2}$$

or

$$\Delta N = \frac{2\Delta a}{[AK^n]_a + [AK^n]_{a+\Delta a}}$$

where;

\bar{a} - average crack length for a given increment.

$$\Delta N = \frac{\Delta a}{[AK^n]_{(\bar{a})}}$$

The stress intensity factors were calculated using the calibration function shown earlier. Fig. 134 shows the variations of K_I with crack length for several values of the bending moment. (Note: the maximum permissible value of K is about 900 psi (in.)^{1/2}, determined from the fracture tests.)

Having obtained the value of K for the increment Δa the crack growth rate was then determined for the increment from Fig. 132. By determining these for a series of increments, the fatigue life increments may be summed to the value of the crack size corresponding to K_{IC} when failure occurs. The fatigue life for any initial crack size can thus be obtained by subtracting the cumulative load cycles to that size from the total number of repetitions at failure.

This procedure was repeated for several values of the bending moment and the results are shown in Fig. 135. Although the laboratory tested specimens were limited in number, they show reasonable agreement with the predicted trends. For convenience this process of fatigue life prediction has been developed in the form of a block diagram Fig. 136 and can be summarized as:

It is started with the initial crack size a_0 and iterated for any arbitrary number of increments r , $0 < r \leq n$, with n being the total number of increments to failure. For any increment Δa_i a corresponding average crack size \bar{a}_i follows. The calibration function together with \bar{a}_i and the applied moment yield the stress intensity factor K_i . If $K_i \leq K_{IC}$, the

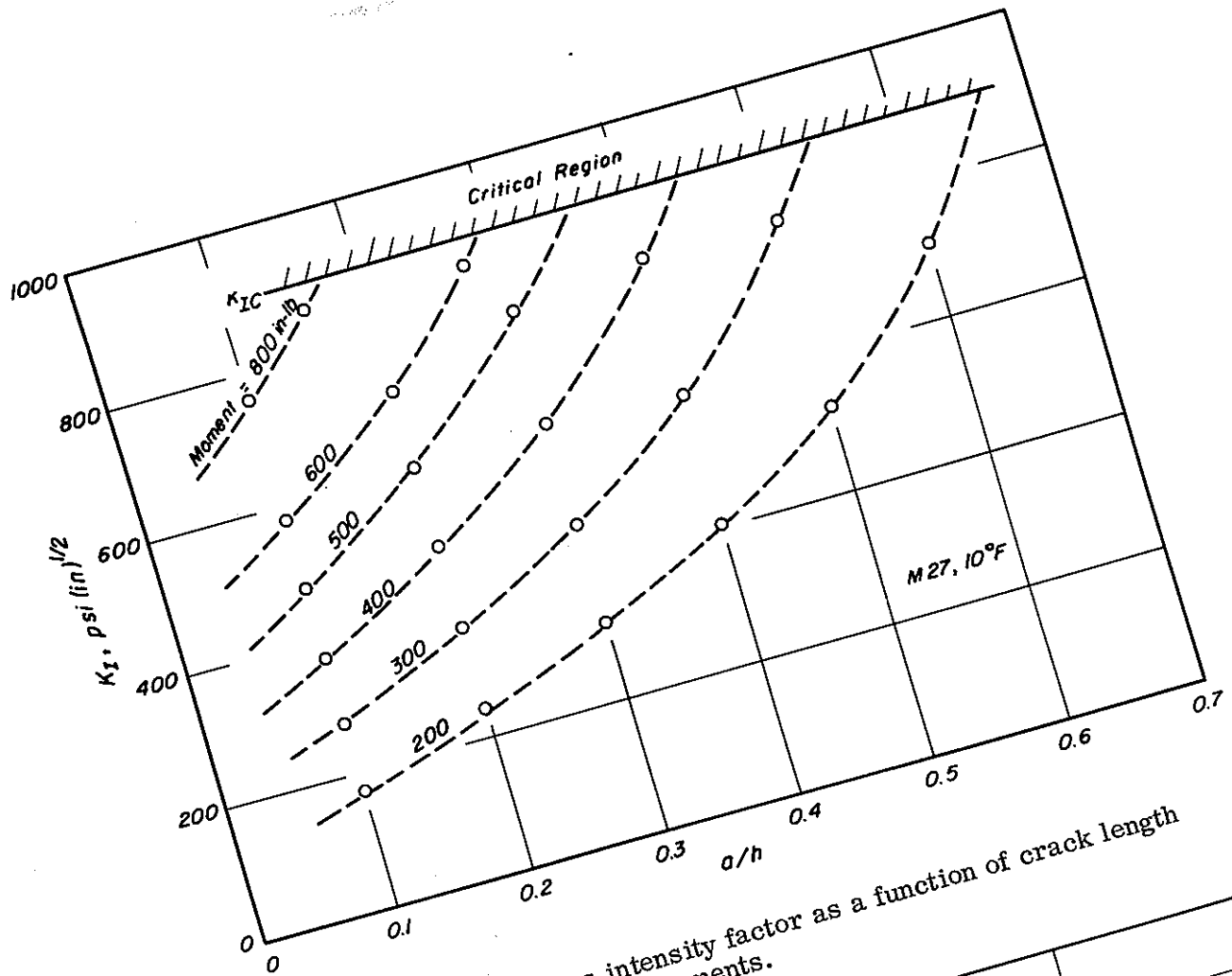


Fig. 134 - Stress intensity factor as a function of crack length for various bending moments.

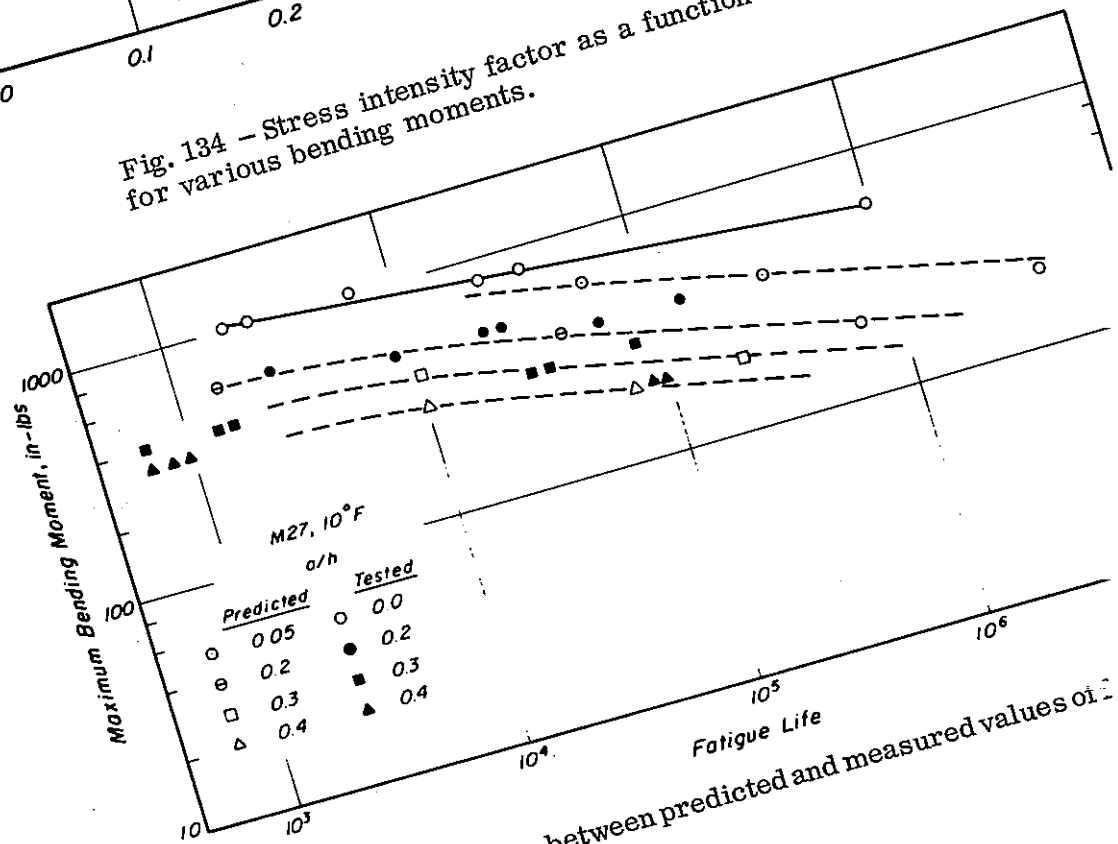


Fig. 135 - Comparison between predicted and measured values of

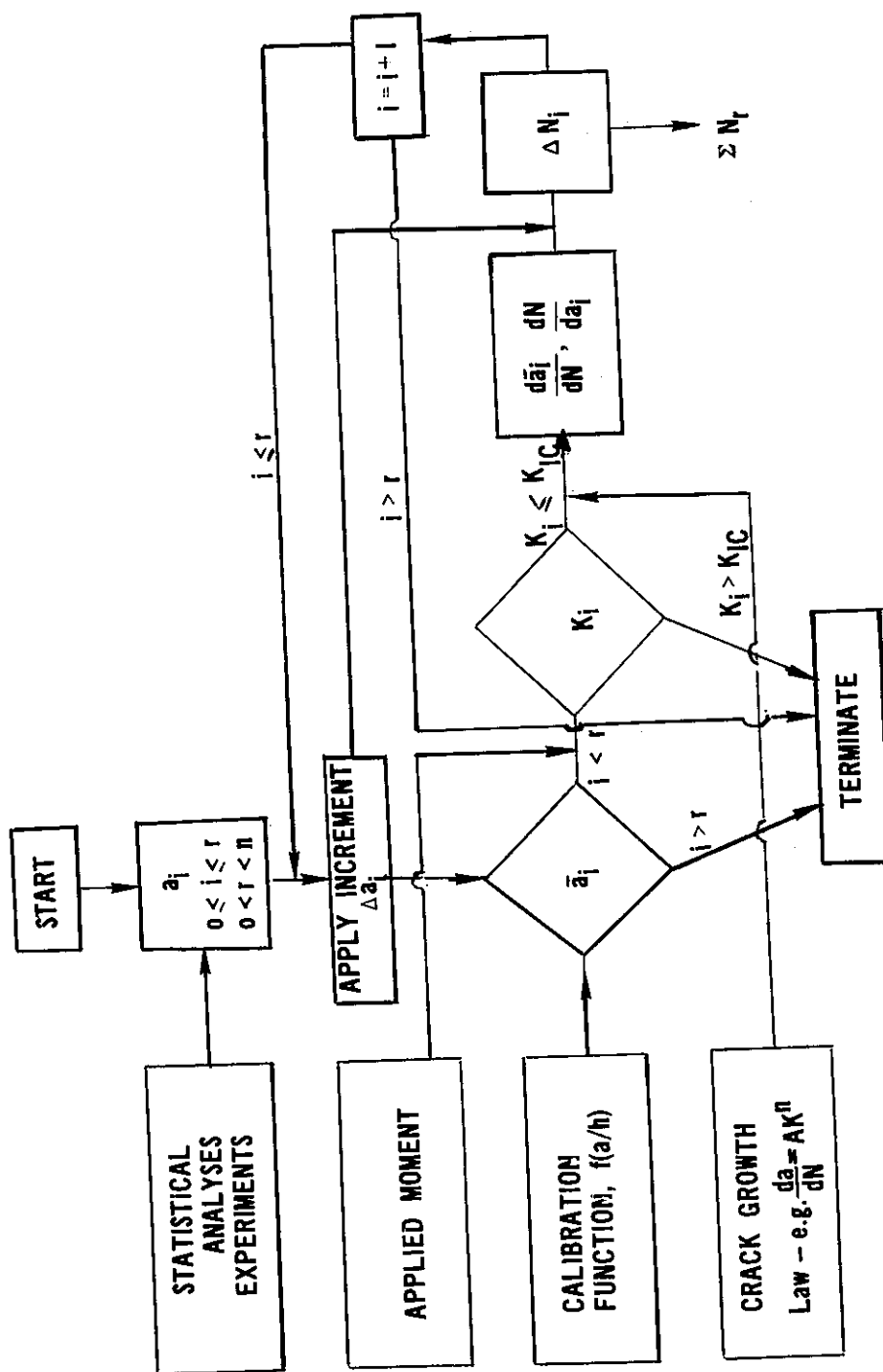


Fig. 136 - Block diagram for fatigue life computations from fracture properties.

rate of crack growth $d\bar{a}_i/dN$ can be determined with the aid of the crack growth law. The resulting fatigue life increment ΔN_i is obtained by multiplying $dN/d\bar{a}_i$ by Δa_i with the process repeated up to any desired value of the crack size corresponding to r increments. The sum of all these increments is the predicted value of the fatigue life.

Summary. The merit of such an approach is that it provides a quantitative description of the fatigue process. Quantification of the method for asphalt mixtures requires a considerable amount of experimental data which are not available at the present. However, it holds the potential for practical design considerations since eventually it may be possible to predict the extent of cracking in a pavement rather than merely the onset as is now done by the procedure described in this report, Fig. 2.

SUMMARY

In this report a subsystem of the pavement design system has been presented to consider the fatigue mode of distress. The proposed procedure permits incorporation of realistic material properties (in the engineering sense) within the framework of multi-layer elastic theory (although other methods, e. g. , finite element procedures, are fast becoming usable) to define the potential for cracking of the pavement structure under repetitive loading. This procedure can be used either for checking the adequacy of existing pavements or for design of new structures.

When this procedure was used to check the Morro Bay pavement, distress, which had been predicted, was ascertained through additional field sampling. The time period in which cracking was estimated to develop was somewhat shorter than that which actually occurred in service (approximately 2 years vs. some less well defined period in the range 3 to 3-1/2 years*). This difference was in part due to potential differences in assumed and actual traffic, use of average conditions for base and subbase materials rather than recognizing potential seasonal variations which, though known to occur, were not well defined, and the use of one fatigue curve rather than a family of curves to recognize the dependence of damage development on asphalt mixture stiffness (e. g. , Fig. 95).

In spite of these limitations the system was shown to be responsive to actual conditions since distress, which was subsequently observed, was predicted in advance.

For the second in-service pavement to be analyzed, the Folsom project, a reasonable estimate of service life (of the order of 10 years) was obtained. In developing this estimate some of the limitations associated with the analysis of the Morro Bay pavement were reduced since additional data became available in the interim.

For the design example, Ygnacio Valley Road in Contra Costa County was selected. The resulting design utilizing the fatigue subsystem resulted in a thickness comparable to those predicted by a number of other procedures. The road was constructed to the recommended thickness in 1969 and at the time of this report has been in service for about two years.

The strength of the type of approach described herein appears to lie in its usefulness as a design tool since it has the potential to consider a number of factors not utilized in present day design practices. It should be emphasized, however, that this type of an approach is not meant to replace existing methods but rather to be used in conjunction with them.

*This is merely an estimate since no cracking was evident at the time of the first samples in December.

Relative to the fatigue data, in tests of the controlled-stress and controlled-strain types, mixture stiffness has been emphasized as an important mix variable. In addition asphalt content has a dominant role to play in improving fatigue behavior.

The data also indicate that a worthwhile field experiment would be to construct an asphalt-bound base course utilizing a mix similar to that defined in the B. S. 594 specifications.

By combining the fatigue data from the various investigations it has been possible to develop a preliminary design diagram which (as demonstrated in the Folsom example and in Appendix G for the revised design of Ygnacio Valley Road for varying traffic conditions) is a useful part of the fatigue subsystem of Fig. 2. The resulting diagram, Fig. 95, should be considered a preliminary guide until substantiated by additional performance studies.

The design example for Ygnacio Valley emphasizes how the mixture design and structural pavement design processes must be blended together to insure the most workable solution to a specific problem.

A simple fracture test such as that described in the report may serve as a useful procedure to define fatigue response and/or to incorporate fatigue considerations in Materials specifications. Stiffnesses (in this test) determined at a particular temperature compare reasonably well with those measured in flexure when the same time of loading is utilized.

While some evidence has been presented to indicate that fracture test data can be used to predict fatigue response using fracture mechanics concepts, additional evidence is required before such a potentially useful technique can be adopted more generally.

Finally there is some indication that by specifying a minimum fracture strength and stiffness (at a particular time of loading and temperature), fatigue response for a mix designed according to the California procedure may be reasonably assured.

ACKNOWLEDGMENTS

The authors wish to acknowledge the support provided by the Institute of Transportation and Traffic Engineering of the University of California in the form of shop and office staff and facilities. Thanks are especially due Messrs. C. K. Chan, R. G. Newcomb, T. W. Pickrell and G. Ahlborn and Mrs. R. H. Mackey. Graduate research assistants also associated with the project included Messrs. P. Lade, R. Stubstead, and C. Espana; their contributions are acknowledged.

1970 Road Test Findings, Basic
1970. (Highway Research

L. Brown, "A
Report 123-1,
Texas
Austin,

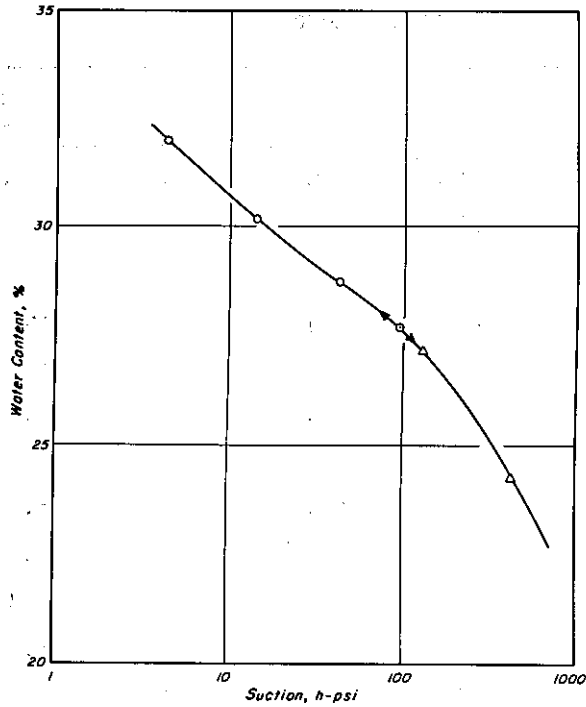


Fig. A1 - Water content vs. suction relation.

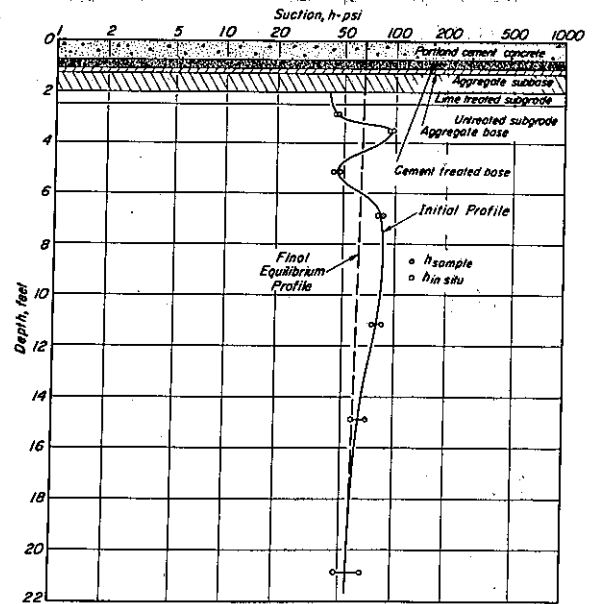


Fig. A3 - Suction profile

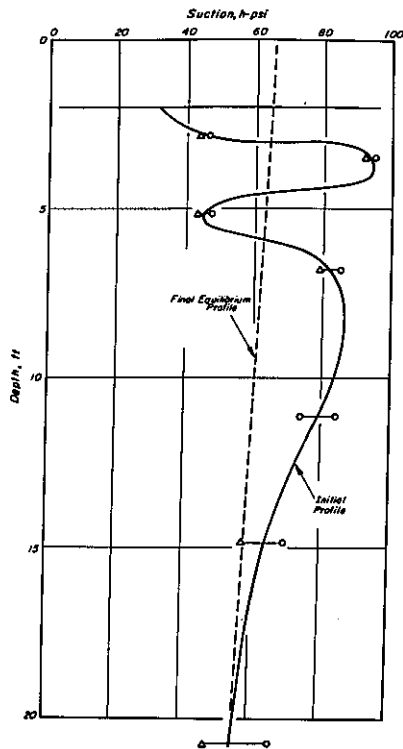


Fig. A2 - Suction profiles.

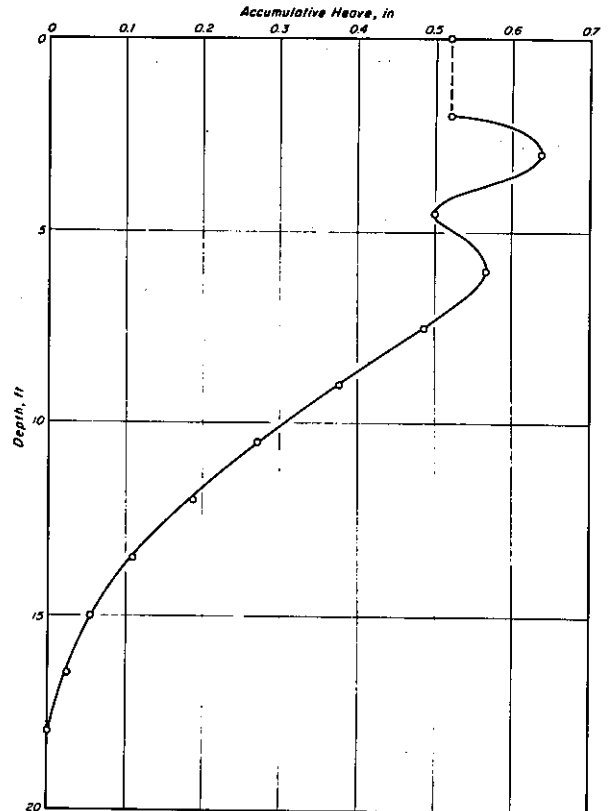


Fig. A4 - Variation of heave with depth below grade surface.

TABLE A1 — HEAVE CALCULATION

Depth ft	h_{ave} psi	w_i percent	h_f psi	w_f percent	Δw	H in.	ΔH in.
2-3	39	30.6	64.5	29.95	-0.65	12	-.116
3-3	89	29.5	63.5	30.0	+0.5	18	+.137
4.5-6	50	30.25	63.0	30.0	-0.25	18	-.068
6-7.5	79	29.7	62	30.0	-0.3	18	+.081
7.5-9	85	29.6	61.5	30.0	+0.4	18	+.108
9-10.5	83	29.6	61	30.0	+0.4	18	+.108
10.5-12	79	29.7	60	30.0	+0.3	18	+.081
12-13.5	72	29.8	59	30.1	+0.3	18	+.081
13.5-15	66	29.9	58	30.1	+0.2	18	+.0541
15-16.5	62	30.0	57	30.1	+0.1	18	+.027
16.5-18	60	30.0	56.5	30.1	+0.1	18	+.027
18-19.5	58	30.1	55.5	30.1	0	18	.0
19.5-20	55.5	30.1	55	30.1	0	18	0
							+.520

i. e. potential heave = $\frac{1}{2}$ in.

For this non-fissuring soil
$$AH \times \frac{\Delta w G_s}{100 + w_i G_s} \cdot H$$

where: $G_s = 2.75$

Substantial heave occurs at depth, i. e. below 10 ft. However, in this case, the total heave is relatively small.

APPENDIX B

RESPONSE OF GRANULAR MATERIALS SUBJECTED TO REPEATED LOADING

Tables B1 through B6 contain a summary of the data by Hicks (30) on which the material such as that presented in Figs. 23 and 24 are based.

Effects of Stress Sequence

Hicks has demonstrated that for dry, and partially saturated granular materials the variation in resilient modulus with stress state can be established on one specimen provided the response at each stress state is measured after about 100 repetitions of the applied axial stress. Typical results of this study are shown in Figs. B1 and B2.

For saturated granular materials it is necessary to subject the specimen to approximately 1,000 stress repetitions at each stress level. Results for one such specimen subjected to this procedure are shown in Fig. B3.

The number of test conditions may also be minimized by noting that the slope, n , of the relation

$$M_R = K \sigma_3^n$$

may be taken as approximately 0.55 for a range in conditions and that the slope, n' , of the relation

$$M_R = K' \theta^{n'}$$

may be taken as 0.65.

Effects of Density and Water Content

To simplify still further the testing required for granular materials, the data presented in Tables B1 through B6 may provide some reasonable estimates of the affects of mix variables such as density and water content.

The data in Fig. 24 indicate that a 6 percent increase in water content, for the range normally encountered, can result in a decrease in modulus in the range 40-50 percent depending on the fineness of the aggregate grading. Accordingly we could reduce the K or K' value by about 7 to 8 percent for each one percent increase in water content. The data in the tables indicate, on the other hand, that n and n' are relatively unaffected by water content. By this process one could approximately account for anticipated changes in water content that might occur seasonally.

Similarly a change in density influences the K or K' values but has little influence on n or n' . Generally a change in relative density of 10 percent for the range normally antic-

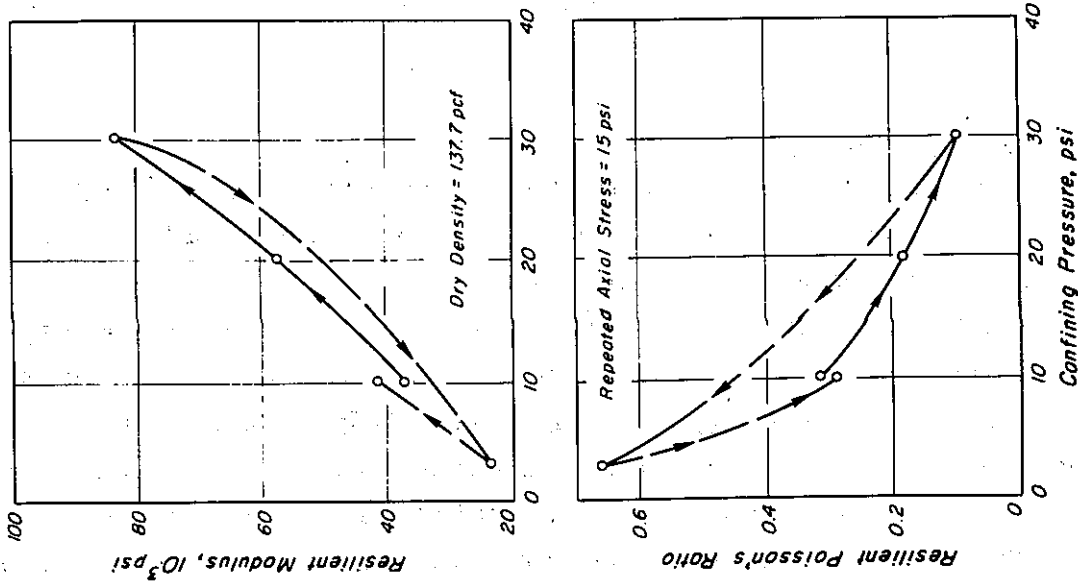


Fig. B1 - Effect of stress sequence on the variation of resilient modulus and Poisson's ratio with confining pressure. Specimen No. C(00)-1D, 100 repetitions per stress level. Crushed aggregate.

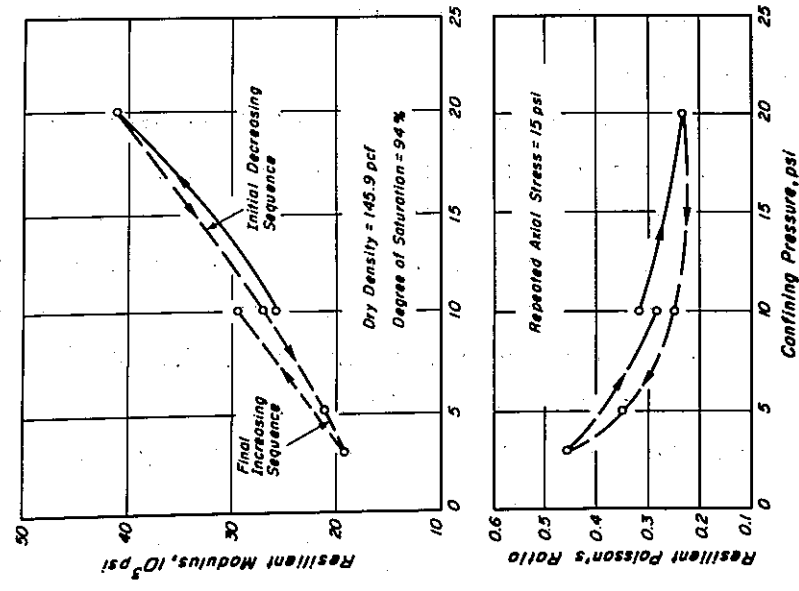


Fig. B2 - Effect of stress sequence on the variation of resilient modulus and Poisson's ratio with confining pressure. Specimen C(2)-2P2, 100 repetitions per stress level. Crushed aggregate.

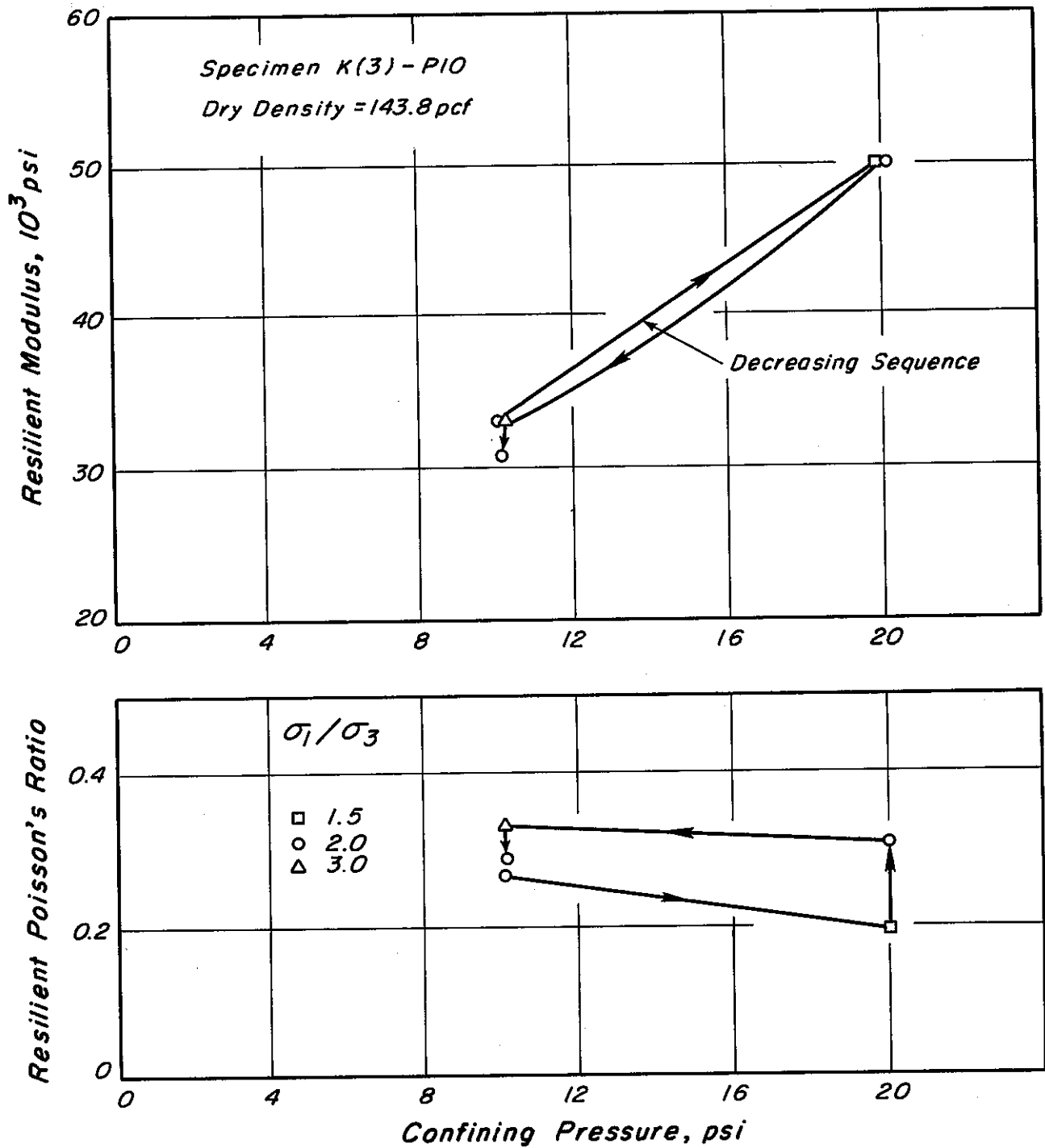


Fig. B3 — Effect of stress sequence on the variation of resilient modulus and Poisson's ratio. Saturated undrained test. 1,000 repetitions per stress level. High density level. Partially crushed aggregate.

ipated in the field may influence K or K' by the order of 10 to 15 percent. Thus it is possible that the influence of different degrees of compaction may be approximated relatively simply.

TABLE B1 — SUMMARY OF CONSTANTS K, n AND K', n' RELATING RESILIENTS MODULUS TO CONFINING PRESSURE (σ_3) AND TO THE SUM OF THE PRINCIPAL STRESSES (θ) AND MEAN POISSON'S RATIO FOR DRY TEST SERIES

Aggregate Type	Percent Passing 200	Relative Density Percent	K	n	K'	n'	Mean Poisson's Ratio*
Partially Crushed	3	74.5	8,036	.60	2,156	.71	0.50+
		89.2	11,752	.53	3,977	.61	0.45
	5	96.4	13,644	.53	4,119	.63	0.47
		85.5	10,252	.64	2,780	.73	0.45
		100.2	11,157	.59	3,289	.67	0.32
		59.1	7,962	.57	2,447	.66	0.49
	8	73.0	9,006	.57	2,543	.68	0.45
		86.5	8,939	.61	2,427	.71	0.34
Crushed	3	89.3	12,338	.55	4,368	.60	0.41
		100.3	10,806	.62	3,103	.70	0.35
	5	77.2	11,446	.59	3,572	.66	0.35
		87.0	13,435	.56	4,340	.63	0.27
	10	91.3	14,874	.51	4,949	.60	0.30
		77.0	14,313	.52	5,017	.57	0.23
		86.0	14,672	.50	5,049	.57	0.27

*Average of values at σ_1/σ_3 of 2.0 and 5.0.

TABLE B2 — SUMMARY OF CONSTANTS K, n AND K', n' RELATING RESILIENT MODULUS TO CONFINING PRESSURE (σ_3) AND TO THE SUM OF THE PRINCIPAL STRESSES (θ) AND MEAN POISSON'S RATIO FOR PARTIALLY SATURATED TEST SERIES

Aggregate Type	Percent Passing #200	Relative Density Percent	Degree of Saturation Percent	K	n	K'	n'	Mean Poisson's Ratio*
Partially Crushed	3	80.7	65	6,786	.59	2,033	.68	0.25
		89.5	67	10,418	.54	3,343	.62	0.34
	5	89.5	68	6,937	.57	2,068	.66	0.39
		102.0	85	7,119	.62	2,039	.70	0.45
		107.0	90	9,795	.56	3,122	.64	0.38
		82.8	75	5,204	.64	1,608	.71	0.50+
	8	92.9	83	7,302	.62	1,901	.73	0.42
		86.1	70	8,818	.57	2,714	.65	0.29
Crushed	3	104.0	74	9,821	.57	2,710	.68	0.25
		78.2	76	7,833	.58	2,351	.66	0.35
	5	78.8	74	8,563	.56	2,589	.65	0.34
		87.3	81	9,032	.58	2,678	.66	0.22
		91.8	94	8,759	.57	2,231	.67	0.45
		98.0	92	9,863	.55	3,038	.64	0.45

*Average of values at σ_1/σ_3 of 2.0 and 5.0.

TABLE B3 — SUMMARY OF CONSTANTS K, n AND K', n' RELATING RESILIENT MODULUS TO CONFINING PRESSURE (σ_3) AND TO THE SUM OF PRINCIPAL STRESSES (θ) AND MEAN POISSON'S RATIO FOR SATURATED TEST SERIES

Aggregate Type	Percent Passing #200	Relative Density Percent	K	n	K'	n'	Mean Poisson's Ratio*
Partially Crushed	3	79.9	9,598	.55	2,681	.67	0.25
		88.7	10,396	.54	3,278	.63	0.20
		90.1	10,771	.50	3,616	.60	0.33
	5	74.2	8,080	.54	2,481	.65	0.36
		83.8	9,430	.50	3,208	.59	0.35
		95.0	9,801	.58	2,612	.71	0.34
		81.5	9,063	.52	2,967	.62	0.25
		92.0	12,015	.49	4,068	.58	0.25
		8					

*Average of values at σ_1/σ_3 of 2.0 and 5.0.

TABLE B4 — INFLUENCE OF AGGREGATE GRADATION ON RESILIENT PROPERTIES OF GRANULAR BASE MATERIALS

Percent Passing #200	Relative Density Percent	Degree of Saturation Percent	K	n	Mean Poisson's Ratio
<u>Partially Crushed Aggregate</u>					
3	89.2	0	11,752	.53	0.45
		0	10,252	.64	0.45
		0	8,939	.61	0.34
5	85.5	0			
		100	9,598	.55	0.25
8	86.5	100	9,430	.50	0.35
		100	9,063	.52	0.25
<u>Crushed Aggregate</u>					
3	89.3	0	12,338	.55	0.41
		0	13,435	.56	0.27
		0	14,672	.50	0.27
5	87.0	0			
		0	11,446	.59	0.35
10	86.0	0	14,313	.52	0.23
		0			

TABLE B5 - INFLUENCE OF AGGREGATE TYPE ON THE RESILIENT PROPERTIES OF GRANULAR BASE MATERIALS

Aggregate Type	Relative Density Percent	Degree of Saturation Percent	K	n	Mean Poisson's Ratio
<u>Coarse Grading</u>					
PC	89.2	0	11,752	.53	0.45
C	89.3	0	12,338	.55	0.41
PC*	86.0	66	9,000	.56	0.30
C	86.1	70	8,818	.57	0.29
<u>Medium Grading</u>					
PC	85.5	0	10,252	.64	0.45
C	87.0	0	13,435	.56	0.27
PC	89.5	68	6,937	.57	0.39
C	87.3	81	9,032	.58	0.22
<u>Fine Grading</u>					
PC	86.5	0	8,939	.61	0.34
C	86.0	0	14,672	.50	0.27
PC	92.9	83	7,302	.62	0.42
C	91.8	94	7,759	.57	0.45

*Values obtained using linear interpolation.

TABLE B6 - INFLUENCE OF DEGREE OF SATURATION ON THE RESILIENT PROPERTIES OF GRANULAR BASE MATERIALS

Percent Passing #200	Relative Density Percent	Degree of Saturation Percent	K	n	Mean Poisson's Ratio
<u>Partially Crushed Aggregate</u>					
3	80.0*	0	9,620*	.57*	0.48*
	80.1	65	6,786	.59	0.24
	79.9	100	9,598	.55	0.25
5	85.5	0	10,252	.64	0.45
	89.5	68	6,937	.57	0.39
	83.8	100	9,430	.50	0.35
8	86.5	0	8,939	.61	0.34
	82.8	75	5,204	.64	0.50
	87.5	100	9,063	.52	0.25
<u>Crushed Aggregate</u>					
3	89.3	0	12,338	.55	0.41
	86.1	70	8,818	.56	0.29
5	87.0	0	13,435	.56	0.27
	87.3	81	9,032	.58	0.22
10	86.0	0	14,672	.50	0.23
	91.8	94	7,759	.57	0.45

*Values obtained using linear interpolation.

APPENDIX C
COMPUTER PROGRAM LISTINGS

PROGRAM INSTRUCTIONS FOR MULTI-LAYERED ELASTIC SYSTEM WITH A SINGLE VERTICAL LOAD

Description

The multi-layered elastic system computer program (CHEV5L) will determine the various component stresses and strains in a three dimensional ideal elastic layered system with a single vertical uniform circular load at the surface of the system. The bottom layer of the system is semi-infinite with all other layers of uniform thickness. All layers extend infinitely in the horizontal direction. The top surface of the system is free of shear and all interfaces between layers have full continuity of stresses and displacements.

With a vertical uniform circular load, the system is axisymmetric with the Z axis perpendicular to the layers and extending through the center of the load. Points in the system are described by a set of cylindrical coordinates consisting of R- and Z-values where R is the horizontal distance out from the center of the load and Z is the depth to the point measured vertically from the surface of the system.

The load is described by the total vertical load in pounds and the tire pressure in psi. The load radius is computed by the program. Each layer of the system is described by a modulus of elasticity in psi, a Poisson's ratio, and thickness in inches. Layers are numbered consecutively downward, the upper layer being designated as layer 1.

Program Operating Notes

The program operates with the various given R- and Z-values as follows: For each R-value a complete set of characterizing functions is developed for all layers, then the stresses and strains are computed at points represented by that R and each of the given Z-values. The program then steps to the next R-value and computes the stresses and strains at points represented by each of the given Z-values continuing until all combinations of R- and Z-values are used.

When a given Z-value is directly on an interface between two layers, the program will first compute the stresses and strains at this point using the functions for the upper of the two layers then will recompute the stresses and strains at this same point using the functions from the lower of the two layers. In the output of the program a negative Z-value indicates that the stresses and strains have been computed at an interface and the characteristics of the upper layer have been used.

Limitations

The following are limitations of the program and/or method.

1. Number of layers in the system; minimum of two and a maximum of five.
2. Number of points in the system where stresses and strains are to be determined; minimum of one (one R and one Z) to a maximum of 121 (maximum of 11R and 11Z)
3. All data are positive, no negative values.
4. Poisson's ratio must not have a value of one.

Input Cards

The notation cc refers to card columns, with the range of columns being inclusive. All "REAL" values are punched with a decimal point as a part of the value and all "INTEGER" values are to be punched without a decimal point and right justified in the data field.

- | | | |
|--------|--|--|
| Card 1 | cc5 | any integer value other than 9. This card is placed at the beginning of each new problem to be solved. The placing of a card, with the integer 9 in cc5, following the last problem to be solved, causes the program to stop (INTEGER) |
| Card 2 | cc1-72 | any combination of alphanumeric characters may be used to identify the problem to be solved.
FORMAT (12 A6) |
| Card 3 | cc1-12
cc13-24 | total load in pounds (REAL)
tire pressure in psi (REAL) FORMAT (2F 12. 0) |
| Card 4 | cc1-2
cc3-10
cc11-16
cc17-24
cc25-30
etc. | number of layers in the system (INTEGER)
modulus of elasticity for layer 1 (REAL)
Poisson's ratio for layer 1 (REAL)
modulus of elasticity for layer 2 (REAL)
Poisson's ratio for layer 2 (REAL)
etc.
FORMAT (I2, 5(F8. 0, F6. 0)) |
| Card 5 | cc1-6
cc7-12
etc. | thickness of layer 1 in inches (REAL)
thickness of layer 2 in inches (REAL)
etc.
FORMAT (4F 6. 0) |
| Card 6 | cc1-3
cc4-10
cc11-20
etc. | number of values in card (INTEGER)
first value in inches (REAL)
second value in inches (REAL)
etc.
FORMAT (I, 3F 6. 0) |

Card 6 cc1-6 number of R-values on card (INTEGER)
cc7-12 first R-value in inches (REAL)
cc13-18 second R-value in inches (REAL)
etc.
FORMAT (I6, 11F6.0)

Card 7 cc1-6 number of Z-values on card (INTEGER)
cc7-12 first Z-value in inches (REAL)
cc12-18 second Z-value in inches (REAL)
etc.
FORMAT (I6, 11F6.0)


```

TZZ = 1.0
34 CONTINUE
CALL CALCIN
IF (TZZ) 36,36+25
35 ZZ(I2T) = -ZZ(I2T)
I2T = I2T-1
36 CONTINUE
GO TO 200
END
SURROUTINE CALCIN
CCALCIN *****SURROUTINE CALCIN - N-LAYER ELASTIC SYSTEM *****
DIMENSION RR(11),ZZ(11),F(5),V(5),H(4),H(4),AZ(184),A(184),S1,
COMMON RR,ZZ,F,V,H,H,AZ,A(184),RJI(184),RJO(184)
DIMENSION TIP,E(12),BZ(47),X(4,4),SC(4),PM(4,4,2),FM(2,2),
1 TEST(11)
COMMON TIP,E,PSI,NLINE,NTEST,TEST,
1 ITN4, LC, JT, TZZ, PR, PA, EP, TIP, TIM, T1, T2, T3, T4,
2 T5, T6, T2P, T2M, MA, BJI, BJO, BZ, 2F, SZ1, SZ2, PM, SGI, SG2,
3 PH, PH2, VK7, VKP2, VK4, VKP4, VKK8, X, SC, FM
DIMENSION W(4)
1 W(1) = 0.34785485
W(2) = 0.65214515
W(3) = W(2)
W(4) = W(1)
2 VL=2.0+V(L)/E(L)
FL=(1.0+VL)/E(L)
VLI=1.0-VL
CSZ=0.0
CST=0.0
CSR=0.0
CTR=0.0
COM=0.0
CMU=0.0
NTS1 = NTEST + 1
ITS = 1
JT = 0
ARP=AR*PSI
10 DO 40 I=1,ITN
C INITIALIZE THE SUB-INTEGRALS
RSZ=0.0
RST=0.0
RTR=0.0
ROM=0.0
RMU=0.0
DO 30 J=1,6
J1 = K + J
P=AZ(J1)
EP=EXP(IP*Z)
TI=BI(J1)*EP
T2=D(I,J1)/EP
TIP=TI+T2
TIM=TI-T2
T1=(A(J1)+H(J1))*Z)*EP
T2=(C(J1)+D(J1)+L)*Z)/EP
T2M=P*(T1-T2)
T2Me=P*(T1-T2)
WA=AJ(J1)*W(J)
IF (R) 20,20+15
15 RJI=RJI(J1)*P
RJO=RJO(J1)*P
RSZ=RSZ+WA*P*BJO*(VL)*TIP-T2M)
ROM=ROM+WA*EL*BJO*(2.0*VL)*TIM-T2P)
RTR=RTR+WA*P*BJ1*(VL)*TIM+T2P)
RMU=RMU+WA*EL*BJ1*(TIP+T2M)
RSR=RSR+WA*P*BJO*(1.0+VL)*TIP+T2M)-RJI*(TIP+T2M)/R)
RST=RST+WA*(VL)*P*BJO*(TIP+T2M)/R)
GO TO 30
C SPECIAL ROUTINE FOR R = ZERO
20 P=PE*P
RSZ=RSZ+WA*PP*(VL)*TIP-T2M)
ROM=ROM+WA*EL*P*(2.0*VL)*TIM-T2P)
RST=RST+WA*PP*(VL+0.5)*TIP+0.5*T2M)
RSR=RST
30 CONTINUE
SF = (AZ(K+4) - AZ(K+1))/1.7222726
CSZ=CSZ+RSZ*SF
CST=CST+RST*SF
CSR=CSR+RSR*SF
CTR=CTR+RTR*SF
COM=COM+ROM*SF
CMU=CMU+RMU*SF
RST = 2.0*RSZ*AR*SF
TESTH = ABS (RSZ) -10.0*(**(-4)
IF (ITS-NTS1) 31,32+32
31 CONTINUE
TEST(ITS) = TESTH
ITS = ITS+1
GO TO 40
32 CONTINUE
TEST(NTS1) = TESTH
DO 33 J = 1,NTST
IF (TESTH-TEST(J)) 35,36+36
35 CONTINUE
TESTH = TEST(J)
36 CONTINUE
TEST(J) = TEST(J+1)
33 CONTINUE
IF (TESTH) 50,50+40
40 CONTINUE
JT = 1
50 CSZ=CSZ+ARP
CST=CST+ARP
CTR=CTR+ARP
CSR=CSR+ARP

```

```

GA 1090
GA 1100
GA 1110
GA 1120
GA 1130
GA 1140
GA 1150
GA 1160
GA 1170
GA 1180
GA 1190
GA 1200
GA 1210
GA 1220
GA 1230
GA 1240
GA 1250
GA 1260
GA 1270
GA 1280
GA 1290
GA 1300
GA 1310
GA 1320
GA 1330
GA 1340
GA 1350
GA 1360
GA 1370
GA 1380
GA 1390
GA 1400
GA 1410
GA 1420
GA 1430
GA 1440
GA 1450
GA 1460
GA 1470
GA 1480
GA 1490
GA 1500
GA 1510
GA 1520
GA 1530
GA 1540
GA 1550
GA 1560
GA 1570
GA 1580
GA 1590
GA 1600
GA 1610
GA 1620
GA 1630
TIP=TI+T2
TIM=TI-T2
T1=(A(J1)+H(J1))*Z)*EP
T2=(C(J1)+D(J1)+L)*Z)/EP
T2M=P*(T1-T2)
T2Me=P*(T1-T2)
WA=AJ(J1)*W(J)
IF (R) 20,20+15
15 RJI=RJI(J1)*P
RJO=RJO(J1)*P
RSZ=RSZ+WA*P*BJO*(VL)*TIP-T2M)
ROM=ROM+WA*EL*BJO*(2.0*VL)*TIM-T2P)
RTR=RTR+WA*P*BJ1*(VL)*TIM+T2P)
RMU=RMU+WA*EL*BJ1*(TIP+T2M)
RSR=RSR+WA*P*BJO*(1.0+VL)*TIP+T2M)-RJI*(TIP+T2M)/R)
RST=RST+WA*(VL)*P*BJO*(TIP+T2M)/R)
GO TO 30
C SPECIAL ROUTINE FOR R = ZERO
20 P=PE*P
RSZ=RSZ+WA*PP*(VL)*TIP-T2M)
ROM=ROM+WA*EL*P*(2.0*VL)*TIM-T2P)
RST=RST+WA*PP*(VL+0.5)*TIP+0.5*T2M)
RSR=RST
30 CONTINUE
SF = (AZ(K+4) - AZ(K+1))/1.7222726
CSZ=CSZ+RSZ*SF
CST=CST+RST*SF
CSR=CSR+RSR*SF
CTR=CTR+RTR*SF
COM=COM+ROM*SF
CMU=CMU+RMU*SF
RST = 2.0*RSZ*AR*SF
TESTH = ABS (RSZ) -10.0*(**(-4)
IF (ITS-NTS1) 31,32+32
31 CONTINUE
TEST(ITS) = TESTH
ITS = ITS+1
GO TO 40
32 CONTINUE
TEST(NTS1) = TESTH
DO 33 J = 1,NTST
IF (TESTH-TEST(J)) 35,36+36
35 CONTINUE
TESTH = TEST(J)
36 CONTINUE
TEST(J) = TEST(J+1)
33 CONTINUE
IF (TESTH) 50,50+40
40 CONTINUE
JT = 1
50 CSZ=CSZ+ARP
CST=CST+ARP
CTR=CTR+ARP
CSR=CSR+ARP

```

GA 1640
GA 1650
GA 1660
GA 1670
GA 1680
GA 1690
GA 1700
GA 1710
GA 1720
GA 1730
GA 1740
GA 1750
GA 1760
GA 1770
GA 1780
GA 1790
GA 1800
GA 1810
GA 1820
GA 1830
GA 1840
GA 1850
GA 1860
GA 1870
GA 1880
GA 1890
GA 1900
GA 1910
GA 1920
GA 1930
GA 1940
GA 1950
GA 1960
GA 1970
GA 1980
GA 1990
GA 2000
GA 2010
GA 2020
GA 2030
GA 2040
GA 2050
GA 2060
GA 2070
GA 2080
GA 2090
GA 2100
GA 2110
GA 2120
GA 2130
GA 2140
GA 2150
GA 2160
GA 2170
GA 2180


```

GA 3260      VK4=2*0*VK2
GA 3270      VKP4=2*0*VKP2
GA 3280      VKK8=8*0*VK(K)*V(K+1)
GA 3290      X(K+1,1)=VK4-3*0-T1
GA 3300      X(K+2,1)=0*0
GA 3310      X(K+3,1)=T1*(PH2-VK4+1*0)
GA 3320      X(K+4,1)=-2*0*T1*MP
GA 3330      T3=PH2*(VK2-1*0)
GA 3340      T4=VKK8+1*0-3*0*VKP2
GA 3350      T5=PH2*(VKP2-1*0)
GA 3360      T6=VKK8+1*0-3*0*VK2
GA 3370      X(K+1,2)=(T3+T4-T1)*(T5+T6))/P
GA 3380      X(K+2,2)=T1*(VKP4-3*0)-1*0
GA 3390      X(K+4,2)=T1*(1*0-PH2-VKP4)
GA 3400      X(K+3,4)=(T3-T4-T1)*(T5-T6))/P
GA 3410      T3=PH2*PH-VKK8+1*0
GA 3420      T4=PH2*(VK2-VKP2)
GA 3430      X(K+1,4)=(T3+T4+VKP2-T1*(T3+T4+VK2))/P
GA 3440      X(K+3,4)=(T3+T4-VKP2+T1*(T3-T4+VK2))/P
GA 3450      X(K+1,3)=T1*(1*0-PH2-VK4)
GA 3460      X(K+2,3)=2*0*T1*MP
GA 3470      X(K+3,3)=VK4-3*0-T1
GA 3480      X(K+4,3)=0*0
GA 3490      X(K+2,4)=T1*(PH2-VKP4+1*0)
GA 3500      X(K+4,4)=T1*(VKP4-3*0)-1*0
GA 3510      K = K
GA 3520      10 CONTINUE
GA 3530      COMPUTE THE PRODUCT MATRICES PM
GA 3540      SC(N)=4*0*(V(N)-1*0)
GA 3550      IF (N-2) 13,11,11
GA 3560      11 DO 12 K1=2,N
GA 3570      M=NS-K1
GA 3580      SC(M)=SC(M)+4*0*(V(M)-1*0)
GA 3590      K = K
GA 3600      12 CONTINUE
GA 3610      13 CONTINUE
GA 3620      K = N
GA 3630      DO 15 I=1,4
GA 3640      DO 14 J=1,2
GA 3650      14 SV(I,J) = X(K+I,J+2)
GA 3660      15 CONTINUE
GA 3670      CV1(I,1) = -2*0*PH*H(K)
GA 3680      K = K-1
GA 3690      IF(K) 50,50,20
GA 3700      20 CONTINUE
GA 3710      DO 42 J=1,4
GA 3720      T(1) = SV3(1,J)
GA 3730      T(2) = SV3(2,J)
GA 3740      T(3) = SV3(3,J)
GA 3750      T(4) = SV3(4,J)
GA 3760      T(5) = SV3(1,J+4)
GA 3770      T(6) = SV3(2,J+4)
GA 3780      T(7) = SV3(3,J+4)
GA 3790      T(8) = SV3(4,J+4)
GA 3800      DO 41 I=1,4
GA 3810      SVA(I,J) = X(K+I,1)*T(1)+X(K+I,2)*T(2)
GA 3820      +X(K+I,3)*T(3)+X(K+I,4)*T(4)
GA 3830      +X(K+I,5)*T(5)+X(K+I,6)*T(6)
GA 3840      +X(K+I,7)*T(7)+X(K+I,8)*T(8)
GA 3850      DO 21 I=1,4
GA 3860      SV2(I,J+1) = X(K+I,1)*T(1)+X(K+I,2)*T(2)
GA 3870      +X(K+I,3)*T(3)+X(K+I,4)*T(4)
GA 3880      +X(K+I,5)*T(5)+X(K+I,6)*T(6)
GA 3890      +X(K+I,7)*T(7)+X(K+I,8)*T(8)
GA 3900      22 CONTINUE
GA 3910      T(1) = CV1(1,1)
GA 3920      T(2) = -2*0*PH*H(K)
GA 3930      CV2(1,1) = T(1)
GA 3940      CV2(1,2) = T(2)
GA 3950      CV2(2,1) = T(1)-T(2)
GA 3960      K = K-1
GA 3970      IF (K) 50,50,30
GA 3980      30 CONTINUE
GA 3990      NO 34 J=1,4
GA 4000      JI = J
GA 4010      IF (JI-2) 32,32,31
GA 4020      31 JI = JI+2
GA 4030      32 CONTINUE
GA 4040      T(1) = SV2(1,J)
GA 4050      T(2) = SV2(2,J)
GA 4060      T(3) = SV2(3,J)
GA 4070      T(4) = SV2(4,J)
GA 4080      DO 33 I=1,4
GA 4090      SV3(I,J+1) = X(K+I,1)*T(1)+X(K+I,2)*T(2)
GA 4100      +X(K+I,3)*T(3)+X(K+I,4)*T(4)
GA 4110      +X(K+I,5)*T(5)+X(K+I,6)*T(6)
GA 4120      +X(K+I,7)*T(7)+X(K+I,8)*T(8)
GA 4130      T(1) = -2*0*PH*H(K)
GA 4140      DO 35 J=1,2
GA 4150      CV3(1,J) = CV2(1,J)
GA 4160      CV3(2,J) = CV2(2,J)-T(1)
GA 4170      CV3(3,J+2) = CV2(3,J)+T(1)
GA 4180      CV3(4,J+2) = CV2(4,J)
GA 4190      35 CONTINUE
GA 4200      K = K-1
GA 4210      IF (K) 50,50,40
GA 4220      40 CONTINUE
GA 4230      DO 42 J=1,4
GA 4240      T(1) = SV3(1,J)
GA 4250      T(2) = SV3(2,J)
GA 4260      T(3) = SV3(3,J)
GA 4270      T(4) = SV3(4,J)
GA 4280      T(5) = SV3(1,J+4)
GA 4290      T(6) = SV3(2,J+4)
GA 4300      T(7) = SV3(3,J+4)
GA 4310      T(8) = SV3(4,J+4)
GA 4320      DO 41 I=1,4
GA 4330      SVA(I,J) = X(K+I,1)*T(1)+X(K+I,2)*T(2)
GA 4340      +X(K+I,3)*T(3)+X(K+I,4)*T(4)
GA 4350      +X(K+I,5)*T(5)+X(K+I,6)*T(6)
GA 4360      +X(K+I,7)*T(7)+X(K+I,8)*T(8)

```

```

GA 3260      VK4=2*0*VK2
GA 3270      VKP4=2*0*VKP2
GA 3280      VKK8=8*0*VK(K)*V(K+1)
GA 3290      X(K+1,1)=VK4-3*0-T1
GA 3300      X(K+2,1)=0*0
GA 3310      X(K+3,1)=T1*(PH2-VK4+1*0)
GA 3320      X(K+4,1)=-2*0*T1*MP
GA 3330      T3=PH2*(VK2-1*0)
GA 3340      T4=VKK8+1*0-3*0*VKP2
GA 3350      T5=PH2*(VKP2-1*0)
GA 3360      T6=VKK8+1*0-3*0*VK2
GA 3370      X(K+1,2)=(T3+T4-T1)*(T5+T6))/P
GA 3380      X(K+2,2)=T1*(VKP4-3*0)-1*0
GA 3390      X(K+4,2)=T1*(1*0-PH2-VKP4)
GA 3400      X(K+3,4)=(T3-T4-T1)*(T5-T6))/P
GA 3410      T3=PH2*PH-VKK8+1*0
GA 3420      T4=PH2*(VK2-VKP2)
GA 3430      X(K+1,4)=(T3+T4+VKP2-T1*(T3+T4+VK2))/P
GA 3440      X(K+3,4)=(T3+T4-VKP2+T1*(T3-T4+VK2))/P
GA 3450      X(K+1,3)=T1*(1*0-PH2-VK4)
GA 3460      X(K+2,3)=2*0*T1*MP
GA 3470      X(K+3,3)=VK4-3*0-T1
GA 3480      X(K+4,3)=0*0
GA 3490      X(K+2,4)=T1*(PH2-VKP4+1*0)
GA 3500      X(K+4,4)=T1*(VKP4-3*0)-1*0
GA 3510      K = K
GA 3520      10 CONTINUE
GA 3530      COMPUTE THE PRODUCT MATRICES PM
GA 3540      SC(N)=4*0*(V(N)-1*0)
GA 3550      IF (N-2) 13,11,11
GA 3560      11 DO 12 K1=2,N
GA 3570      M=NS-K1
GA 3580      SC(M)=SC(M)+4*0*(V(M)-1*0)
GA 3590      K = K
GA 3600      12 CONTINUE
GA 3610      13 CONTINUE
GA 3620      K = N
GA 3630      DO 15 I=1,4
GA 3640      DO 14 J=1,2
GA 3650      14 SV(I,J) = X(K+I,J+2)
GA 3660      15 CONTINUE
GA 3670      CV1(I,1) = -2*0*PH*H(K)
GA 3680      K = K-1
GA 3690      IF(K) 50,50,20
GA 3700      20 CONTINUE
GA 3710      DO 42 J=1,4
GA 3720      T(1) = SV3(1,J)
GA 3730      T(2) = SV3(2,J)
GA 3740      T(3) = SV3(3,J)
GA 3750      T(4) = SV3(4,J)
GA 3760      T(5) = SV3(1,J+4)
GA 3770      T(6) = SV3(2,J+4)
GA 3780      T(7) = SV3(3,J+4)
GA 3790      T(8) = SV3(4,J+4)
GA 3800      DO 41 I=1,4
GA 3810      SVA(I,J) = X(K+I,1)*T(1)+X(K+I,2)*T(2)
GA 3820      +X(K+I,3)*T(3)+X(K+I,4)*T(4)
GA 3830      +X(K+I,5)*T(5)+X(K+I,6)*T(6)
GA 3840      +X(K+I,7)*T(7)+X(K+I,8)*T(8)

```

```

41 5V4(I,J+2) = X(K,I,3)*T(I,7)+X(K,I,4)*T(I,8)
42 CONTINUE
DO 43 J=1,4
  CV4(I,J) = CV3(I,J)
  CV4(I,J+4) = CV3(I,J)-T(I)
  CV4(I,J+8) = CV3(I,2)+J+T(I)
  CV4(I,J+8) = CV3(I,2)+J
43 CONTINUE
C
50 CONTINUE
NT(I) = 1
DO 51 K=2,N
  NT(K) = NT(K-1)+NT(K-1)
50 80 K=1:N
  K1 = NS-K
  DO 52 I=1,4
    PM(K1,I) = 0.0
    PM(K1,I+2) = 0.0
52 CONTINUE
I1 = NT(K)
DO 80 I=1,I1
  I2 = I+1
  GO TO (61,62,63,64),K
61 CONTINUE
T(3) = CV1(I,1)
T(4) = CV1(I,1)
GO TO 65
62 CONTINUE
T(3) = CV2(I,1)
T(4) = CV2(I,1)
GO TO 65
63 CONTINUE
T(3) = CV3(I,1)
T(4) = CV3(I,1)
GO TO 65
64 CONTINUE
T(3) = CV4(I,1)
T(4) = CV4(I,1)
65 CONTINUE
T(1) = 0.0
T(2) = 0.0
IF (T(3)+68.0).67.66.66
66 T(1) = EXP (T(3))
67 IF (T(4)+68.0).69.68.68
68 T(7) = EXP (T(4))
69 CONTINUE
DO 80 J=1,2
  GO TO (71,72,73,74),K
71 CONTINUE
T(3) = 5V1(I,1)
T(4) = 5V1(I,2)
T(5) = 5V1(I,2+1)

```

```

GA 4360
GA 4370
GA 4380
GA 4390
GA 4400
GA 4410
GA 4420
GA 4430
GA 4440
GA 4450
GA 4460
GA 4470
GA 4480
GA 4490
GA 4500
GA 4510
GA 4520
GA 4530
GA 4540
GA 4550
GA 4560
GA 4570
GA 4580
GA 4590
GA 4600
GA 4610
GA 4620
GA 4630
GA 4640
GA 4650
GA 4660
GA 4670
GA 4680
GA 4690
GA 4700
GA 4710
GA 4720
GA 4730
GA 4740
GA 4750
GA 4760
GA 4770
GA 4780
GA 4790
GA 4800
GA 4810
GA 4820
GA 4830
GA 4840
GA 4850
GA 4860
GA 4870
GA 4880
GA 4890
GA 4900

```

```

T(6) = 5V1(I,2+1,2)
GO TO 75
72 T(3) = 5V2(I,1)
T(4) = 5V2(I,2)
T(5) = 5V2(I,2+1)
T(6) = 5V2(I,2+1,2)
GO TO 75
73 T(3) = 5V3(I,1)
T(4) = 5V3(I,2)
T(5) = 5V3(I,2+1)
T(6) = 5V3(I,2+1,2)
GO TO 75
74 T(3) = 5V4(I,1)
T(4) = 5V4(I,2)
T(5) = 5V4(I,2+1)
T(6) = 5V4(I,2+1,2)
75 CONTINUE
C
PM(K1,J,1) = PM(K1,J,1)+T(1)+T(3)
PM(K1,J,2) = PM(K1,J,2)+T(1)+T(4)
PM(K1,J+2,1) = PM(K1,J+2,1)+T(2)+T(5)
PM(K1,J+2,2) = PM(K1,J+2,2)+T(2)+T(6)
80 CONTINUE
C
SOLVE FOR C(NS) AND D(NS)
VZ=2.0*V(I)
VZ1=VZ-1.0
DO 90 J=1,2
  FM(1,J)=P*PM(1,1,J)+VZ1*PM(1,2,J)+P*PM(1,3,J)-VZ*PM(1,4,J)
  FM(2,J)=P*PM(1,1,J)+VZ1*PM(1,2,J)-P*PM(1,3,J)+VZ1*PM(1,4,J)
  DFAC=5C(1)/(FM(1,1)*FM(2,2)-FM(2,1)*FM(1,2))*P*P
  A(LC,NS) = 0.0
  B(LC,NS) = 0.0
  C(LC,NS) = -FM(1,2)*DFAC
  D(LC,NS) = FM(1,1)*DFAC
DO 91 K1=1,N
  A(LC,K1)=[PM(K1,1,1)*C(LC,NS)+PM(K1,2,1)*D(LC,NS)]/5C(K1)
  B(LC,K1)=[PM(K1,2,1)*C(LC,NS)+PM(K1,3,2)*D(LC,NS)]/5C(K1)
  C(LC,K1)=[PM(K1,3,1)*C(LC,NS)+PM(K1,4,2)*D(LC,NS)]/5C(K1)
  D(LC,K1)=[PM(K1,4,1)*C(LC,NS)+PM(K1,4,2)*D(LC,NS)]/5C(K1)
91 RETURN
FND
SUBROUTINE BESSELINI, XI, Y1
CBESSEL *****SUBROUTINE BESSEL - 5-LAYER ELASTIC SYSTEM *****
DIMENSION PZ(16),QZ(16),P(16),D(16),D(20)
C
1 PZ(1)=1.0
PZ(2) = -1.125E-4
PZ(3) = 2.6710938E-7
PZ(4) = -2.3449658E-9
PZ(5) = 3.5980684E-11
PZ(6) = -1.1536133E-12
C
QZ(1) = -5.0E-3

```

```

GA 4910
GA 4920
GA 4930
GA 4940
GA 4950
GA 4960
GA 4970
GA 4980
GA 4990
GA 5000
GA 5010
GA 5020
GA 5030
GA 5040
GA 5050
GA 5060
GA 5070
GA 5080
GA 5090
GA 5100
GA 5110
GA 5120
GA 5130
GA 5140
GA 5150
GA 5160
GA 5170
GA 5180
GA 5190
GA 5200
GA 5210
GA 5220
GA 5230
GA 5240
GA 5250
GA 5260
GA 5270
GA 5280
GA 5290
GA 5300
GA 5310
GA 5320
GA 5330
GA 5340
GA 5350
GA 5360
GA 5370
GA 5380
GA 5390
GA 5400
GA 5410
GA 5420
GA 5430
GA 5440
GA 5450

```

```

OZ(2) = 4.6875E-6
OZ(3) = -2.3255859E-8
OZ(4) = 2.8307087E-10
OZ(5) = -8.9912096E-12
OZ(6) = 2.3124704E-13
C
C
PI(1) = 1.0
PI(2) = 1.875E-4
PI(3) = -3.6914083E-7
PI(4) = 2.7713225E-9
PI(5) = -4.5114421E-11
PI(6) = 1.2750463E-12
C
O1(1) = 1.5E-2
O1(2) = -6.5625E-6
O1(3) = 2.8423828E-8
O1(4) = -3.2662024E-10
O1(5) = 7.1431166E-12
O1(6) = -2.537056E-13
C
C
PI = 3.1415927
PI2 = 2.0*PI
C
C
9 N = NI
X = XI
IF (X-T*O) 10,10,160
C
10 X2=X/2.0
FAC=-X2*X2
IF (N) 11,11,14
11 C=1.0
Y=C
DO 13 I=1,34
T=I
C=FAC*C/(T*T)
TEST=ABS (C) - 10.0**(-8)
IF (TEST) 17,17,12
12 Y=Y+C
13 CONTINUE
14 C=C*X
Y=C
DO 16 I=1,34
T=I
C=FAC*C/(T*(T+1.01))
TEST=ABS (C) - 10.0**(-8)
IF (TEST) 17,17,15
15 Y=Y+C
16 CONTINUE
17 RETURN
160 IF (N) 161,161,164
C
C
OZ(2) = 4.6875E-6
OZ(3) = -2.3255859E-8
OZ(4) = 2.8307087E-10
OZ(5) = -8.9912096E-12
OZ(6) = 2.3124704E-13
C
C
PI(1) = 1.0
PI(2) = 1.875E-4
PI(3) = -3.6914083E-7
PI(4) = 2.7713225E-9
PI(5) = -4.5114421E-11
PI(6) = 1.2750463E-12
C
O1(1) = 1.5E-2
O1(2) = -6.5625E-6
O1(3) = 2.8423828E-8
O1(4) = -3.2662024E-10
O1(5) = 7.1431166E-12
O1(6) = -2.537056E-13
C
C
PI = 3.1415927
PI2 = 2.0*PI
C
C
9 N = NI
X = XI
IF (X-T*O) 10,10,160
C
10 X2=X/2.0
FAC=-X2*X2
IF (N) 11,11,14
11 C=1.0
Y=C
DO 13 I=1,34
T=I
C=FAC*C/(T*T)
TEST=ABS (C) - 10.0**(-8)
IF (TEST) 17,17,12
12 Y=Y+C
13 CONTINUE
14 C=C*X
Y=C
DO 16 I=1,34
T=I
C=FAC*C/(T*(T+1.01))
TEST=ABS (C) - 10.0**(-8)
IF (TEST) 17,17,15
15 Y=Y+C
16 CONTINUE
17 RETURN
160 IF (N) 161,161,164
C
C
161 DO 162 I=1,6
D(I) = PZ(I)
D(I+10) = QZ(I)
162 CONTINUE
GO TO 163
C
164 DO 165 I=1,6
D(I) = P1(I)
D(I+10) = Q1(I)
165 CONTINUE
163 CONTINUE
T1 = 25.0/X
T2=T1*T1
P = D(6)*T2+D(5)
DO 170 I=1,4
J = 5-I
P = P*T2+D(J)
170 CONTINUE
DO 171 I=1,4
J = 5-I
O = D(16)*T2+D(15)
J = 5-I
O = O*T2+D(J+10)
171 CONTINUE
O = O*T1
C
T4 = SORT (X*PI)
T6 = SIN (X)
T7 = COS (X)
C
IF (N) 180,180,185
180 T5 = ((P-O)*T6 + (P+O)*T7)/T4
185 T5 = ((P+O)*T6 - (P-O)*T7)/T4
99 Y = T5
RETURN
END
GA 5460
GA 5470
GA 5480
GA 5490
GA 5500
GA 5510
GA 5520
GA 5530
GA 5540
GA 5550
GA 5560
GA 5570
GA 5580
GA 5590
GA 5600
GA 5610
GA 5620
GA 5630
GA 5640
GA 5650
GA 5660
GA 5670
GA 5680
GA 5690
GA 5700
GA 5710
GA 5720
GA 5730
GA 5740
GA 5750
GA 5760
GA 5770
GA 5780
GA 5790
GA 5800
GA 5810
GA 5820
GA 5830
GA 5840
GA 5850
GA 5860
GA 5870
GA 5880
GA 5890
GA 5900
GA 5910
GA 5920
GA 5930
GA 5940
GA 5950
GA 5960
GA 5970
GA 5980
GA 5990
GA 6000
GA 6010
GA 6020
GA 6030
GA 6040
GA 6050
GA 6060
GA 6070
GA 6080
GA 6090
GA 6100
GA 6110
GA 6120
GA 6130
GA 6140
GA 6150
GA 6160
GA 6170
GA 6180
GA 6190
GA 6200
GA 6210
GA 6220
GA 6230
GA 6240
GA 6250
GA 6260
GA 6270
GA 6280
GA 6290
GA 6300
GA 6310
GA 6320
GA 6330
GA 6340
GA 6350
GA 6360
GA 6370

```

PROGRAM INSTRUCTIONS FOR MULTI-LAYERED ELASTIC SYSTEM
WITH STRESS-MODULUS ITERATION

Description

Program PSAD2, multi-layered elastic system with stress-modulus iteration uses program CHEV5L to determine the various component stresses and deformations in a three dimensional ideal layered elastic system with a single, vertical load of uniform pressure and of circular area. As with the CHEV5L system, the bottom layer is of semi-infinite vertical extent; all layers are of uniform thickness and of infinite horizontal extent, the surface is free of shear; and full continuity of stresses and displacements exist at all interfaces. Points in the axisymmetric system are described by cylindrical coordinates consisting of a radius from the center of the wheel load (R-value) and the depth from the surface of the system (Z-value).

Certain geometric restrictions are imposed on the system. These restrictions result in a symmetrical relationship between the stresses and deformations due to the applied load and those due to a second load assumed to be located at a distance D from the first. Stresses due to both wheel loads, on a vertical plane through the center of the loads, plus those due to gravity effects are combined for use in the stress-modulus iteration.

Geometric restrictions are:

1. The number of layers in the system must be five.
2. The R-values must be those to the six locations shown in Fig. C1.
3. The Z-values must be those to the eight locations shown in Fig. C1.
4. The spacing between the wheels, D, should not normally exceed twice the radius of the loaded area to maintain a relatively uniform modulus condition on any horizontal plane.

The load is described by the total vertical load in pounds and by the pressure in psi. Layers are numbered consecutively downward, the upper layer being designated as layer 1. Each layer is described by an initial elastic modulus (psi) and by a Poisson's Ratio. The upper four layers are further described; by the K coefficients of a stress-modulus relationship of the form $E = K_1 \theta^{K_2}$ where θ is the sum of the principal stresses; by the unit weight of the material in pounds per cubic foot; and by the thickness of the layer. For a linear elastic layer $K_1 = E$ and $K_2 = 0.0$. The stress-modulus relationship for layer five has the form $E = f(\sigma_d)$ where σ_d is the stress difference. This relationship is specified by coordinate pairs of E and σ_d , assuming linear segments between adjacent coordinates σ_d . Assuming linear segments between adjacent coordinates σ_d .

Operation

Stresses and deformations at each of the specified R and Z-values are determined using the CHEV5L characterizing functions. These values are stored for use in the stress-modulus subroutine. In the stress-modulus subroutine, the total effect of both wheel loads and of gravity is determined. For each layer, an average modulus (modulus required) is calculated from the stresses and is compared to the "modulus used". If these values differ by more than 2.5 percent in any layer, a new modulus, the average of the "modulus used" and "modulus required" is determined for each layer. The new moduli are communicated back to the CHEV5L portion and a new set of stresses and deformations computed.

Computations are stopped and stresses printed when the difference between the "modulus used" and the "modulus required" is less than 2.5 percent in each layer or when the maximum allowable number of iterations, specified in the input, is reached.

Stresses and deformations are output in four parts. Part 1 shows the stresses, deflection and strains, due to the single wheel load, at each R- and Z-value. Part 2 shows the stresses and resulting moduli at each point due to the total stresses. (Note: a zero modulus in a stress dependent material occurs when the sum of the principal stresses is zero or when the algebraic sum of these values results in a tensile stress). Part 3 shows the total strain at each point due to both wheel loads. Part 4 shows the maximum and minimum total stresses and their ratios at each point in the system.

Input Cards

The notation cc refers to card columns, with the range of columns being inclusive. All "REAL" values are punched with a decimal point as a part of the value and all "INTEGER" values are to be punched without a decimal point and right justified in the data field.

Card 1	cc1-5	number of problems to be solved (INTEGER) FORMAT (I5)
Card 2	cc1-80	any combination of alphanumeric characters may be used to identify the problems to be solved. FORMAT (8A10)
Card 3	cc1-10	total load on wheel in pounds (REAL)
	cc11-20	tire pressure in psi (REAL)
	cc21-25	number of layers in system (INTEGER)
	cc26-30	maximum number of iterations (INTEGER) FORMAT (2F10.0, 2I5)

Card 4 cc1-10 initially assumed modulus of elasticity of layer i in psi (REAL)
 cc11-20 Poisson's Ratio for layer i (REAL)
 cc21-30 coefficient K_1 for layer i (REAL)
 cc31-40 coefficient K_2 for layer i (REAL)
 cc41-50 unit weight of material in layer i in pcf (REAL)
 cc51-60 thickness of layer i in inches (REAL)
 FORMAT (6F10.0)

One card is required for each of the upper four layers (i = 1 to 4), the card for layer 1 being placed first followed by a card for each successive lower layer.

Card 5 cc1-10 initial assumed modulus of elasticity for layer 5 in psi (REAL)
 cc11-20 Poisson's Ratio for layer 5 (REAL)
 FORMAT (2F10.0)

Card 6 cc1-5 the number of coordinate points in the modulus deviator stress relationship for layer 5; maximum 20 (INTEGER)
 FORMAT (I5)

Card 7 cc1-10 least value of deviator stress in psi (REAL)
 cc11-20 corresponding modulus in psi (REAL)
 cc21-30 second value of deviator stress in psi (REAL)
 cc31-40 corresponding modulus in psi (REAL)
 etc repeat card 7 as required
 FORMAT (8F10.0)

Card 8 cc1-5 the number of R-values (INTEGER)
 cc6-10 the number of Z-values (INTEGER)
 FORMAT (2I5)

Card 9 cc1-10 first R-value-inches (REAL)
 cc11-20 second R-value-inches (REAL)
 etc
 FORMAT (6F10.0)

Card 10 cc1-10 first Z-value-inches (REAL)
 cc11-20 second Z-value-inches (REAL)
 etc.
 FORMAT (8F10.0)

REPEAT CARDS 2 THROUGH 10 FOR EACH NEW SYSTEM TO BE SOLVED AS INDICATED BY CARD 1.

15.51. 000001

```

PROGRAM 05A02 (INPUT,OUTPUT)
C *****
C STRESS ANALYSIS ITERATION IN THE CHEVRON FIVE LAYER PROGRAM
DIMENSION NR(6),Z(8),E(5),V(5),HH(4),AZ(184),A(184,5),H(4),
1 R(184,4),C(184,3),D(184,2),J(184),RJI(184),RJO(184)
COMMON R9,ZZ,ZZY,ZZJ,AA,AB,AC,DA,EA,EAJ,RJ,RJO
COMMON R7,R8,R9,R10,R11,P,R5Z,R5T,R5R,RT,R,RO4,RMO,SF
DIMENSION TITL(4),BZ(47),X(5,4,4),SC(4),PH(4,4,4),PH(2,2),
1 TEST(11)
COMMON TITLE,PSI,MLINE,TEST,MGT,MARK,IQ,
1 IJN4, LC, JT, YZ, PR, PA, EP, TIP, IJH, T1, T2, T3, T4,
2 T5, T6, T7, T8, T9, T10, T11, T12, T13, T14,
3 T15, T16, T17, T18, T19, T20, T21, T22, T23, T24, T25,
4 T26, T27, T28, T29, T30, T31, T32, T33, T34, T35,
5 T36, T37, T38, T39, T40, T41, T42, T43, T44, T45,
6 T46, T47, T48, T49, T50, T51, T52, T53, T54, T55,
7 T56, T57, T58, T59, T60, T61, T62, T63, T64, T65,
8 T66, T67, T68, T69, T70, T71, T72, T73, T74, T75,
9 T76, T77, T78, T79, T80, T81, T82, T83, T84, T85,
10 T86, T87, T88, T89, T90, T91, T92, T93, T94, T95,
11 T96, T97, T98, T99, T100, T101, T102, T103, T104, T105,
12 T106, T107, T108, T109, T110, T111, T112, T113, T114, T115,
13 T116, T117, T118, T119, T120, T121, T122, T123, T124, T125,
14 T126, T127, T128, T129, T130, T131, T132, T133, T134, T135,
15 T136, T137, T138, T139, T140, T141, T142, T143, T144, T145,
16 T146, T147, T148, T149, T150, T151, T152, T153, T154, T155,
17 T156, T157, T158, T159, T160, T161, T162, T163, T164, T165,
18 T166, T167, T168, T169, T170, T171, T172, T173, T174, T175,
19 T176, T177, T178, T179, T180, T181, T182, T183, T184, T185,
20 T186, T187, T188, T189, T190, T191, T192, T193, T194, T195,
21 T196, T197, T198, T199, T200, T201, T202, T203, T204, T205,
22 T206, T207, T208, T209, T210, T211, T212, T213, T214, T215,
23 T216, T217, T218, T219, T220, T221, T222, T223, T224, T225,
24 T226, T227, T228, T229, T230, T231, T232, T233, T234, T235,
25 T236, T237, T238, T239, T240, T241, T242, T243, T244, T245,
26 T246, T247, T248, T249, T250, T251, T252, T253, T254, T255,
27 T256, T257, T258, T259, T260, T261, T262, T263, T264, T265,
28 T266, T267, T268, T269, T270, T271, T272, T273, T274, T275,
29 T276, T277, T278, T279, T280, T281, T282, T283, T284, T285,
30 T286, T287, T288, T289, T290, T291, T292, T293, T294, T295,
31 T296, T297, T298, T299, T300, T301, T302, T303, T304, T305,
32 T306, T307, T308, T309, T310, T311, T312, T313, T314, T315,
33 T316, T317, T318, T319, T320, T321, T322, T323, T324, T325,
34 T326, T327, T328, T329, T330, T331, T332, T333, T334, T335,
35 T336, T337, T338, T339, T340, T341, T342, T343, T344, T345,
36 T346, T347, T348, T349, T350, T351, T352, T353, T354, T355,
37 T356, T357, T358, T359, T360, T361, T362, T363, T364, T365,
38 T366, T367, T368, T369, T370, T371, T372, T373, T374, T375,
39 T376, T377, T378, T379, T380, T381, T382, T383, T384, T385,
40 T386, T387, T388, T389, T390, T391, T392, T393, T394, T395,
41 T396, T397, T398, T399, T400, T401, T402, T403, T404, T405,
42 T406, T407, T408, T409, T410, T411, T412, T413, T414, T415,
43 T416, T417, T418, T419, T420, T421, T422, T423, T424, T425,
44 T426, T427, T428, T429, T430, T431, T432, T433, T434, T435,
45 T436, T437, T438, T439, T440, T441, T442, T443, T444, T445,
46 T446, T447, T448, T449, T450, T451, T452, T453, T454, T455,
47 T456, T457, T458, T459, T460, T461, T462, T463, T464, T465,
48 T466, T467, T468, T469, T470, T471, T472, T473, T474, T475,
49 T476, T477, T478, T479, T480, T481, T482, T483, T484, T485,
50 T486, T487, T488, T489, T490, T491, T492, T493, T494, T495,
51 T496, T497, T498, T499, T500, T501, T502, T503, T504, T505,
52 T506, T507, T508, T509, T510, T511, T512, T513, T514, T515,
53 T516, T517, T518, T519, T520, T521, T522, T523, T524, T525,
54 T526, T527, T528, T529, T530, T531, T532, T533, T534, T535,
55 T536, T537, T538, T539, T540, T541, T542, T543, T544, T545,
56 T546, T547, T548, T549, T550, T551, T552, T553, T554, T555,
57 T556, T557, T558, T559, T560, T561, T562, T563, T564, T565,
58 T566, T567, T568, T569, T570, T571, T572, T573, T574, T575,
59 T576, T577, T578, T579, T580, T581, T582, T583, T584, T585,
60 T586, T587, T588, T589, T590, T591, T592, T593, T594, T595,
61 T596, T597, T598, T599, T600, T601, T602, T603, T604, T605,
62 T606, T607, T608, T609, T610, T611, T612, T613, T614, T615,
63 T616, T617, T618, T619, T620, T621, T622, T623, T624, T625,
64 T626, T627, T628, T629, T630, T631, T632, T633, T634, T635,
65 T636, T637, T638, T639, T640, T641, T642, T643, T644, T645,
66 T646, T647, T648, T649, T650, T651, T652, T653, T654, T655,
67 T656, T657, T658, T659, T660, T661, T662, T663, T664, T665,
68 T666, T667, T668, T669, T670, T671, T672, T673, T674, T675,
69 T676, T677, T678, T679, T680, T681, T682, T683, T684, T685,
70 T686, T687, T688, T689, T690, T691, T692, T693, T694, T695,
71 T696, T697, T698, T699, T700, T701, T702, T703, T704, T705,
72 T706, T707, T708, T709, T710, T711, T712, T713, T714, T715,
73 T716, T717, T718, T719, T720, T721, T722, T723, T724, T725,
74 T726, T727, T728, T729, T730, T731, T732, T733, T734, T735,
75 T736, T737, T738, T739, T740, T741, T742, T743, T744, T745,
76 T746, T747, T748, T749, T750, T751, T752, T753, T754, T755,
77 T756, T757, T758, T759, T760, T761, T762, T763, T764, T765,
78 T766, T767, T768, T769, T770, T771, T772, T773, T774, T775,
79 T776, T777, T778, T779, T780, T781, T782, T783, T784, T785,
80 T786, T787, T788, T789, T790, T791, T792, T793, T794, T795,
81 T796, T797, T798, T799, T800, T801, T802, T803, T804, T805,
82 T806, T807, T808, T809, T810, T811, T812, T813, T814, T815,
83 T816, T817, T818, T819, T820, T821, T822, T823, T824, T825,
84 T826, T827, T828, T829, T830, T831, T832, T833, T834, T835,
85 T836, T837, T838, T839, T840, T841, T842, T843, T844, T845,
86 T846, T847, T848, T849, T850, T851, T852, T853, T854, T855,
87 T856, T857, T858, T859, T860, T861, T862, T863, T864, T865,
88 T866, T867, T868, T869, T870, T871, T872, T873, T874, T875,
89 T876, T877, T878, T879, T880, T881, T882, T883, T884, T885,
90 T886, T887, T888, T889, T890, T891, T892, T893, T894, T895,
91 T896, T897, T898, T899, T900, T901, T902, T903, T904, T905,
92 T906, T907, T908, T909, T910, T911, T912, T913, T914, T915,
93 T916, T917, T918, T919, T920, T921, T922, T923, T924, T925,
94 T926, T927, T928, T929, T930, T931, T932, T933, T934, T935,
95 T936, T937, T938, T939, T940, T941, T942, T943, T944, T945,
96 T946, T947, T948, T949, T950, T951, T952, T953, T954, T955,
97 T956, T957, T958, T959, T960, T961, T962, T963, T964, T965,
98 T966, T967, T968, T969, T970, T971, T972, T973, T974, T975,
99 T976, T977, T978, T979, T980, T981, T982, T983, T984, T985,
100 T986, T987, T988, T989, T990, T991, T992, T993, T994, T995,
101 T996, T997, T998, T999, T1000, T1001, T1002, T1003, T1004, T1005,
102 T1006, T1007, T1008, T1009, T1010, T1011, T1012, T1013, T1014, T1015,
103 T1016, T1017, T1018, T1019, T1020, T1021, T1022, T1023, T1024, T1025,
104 T1026, T1027, T1028, T1029, T1030, T1031, T1032, T1033, T1034, T1035,
105 T1036, T1037, T1038, T1039, T1040, T1041, T1042, T1043, T1044, T1045,
106 T1046, T1047, T1048, T1049, T1050, T1051, T1052, T1053, T1054, T1055,
107 T1056, T1057, T1058, T1059, T1060, T1061, T1062, T1063, T1064, T1065,
108 T1066, T1067, T1068, T1069, T1070, T1071, T1072, T1073, T1074, T1075,
109 T1076, T1077, T1078, T1079, T1080, T1081, T1082, T1083, T1084, T1085,
110 T1086, T1087, T1088, T1089, T1090, T1091, T1092, T1093, T1094, T1095,
111 T1096, T1097, T1098, T1099, T1100, T1101, T1102, T1103, T1104, T1105,
112 T1106, T1107, T1108, T1109, T1110, T1111, T1112, T1113, T1114, T1115,
113 T1116, T1117, T1118, T1119, T1120, T1121, T1122, T1123, T1124, T1125,
114 T1126, T1127, T1128, T1129, T1130, T1131, T1132, T1133, T1134, T1135,
115 T1136, T1137, T1138, T1139, T1140, T1141, T1142, T1143, T1144, T1145,
116 T1146, T1147, T1148, T1149, T1150, T1151, T1152, T1153, T1154, T1155,
117 T1156, T1157, T1158, T1159, T1160, T1161, T1162, T1163, T1164, T1165,
118 T1166, T1167, T1168, T1169, T1170, T1171, T1172, T1173, T1174, T1175,
119 T1176, T1177, T1178, T1179, T1180, T1181, T1182, T1183, T1184, T1185,
120 T1186, T1187, T1188, T1189, T1190, T1191, T1192, T1193, T1194, T1195,
121 T1196, T1197, T1198, T1199, T1200, T1201, T1202, T1203, T1204, T1205,
122 T1206, T1207, T1208, T1209, T1210, T1211, T1212, T1213, T1214, T1215,
123 T1216, T1217, T1218, T1219, T1220, T1221, T1222, T1223, T1224, T1225,
124 T1226, T1227, T1228, T1229, T1230, T1231, T1232, T1233, T1234, T1235,
125 T1236, T1237, T1238, T1239, T1240, T1241, T1242, T1243, T1244, T1245,
126 T1246, T1247, T1248, T1249, T1250, T1251, T1252, T1253, T1254, T1255,
127 T1256, T1257, T1258, T1259, T1260, T1261, T1262, T1263, T1264, T1265,
128 T1266, T1267, T1268, T1269, T1270, T1271, T1272, T1273, T1274, T1275,
129 T1276, T1277, T1278, T1279, T1280, T1281, T1282, T1283, T1284, T1285,
130 T1286, T1287, T1288, T1289, T1290, T1291, T1292, T1293, T1294, T1295,
131 T1296, T1297, T1298, T1299, T1300, T1301, T1302, T1303, T1304, T1305,
132 T1306, T1307, T1308, T1309, T1310, T1311, T1312, T1313, T1314, T1315,
133 T1316, T1317, T1318, T1319, T1320, T1321, T1322, T1323, T1324, T1325,
134 T1326, T1327, T1328, T1329, T1330, T1331, T1332, T1333, T1334, T1335,
135 T1336, T1337, T1338, T1339, T1340, T1341, T1342, T1343, T1344, T1345,
136 T1346, T1347, T1348, T1349, T1350, T1351, T1352, T1353, T1354, T1355,
137 T1356, T1357, T1358, T1359, T1360, T1361, T1362, T1363, T1364, T1365,
138 T1366, T1367, T1368, T1369, T1370, T1371, T1372, T1373, T1374, T1375,
139 T1376, T1377, T1378, T1379, T1380, T1381, T1382, T1383, T1384, T1385,
140 T1386, T1387, T1388, T1389, T1390, T1391, T1392, T1393, T1394, T1395,
141 T1396, T1397, T1398, T1399, T1400, T1401, T1402, T1403, T1404, T1405,
142 T1406, T1407, T1408, T1409, T1410, T1411, T1412, T1413, T1414, T1415,
143 T1416, T1417, T1418, T1419, T1420, T1421, T1422, T1423, T1424, T1425,
144 T1426, T1427, T1428, T1429, T1430, T1431, T1432, T1433, T1434, T1435,
145 T1436, T1437, T1438, T1439, T1440, T1441, T1442, T1443, T1444, T1445,
146 T1446, T1447, T1448, T1449, T1450, T1451, T1452, T1453, T1454, T1455,
147 T1456, T1457, T1458, T1459, T1460, T1461, T1462, T1463, T1464, T1465,
148 T1466, T1467, T1468, T1469, T1470, T1471, T1472, T1473, T1474, T1475,
149 T1476, T1477, T1478, T1479, T1480, T1481, T1482, T1483, T1484, T1485,
150 T1486, T1487, T1488, T1489, T1490, T1491, T1492, T1493, T1494, T1495,
151 T1496, T1497, T1498, T1499, T1500, T1501, T1502, T1503, T1504, T1505,
152 T1506, T1507, T1508, T1509, T1510, T1511, T1512, T1513, T1514, T1515,
153 T1516, T1517, T1518, T1519, T1520, T1521, T1522, T1523, T1524, T1525,
154 T1526, T1527, T1528, T1529, T1530, T1531, T1532, T1533, T1534, T1535,
155 T1536, T1537, T1538, T1539, T1540, T1541, T1542, T1543, T1544, T1545,
156 T1546, T1547, T1548, T1549, T1550, T1551, T1552, T1553, T1554, T1555,
157 T1556, T1557, T1558, T1559, T1560, T1561, T1562, T1563, T1564, T1565,
158 T1566, T1567, T1568, T1569, T1570, T1571, T1572, T1573, T1574, T1575,
159 T1576, T1577, T1578, T1579, T1580, T1581, T1582, T1583, T1584, T1585,
160 T1586, T1587, T1588, T1589, T1590, T1591, T1592, T1593, T1594, T1595,
161 T1596, T1597, T1598, T1599, T1600, T1601, T1602, T1603, T1604, T1605,
162 T1606, T1607, T1608, T1609, T1610, T1611, T1612, T1613, T1614, T1615,
163 T1616, T1617, T1618, T1619, T1620, T1621, T1622, T1623, T1624, T1625,
164 T1626, T1627, T1628, T1629, T1630, T1631, T1632, T1633, T1634, T1635,
165 T1636, T1637, T1638, T1639, T1640, T1641, T1642, T1643, T1644, T1645,
166 T1646, T1647, T1648, T1649, T1650, T1651, T1652, T1653, T1654, T1655,
167 T1656, T1657, T1658, T1659, T1660, T1661, T1662, T1663, T1664, T1665,
168 T1666, T1667, T1668, T1669, T1670, T1671, T1672, T1673, T1674, T1675,
169 T1676, T1677, T1678, T1679, T1680, T1681, T1682, T1683, T1684, T1685,
170 T1686, T1687, T1688, T1689, T1690, T1691, T1692, T1693, T1694, T1695,
171 T1696, T1697, T1698, T1699, T1700, T1701, T1702, T1703, T1704, T1705,
172 T1706, T1707, T1708, T1709, T1710, T1711, T1712, T1713, T1714, T1715,
173 T1716, T1717, T1718, T1719, T1720, T1721, T1722, T1723, T1724, T1725,
174 T1726, T1727, T1728, T1729, T1730, T1731, T1732, T1733, T1734, T1735,
175 T1736, T1737, T1738, T1739, T1740, T1741, T1742, T1743, T1744, T1745,
176 T1746, T1747, T1748, T1749, T1750, T1751, T1752, T1753, T1754, T1755,
177 T1756, T1757, T1758, T1759, T1760, T1761, T1762, T1763, T1764, T1765,
178 T1766, T1767, T1768, T1769, T1770, T1771, T1772, T1773, T1774, T1775,
179 T1776, T1777, T1778, T1779, T1780, T1781, T1782, T1783, T1784, T1785,
180 T1786, T1787, T1788, T1789, T1790, T1791, T1792, T1793, T1794, T1795,
181 T1796, T1797, T1798, T1799, T1800, T1801, T1802, T1803, T1804, T1805,
182 T1806, T1807, T1808, T1809, T1810, T1811, T1812, T1813, T1814, T1815,
183 T1816, T1817, T1818, T1819, T1820, T1821, T1822, T1823, T1824, T1825,
184 T1826, T1827, T1828, T1829, T1830, T1831, T1832, T1833, T1834, T1835,
185 T1836, T1837, T1838, T1839, T1840, T1841, T1842, T1843, T1844, T1845,
186 T1846, T1847, T1848, T1849, T1850, T1851, T1852, T1853, T1854, T1855,
187 T1856, T1857, T1858, T1859, T1860, T1861, T1862, T1863, T1864, T1865,
188 T1866, T1867, T1868, T1869, T1870, T1871, T1872, T1873, T1874, T1875,
189 T1876, T1877, T1878, T1879, T1880, T1881, T1882, T1883, T1884, T1885,
190 T1886, T1887, T1888, T1889, T1890, T1891, T1892, T1893, T1894, T1895,
191 T1896, T1897, T1898, T1899, T1900, T1901, T1902, T1903, T1904, T1905,
192 T1906, T1907, T1908, T1909, T1910, T1911, T1912, T1913, T1914, T1915,
193 T1916, T1917, T1918, T1919, T1920, T1921, T1922, T1923, T1924, T1925,
194 T1926, T1927, T1928, T1929, T1930, T1931, T1932, T1933, T1934, T1935,
195 T1936, T1937, T1938, T1939, T1940, T1941, T1942, T1943, T1944, T1945,
196 T1946, T1947, T1948, T1949, T1950, T1951, T1952, T1953, T1954, T1955,
197 T1956, T1957, T1958, T1959, T1960, T1961, T1962, T1963, T1964, T1965,
198 T1966, T1967, T1968, T1969, T1970, T1971, T1972, T1973, T1974, T1975,
199 T1976, T1977, T1978, T1979, T1980, T1981, T1982, T1983, T1984, T1985,
200 T1986, T1987, T1988, T1989, T1990, T1991, T1992, T1993, T1994, T1995,
201 T1996, T1997, T1998, T1999, T2000, T2001, T2002, T2003, T2004, T2005,
202 T2006, T2007, T2008, T2009, T2010, T2011, T2012, T2013, T2014, T2015,
203 T2016, T2017, T2018, T2019, T2020, T2021, T2022, T2023, T2024, T2025,
204 T2026, T2027, T2028, T2029, T2030, T2031, T2032, T2033, T2034, T2035,
205 T2036, T2037, T2038, T2039, T2040, T2041, T2042, T2043, T2044, T2045,
206 T2046, T2047, T2048, T2049, T2050, T2051, T2052, T2053, T2054, T2055,
207 T2056, T2057, T2058, T2059, T2060, T2061, T2062, T2063, T2
```


12 CONTINUE
13 CONTINUE

K = N
DO 15 I=1,4
DO 14 J=1,2
14 SVI(I,J) = X(K,I,J+2)
15 CONTINUE
CVI(1,1) = -2.0*P*H(K)
CVI(2,1) = 0.0
K = K-1
IF (K) 50,50,20

20 CONTINUE

DO 22 J=1,2
J1 = J+J
T(1) = SVI(1,J1)
T(2) = SVI(2,J1)
T(3) = SVI(3,J1)
T(4) = SVI(4,J1)
DO 21 I=1,4
SV2(I,J1-1) = X(K,I,1)*T(1)+X(K,I,2)*T(2)
SV2(I,J1) = X(K,I,3)*T(3)+X(K,I,4)*T(4)
22 CONTINUE
T(1) = CVI(1,1)
T(2) = -2.0*P*H(K)
CV2(1,2) = T(1)
CV2(1,1) = T(2)
CV2(2,1) = T(1)-T(2)
CV2(2,2) = 0.0
K = K-1
IF (K) 50,50,30

30 CONTINUE

DO 34 J=1,4
J1 = J
IF (J1-2) 32,32,31
31 J1 = J1+2
32 CONTINUE
T(1) = SV2(1,J1)
T(2) = SV2(2,J1)
T(3) = SV2(3,J1)
T(4) = SV2(4,J1)
DO 33 I=1,4
SV3(I,J1+2) = X(K,I,1)*T(1)+X(K,I,2)*T(2)
SV3(I,J1+1) = X(K,I,3)*T(3)+X(K,I,4)*T(4)
34 CONTINUE
T(1) = -2.0*P*H(K)
DO 35 J=1,2

CV3(1,J1) = CV2(1,1)
CV3(2,J1) = CV2(1,J1)-T(1)
CV3(1,J1+2) = CV2(2,J1)+T(1)
CV3(2,J1+2) = CV2(2,J1)
35 CONTINUE
K = K-1
IF (K) 50,50,40

40 CONTINUE

DO 42 J=1,4
T(1) = SV3(1,J)
T(2) = SV3(2,J)
T(3) = SV3(3,J)
T(4) = SV3(4,J)
T(5) = SV3(1,J+4)
T(6) = SV3(2,J+4)
T(7) = SV3(3,J+4)
T(8) = SV3(4,J+4)
DO 41 I=1,4

SV4(I,J) = X(I,1)*T(1)+X(I,2)*T(2)
SV4(I,J+4) = X(K,I,3)*T(3)+X(K,I,4)*T(4)
SV4(I,J+8) = X(K,I,1)*T(5)+X(K,I,2)*T(6)
41 SV4(I,J+12) = X(K,I,3)*T(7)+X(K,I,4)*T(8)
42 CONTINUE
T(1) = -2.0*P*H(K)

DO 43 I=1,4

CV4(1,J) = CV3(1,J)
CV4(2,J) = CV3(1,J)-T(1)
CV4(1,J+4) = CV3(2,J)+T(1)
CV4(2,J+4) = CV3(2,J)
43 CONTINUE

50 CONTINUE

NT(1) = 1
DO 51 K=2,N
NT(K) = NT(K-1)+NT(K-1)
DO 80 K=1,N
KI = NS-K
DO 52 I=1,4
PM(K,I,1) = 0.0
PM(K,I,2) = 0.0
52 CONTINUE
I1 = NT(K)

DO 80 I=1,1

I2 = I+1
GO TO (61,62,63,64),K
61 CONTINUE
T(3) = CVI(1,I)
T(4) = CVI(2,I)

GO TO 65

62 CONTINUE
T(3) = CV2(1,I)
T(4) = CV2(2,I)

GO TO 65

63 CONTINUE
T(3) = CV3(1,I)
T(4) = CV3(2,I)

GO TO 65

64 CONTINUE
T(3) = CV4(1,I)
T(4) = CV4(2,I)

GO TO 65

65 CONTINUE

T(1) = 0.0


```

VS(4) = -(CSZ(3,J)+CSZ(3,J)*(-S(VI,J)))
VS(5) = VS(3)
VS(6) = VS(2)
VS(7) = VS(1)
DO 452 I = 1,7
  AMX(I) = AMAXI(RS(I),TS(I),VS(I))
  PAT(I) = AMX(I)/AMN(I)
  AMX(I) = -AMX(I)
  IF(J.EQ.1.OR.J.EQ.2) LAY = 1
  IF(J.EQ.3.OR.J.EQ.4.OR.J.EQ.5) LAY = 2
  IF(J.EQ.6.OR.J.EQ.7.OR.J.EQ.8) LAY = 3
  IF(J.EQ.9.OR.J.EQ.10.OR.J.EQ.11) LAY = 4
  IF(J.EQ.12) LAY = 5
  GO TO (8,10,8,9,10,8,9,10,8)J
  PRINT 604
  PRINT 616,LAY,(AMX(I),I=1,7)
  PRINT 617,TRAY(I),I=1,7)
  PRINT 613,(PAT(I),I=1,7)
  GO TO 663
9 PRINT 604
  PRINT 619,LAY,(AMX(I),I=1,7)
  PRINT 617,(AMX(I),I=1,7)
  PRINT 618,TRAY(I),I=1,7)
  GO TO 662
10 PRINT 604
  PRINT 620,LAY,(AMX(I),I=1,7)
  PRINT 617,(AMX(I),I=1,7)
  PRINT 618,(PAT(I),I=1,7)
660 CONTINUE
616 FORMAT(IHX,6H LAYER,12,12H TOP MAXIMUM,7(3X,3PE12.3))
617 FORMAT(IHX,13X,7HMINIMUM,7(3X,3PE12.3))
618 FORMAT(IHX,15X,5HAT 10,7(3X,3PE12.3))
619 FORMAT(IHX,6H LAYER,12,12H MID MAXIMUM,7(3X,3PE12.3))
620 FORMAT(IHX,6H LAYER,12,12H BTM MAXIMUM,7(3X,3PE12.3))
500 * * * * *
END

```

PROGRAM INSTRUCTIONS FOR FATIGUE LIFE SIMULATION

Description

Program FATIG, fatigue life simulation system combines output data obtained from the multi-layered elastic system and the temperature simulation system with traffic and fatigue fracture data to obtain the expected fatigue life of an asphalt concrete layer. The simulation is based on the prevailing conditions of the average day of each month of the year, the total monthly truck traffic being applied during the average day.

Operation

Input data specifying the average daily truck traffic, the axle load distribution of this traffic and the hourly variation of the traffic is used to obtain the distribution of the monthly total of axle loads in each hour of the average day.

Hourly means of stiffness modulus in the layer (from program TEMPS), reduced to the form of a frequency distribution of stiffness modulus with time of day is then combined with the axle load distribution to obtain, on an annual basis, the distribution of the number of applications, to the pavement, of each axle load type while the asphalt concrete stiffness modulus is within a certain range.

The multi-layered elastic system is used to obtain graphical relationships showing tensile strain as a function of axle load magnitude and stiffness modulus. These strains are then used to obtain a fatigue life distribution as a function of axle load and stiffness modulus. The fatigue life distribution is then combined with distribution of axle load applications described previously. Linear summation of applications to failure is used to determine the annual fatigue life damage.

The volume of truck traffic is then increased and the computations repeated. Computations are continued until a maximum specified number of years has been reached, or until the accumulated fatigue damage reaches a value of 1.0. Data for a new system is then read and the process repeated.

Limitations

The following limitations of the program and/or method.

1. The maximum number of axle groups is 12. Refer to program statement number 123 for the output headings used. Other groupings will require appropriate changes to statement 123.
2. The maximum number of stiffness groups is 15.
3. Traffic data must be in the form of monthly Wheel Load Distribution Factors (WLDF) described in the main body of the report.
4. The order of input of WLDF's must be from least to greatest.
5. The order of input of stiffness modulus groups must be consistent.

Input Cards

The notation cc refers to card columns, with the range of columns being inclusive. All "REAL" values on F-FORMAT are punched with a decimal point as a part of the value. All "REAL" values on E-FORMAT are punched with a decimal point as part of the value and right justified in the data field. All "INTEGER" values are to be punched without a decimal point and right justified in the data field.

- Card 1 cc1-5 the number of pavement systems to be solved (INTEGER)
FORMAT (I5)
- Card 2 cc-1-80 any combination of alphanumeric characters may be used to describe the problem to be solved
FORMAT (8A10)
- Card 3 cc1-10 average daily number of trucks, both directions (ADTT) (REAL)
cc11-20 percent of 2 axle trucks in ADTT (REAL)
cc21-30 percent of 3 axle trucks in ADTT (REAL)
cc31-40 percent of 4 axle trucks in ADTT (REAL)
cc41-50 percent of 5 axle trucks in ADTT (REAL)
cc51-60 percent of 6 axle trucks in ADTT (REAL)
cc61-70 percent of one-way truck traffic using the design lane (REAL)
FORMAT (7F10.0)
- Card 4 cc1-5 the number of axle load groups, maximum of 12 (INTEGER)
cc6-10 the number of stiffness modulus groups, maximum of 15 (INTEGER)
cc11-20 the annual rate of traffic expansion (REAL)
cc21-25 the maximum number of years for which calculations are to be performed (INTEGER)
FORMAT (2I5, F10.0, I5)
- Card 5 cc1-10 the WLDF for axle group 1 and 2 axle trucks (REAL)
cc11-20 the WLDF for axle group 1 and 3 axle trucks (REAL)
cc21-30 the WLDF for axle group 1 and 4 axle trucks (REAL)
cc31-40 the WLDF for axle group 1 and 5 axle trucks (REAL)
cc41-50 the WLDF for axle group 1 and 6 axle trucks (REAL)
One card of this type is required for each axle group specified on card 4.
FORMAT (5F10.0)

- Card 6 cc1-10 percent of ADTT in hourly period midnight to 1 a. m. (REAL)
 cc11-20 percent of ADTT in hourly period 1 to 2 a. m. (REAL)
 etc. 3 cards of this type are required to complete the 24 hourly periods.
 FORMAT (8F10. 0)
- Card 7 cc1-5 frequency of occurrence of stiffness group 1 in time interval mid-
 night to 1 a. m. (REAL)
 cc6-10 frequency of occurrence of stiffness group 2 in time interval mid-
 night to 1 a. m. (REAL)
 etc one such entry required for each of the stiffness groups specified
 in card 4
 24 such cards required, one for each hourly time period.
 FORMAT (15F5. 0)
- Card 8 cc1-10 fatigue life for axle group 1 and stiffness group 1 (REAL)
 cc11-20 fatigue life for axle group 2 and stiffness group 1 (REAL)
 etc 2 such cards are required for each of the stiffness groups
 specified in card 4.
 FORMAT (6E10. 0)

CARDS 2 THROUGH 8 ARE REPEATED FOR EACH NEW PAVEMENT SYSTEM TO BE SOLVED AS INDICATED CARD 1.

PROGRAM INSTRUCTIONS FOR TEMPERATURE SIMULATION SYSTEM

Description

Program TEMPS2 solves for temperatures at various specified depths in a semi-infinite mass having constant thermal properties. The surface of the mass is subjected to a heat flux which varies with time. Using specified thermal characteristics of an asphalt concrete and relationships between meteorological conditions and heat flux, time and depth dependent temperatures in an asphalt concrete layer are simulated.

Operation

The specified daily meteorological conditions and thermal character of the asphalt concrete are used to determine the first value of depth and of time. This temperature is then used to interpolate, from input values relating temperature and stiffness modulus of an asphalt cement, a corresponding stiffness modulus of asphalt cement. A stiffness modulus for the asphalt concrete is then determined using the Heukelom-Klomp equation, these values being stored for later computation of means. The program then steps to the next value of time. Computations are performed at 25 values of time representing the beginning and end of each hour of the day. A daily mean and a traffic weighted mean of temperature and stiffness modulus of the asphalt concrete is then determined. The program then proceeds to the next value of depth. When values have been determined at each depth, an hourly mean of temperature and stiffness modulus in the layer is computed. The program then repeats the computation for a new set of meteorological conditions or a new pavement system.

Input Cards

The notation cc refers to card columns, with the range of columns being inclusive. All "REAL" values are punched with a decimal point as part of the value and all "INTEGER" values are to be punched without a decimal and right justified in the data field.

- | | | |
|--------|--------|---|
| Card 1 | cc1-5 | the number of pavement systems to be solved (INTEGER)
FORMAT (I5) |
| Card 2 | cc1-5 | the number of days on which computations are to be
performed (INTEGER)
FORMAT (I5) |
| Card 3 | cc1-80 | any combination of alphanumeric characters may be used
to identify the problem to be solved
FORMAT (8A10) |

- Card 4 cc1-80 any combination of alphanumeric characters may be used to identify the nature of traffic variables
FORMAT (8A10)
- Card 5 cc1-10 percent of average daily truck traffic in the time interval, midnight to 1 a. m. (REAL)
cc11-20 percent of average daily truck traffic in the time 1 to 2 a. m. (REAL)
etc.
FORMAT (8F10.0)
three cards are required for the 24 hours of the day.
- Card 6 cc1-10 penetration at 77⁰F of the asphalt cement in the pavement, in dmm (REAL)
cc11-20 ring and ball softening temperature of the asphalt cement in the pavement in degrees F (REAL)
cc21-30 loading time of the asphalt cement in the pavement in seconds (REAL)
FORMAT (3F10.0)
- Card 7 cc1-5 the number of points in the temperature-stiffness modulus of the asphalt cement (INTEGER)
FORMAT (I5)
- Card 8 cc1-10 least temperature in temperature-stiffness modulus relationship (REAL)
cc11-20 corresponding stiffness modulus of the asphalt cement -Kg/cm² (REAL)
cc21-30 second temperature (REAL)
cc31-40 corresponding stiffness modulus (REAL)
etc
repeat card 8 as required
FORMAT (8F10.0)
- Card 9 cc1-10 coefficient describing the energy reflecting character of the layer surface (REAL)
cc11-20 specific heat of the asphalt concrete (REAL)
cc21-30 unit weight of the asphalt concrete (REAL)
cc31-40 conductivity of the asphalt concrete (REAL)
cc41-50 coefficient of volume concentration of aggregate in the asphalt concrete (REAL)

- Card 9 cc51-60 the air voids in the asphalt concrete as a decimal fraction
(REAL)
FORMAT (6F10. 0)
- Card 10 cc1-5 the number of depth values at which computations are to be
performed. Maximum of 12 (INTEGER)
FORMAT (I5)
- Card 11 cc1-10 the first depth value in inches (REAL)
cc1-20 the second depth value in inches (REAL)
etc. repeat card 11 as required
FORMAT (6F10. 0)
- Card 12 cc1-10 total depth of layer in inches (REAL)
FORMAT (F10. 0)
- Card 13 cc1-30 any combination of alphanumeric characters may be used to
describe the day type
cc31-40 the mean daily air temperature in °F (REAL)
cc41-50 the daily range of air temperature in °F (REAL)
cc51-60 the mean wind velocity in mph (REAL)
cc61-70 the daily solar insolation in langleys (REAL)
cc71-80 mean daily sky cover in tenths (REAL)
repeat card 12 as required by the values specified on card 2.
FORMAT (3A10, 5F10. 0)

CARDS 2 THROUGH 13 ARE REPEATED FOR THE NUMBER OF PAVEMENT SYSTEMS
SPECIFIED IN CARD 1.


```
PRINT CRILL  
92 FORMAT(5X,11HUNITS WEIGHT ,15X,F7.1,12H LBS/CL.FT. )  
93 FORMAT(5X,16H-AIR VOIC CONTENT ,14X,F7.1,11H PER CENT )  
94 FORMAT(5X,25H-VOLUME CONC. CF AGGREGATE ,15X,F6.2 )  
95 FORMAT(5X,21H-FORMAL CONDUCTIVITY ,10X,F8.2 )  
96 FORMAT(5X,13H-SPECIFIC HEAT ,17X,F6.2 )  
97 FORMAT(5X,13H-SUREAGE COEFFICIENT ,11X,F8.2 )  
98 FORMAT(5X,31H-LOADING TIME ,18.2,6H SEC.)  
PRINT*  
997 FORMAT(1P1)  
RETURN  
END
```

PROGRAM INSTRUCTIONS FOR FINITE ELEMENT ANALYSIS OF PAVEMENTS

Description

The Finite Element Pavement program (FEPAVE 2) will determine stresses and deformations in an axisymmetric pavement system supporting a single load, uniformly distributed over a circular area. All layer boundaries, the surface and the base of the system are horizontal plane surfaces. The lateral extremity of the system is a vertical plane. This geometric regularity is used to advantage in simplifying the specification of nodal point coordinates. The system is composed of a combination of elastic materials which may be linear, linear-temperature dependent, or non-linear. The load is applied to the system using one or more equal increments.

Operation

The mesh configuration, the lateral extremity, the material boundaries and the edge of the loaded area are specified by horizontal and vertical offsets from the center of the loaded area. As is shown in Figs. C-2 and C-3, the mesh configuration is a finer fabric near the load becoming coarser at the extremities. For a flexible loaded area, the upper layer of the pavement is designated as material 1, with numbering following successively downward as shown in Fig. C-2. However, where the load is applied through a rigid plate as is shown in Fig. C-3, the plate material is designated as material 1. The thickness of the plate is entered as negative vertical offset.

When the mesh configuration has been determined, stresses due to gravity effects are determined and printed; the first increment of load is then applied and the resulting stresses and deformations determined. If all materials in the system are linear elastic, the first increment is the total load. For non-linear materials, the gravity stresses and load stresses are summed to obtain an appropriate stress dependent modulus. Stresses and deformations are then printed. A second increment of the load is applied and stresses and deformations due to this increment plus the preceding increment are determined and printed. This process is continued, stresses and deformations due to each succeeding increment being added to the sum of all preceding increments. When the total load has been applied, the total stresses and deformations are printed and a plot of the major and minor principal stresses is prepared.

Limitations

The following are limitations of the method and/or program:

1. Refer to Subroutine QUAD for the forms of specifying non-linear material properties.

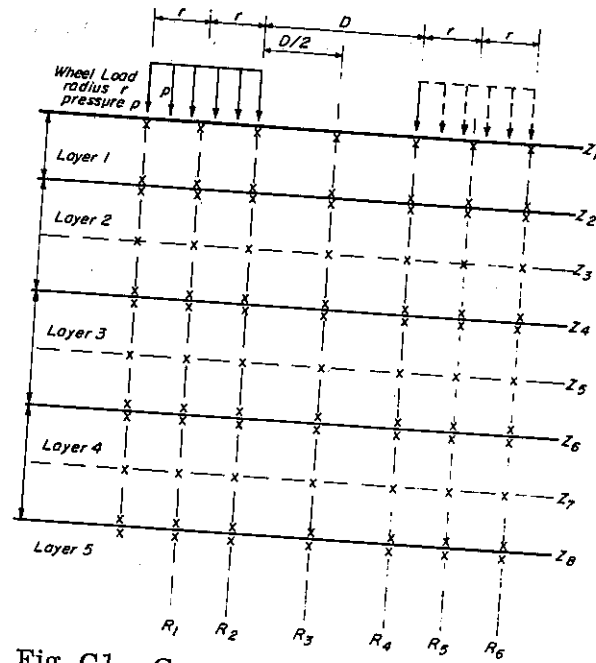


Fig. C1 - Computer representation of pavement structure for stress-modulus iteration.

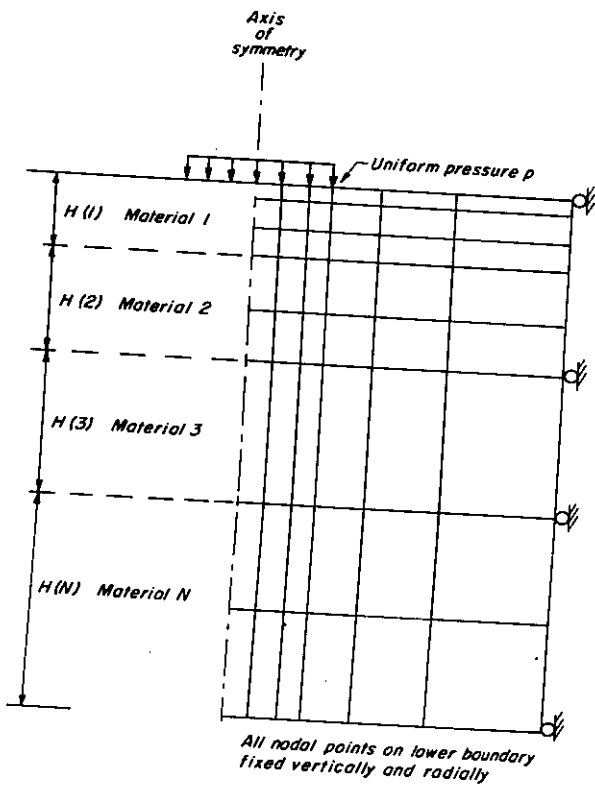


Fig. C2 - Mesh configuration and boundary conditions (flexible plate FEPAVE 2).

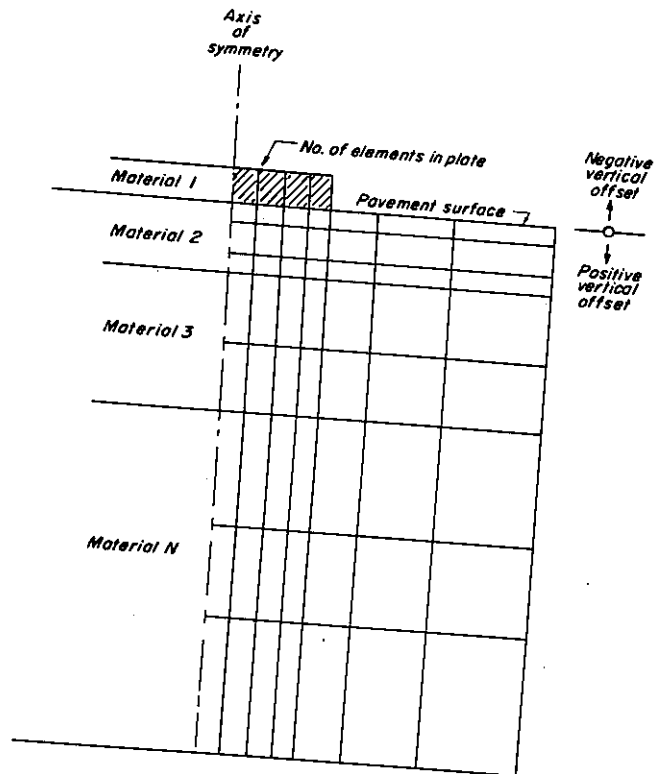


Fig. C3 - Mesh configuration and boundary conditions (rigid plate FEPAVE 2).

2. Poisson's Ratio is a constant for each material and must have a value less than 0.5.
3. The number of material types in the system cannot exceed 12. Material identification must begin with "1" at the top and increase downward.
4. The number of rows of elements cannot exceed 32.
5. The number of columns of elements cannot exceed 24.
6. Layer and/or material interfaces must coincide with a nodal point row.
7. The horizontal offset to the first nodal point column must be zero.
8. The edge of the loaded area must coincide with a nodal point column.
9. The vertical offset to the first nodal point row must be zero (flexible loaded area) or negative (rigid plate loading).
10. All units must be pounds and inches.
11. All nodal points on the lower horizontal boundary are constrained from horizontal and vertical movement.
12. All nodal points on the vertical boundary are constrained from horizontal movement.

Input Cards

The notation cc refers to card columns with the range of columns being inclusive. All "REAL" values are punched with a decimal point as a part of the value and all "INTEGER" values are to be punched without a decimal point and right justified in the field.

- | | | |
|--------|--|---|
| Card 1 | cc1 | any integer value other than 9. This card is placed at the beginning of each new problem to be solved. A card, with the integer 9 in cc 1, placed following the last system to be solved, causes the program to stop. |
| Card 2 | cc1-80 | any combination of alphanumeric characters may be used to identify the problem to be solved.
FORMAT (8A10). |
| Card 3 | cc1-10
cc11-20
cc21-25
cc26-30
cc31-35
cc36-40
cc41-45 | radius of loaded area in inches (REAL)
pressure on loaded area in inches (REAL)
number of materials (INTEGER)
number of element columns (INTEGER)
number of element rows (INTEGER)
number of elements in rigid plate (INTEGER)
number of load increments to be used (INTEGER)
FORMAT (2F10.0, 5I5) |

Card 4 cc1-5 material identification (INTEGER)
 cc6-10 number of temperature cards (INTEGER)
 cc11-20 layer thickness in inches (REAL)
 cc21-30 layer density in lbs/in³ (REAL)
 cc31-40 coefficient of earth pressure at rest (REAL)
 cc41-50 material code (REAL)
 cc51-60 estimated maximum stress, positive or negative, to provide a
 scale for the plotting routine (REAL)
 FORMAT (2I5, 5F10.0)

Card 5 cc1-10 Temperature in °F (REAL)
 cc11-20 linear elastic modulus in psi (REAL)
 cc21-30 Poisson's Ratio (REAL)
 cc31-40 non-linear coefficient K_1 (REAL)
 cc41-50 non-linear coefficient K_2 (REAL)
 cc51-60 non-linear coefficient K_3 (REAL)
 cc61-70 non-linear coefficient K_4 (REAL)
 cc71-80 non-linear coefficient K_5 (REAL)
 FORMAT (8F10.0)

Note: Card order - a card 4 for material identification 1 followed by 'n'
 type 5 cards where 'n' is the number specified in card 4 cc6=10. Repeat
 as required in the order, card 4 and n card 5's according to the number
 of materials specified on card 3.

Card 6 cc1-10 radius to first nodal point column in inches (REAL)
 cc11-20 radius to second nodal point column in inches (REAL)
 etc.
 FORMAT (8F10.0)
 Repeat card 6 as required.

Card 7 cc1-10 temperature in °F of first nodal point row (REAL)
 cc11-20 vertical offset to first nodal point row in inches (REAL)
 cc21-30 temperature in °F of second nodal point row (REAL)
 cc31-40 vertical offset to second nodal point row in inches (REAL)
 etc.
 FORMAT (8F10.0)
 Repeat card 7 as required.

REPEAT CARDS 1 THROUGH 7 FOR EACH NEW SYSTEM TO BE SOLVED.

FINITE ELEMENT PAVEMENT PROGRAM

```

C AXISYMMETRIC PAVEMENT STRUCTURE(WILSON MOD DUNCAN MOD DEHLEN)
C INCREMENTAL PROCEDURE (EPFAVE 2)
C*****
COMMON NUMNP,NUMEL,NUMMAT,NUMPC,ACELZ,ANGFQ, BAND,TEMP,MTYPE,NUM
1IN,NUMCOL,NUMROW,NPLATE,NPPI,NNH,HED(8),E(8,8,12),RO(12),KO(12),CL
2ASS(12), THICK(12),TOP(12),R(900),Z(900),UR(900),UZ(900),CODE(900)
3AT(900),ZS(900),IRC(25), JBC(25), PR(25), ANGLE(4),SIG(10),SIGT(80
40,4),SIG3(800),SIGD(800),URT(900),UZT(900),ROWTMP(34),MATYP(34),DE
5PTH(34),RADIST(25),MAXSTR(12),RZFERO,PZERO
COMMON /ARG/ RRR(15),ZZZ(15),VS(10),P(10),TT(4),LM(4),DD(3,3),
1 HH(6,10),RR(4),ZZ(4),C(14,4),H(6,10),D(16,6),F(6,10),IP(6),X(110)
2,EE(17),X(1800,5)
COMMON /BANARG/ MBAND,NUMBLK*B(108),A(108,54)
COMMON /PLANE/ NPP
REAL KO,MAXSTR
C*****
C READ AND PRINT OF CONTROL INFORMATION AND MATERIAL PROPERTIES
C*****
50 READ 1103,WERK
IF (WERK.EQ.9) STOP
NPP=0
ACELZ=0.
ANGFQ=0.
Q=0.
READ 1000,HED,RZERO,PZERO,NUMMAT,NUMCOL,NUMROW,NPLATE,NUMIN
PRINT 2000,HED,RZERO,PZERO
IF(NPLATE.GT.0)PRINT 2009
56 DO 59 M=1,NUMMAT
READ 1001,MTYPE,NUMTC,THICK(MTYPE),RO(MTYPE),KO(MTYPE),CLASS(MTYPE)
1),MAXSTR(MTYPE)
PRINT 2002,MTYPE,THICK(MTYPE),RO(MTYPE),KO(MTYPE),CLASS(MTYPE)
READ 1005,((F(I,J,MTYPE),J=1,8),I=1,NUMTC)
PRINT 2004,((E(I,J,MTYPE),J=1,8),I=1,NUMTC)
DO 58 J=1,NUMTC,8
DO 58 I=1,8
58 E(I,J,MTYPE)=E(NUMTC,J,MTYPE)
59 CONTINUE
PRINT 2008
NCP1=NUMCOL+1
NRPI=NUMROW+1
NPP2=NPP1+1
IF(NPLATE.EQ.0) GO TO 60
NUMEL = NUMROW*NUMCOL + NPLATE - NUMCOL
NUMNP = NRPI*NCPI + NPLATE - NUMCOL
GO TO 61
60 NUMEL = NUMROW*NUMCOL
NUMNP = NRPI*NCPI
61 PRINT 2010,NUMCOL,NUMROW,NPLATE,NUMNP,NUMEL
C*****
C READ AND GENERATE NODAL POINT CO-ORDINATES
C*****
READ 1005,(RADIST(INCOL),NCOL=1,NCPI)
READ 1005,(ROWTMP(INROW),DEPTH(INROW),NROW=1,NRPI)

```

```

PRINT 1005,(ROWTMP(INROW),DEPTH(INROW),NROW=1,NRPI)
TOP(1)=DEPTH(1)
DO 100 MTYPE=2,NUMHAT
100 TOP(MTYPE)=TOP(MTYPE-1)+THICK(MTYPE-1)
3002 FORMAT(15,F10.2)
TOP(NUMHAT + 1) = DEPTH(NRPI) + 0.1
102 MTYPE=1
DO 104 NROW=1,NUMROW
DEPNTH = DEPTH(NROW)-TOP(MTYPE+1)
IF(ABS(DEPNTH).LT.0.0001) MTYPE = MTYPE+1
104 MATYP(INROW)=MTYPE
MATYP(NRPI)=MATYP(INROW)
PRINT 3001
STOP
105 NCOL=0
NROW=0
DO 107 N=1,NUMNP
NCOL=NCOL+1
NROW=NROW+1
CODE(N)=0.0
IF(NCOL.EQ.NCPI) CODE(N)=1.0
IF(NROW.EQ.NRPI) CODE(N)=3.0
R(N)=RADIST(NCOL)
Z(N)=DEPTH(NRPI)-DEPTH(NROW)
ZS(N)=DEPTH(NROW)
T(N)=ROWTMP(NROW)
IF(NCOL.LT.NCPI) NROW=NROW-1
IF(N.EQ.NPPI.AND.N.GT.1) NROW=NROW+1
IF(NCOL.EQ.NCPI) NCOL=0
IF(N.EQ.NPPI.AND.N.GT.1) NCOL=0
107 CONTINUE
DO 106 N=1,900
UR(N)=0.0
UZ(N)=0.0
106 CONTINUE
C*****
C COMPUTE ELEMENT PROPERTIES
C*****
PRINT 2001
NROW=0
NCOL=0
DO 110 N=1,NUMEL
NCOL=NCOL+1
NROW=NROW+1
IX(N,1)=N+NROW-1
IX(N,2)=IX(N,1)+NUMCOL+1
IF(N.LE.NPLATE) IX(N,2)=IX(N,1)+NPLATE+1
IX(N,3)=IX(N,2)+1
IX(N,4)=IX(N,3)+1
IX(N,5)=MATYP(INROW)
IF(N.EQ.NPLATE) NROW=NROW-1
IF(NCOL.EQ.NUMCOL) NCOL=0

```

```

IF (N*EQ,NPLATE) NCOL=0
PRINT 2005,N*(IX(N),I,I=1,5)
110 CONTINUE
C*****
C GENERATE PRESSURE BOUNDARY CONDITIONS
C*****
PRINT 2005
IF (NPLATE)290,290,280
280 NUMP=NPLATE
IF (R(NPPI)*RE+RZERO)GO TO 310
GO TO 315
290 DO 300 N=1,NCP1
IF (R(N)-RZERO)300,305,310
305 NUMP=N-1
GO TO 315
300 CONTINUE
310 PRINT 3000
STOP
315 DO 318 L=1,NUMP
IBC(L)=NUMP+2-L
JBC(L)=NUMP+1-L
PR(L)=PZERO/NUMIN
PRINT 2007,IBC(L),JBC(L),PZERO
318 CONTINUE
C*****
C DETERMINE BAND WIDTH
C*****
J=0
DO 340 N=1,NUMEL
DO 340 I=1,4
DO 325 L=1,4
KK=IABS(IX(N,I)-IX(N,L))
IF (KK-J) 325,325,320
320 J=KK
325 CONTINUE
340 CONTINUE
MBAND=2*J+2
C*****
C NNN=0
C*****
C COMPUTE GRAVITY STRESSES
C*****
PRINT 2012
CALL STRESS
C*****
C SET DISPLACEMENTS BEFORE LOAD APPLICATION TO ZERO
C*****
DO 350 M=1,NUMNP
URT(M)=0.
350 UZT(M)=0.
C*****
C APPLY LOAD IN INCREMENTS, COMPUTE DISPLACEMENT AND STRESS INCREMENT
C DUE TO EACH LOAD INCREMENT AND ADD TO VALUES AT PRIOR LOAD LEVEL
C*****
DO 500 NNN=1,NUMIN

```

```

C*****
C FORM STIFFNESS MATRIX
C*****
CALL STIFF
C*****
C SOLVE FOR DISPLACEMENTS
C*****
CALL BANPOL
PRINT 2006,NNN
DO 400 N=1,NUMNP
URT(N)=URT(N)+B(2,N-1)
UZT(N)=UZT(N)+B(2,N)
PRINT 2011,N,UR(N),R(N),ZS(N),URT(N),UZT(N)
400 CONTINUE
C*****
C COMPUTE STRESSES
C*****
CALL STRESS
500 CONTINUE
GO TO 50
1000 FORMAT(8A10,2F10.0,5I5)
1001 FORMAT(2I5,5F10.0)
1003 FORMAT(6I5)
1005 FORMAT(8F10.0)
1103 FORMAT(11)
2000 FORMAT (1H1,15X,100H-----
2--- 8A10,10H -----6(/140X,33HMEAN PRESSURE ON LOADED AREA = *F10.3)
3EA = *F10.3/40X,33HMEAN PRESSURE ON LOADED AREA = *F10.3)
2001 FORMAT (49H-ELEMENT NO. I J K L MATERIAL )
2002 FORMAT(1H-//8H LAYER =:12,15H THICKNESS = *F8.2,13H DENSITY =
1, F9.6,23H EARTH PRESS COEFF = *F5.2,19H MATERIAL CODE = *F4.1)
2003 FORMAT (11I3,4I6,11I12)
2004 FORMAT (1H0,13X,96H AT TEMP RESIL MOD POISS RAT K
11 K2 K3 K4 K5/(14X,8F12.2))
2005 FORMAT (1H-,40X,28HPRESSURE BOUNDARY CONDITIONS//36X,35HBETWEEN N
10DAL POINTS PRESSURE//)
2006 FORMAT (1H1,35X,53H-----D I S P L A C E M E N T S
1-----//88H NODAL POINT NP CODE R-ORDINATE Z-ORDINATE
2 RADIAL DISPL VERTICAL DISPL,15X,17HINCREMENT NUMBER *I2)
2007 FORMAT (32X,2I10,8X,F10.3)
2008 FORMAT(1H-//6H NOTES/28H ALL UNITS POUNDS AND INCHES/92H MATERIAL C
10DES- BITUMINOUS 0. GRANULAR 1. COHESIVE 2. LINEAR 3.
2 STAB CLAY 5.)
2009 FORMAT (1H ,39X,26HLOAD APPLIED THROUGH PLATE)
2010 FORMAT (1H1,30X,55H-----FINITE ELEMENT MESH
1-----9(/141X,30HNUMBER OF COLUMNS
3TE = *I3//41X,30HNUMBER OF NODAL POINTS = *I3//41X,30HNUMBE
4R OF ELEMENTS = *I3//)
2011 FORMAT (11I2,1,2F12.3,2F20.10)
2012 FORMAT (1H8//48X,25HG R A V I T Y)
3000 FORMAT (36H-LAYER THICKNESSES DO NOT MATCH MESH)
C*****

```



```

          SIGMA=(RO(MTYPE))*Z(IL)-Z(JL)})*SIGMA
4 CONTINUE
  SIGMA=SIGMA-0.5*(RO(MTYPE))*Z(IL)-Z(JL)}
281 SIG(I)=-RO(MTYPE)*SIGMA
    SIG(2)=-SIGMA
    SIG(3)=-KO(MTYPE)*SIGMA
    CIG(4)=0.
    DO 282 I=1,4
282 STGT(N,I)=0.
C
C ADD STRESS INCREMENTS TO PREVIOUS STRESSES
C
283 DO 284 I=1,4
    SIG(N,I)=SIG(N,I)+SIG(I)
284 SIG(I)=SIG(N,I)
C
C CALCULATE PRINCIPAL STRESSES
C
    CC=(SIG(1)+SIG(2))/2*0
    PR=(SIG(1)-SIG(2))/2*
    CR=SQRT(BR**2+SIG(4)**2)
    SIG(5)=CC+CR
    SIG(6)=CC-CR
C
    SIG(7)=999.
    TFSIG(4)=EQ.0.AND.8B.EQ.0IGO TO 287
    SIG(7)=28.648*ATAN2(SIG(4),BR)
C
C CALCULATE OCTAHEDRAL STRESSES
C
287 SIG(8)=(SIG(3)+SIG(5)+SIG(6))/3.
    SIG(9)=-ISQRT((SIG(3)-SIG(5))**2+((SIG(5)-SIG(6))**2)+(SIG(6)-S
    IIG(3))**2))/3.
C
C FIND MAJOR AND MINOR PRINCIPAL STRESSES
C
    TFSIG(3)=GT.SIG(5)SIG(5)SIG(5)=SIG(3)
    TFSIG(3)=LT.SIG(6)SIG(6)=SIG(3)
C
C DETERMINE PLOTTING CO-ORDINATES
C
    IF(INN.NE.NUMINIGO TO 104
    I=51.5-(SIG(5)*50.)/MAXSTR(MTYPE)
    J=31.5+(SIG(6)*30.)/MAXSTR(MTYPE)
    TFI(LT,I) I=1
    TFI(GT,101) I=101
    TFI(J,LT,I) J=1
    TFI(J,GT,31) J=31
    PLOT(I,J,MTYPE)=ASTER
C*****
C OUTPUT STRESSES
C*****
104 IF (MPRINT) 110,105,110
105 PRINT 2000
    MPRINT=50

```

```

          P(I+1)=B(JJ-I)
120 P(I+1)=B(JJ)
C
    DO 150 I=1,2
    RR(I)=P(I+8)
    DO 150 K=1,8
150 RR(I)=RR(I)-S(1+B*K)*P(K)
C
    COMW=S(9,9)*S(10,10)-S(9,10)*S(10,9)
    IF (COMM) 155,160,155
155 P(9)=S(10,10)*RR(11)-S(9,10)*RR(12)/COMM
    P(10)=[-S(10,9)*RR(11)+S(9,9)*RR(12)]/COMM
C
160 DO 170 I=1,6
    TP(I)=0.0
    DO 170 K=1,10
170 TP(I)=TP(I)+HH(I,K)*P(K)
171 RR(1)=TP(2)
    RR(2)=TP(6)
    RR(3)=(TP(1)+TP(2)+TP(3)+TP(4)+TP(5))/RRR(5)
    RR(4)=TP(3)+TP(5)
C
C CALCULATE STRESSES DUE TO STRAINS
C
10 DO 5 K=1,3
5 SIG(K)=0.0
    DO 6 I=1,3
    DO 6 K=1,3
6 SIG(I)=SIG(I)+C(I,K)*RR(K)
    SIG(4)=C(4,4)*RR(4)
C
C CALCULATE EFFECTIVE STRAIN
C
252 CC=(RR(1)+RR(2))/2*0
    CR=SQRT((RR(2)-RR(1))/2*0)**2 + (RR(4)/2*0)**2 )
    RR(1)=CC+CR
    RR(2)=CC-CR
    GO TO 283
C
C CALCULATE GRAVITY STRESSES
C
280 DO 2 NROW=1,NUMROW
    IF(IN*GT*NP(LATE)GO TO 1
    SIGMA=0.
    GO TO 281
1 NRM1=NROW-1
    WRITE(NPLATE+NRM1)NUMCOL
    IF (NRITE*GE*N) GO TO 3
2 CONTINUE
3 NTOP=N-(NROW-2)*(NUMCOL)
    SIGMA=N.
    DO 4 NL=NTOP,N,NUMCOL
    MTYPE=IX(NL,5)
    IL=IX(NL,1)
    JL=IX(NL,2)

```

```

C*****
C INITIALIZATION
C*****
REWIND 2
NR=27
ND=2*NR
ND2=2*ND
STOP=0.0
NUMBLK=0
DO 50 N=1,ND2
  B(N)=0.0
DO 50 M=1,ND
  A(N,M)=0.0
C*****
FORM STIFFNESS MATRIX IN BLOCKS
C*****
60 NUMBLK=NUMBLK+1
MH=NH-NB
NL=NH-NB+1
KSHIFT=2*NL-2
DO 210 N=1,NUMEL
  IF (IX(N,5)) 210,210,65
  65 DO 80 I=1,4
  IF (IX(N,I)-NL) 80,70,70
  70 IF (IX(N,I)-NM) 90,90,80
  80 CONTINUE
  GO TO 210
C 90 CALL QUAD(N,VOL)
  IF (VOL) 142,142,144
  142 PRINT 2003,N
  STOP=1.0
  144 IF (IX(N,3)-IX(N,4)) 145,165,145
  145 DO 150 II=1,9
  CC=S(II,10)/S(10,10)
  P(II)=P(II)-CC*P(10)
  DO 150 JJ=1,9
  150 S(II,JJ)=S(II,JJ)-CC*S(10,JJ)
C
DO 160 II=1,8
  CC=S(II,9)/S(9,9)
  P(II)=P(II)-CC*P(9)
  DO 160 JJ=1,8
  160 S(II,JJ)=S(II,JJ)-CC*S(9,JJ)
C
ADD ELEMENT STIFFNESS TO TOTAL STIFFNESS
  165 DO 166 I=1,4
  166 LM(I)=2*IX(N,I)-2
C

```

```

110 MPRINT=MPRINT-1
DO 8 I=1,10
  SIG(I)=-SIG(I)
8 CONTINUE
IF (NN,EQ,0) GO TO 290
ZZS=DEPTH(NUMROW+1)-ZZZ(5)
PRINT 2001,N,RRR(5),ZZS,(SIG(I),I=1,9),EE(1),EE(2)
GO TO 292
290 PRINT 2002,N,(SIG(I),I=1,9)
292 SIG3(N)=SIG(5)
298 SIGD(N)=SIG(6)-SIG(5)
300 CONTINUE
C
C PLOT MAJOR AND MINOR PRINCIPAL STRESSES OCCURRING IN EACH LAYER
C
IF (NN,NE,NUMIN) GO TO 911
DO 910 MTYPE=1,NUMMAT
  IACH2=MAXSTR(MTYPE)/10.
  PRINT 2200
  PRINT 2201,((PLOT(I,J,MTYPE),I=1,101),J=1,31)
  PRINT 2203
  PRINT 2202,MTYPE,INCH2
910 CONTINUE
911 CONTINUE
C
RETURN
C
2000 FORMAT(1H1,35X,52H-----S T R E S S E S-----
1---//132H EL R Z RADIAL VERTICAL TANGENL RZ SHE
2AR MIN PRIN MAJ PRIN ANGLE OCT NOR OCT SHE RESIL
3MOD POI RA)
2001 FORMAT(14,2F7.2,6F10.4,F8.2,2F10.4,9X,F11.1,F6.3)
2002 FORMAT(14,14X,6F10.4,F8.2,2F10.4)
2200 FORMAT(1H1,60X,9H MAJOR /61X,9HPRINCIPAL/61X,9H STRESS )
2201 FORMAT(1H,56X,14H LAYER NUMBER ,12/52X,17HSCALE-HALF INCH =,15,4H
1 PSI)
2203 FORMAT(1H,106X,9H MINOR /107X,9HPRINCIPAL/107X,9H STRESS )
C
END
SUBROUTINE STIFF
C*****
COMMON NUMNP,NUMEL,NUMMAT,NUMPC,ACELZ,ANGFO, BAND,TEMP,MTYPE,NUM
1H,NH,NHCOL,NUMROW,NPLATE,NPPI,ANN,HEDI(8),E(8,8,12),RO(12),CL
2AS(12), THICK(12),TOP(12),R(900),Z(900),UR(900),UZ(900),CODE(900)
3,T(900),ZS(900),IBC(25), JBC(25), PRI(25), ANGLE(4),SIG(110),SIGI(80
40,4),SIG3(800),SIGD(800),URTI(800),URZ(800),ROWTMP(34),MATYP(34),DE
5PH(34),RADIST(25),MAXSTR(12),RZERO,PZERO
COMMON /ARG/ RRR(5),ZZ(5),S(10,10),P(10),TT(4),LM(4),DD(3,3),
1 RH(6,10),RR(4),ZZ(4),C(4,4),H(6,10),D(6,6),F(6,10),P(6),X(110)
2,EE(7),IX(800,5)
COMMON /BANARG/ MBAND,NUMBLK,B(108),A(108,54)
COMMON /PLANE/ NPP
REAL K0,MAXSTR
C

```

```

DO 200 I=1,4
DO 200 K=1,2
I=LM(I)+K-KSHIFT
KK=2*I-2+K
R(I)=R(I)+P(KK)
DO 200 J=1,4
DO 200 L=1,2
JJ=LM(J)+L-1+1-KSHIFT
LL=2*J-2+L
IF(JJ) 200,200,175
175 IF(ND-JJ) 180,195,195
180 PRINT 2004,N
STOP=1.0
GO TO 210
195 A(I),JJ=A(I),JJ+5(KK+LL)
200 CONTINUE
210 CONTINUE
C
C ADD CONCENTRATED FORCES WITHIN BLOCK
C
DO 250 N=NL,NM
K=2*N-KSHIFT
R(K)=B(K)+U(N)
C*****
250 B(K)=B(K)+U(N)
C*****
C BOUNDARY CONDITIONS
C*****
C 1. PRESSURE B.C.
C
IF (NUMPC) 260,310,260
260 DO 300 L=1,NUMPC
I=IRC(L)
J=JRC(L)
PP=PR(L)/6.
DZ=(Z(I)-Z(J))*PP
DR=(R(J)-R(I))*PP
RX=2.0*(R(I)+R(J))
ZX=R(I)+2.0*(R(J))
IF (NPP) 262,264,262
262 RX=3.0
ZX=3.0
264 I=2*I-KSHIFT
J=2*J-KSHIFT
IF (I) 260,280,265
265 IF (I-ND) 270,270,280
270 SINA=0.0
COSA=1.0
IF (CODE(I)) 271,272,272
271 SINA=SINI(CODE(I)/57.3)
COSA=COS(CODE(I)/57.3)
272 B(I)=B(I)+RX*(COSA*DZ+SINA*DR)
B(I)=B(I)-RX*(SINA*DZ-COSA*DR)
280 IF (JJ) 300,300,285
285 IF (JJ-ND) 290,290,300
290 SINA=0.0

```

```

COSA=1.0
IF (CODE(J)) 291,292,292
291 SINA=SINI(CODE(J)/57.3)
COSA=COS(CODE(J)/57.3)
292 B(J)=B(J)+ZX*(COSA*DZ+SINA*DR)
B(J)=B(J)-ZX*(SINA*DZ-COSA*DR)
300 CONTINUE
C
C 2. DISPLACEMENT B.C.
C
310 DO 400 M=NL,NH
IF (M-NUMMP) 315,315,400
315 U=UR(M)
N=2*M-1-KSHIFT
IF (CODE(M)) 390,400,316
316 IF (CODE(M)-1) 317,370,317
317 IF (CODE(M)-2) 318,390,318
318 IF (CODE(M)-3) 390,380,390
370 CALL MODIFY(A,B,ND2,MBAND,N,U)
GO TO 400
380 CALL MODIFY(A,B,ND2,MBAND,N,U)
390 U=U*(M)
N=N+1
CALL MODIFY(A,B,ND2,MBAND,N,U)
400 CONTINUE
C
C WRITE BLOCK OF EQUATIONS ON TAPE AND SHIFT UP LOWER BLOCK
C
WRITE (2) (B(N),A(N,M),M=1,MBAND),N=1,ND)
C
DO 420 N=1,ND
K=N+ND
B(N)=B(K)
R(K)=0.0
DO 420 M=1,ND
A(N,M)=A(K,M)
420 A(K,M)=0.0
C
C CHECK FOR LAST BLOCK
C
IF (NM-NUMMP) 60,480,480
480 CONTINUE
C*****
IF (STOP) 490,500,490
490 CALL EXIT
500 RETURN
C
2003 FORMAT (26HNEGATIVE AREA ELEMENT NO. I4)
2004 FORMAT (29HOBAND WIDTH EXCEEDS ALLOWABLE I4)
END
SUBROUTINE BANSON
COMMON /BANARG/ MH,NUREBLK,B(108),A(108,54)
NN=54

```

```

NL=NN+1
NH=NN+NN
REWIND 1
REWIND 2
NB=0
GO TO 150
C*****
C REDUCE EQUATIONS BY BLOCKS
C*****
C 1. SHIFT BLOCK OF EQUATIONS
C
100 NB=NB+1
DO 125 N=1,NN
NM=NN+NN
R(N)=B(N)
R(NM)=0.0
DO 125 M=1,MM
A(N,M)=A(NM,M)
125 A(NM,M)=0.0
C
C 2. READ NEXT BLOCK OF EQUATIONS INTO CORE
C
IF (NUMBLK-NB) 150,200,150
150 READ (2) (B(N),(A(N,M),M=1,MM),N=NL,NH)
IF (NB) 200,100,200
C
C 3. REDUCE BLOCK OF EQUATIONS
C
200 DO 300 N=1,NN
IF (A(N,1)) 225,300,225
225 B(N)=B(N)/A(N,1)
DO 275 L=2,MM
IF (A(N,L)) 230,275,230
230 C=A(N,L)/A(N,1)
I=N+L-1
J=0
DO 250 K=L,MM
JF=J+1
250 A(I+J)=A(I,J)-C*A(N,K)
R(I)=B(I)-A(N,L)*B(N)
A(N,L)=C
275 CONTINUE
300 CONTINUE
C
C 4. WRITE BLOCK OF REDUCED EQUATIONS ON TAPE 2
C
IF (NUMBLK-NB) 375,400,375
375 WRITE (1) (B(N),(A(N,M),M=2,MM),N=1,NN)
GO TO 100
C*****
C RACK-SUBSTITUTION
C*****
400 DO 450 M=1,NN
N=NN+1-M

```

```

DO 425 K=2,MM
L=N+K-1
425 B(N)=B(N)-A(N,K)*B(L)
NM=NN+NN
R(NM)=B(N)
450 A(NM,NB)=B(N)
NB=NB-1
IF (NB) 475,500,475
475 RACKSPACE 1
BACKSPACE 1
GO TO 400
C*****
C ORDER UNKNOWN IN B ARRAY
C*****
500 K=0
DO 600 NB=1,NUMBLK
DO 600 N=1,NN
NM=NN+NN
K=K+1
600 R(K)=A(NM,NB)
C
RETURN
C
END
SUBROUTINE TRISTF(II,JJ,KK)
COMMON NUMNP,NUMEL,NUMMAT,NUMPC,ACELZ,ANGFQ,MBAND,TEMP,MTYPE,Q,NUM
1IN,NUMCOL,NUMROW,NPLATE,NPP1,NNN,HED(8),E(8,8,12),RO(12),KO(12),CL
ZASS(12),THICK(12),TOP(12),R(900),Z(900),UR(900),UZ(900),CODE(900)
3,T(900),ZS(900),IBC(125),JBC(25),PR(25),ANGLE(4),SIGT(10),SIGT180
40,4),SIG3(800),URT(900),UZT(900),ROTMP(34),MATYP(34),DE
5PTH(34),RADI(25),MAXSTR(12),RZERO,PZERO
COMMON /ARG/ RRR(5),ZZZ(5),VST(10),PIIO,TT(4),LM(4),DD(3,3),
1 HR(6,10),RR(4),ZZ(4),C(4,4),H(6,10),D(6,6),F(6,10),TP(6),XI(10)
2 EE(7),X(1800,9)
COMMON /PLANE/ NPP
REAL KO,MAXSTR
C
C 1. INITIALIZATION
C
LM(1)=II
LM(2)=JJ
LM(3)=KK
C
RR(1)=RRR(II)
RR(2)=RRR(IJJ)
RR(3)=RRR(KK)
RR(4)=RRR(II)
ZZ(1)=ZZZ(II)
ZZ(2)=ZZZ(IJJ)
ZZ(3)=ZZZ(KK)
ZZ(4)=ZZZ(II)
C
85 DO 100 I=1,6

```

```

DO 90 J=1,10
F(I,J)=0.0
90 H(I,J)=0.0
DO 100 J=1,6
100 D(I,J)=0.0
C
C 3. FORM INTEGRAL(G)*C*(G)
C
C CALL INTER(XI,RR,ZZ)
C
D(2,6)=X(1)*C(1,2)+C(2,3)
D(3,5)=X(1)*C(4,4)
D(5,5)=X(1)*C(4,4)
D(6,6)=X(1)*C(2,2)
106 D(1,1)=X(1)*C(3,3)
D(1,2)=X(1)*C(1,3)+C(3,3)
D(1,3)=X(1)*C(3,3)
D(2,2)=X(1)*C(2,3)
D(2,3)=X(1)*C(1,1)+2.*C(1,3)+C(3,3)
D(2,3)=X(1)*C(1,3)+C(3,3)
D(3,3)=X(1)*C(3,3)+X(1)*C(4,4)
D(3,6)=X(1)*C(2,3)
C
C 108 DO 110 I=1,6
DO 110 J=1,6
110 D(I,J)=D(I,J)
C
C 4. FORM COEFFICIENT-DISPLACEMENT TRANSFORMATION MATRIX
C
COMM=RR(2)*ZZ(3)-ZZ(1)*RR(1)+RR(3)*ZZ(2)-ZZ(2)*RR(3)+ZZ(1)-ZZ(2)
DD(1,1)=(RR(2)*ZZ(3)-RR(3)*ZZ(2))/COMM
DD(1,2)=(RR(3)*ZZ(1)-RR(1)*ZZ(3))/COMM
DD(1,3)=(RR(1)*ZZ(2)-RR(2)*ZZ(1))/COMM
DD(2,1)=(ZZ(2)-ZZ(3))/COMM
DD(2,2)=(ZZ(3)-ZZ(1))/COMM
DD(2,3)=(RR(3)-RR(2))/COMM
DD(3,1)=(RR(1)-RR(2))/COMM
DD(3,2)=(RR(2)-RR(1))/COMM
DD(3,3)=(RR(2)-RR(1))/COMM
C
DO 120 I=1,3
J=2*LM(I)-1
H(I,J)=DD(1,1)
H(2,J)=DD(2,1)
H(3,J)=DD(3,1)
H(4,J)=DD(1,1)
H(5,J+1)=DD(2,1)
120 H(6,J+1)=DD(3,1)
C
C ROTATE UNKNOWN IF REQUIRED
C
C I=LM(J)
IF (ANGLE(I),122,125,125)
122 SIN=STN(ANGLE(I))

```

```

COSA=COS(ANGLE(I))
I=2*I
DO 124 K=1,6
TEM=H(K,J)-1
H(K,I,J)=TEM*COSA+HI(K,I)*SINA
124 H(K,I,J)= -TEM*SINA+HI(K,I)*COSA
125 CONTINUE
C
C 5. FORM ELEMENT STIFFNESS MATRIX (H)*D)*(H)
C
DO 130 J=1,10
DO 130 K=1,6
IF (H(K,J)) 128,130,128
128 DO 129 I=1,6
129 F(I,J)=F(I,J)+D(I,K)*H(K,J)
130 CONTINUE
C
DO 140 I=1,10
DO 140 K=1,6
IF (H(K,I)) 138,140,138
138 DO 139 J=1,10
139 S(I,J)=S(I,J)+H(K,I)*F(K,J)
140 CONTINUE
C
C 6. FORM THERMAL LOAD MATRIX
C
150 COMM=RO(IMTYPE)*ANGFO**2
TP(1)=COMM*X(7) + X(2)*TT(3)
TP(2)=COMM*X(9) + X(1)*TT(1)+TT(3)
TP(3)=COMM*X(10)+ X(4)*TT(3)
COMM=-RO(IMTYPE)*ACELZ
TP(4)=COMM*X(7)
TP(5)=COMM*X(7)
TP(6)=COMM*X(8) +X(1)*TT(2)
C
DO 160 I=1,10
DO 160 K=1,6
160 P(I)=P(I)+H(K,I)*TP(K)
C
C FORM STRAIN TRANSFORMATION MATRIX
C
400 DO 410 I=1,6
DO 410 J=1,10
410 HH(I,J)=HH(I,J)+H(I,J)
C
C RETURN
C
C FND
C SUBROUTINE SYNTHV(A,NMAX)
C *****
C DIMENSION A(4,4)
C
C DO 200 N=1,NMAX
C

```

```

D=A(N,N)
DO 100 J=1,NMAX
  100 A(N,J)=-A(N,J)/D
C
DO 150 I=1,NMAX
  150 DO 140 J=1,NMAX
    140 A(I,J)=A(I,J)+A(I,N)*A(N,J)
  140 CONTINUE
  150 A(I,N)=A(I,N)/D
C
A(N,N)=1.0/D
C
200 CONTINUE
C
RETURN
C
FND
SUBROUTINE MODIFY(A,D,NEG,MBAND,N,U)
*****
DIMENSION A(108,54),B(108)
C
DO 250 M=2,MBAND
  K=N-M+1
  235 R(K)=B(K)-A(K,M)*U
  A(K,M)=0.0
  235 K=N-M-1
  IF(NEG-K) 250,240,240
  240 R(K)=B(K)-A(N,M)*U
  A(N,M)=0.0
  250 CONTINUE
  A(N,1)=1.0
  R(N)=U
  RETURN
END
SUBROUTINE INTER(X,RR,ZZ)
*****
DIMENSION RR(1),ZZ(1),XI(1),XM(6),R(6),Z(6),XX(6)
COMMON /PLANE/ NPP
DATA (XX(I),I=1,6)/3*1.0,3*3.0/
C
COMM=RR(2)*(ZZ(3)-ZZ(1))+RR(1)*ZZ(2)-ZZ(3)+RR(3)*(ZZ(1)-ZZ(2))
COMM=COMM/24.0
R(1)=RR(1)
R(2)=RR(2)
R(3)=RR(3)
R(4)=(R(1)+R(2))/2.0
R(5)=(R(2)+R(3))/2.0
R(6)=(R(3)+R(1))/2.0
C
Z(1)=ZZ(1)
Z(2)=ZZ(2)
Z(3)=ZZ(3)
Z(4)=(Z(1)+Z(2))/2.0
Z(5)=(Z(2)+Z(3))/2.0
Z(6)=(Z(3)+Z(1))/2.0
C
DO 30 I=1,6
  35 XM(I)=XX(I)*R(I)
C
DO 40 I=1,10
  50 XI(I)=0.0
C
DO 100 I=1,6
  XI(1)=XI(1)+XM(I)
  XI(2)=XI(2)+XM(I)/R(I)
  XI(3)=XI(3)+XM(I)/R(I)**2
  XI(4)=XI(4)+XM(I)*Z(I)/R(I)
  XI(5)=XI(5)+XM(I)*Z(I)/(R(I)**2)
  XI(6)=XI(6)+XM(I)*Z(I)**2/(R(I)**2)
  XI(7)=XI(7)+XM(I)*R(I)
  XI(8)=XI(8)+XM(I)*Z(I)
  XI(9)=XI(9)+XM(I)*R(I)**2
  XI(10)=XI(10)+XM(I)*R(I)*Z(I)
  100 CONTINUE
C
DO 150 I=1,10
  150 XI(I)=XI(I)*COMM
C
RETURN
END

```

INSTRUCTION FOR ANALYSIS OF PRISMATIC SOLIDS PROGRAM

The first step is to select a finite element representation of the two-dimensional cross-section of the body. Elements and nodal points are then numbered in two numerical sequences, each starting with one. The following group of punched cards numerically defines the two-dimensional structure to be analyzed.

Card 1 - Identification Card - (12A6)

cc1-72 Of this card contain information to be with results.

Card 2 - Control Card - (4I5, F10.2)

cc1-5 number of nodal points (350 max.)
 cc6-10 number of elements (300 max.)
 cc11-15 number of different materials (12 max.)
 cc16-20 number of harmonics
 cc21-30 ZL - length

The ZL length is half of the period length (length to next load).

Card 3 - Material Property Information

The following group of cards for each material:

First Card: (2I5, 2F10.0)

cc1-5 material identification - any number from 1 -12
 cc6-10 number of different Y-ordinates for which properties are given - 8 maximum

Second Card: (3F10.0) One card for each Y-ordinate

cc1-10 Y-ordinate of material for which property is given
 cc11-20 Young's Modulus
 cc21-30 Poisson's Ratio

Card 4 - Nodal Point Data - (I5, F5.0, 5F10.0)

One card for each nodal point with the following information:

cc1-5 nodal point number
 cc6-10 code number
 cc11-20 X-ordinate
 cc21-30 Y-ordinate
 cc31-40 UX
 cc41-50 UY
 cc51-60 Loaded length in Z-direction

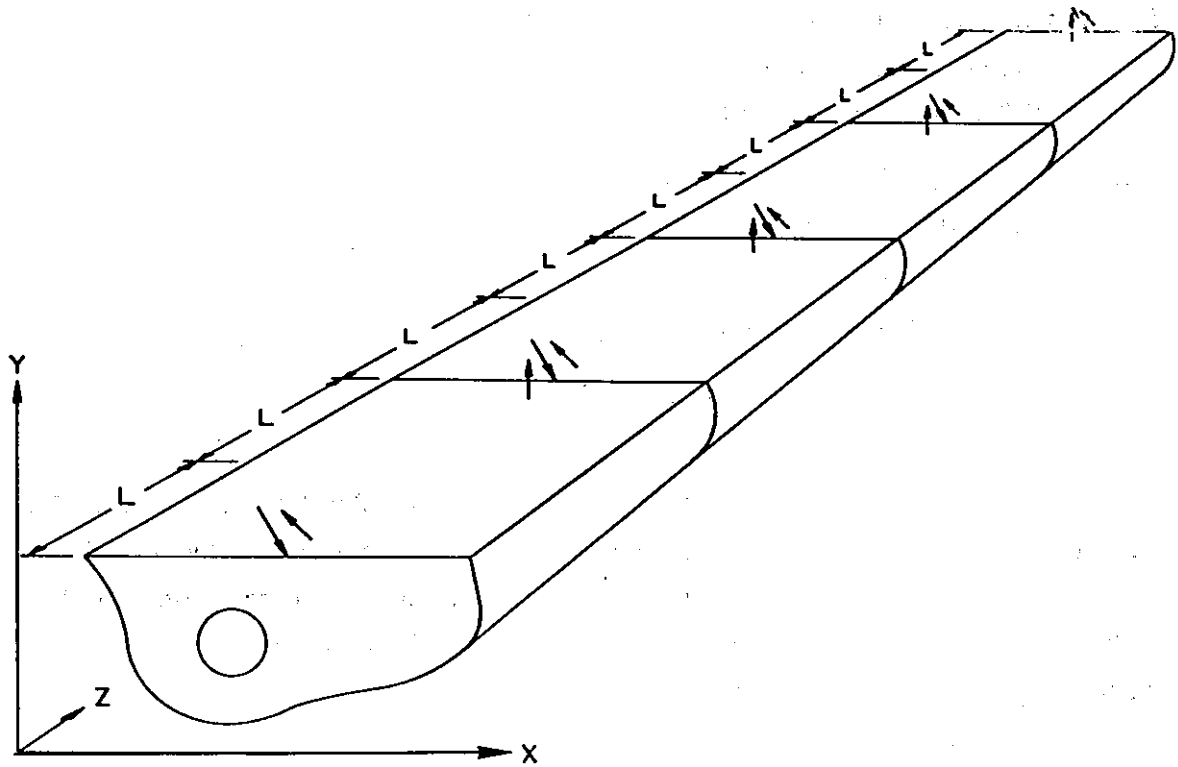


Fig. C4 — The prismatic space.

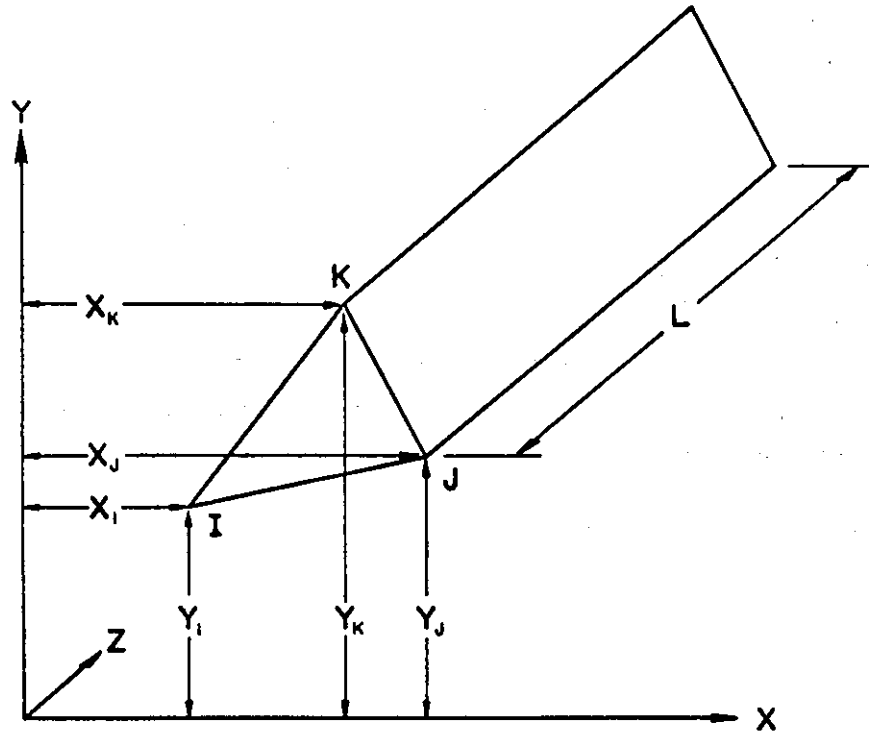


Fig. C5 — The prismatic space finite element.

If the number of column 10 is

- 0, UX is specified X-load
 UY is specified Y-load
- 1, UX is specified X-displacement
 UY is specified Y-load
- 2, UX is specified X-load
 UY is specified Y-displacement
- 3, UX is specified X-displacement
 UY is specified Y-displacement

All loads are total forces acting on the nodal point. Loaded length is half the loaded length in the Z-direction. Nodal point cards must be in numerical sequence. If cards are omitted, the omitted nodal points are generated at equal intervals along a straight line between the defined nodal points. The boundary code (column 10), UX, UY, and loaded length, are set equal to zero.

Card 5 - Element Properties: (6I5)

One card for each element

- cc1-5 element number
- cc6-10 nodal point I
- cc11-15 nodal point J
- cc16-20 nodal point K
- cc21-25 nodal point L
- cc26-30 material identification

Card 6 - Longitudinal Distance: (F10.0)

- cc1-10 ZZ - length

This distance defines the cross-sections in the longitudinal (Z) direction where stresses and strains are to be printed. Nodal point displacements and element stresses for the defined finite element mesh are obtained.


```

1001 FORMAT (215,ZELL,0)
1002 FORMAT (15,F5.1,5F11.0)
1003 FORMAT (15)
1005 FORMAT (3F11.0)
2000 FORMAT (1F11,2Ae/
1 30HC NUMBER OF NODAL POINTS----- 13 /
2 30HC NUMBER OF ELEMENTS----- 13 /
3 30HC NUMBER OF CIPF, MATERIALS----- 13 /
4 30HC NUMBER OF PARONITICS----- 13 /
5 30HC Z-LENGTH----- F10.3)
2001 FORMAT (49,ELEMENT NO. I J K L MATERIAL )
2003 FORMAT (11I3,4I6,11I2)
2004 FORMAT (48H,ADDDAL PCINT TYPE X-COORDINATE Y-COORDINATE
1:8X GHK-LC3D 18X 6HV-LCAD 2X 12-LCAD LENGTH )
2002 FORMAT (11I2,F12.2,2F12.3,2E24.7,F12.3)
2006 FORMAT (12F10.4,P. NUMBER 18X 2PLX 16X 2PLY 18X 2HUL / (11I2,3E20.7))
2007 FORMAT (3I6,F12.3)
2008 FORMAT (3LUGN,P. CIEF, 10C LARGE EL.NC.= 14)
2009 FORMAT (26H,ADDDAL PCINT C66L EPRC M= 15)
2010 FORMAT (17X 1PY 14X 1PE 13X 2HUL / (F15.3,E15.7,F15.3))
2011 FORMAT (17HP,MATERIAL NUMBER= 13, 20HP, NUMBER OF Y CARDS= 13)
C
ENC
SUBROUTINE STIFF
C
CCMPCN NMAP,NUMEL,NUMMAT,NUMPAR,NUMPAR,ZL,PI,PCD(12),C11,C12,G
1 ,WBANC,NWBK,R(100),A(108,54)
CCMPCN /ELCARG/ IX(300,5),E(18,3,12),NUMTC(12),Y(400),SIG(300,6)
CCMPCN /ELCARG/ Y(350),X(350),UM(350),LY(350),WZ(350),CODE(35C)
COMMON /CLCARG/ N,VEL,HTYPE,ST(15,15),DC(13,3),E(13,3),S(9,9),
1 ,XX(3),YY(3),JJ,EE(7),LW(4),DI(3),EAL(5),EPS(E)
C
*****
C INITIALIZATION
C *****
REMI=2
NB=18
ND=2*NB
AD2=2*ND
NUMBLK=0
DC 40 N=1,NUMEL
4) IXIN,5)=IARS(IX(N,5))
C
CC 5C N=1,AD2
B(N)=1.0
DO 5C M=1,ND
5) A(N,M)=0.0
C *****
C FORM STIFFNESS MATRIX IN BLOCKS
C *****
60 NUMBLK=NUMBLK+1
N=NB*(NUMBLK+1)
NENB=NB
NENB=NB+1
KSHIF1=3UN-3
C

```

```

DC 210 N=1,NMEL
IF (IXIN,5) 210,212,65
65 DO BC I=1,4
IF (IXIN,I)-AL1 6C,7C,70
70 IF (IXIN,I)-NM 99,90,99)
90 CONTINUE
GC TC 21C
99 CALL QLAC
IXIN,5)=-NTYPE
ACC ELEMENT STIFFNESS, TC, TOTAL STIFFNESS
165 DO 166 I=1,4
166 UM(I)=3*IX(N,11)-3
CC 200 I=1,4
CC 200 K=1,3
II=LM(I)*NK-KSHIF1
KK=3*I-34K
DC 200 J=1,4
CC 210 L=1,3
JJ=L*(J)+L-I+1-KSHIF1
LL=3*J-34L
IF (JJ) 200,200,155
195 A(II,JJ)=A(II,JJ)+ST(KK,LL)
200 CONTINUE
210 CCNTINE
C
APP CONCENTRATE FORCES WITHIN BLOCK
DO 250 N=NL,NM
IF (N-NUMNP) 240,243,210
240 K=3*N-KSHIF1-1
IF (TN).EC.C.C) TM=1.0)
IF (LX*AR.EC.U.O) TM=0.5
IF (TN)*N*AR.NE.J.) TP=ZL*SIN(X*AR*PI*(N)/ZL)/(X*AP*PI*(N))
245 R(K)=E(K)*LY(N)*TM
250 C(K-1)=B(K-1)*LX(N)*TM
C
BOUNDARY CONDITIONS
310 DO 400 M=NL,NM
IF (M-NUMNP) 315,315,440C
315 U=UX(M)
N=3*M-1-KSHIF1-1
IF (CODE(M)) 350,410,316
316 IF (CODE(M)-1) 317,37C,217
317 IF (CODE(M)-2) 318,35C,319
318 IF (CODE(M)-3) 39C,36C,397
370 CALL MODIFY(A,E,AC2,WBANC,N,L)
CC TO 40C
380 CALL MODIFY(A,E,AC2,WBANC,N,L)
390 L=LY(M)
N=N*Y
C

```



```

DC 145 J=1,3
JJ=LW(J)/3 + 1
DC 145 I=1,3
145 CT(I,JJ)=CT(I,JJ)+DC(I,J)
C
150 CONTINUE
IX(IN,5)=I*TYPE
C
C ELIMINATE CENTRAL UNKNKANS
C
DC 160 KF=1,3
IR=15-NK
IC=IP+1
DO 160 II=1,IP
ST(II,IO)=ST(II,IO)/ST(IC,IO)
DO 160 JJ=1,IR
DO 160 JJ=1,IR
160 ST(II,JJ)=ST(II,JJ)-ST(II,IO)*ST(IC,JJ)
C
RETURN
C
C SUBROUTINE OUTPUT
C
CCMPKN NUMP,NUMEL,NUMPAT,NUMPAR,XI,AR,ZL,PI,PEC(12),C11,C12,G
I *MBAND,NUMBLK,B(109),A(106,54)
CCMKN /FEARG/ XI(350),Y(106,54),Z(106,54),I(106,54)
CCMKN /CROARG/ XI(350),Y(350),UZ(350),UZ(350),CODE(350)
C
DC 50 N=1,NUMEL
CODE(IN)=0
T(N)=0
DC 50 I=1,4
II=T(N,1)
T(N)=T(N,II)/4.
50 CCDE(IN)=CCDE(IN)+T(II)/4.
C
NUMST=6*NUMEL
NUMUR=3*NUMP
100 RENTING 4
C
FEAD (5,1000) ZZ
C
CC 550 N=1,NUMP
LX(IN)=C,0
LY(IN)=C,C
C
550 UZ(IN)=C,C
C
DC 675 N=1,NUMEL
DO 675 I=1,5
SIG(I,II)=C,0
C
DC 800 NPAR=1,NUMPAR
XPAR=NHAR-1
ZP=PI+XPAR*ZL/ZL
SINZ=SIN(ZX)
COSZ=COS(ZX)
C

```

READ (4) (R(N),N=1,NUMUR)

DO 600 N=1,NUMP
UX(N)=UX(N)+B(3*N-2)*CCSZ
LY(N)=UY(N)+E(3*N-1)*CCSZ
600 UZ(N)=UZ(N)+E(3*N)*SINZ

READ (4) (R(N),N=1,NUMST)

DO 700 N=1,NUMEL
SIG(N,1)=SIG(N,1)+B(6*N-5)*CCSZ
SIG(N,2)=SIG(N,2)+B(6*N-4)*CCSZ
SIG(N,3)=SIG(N,3)+B(6*N-3)*CCSZ
SIG(N,4)=SIG(N,4)+B(6*N-2)*CCSZ
SIG(N,5)=SIG(N,5)+B(6*N-1)*CCSZ
700 SIG(N,6)=SIG(N,6)+B(6*N)*SINZ

800 CONTINUE

WRITE (6,2001) (N,X(N),Y(N),Z,UZ(N),LY(N),UZ(N),N=1,NUMNP)

WRITE (6,2002) (N,T(N),CCDE(N),ZZ,(SIG(N,I),I=1,6),N=1,NUMEL)

GO TO 100

1000 FORMAT (1F10.0)
2001 FORMAT (10P1,N,P,NO, 9X 1M, 9X 1M, 9X 1PZ 13X 2HUY 13X 2HUY 13X
1 2HYZ /110,3F10.2,3E15.7)
2002 FORMAT (1CHI EL,NO, 5X 1M, 9X 1M, 9X 1M, 12X 2HSHX 12X 2HSHY 12X
1 3HSZZ 12X 3P-SYZ 12X 3P-SXZ 12X 3HSYZ /110,3F10.2,3E15.7)

END

SUBROUTINE STRESS
COMMON NUMP,NUMEL,NUMPAT,NUMPAR,XI,AR,ZL,PI,PEC(12),C11,C12,G
I *MBAND,NUMBLK,B(109),A(106,54)
CCMKN /FEARG/ XI(350),Y(106,54),Z(106,54),I(106,54)
CCMKN /CROARG/ XI(350),Y(350),UZ(350),UZ(350),CODE(350)
CCMKN /CLAEAR/ A,VOL,TYPE,ST(12,5),DD(3,3),C(3,3),S(9,9),
1 XX(3),YY(3),IJ,JJ,EE(7),LH(4),DT(3,3),U(15),EPSIG

CCP =PI*XPAR/ZL
DO 500 N=1,NUMEL

N=N

CALL QUAC

SELECT CGRNER DISPLACEMENTS

II=0

DC 100 I=1,4
JJ=3+IX(IN,II)-3
DO 100 J=1,3
II=II+1
JJ=JJ+1
100 UZ(II)=BL(JJ)


```

C ***** CRDES LANCHEAS IN P ZFRAY ***** RANSC074
C ***** RANSC075 *****
500 M=0 RANSC076
DE 600 N=0,ALPBLK RANSC077
CC 500 N=J,AN RANSC078
AP=*** RANSC079
R=K+L RANSC080
60) P(K)=A(N+NB) RANSC081
C RANSC082
C RETL:P RANSC083
C ENF RANSC084
RANSC085

```

APPENDIX D
STATISTICAL TESTS

TABLE D1 - t-TEST- TEST OF THE EQUALITY OF TWO MEANS

Applied Stress psi	\bar{x}_1	\bar{x}_2	n_1	n_2	$S_1^2 \times 10^6$	$S_2^2 \times 10^6$	t	$\pm t \frac{\sigma}{2}$	Reject	Accept or Reserve Judgment
Comparison of mean fracture life - granite aggregate, 6 percent asphalt, 85-100 penetration asphalt, California fine and coarse graded mixes:										
150	1,605	3,800	9	11	325	5.86	2.10	2.09	x	-
100	7,885	15,271	10	11	9.34	233	2.10	2.10	-	x
75	23,017	97,541	9	11	165	9,500	1.49	2.09	-	x
Comparison of mean fatigue life - California medium graded mix:										
<u>Granite vs. Limestone</u>										
75	19,925	23,556	8	8	175	236	0.628	2.15	-	x
<u>Granite vs. Crushed Gravel</u>										
75	19,925	42,474	8	9	175	956	1.91	2.13	-	x
<u>Limestone vs. Crushed Gravel</u>										
75	23,556	42,474	8	9	236	956	1.74	2.13	-	x
Comparison of mean stiffness - California medium graded mix:										
<u>Granite vs. Limestone</u>										
75	288,625	292,625	8	8	625	2,500	0.20	2.15	-	x
<u>Granite vs. Crushed Gravel</u>										
75	288,625	370,777	8	9	625	2,304	4.33	2.13	x	-
<u>Limestone vs. Crushed Gravel</u>										
75	292,625	370,777	8	9	2,500	2,304	3.29	2.13	x	-

TABLE D2 - t-TEST - SIGNIFICANCE OF THE DIFFERENCE BETWEEN THE REGRESSION COEFFICIENTS b_1 AND b_2 OF TWO SEPARATE EQUATIONS.

Comparison of:		With:		Regression Equation		b_1	b_2	n_1	n_2	t	t ^a	Reject	Accept or Reserve Judg.
Aggregate Percent Grading	Asphalt Percent Pen.	Aggregate Percent Grading	Asphalt Percent Pen.	$\sigma-N_f$	$\epsilon-N_f$								
Granite 6	Fine 85-100	Granite 6	Coarse 85-100	$\sigma-N_f$	$\epsilon-N_f$	3.843	3.685	33	28	0.25	2.01	-	x
Granite 6	Fine 85-100	Granite 6	Medium 85-100	$\sigma-N_f$	$\epsilon-N_f$	2.952	9.486	33	28	1.42	2.01	-	x
Granite 6	Medium 85-100	Granite 6	Coarse 85-100	$\sigma-N_f$	$\epsilon-N_f$	3.843	4.037	33	19	0.27	2.00	-	x
Granite 6	Medium 85-100	Granite 6	Medium 85-100	$\sigma-N_f$	$\epsilon-N_f$	2.952	2.833	33	19	0.21	2.00	-	x
Granite 6	Medium 85-100	Granite 6	Coarse 85-100	$\sigma-N_f$	$\epsilon-N_f$	4.037	3.685	19	28	0.60	2.02	-	-
Granite 6	Medium 60-70	Granite 6	Coarse 85-100	$\sigma-N_f$	$\epsilon-N_f$	2.833	2.486	19	28	0.90	2.02	-	x
Granite 6	Coarse 85-100	Granite 6	Coarse 85-100	$\sigma-N_f$	$\epsilon-N_f$	3.256	2.486	27	28	2.71	2.02	-	x
Granite 6	Coarse 85-100	Granite 6	Medium 40-50	$\sigma-N_f$	$\epsilon-N_f$	2.486	4.011	28	33	4.88	2.02	x	-
Granite 6	Medium 85-100	Granite 6	Medium 40-50	$\sigma-N_f$	$\epsilon-N_f$	4.037	4.928	19	23	1.20	2.02	-	x
Granite 6	Medium 85-100	Granite 6	Medium 40-50	$\sigma-N_f$	$\epsilon-N_f$	2.833	4.011	19	23	3.21	2.02	x	-
Granite 6	Medium 60-70	Basalt 6.2	Medium 60-70	$\sigma-N_f$	$\epsilon-N_f$	4.206	3.238	27	24	1.65	2.02	-	x
Granite 6	Medium 60-70	Granite 6	Medium 40-50	$\sigma-N_f$	$\epsilon-N_f$	3.256	4.011	27	33	2.32	2.01	x	-
Granite 6	Medium 85-100	Granite 6	Medium 60-70	$\sigma-N_f$	$\epsilon-N_f$	4.207	4.037	19	27	0.26	2.02	-	x
Granite 6	Medium 85-100	Granite 6	Medium 60-70	$\sigma-N_f$	$\epsilon-N_f$	2.833	3.256	19	27	1.07	2.02	-	x
Granite 6	Medium 85-100	Granite 6	Medium 60-70	$\sigma-N_f$	$\epsilon-N_f$	2.952	3.256	33	27	1.03	2.01	-	x
Morro Bay Field Loc. 4, 1965	85-100	Morro Bay Field Loc. 4, 1967	85-100	$\sigma-N_f$	$\epsilon-N_f$	2.713	3.671	14	36	1.08	2.00	-	x

a. $t_{\alpha/2, n_1 + n_2 - 4}$

TABLE D3 - F TEST - TEST OF THE EQUALITY OF THE POPULATIONS STANDARD ERROR OF ESTIMATE

Comparison of:		With:		Asphalt Aggregate Percent Grading	Asphalt Aggregate Asphalt Pen.	Regression Equation	S ₁ ²	S ₂ ²	F	F ^a	Rejection	Accept or Reserve Judg.
Aggregate Percent Grading	Asphalt Pen.	Aggregate Percent Grading	Asphalt Pen.									
Granite 6	Fine 85-100	Granite 6	Coarse 85-100			$\sigma-N_f$.1488	.0406	2.67	2.04	x	-
						$\epsilon-N_f$.0678	.0339	2.00	2.04	-	x
Granite 6	Fine 85-100	Granite 6	Medium 85-100			$\sigma-N_f$.1488	.0702	2.11	2.35	-	x
						$\epsilon-N_f$.0678	.0676	1.01	2.35	-	x
Granite 6	Medium 85-100	Granite 6	Coarse 85-100			$\sigma-N_f$.0702	.0406	1.73	2.40	-	x
						$\epsilon-N_f$.0676	.0339	1.97	2.40	-	x
Granite 6	Medium 60-70	Granite 6	Coarse 85-100			$\epsilon-N_f$.0350	.0339	1.03	2.16	-	x
Granite 6	Coarse 85-100	Granite 6	Medium 40-50			$\epsilon-N_f$.0339	.0225	1.50	2.36	-	x
Granite 6	Medium 85-100	Granite 6	Medium 40-50			$\sigma-N_f$.0700	.0651	1.08	2.46	-	x
+++						$\epsilon-N_f$.0676	.0225	3.00	2.46	x	-
Granite 6	Medium 60-70	Basalt 6.2	Medium 60-70			$\sigma-N_f$.0778	.0553	1.41	2.26	-	x
Granite 6	Medium 60-70	Granite 6	Medium 40-50			$\epsilon-N_f$.0350	.0225	1.55	2.32	-	x
Granite 6	Medium 85-100	Granite 6	Medium 60-70			$\sigma-N_f$.0782	.0700	1.12	2.30	-	x
						$\epsilon-N_f$.0676	.0350	1.93	2.30	-	x
Granite 6	Fine 85-100	Granite 6	Medium 60-70			$\epsilon-N_f$.0678	.0350	1.94	2.10	-	x
Morro Bay Field Loc. 4, 1965		Morro Bay Field Loc. 4, 1967				$\epsilon-N_f$.244	.0968	2.52	2.30	-	^b x
In-service pavement field results		California graded granite mixes				$\epsilon-N_f$.194	.073	2.65	1.50	x	-

a. At $\alpha = 1$ percent

b. $F_{\alpha/2, (n_1-1, n_2-1)}$

TABLE D4 — t-TEST — TEST FOR HYPOTHESIS THAT SLOPE OF
POPULATION REGRESSION LINE HAS A VALUE OF FIVE —
CALIFORNIA GRADED GRANITE MIXES

Aggregate Grading	Asphalt Penetration	S_b	b	n	t	t^a	Reject	Accept or Reserve Judgment
Fine	85-100	.1357	2.952	53	15.1	2.01	x	-
Coarse	85-100	.1899	2.486	28	13.2	2.06	x	-
Medium	85-100	.3351	2.833	19	6.58	2.11	x	-
Medium	60-70	.2105	3.256	27	8.28	2.06	x	-
Medium	40-50	.2480	4.011	23	3.99	2.08	x	-

a. $t_{\alpha/2, n-2}$

APPENDIX E

PROJECT DESCRIPTIONS

Morro Bay Project (V-SLO-56C,D)

The structural section for this pavement, shown in Fig. E1, consists of 0.21 ft of asphalt concrete with a type B aggregate, together with 1.67 of class 2 aggregate base and subbase. The wearing course consists of 0.06 ft of open-graded material; this, however, was not considered as part of the structural section for the structural analyses.

Field samples were obtained at the locations shown in Table E1 and consisted of 15 in. by 15 in. specimens of the asphalt concrete together with samples of the other materials in the structural section.

Folsom Project (03-SAC, Ed-50)

The structural pavement section, Fig. E2, consists of 0.33 ft of asphalt concrete and 0.25 ft of asphalt-treated base, together with 1.50 ft of untreated base and subbase on a subgrade of compacted dredger tailings.

The portion of the project selected for study included a test section in which an experimental asphalt meeting new specifications proposed by the Materials and Research Department (56) as well as a conventional paving asphalt (control) were utilized in the 0.33 ft of asphalt concrete surface course (Fig. E2). Sections from which the pavement samples were obtained are also a part of an experimental compaction study, the details of which are shown in Fig. E3 and described in Ref. (75). Sampling locations are also shown in Fig. E3. Locations 3 and 4 correspond to the sections containing the experimental asphalt while locations 1 and 2 the control asphalt.

TABLE E1 — PAVEMENT SAMPLE* SUMMARY, V-SLO-56-C,D

U. C. Designation	Station and Location	Thickness, ft	
		Plan	Actual
Blocks 1. 1, 1. 2, 1. 3 (1)	625 + 00 Northbound travel lane; outer wheel track	0.27	0.27
Blocks 2. 1, 2. 2, 2. 3 (2)	626 + 00 Northbound passing lane; outer wheel track	0.27	0.29
Blocks 3. 1, 3. 2, 3. 3 (3)	100 + 00 Southbound passing lane; outer wheel track	0.27	0.27
Blocks 4. 1, 4. 2, 4. 3 (4)	718 + 00 Northbound travel lane; outer wheel track	0.27	0.25

*Samples taken December 14-16, 1965.

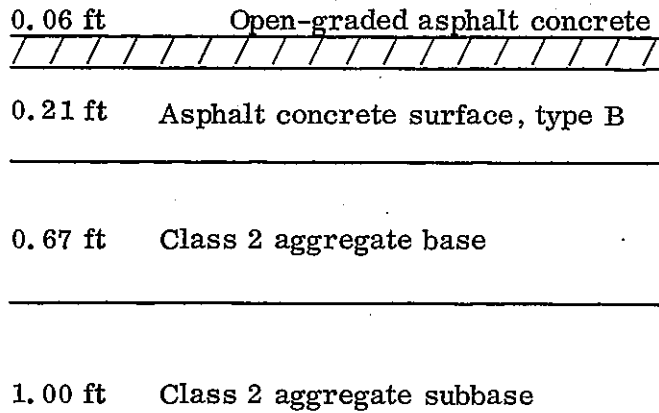


Fig. E1 - Structural section, Morro Bay pavement (V-SLO-56-C, D).

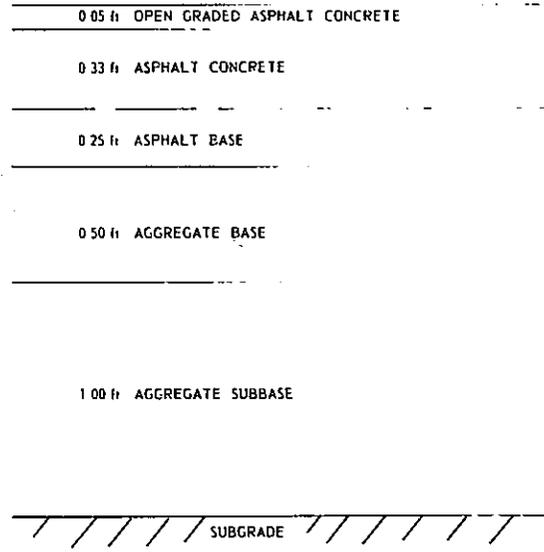


Fig. E2 - Structural pavement section - Folsom project (03-SAC, ED-11-B, A).

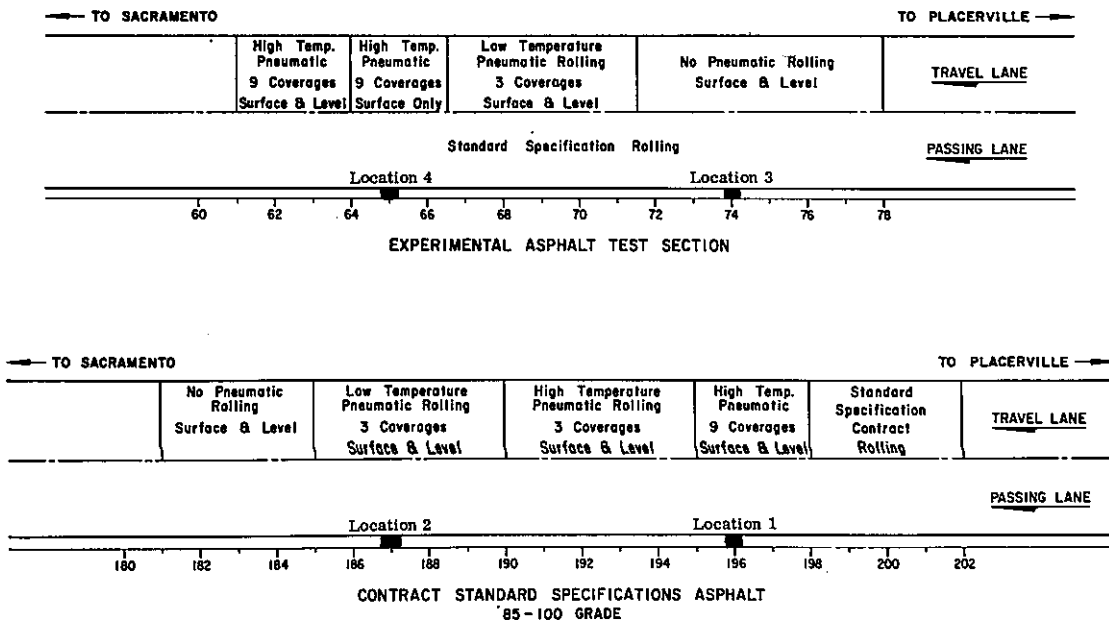


Fig. E3 - Pneumatic rolling test sections - Folsom project (03-SAC, ED-50).

TABLE E2 — RESULTS OF REPEATED LOAD TESTS ON
SUBBASE MATERIAL, FOLSOM PROJECT

Test No.	Degree of Saturation	Dry Density pcf	$k_1(\theta)^{k_2}$			$k_3(\sigma)^{k_4}$		
			k_1	k_2	Corr. Coef.	k_3	k_4	Corr. Coef.
5A	52	132.5	4,945.	0.48	0.86	9,589.	0.50	0.88
5B	42	131.0	10,745.	0.41	0.85	18,273.	0.44	0.91
5C	44	132.8	7,387	0.45	0.94	13,896.	0.45	0.97
5D	39	131.0	4,752	0.54	0.87	10,669.	0.55	0.94
6B		133.3	4,899.	0.55	0.94	12,014.	0.52	0.95
6C	37	133.0	9,967.	0.48	0.87	20,638.	0.48	0.94
6D	43	135.0	19,464.	0.29	0.58	26,155.	0.37	0.79
6E	44	132.3	4,855.	0.55	0.90	12,489.	0.50	0.89
6F	39	131.7	10,895.	0.37	0.84	19,223.	0.38	0.91
All tests			7,729.	0.46	0.68	15,570.	0.46	0.70

TABLE E3 — IN SITU PROPERTIES OF BASE COURSE
FOLSOM PROJECT

Location/station	Wet Density pcf	Dry Density pcf	Water Content Percent	Degree of Saturation
1/196+00	142.7	138.8	2.8	31
	161.1	156.6	2.9	76
2/187+00	151.5	146.6	3.3	51
	135.6	130.7	3.5	30
3/70+00	137.8	133.5	3.2	30
	148.1	143.4	3.3	44
4/65+00	148.8	144.5	3.0	42
	156.5	152.0	2.9	57

TABLE E4 — RESULTS OF REPEATED LOAD TESTS ON
BASE MATERIAL, FOLSOM PROJECT

Test No.	Degree of Saturation	Dry Density pcf	$k_1(\theta)^{k_2}$			$k_3(\sigma)^{k_4}$		
			k_1	k_2	Corr. Coef.	k_3	k_4	Corr. Coef.
7A	32.0	136.2	2,771.	0.72	0.98	11,968.	0.59	0.90
7B	30.0	134.5	3,662.	0.60	0.99	12,102.	0.50	0.89
7C	27.3	134.8	3,232.	0.66	0.98	12,297.	0.54	0.87
7D	23.1	134.8	4,411.	0.61	0.96	14,102.	0.53	0.91
All			3,468.	0.65	0.96			

*All values are in SI units unless otherwise specified.

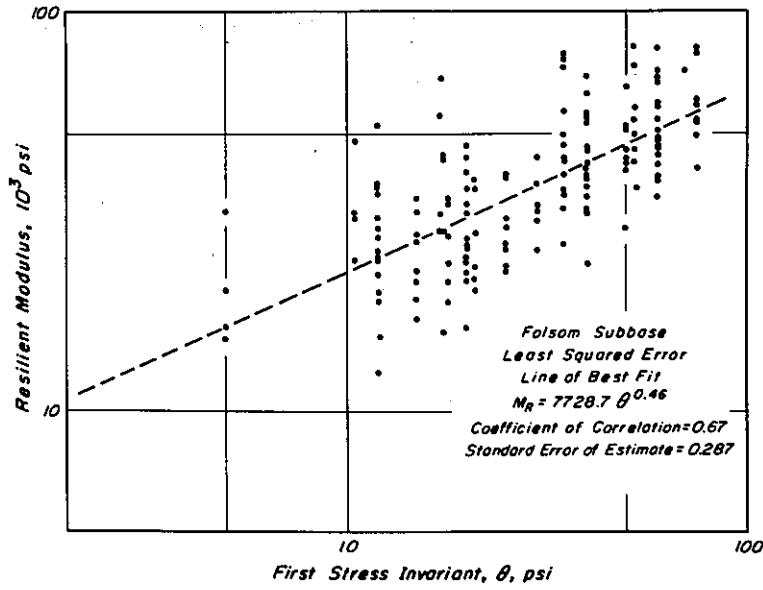


Fig. E4 – Individual test results of modulus vs. sum of principal stresses, Folsom subbase material.

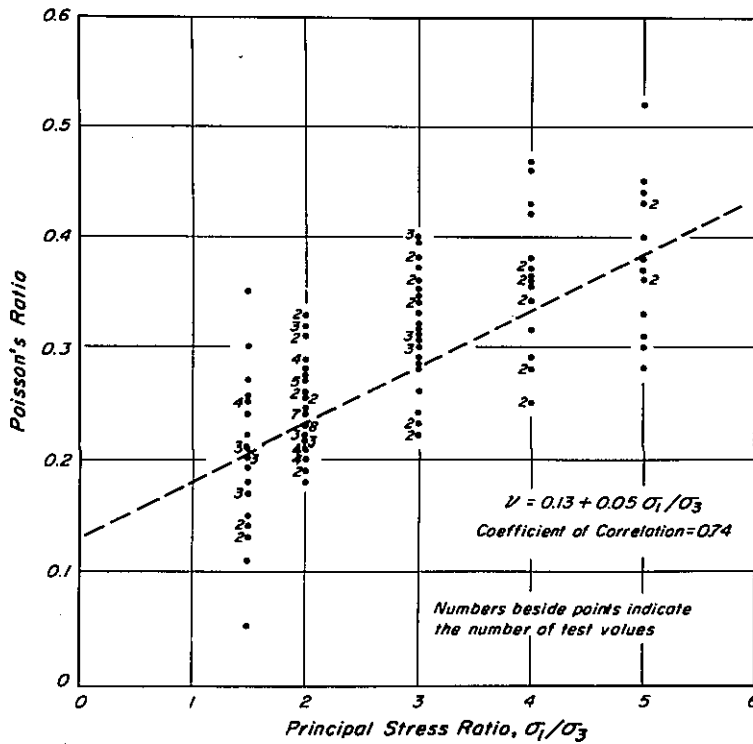


Fig. E5 – Effect of principal stress ratio on resilient Poisson's ratio.

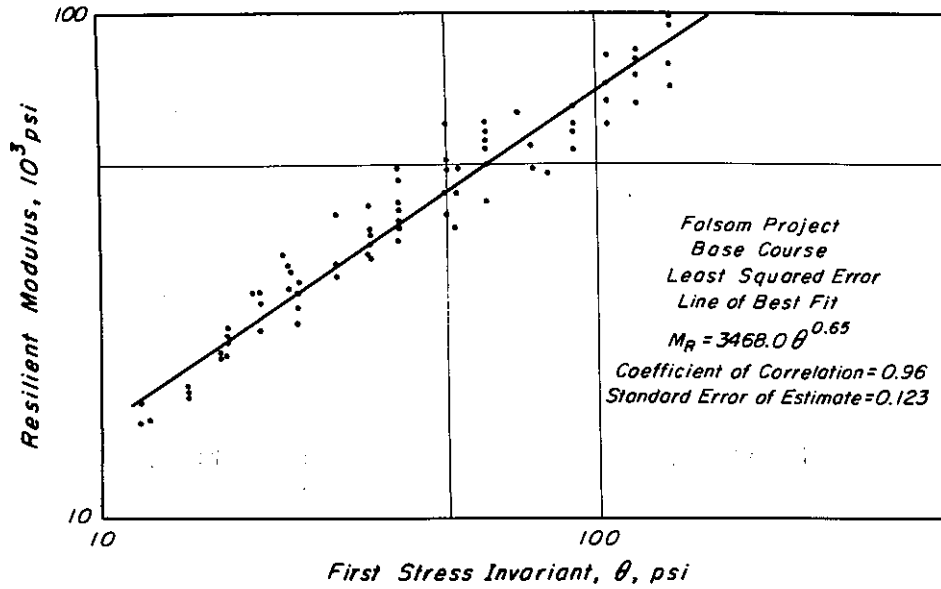


Fig. E6 – Individual test results of modulus vs. sum of principal stresses, Folsom base course aggregate.

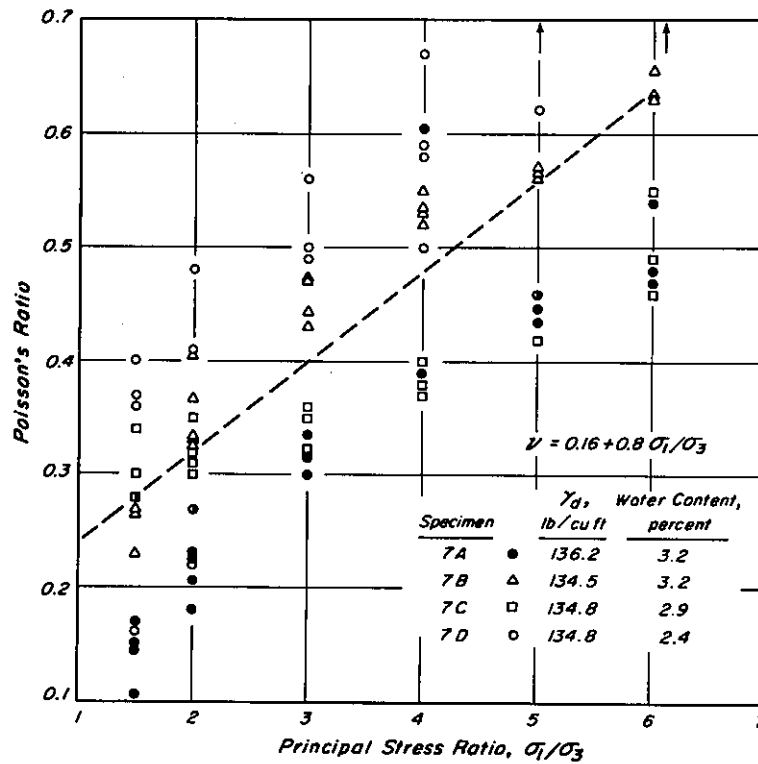


Fig. E7 – Effect of principal stress ratio on resilient Poisson's ratio, Folsom base course aggregate.

APPENDIX F

SUMMARY OF FATIGUE DATA OF OTHER INVESTIGATORS

Authors	Mix Designation	Asphalt Type	Asphalt Content	Grading and Aggregate Type	Air Voids $\times 10^3$ psi	Temperature of	Loading Rate, Applications Per Minute	Controlled Stress Strain	K_1	n_1	Corr. Coef.	Mix $\epsilon - 10^{-6}$ in./in. at N			K_2	n_2	Corr. Coef.	Mix $\sigma -$ psi at N				
												10^8	10^4	10^5				10^3	10^4	10^5	10^6	
	British 594	40-50	7.9	Granite	5.38	68	100	x	6.1×10^{-6}	3.38	.79	1,000	500	250	125	1.36×10^{11}	2.87	.45	650	300	140	65
	California	85-100	6.0	Granite Coarse	5.71	68	100	x	3.20×10^{-5}	2.49	.93	730	390	150	60	1.64×10^{11}	3.69	.92	170	90	48	26
	California	85-100	6.0	Granite Fine	5.71	68	100	x	8.9×10^{-7}	2.95	.95	860	400	180	88	1.58×10^{11}	3.51	.95	215	130	79	30
	California	85-100	6.0	Granite Medium	4.49	68	100	x	2.87×10^{-6}	2.83	.90	960	430	190	84	2.1×10^{12}	4.04	.90	200	115	65	37
	California	60-70	6.0	Granite Medium	4.80	68	100	x	1.12×10^{-7}	3.26	.95	900	440	210	105	7.29×10^{12}	4.21	.89	220	130	74	42
	California	40-50	6.0	Granite Medium	4.73	68	100	x	1.03×10^{-10}	4.01	.86	590	330	185	105	1.97×10^{15}	4.93	.83	330	200	122	76
	California	60-70	6.2	Basalt Medium	6.72	68	100	x	1.34×10^{-7}	3.22	.90	880	420	205	100	6.0×10^{10}	3.24	.87	260	125	60	29
	California	60-70	4.7	Limestone Medium	6.40	68	100	x	-	-	-	-	-	-	-	-	-	-	-	-	-	-
	California	60-70	4.6	Cravel Medium	8.18	68	100	x	-	-	-	-	-	-	-	-	-	-	-	-	-	-
	California	60-70	5.2	Granite Medium	7.06	68	100	x	-	-	-	-	-	-	-	-	-	-	-	-	-	-
Monismith and Epps	Gonzales Field Surface	85-100	5.9	Granite Gneissic	7.63	40	100	x	4.35×10^{-8}	3.37	.96	860	420	220	110	4.10×10^{18}	6.06	.86	390	260	180	120
	Gonzales Lab Surface	85-100	5.9	Shale	7.93	68	100	x	2.12×10^{-8}	3.60	.87	1,100	600	315	165	2.4×10^{13}	4.82	.90	140	87	54	33
	Gonzales Lab Surface	85-100	6.0	Shale	5.46	40	100	x	1.10×10^{-10}	4.17	.79	780	460	260	150	1.78×10^{16}	5.09	.79	400	260	165	105
	Gonzales Field Base	85-100	4.6	Shale	5.00	68	100	x	2.10×10^{-8}	-1.25	.58	1,200	720	420	250	6.68×10^{12}	4.48	.73	160	94	56	31
	Gonzales Field Base	85-100	4.7	Granite	8.66	40	100	x	1.0×10^{-12}	4.56	.79	520	310	190	115	4.64×10^{16}	5.72	.75	240	165	110	78
	Gonzales Lab Base	85-100	4.7	Granite	6.03	68	100	x	8.15×10^{-9}	3.62	.72	880	460	240	130	2.2×10^9	2.82	.75	150	70	32	15
	Gonzales Lab Base	85-100	4.7	Granite	5.34	68	100	x	6.48×10^{-3}	3.53	.96	680	350	180	96	2.26×10^3	- .33	.0426	-	-	-	-
	Morro Bay Field Surface 65	85-100	4.7	Granite	6.03	68	100	x	6.54×10^{-12}	4.69	.83	980	600	360	220	1.87×10^{13}	3.86	.64	130	72	40	22
	Morro Bay Field Surface 65	85-100	5.9	Sandstone Chert	8.12	40	100	x	7.08×10^1	0.70	.23	-	-	-	-	1.58×10^{16}	5.16	.73	350	220	145	90
	Morro Bay Field Surface 65	85-100	5.9	Sandstone Chert	8.40	68	100	x	1.60×10^{-4}	2.95	.59	1,300	480	185	70	1.47×10^{14}	5.07	.67	160	100	65	41
	Morro Bay Field Surface 67	85-100	5.9	Sandstone Chert	8.08	68	100	x	8.28×10^{-0}	3.67	.84	960	510	270	140	1.18×10^{14}	4.72	.89	-	-	-	-
	Morro Bay Lab Surface	85-100	5.9	Sandstone Chert	5.14	40	100	x	4.87×10^{-1}	1.43	.30	-	-	-	-	5.98×10^{17}	5.22	.52	-	-	-	-
	Morro Bay Lab Surface	85-100	5.9	Sandstone Chert	5.26	68	100	x	7.51×10^{-6}	2.79	.89	1,250	540	240	105	8.99×10^{15}	5.34	.83	-	-	-	-
	Morro Bay Lab Surface*	85-100	5.9	Sandstone Chert	5.57	68	100	x	2.78×10^{-7}	3.38	.87	1,500	760	390	195	8.48×10^{10}	2.89	.64	-	-	-	-

*Controlled strain - 50% reduction in stiffness.

Authors	Mix Designation	Asphalt Type	Asphalt Content	Grading Aggregate Type	Air Voids	Stiffness $\times 10^3$, psi	Temperature	Loading Rate Applications per Minute	Controlled Stress Strain	K ₁	n ₁	Corr. Coef.	Mix $\epsilon - 10^{-6}$ in./in. at N		K ₂	n ₂	Corr. Coef.	Mix $\sigma -$ psi at N			
													10^3	10^5				10^3	10^5		
	San Diego Road	Field Surface	85-100	-	4.22	273	68°F	100	x	1.5×10^{-6}	2.87	.90	860	360	3.1×10^{13}	4.86	.82	145	90	56	34
	Folsom	Field Surface	85-100	Igneous Quartzitic	8.18	362	68°F	100	x	2.21×10^{-6}	2.86	.79	950	420	3.55×10^{13}	4.51	.78	220	130	78	46
	Folsom	Field Surface	85-100	Igneous Quartzitic	7.01	500	68°F	100	x	8.52×10^{-6}	2.70	.85	1,050	440	5.32×10^{13}	4.40	.85	280	160	98	58
	Folsom	Field Surface	85-100	Igneous Quartzitic	7.62	430	68°F	100	x	3.58×10^{-6}	2.80	.84	-	-	5.58×10^{13}	4.51	.76	-	-	-	-
	Folsom	Field Base	85-100	Igneous Quartzitic	8.00	425	68°F	100	x	1.09×10^0	1.17	.37	-	-	8.00×10^7	1.85	.24	-	-	-	-
	Folsom	Lab Surface	85-100	Igneous Quartzitic	6.6	1,040	40°F	100	x	5.20×10^{-11}	4.08	.95	550	320	1.16×10^{18}	5.71	.92	440	290	185	130
	Folsom	Lab Surface	85-100	Igneous Quartzitic	7.0	151	68°F	100	x	2.91×10^{-8}	3.47	.91	910	470	3.29×10^{14}	5.72	.79	100	64	46	31
	Folsom	Lab Surface	85-100	Igneous Quartzitic	7.3	1,220	40°F	100	x	8.35×10^{-12}	4.17	.92	420	240	1.55×10^{15}	4.97	.90	440	240	175	110
	Folsom	Lab Surface	85-100	Igneous Quartzitic	7.3	226	68°F	100	x	9.57×10^{-7}	2.97	.86	900	410	3.97×10^{14}	5.36	.80	145	94	61	40
	Folsom	Lab Surface	85-100	Watsonville Granite	5.1	-	40°F	30	-	x	-	-	1,050	600	-	-	-	-	-	-	-
	Folsom	Lab Surface	85-100	Watsonville Granite	4.4	-	75°F	30	-	x	-	-	2,200	1,500	-	-	-	-	-	-	-
	Folsom	Lab Surface	85-100	Watsonville Granite	5.4	-	40°F	30	-	x	-	-	400	290	-	-	-	-	-	-	-
	Folsom	Lab Surface	85-100	Watsonville Granite	3.9	-	75°F	30	-	x	-	-	1,200	850	-	-	-	-	-	-	-
	Folsom	Lab Surface	85-100	Watsonville Granite	5.5	-	40°F	30	-	x	-	-	710	480	-	-	-	-	-	-	-
	Folsom	Lab Surface	85-100	Watsonville Granite	4.8	-	75°F	30	-	x	-	-	1,600	1,150	-	-	-	-	-	-	-
	Folsom	Lab Surface	85-100	Cheche Creek	3.6	-	40°F	30	-	x	-	-	540	390	-	-	-	-	-	-	-
	Folsom	Lab Surface	85-100	Watsonville Granite	5.1	-	40°F	30	-	x	-	-	580	400	-	-	-	-	-	-	-
	Folsom	Lab Surface	85-100	Watsonville Granite	4.3	-	40°F	30	-	x	-	-	800	550	-	-	-	-	-	-	-
	Folsom	Lab Surface	85-100	Cheche Creek	4.3	-	68°F	30	-	x	-	-	1,000	700	-	-	-	-	-	-	-
	Shell Ave. Test Road	Lab Surface	40-50	Basalt	5.2-5.4	-	40°F	30	-	x	-	-	650	450	-	-	-	-	-	-	-
	Shell Ave. Test Road	Lab Surface	85-100	Basalt	5.2-5.4	-	75°F	30	-	x	-	-	880	560	-	-	-	-	-	-	-
	Field	Surface	40-50	Basalt	-	-	32°F	30	-	x	-	-	380	270	-	-	-	-	-	-	-
	Field	Surface	85-100	Basalt	-	-	32°F	50	-	x	-	-	280	200	-	-	-	-	-	-	-

**Test Location 1 & 2 - standard asphalt specifications
 Test Location 3 & 4 - experimental asphalt specifications

Authors	Mix Designation	Asphalt Type	Asphalt Content	Grading and Aggregate Type	Air Voids	Stiffness, $\times 10^3$, psi	Temperature	Loading Rate Applications per Minute	Controlled Stress Strain	K_1	n_1	Corr. Coef.	Mix $\epsilon - 10^{-6}$ in./in. at N		Mix $\sigma -$ psi at N									
													10^3	10^4	10^5	10^6	10^3	10^4	10^5	10^6				
	- Rotating Sandsheet	40-50	9.5	Sand Lime-stone Filler	3.5	2,900	7°F	1,000	X	1.44×10^{-16}	-	-	-	-	-	910	630							
	- Rotating Sandsheet	40-50	9.5	Sand Lime-stone Filler	3.5	2,610	15°F	3,000	X	1.44×10^{-16}	-	-	-	-	-	1,800	1,200	810	570					
	- Rotating Sandsheet	40-50	9.5	Sand Lime-stone Filler	3.5	1,740	32°F	2,300	X	1.44×10^{-16}	6.0	-	-	700	480	330	230	1,500	910	600	400			
	- Rotating Sandsheet	40-50	9.5	Sand Lime-stone Filler	3.5	1,280	45°F	2,300	X	1.44×10^{-16}	-	-	-	-	-	-	-	980	670	480	300			
	- Rotating Sandsheet	40-50	9.5	Sand Lime-stone Filler	3.5	465	77°F	3,000	X	1.44×10^{-16}	-	-	-	-	-	-	-	310	220	160	110			
	- Torsional Sandsheet	40-50	9.5	Sand Lime-stone Filler	3.5	-	-4°F	1,450	-	X	7.5	-	-	650	480	350	270	-	-	-	-			
	- Torsional Sandsheet	40-50	9.5	Sand Lime-stone Filler	3.5	-	15°F	1,450	-	X	7.5	-	-	580	420	310	230	-	-	-	-			
	- Torsional Sandsheet	40-50	9.5	Sand Lime-stone Filler	3.5	-	32°F	1,450	-	X	7.5	-	-	620	460	330	240	-	-	-	-			
	- Torsional Sandsheet	40-50	9.5	Sand Lime-stone Filler	3.5	-	59°F	1,460	-	X	7.0	-	-	820	580	410	290	-	-	-	-			
	- Torsional Sandsheet	40-50	9.5	Sand Lime-stone Filler	3.5	-	86°F	1,450	-	X	4.5	-	-	2,000	1,300	820	570	-	-	-	-			
	- Torsional Sandsheet	40-50	9.5	Sand Lime-stone Filler	3.5	-	104°F	1,450	-	X	4.2	-	-	4,000	2,500	1,600	830	-	-	-	-			
	- Torsional Mastic	40-50	80 by volume	Glass	2.5	-	32°F	1,450	-	X	6.0	-	-	3,400	2,100	1,200	800	-	-	-	-			
	- Torsional Mastic	40-50	60 by volume	Glass	2.5	-	32°F	1,450	-	X	6.0	-	-	2,100	1,600	960	650	-	-	-	-			
	- Torsional Mastic	40-50	50 by volume	Sand	1.2	-	32°F	1,450	-	X	6.0	-	-	2,000	1,500	900	600	-	-	-	-			
	- Torsional Mastic	40-50	40 by volume	Glass	6.0	-	32°F	1,450	-	X	5.5	-	-	1,700	1,100	650	410	-	-	-	-			
	- Torsional Mastic	40-50	30 by volume	Sand	2.7	-	32°F	1,450	-	X	5.5	-	-	1,100	720	470	310	-	-	-	-			
	- Rotating Bitumen	40-50	100	None	-	-	10°F	2,600	X	-	5.5	-	-	2,500	1,700	1,100	700	-	6.0	-	420	230	190	120
	- Rotating Bitumen	40-50	100	None	-	-	25°F	2,600	X	-	4.8	-	-	3,000	2,000	1,400	780	-	4.8	-	370	195	110	76
	- Rotating Bitumen	40-50	100	None	-	-	39°F	1,600	X	-	5.2	-	-	6,800	3,800	2,400	140	-	4.2	-	-	-	-	-
	- Torsional Bitumen	-	100	None	-	-	50°F	1,450	-	X	4.5	-	-	8,500	4,800	2,800	1,800	-	-	-	-	-	-	-
	- Torsional Bitumen	-	100	None	-	-	43°F	1,450	-	X	4.5	-	-	7,300	4,300	2,600	1,700	-	-	-	-	-	-	-
	- Torsional Bitumen	-	100	None	-	-	39°F	1,450	-	X	4.5	-	-	5,500	3,200	1,900	1,300	-	-	-	-	-	-	-
	- Torsional Bitumen	-	100	None	-	-	32°F	1,450	-	X	4.5	-	-	4,500	2,700	1,700	970	-	-	-	-	-	-	-
	- Torsional Bitumen	-	100	None	-	-	21°F	1,450	-	X	4.5	-	-	3,500	2,100	1,400	790	-	-	-	-	-	-	-
	- Torsional Bitumen	-	100	None	-	-	14°F	1,450	-	X	4.5	-	-	3,200	1,900	1,200	680	-	-	-	-	-	-	-

Pell

Authors	Mix Designation	Asphalt Type	Asphalt Content	Grading and Aggregate Type	Air Voids	Stiffness, $\times 10^3$, psi	Temperature	Loading Rate, Applications per Minute	Controlled Stress Strain	K ₁	n ₁	Corr. Coef.	Mix $\epsilon - 10^{-6}$ in./in. at N			K ₂	n ₂	Corr. Coef.	Mix $\sigma -$ psi at N					
													10 ³	10 ⁴	10 ⁵				10 ³	10 ⁴	10 ⁵	10 ³	10 ⁴	10 ⁵
Pell	BS 594 - Surface A	40-50	8.1	Gravel	2-6	1,880	32°F	1,000	x	-	-	-	-	-	-	6.0	-	-	870	600	420	290		
	BS 594 - Surface A	40-50	8.1	Gravel	2-6	1,020	50°F	1,000	x	-	5.8	-	-	560	380	255	173	-	7.7	-	480	360	270	200
	BS 594 - Surface A	40-50	8.1	Gravel	2-6	510	68°F	1,000	x	-	-	-	-	-	-	-	-	-	5.8	-	330	220	140	95
	BS 594 - Surface B	40-50	7.2	Gravel	1-5	2,150	32°F	1,000	x	-	6.3	-	-	450	320	217	150	-	6.2	-	810	560	400	290
	BS 594 - Surface C	90-110	7.2	Gravel	3-6	1,460*	32°F	1,000	x	-	5.3	-	-	560	340	210	150	-	5.3	-	750	480	310	200
	BS 594 - Surface D	40-50	6.3	Gravel	1-5	2,450	32°F	1,000	x	-	5.6	-	-	450	300	195	130	-	5.8	-	950	620	410	280
	USA - Surface E	90-100	5.4	Gravel	2-4	1,460	50°F	1,000	x	-	5.2	-	-	310	200	130	85	-	5.7	-	480	320	220	140
	BS 594 - Base F	40-50	6.0	Gravel	5.8	950*	50°F	1,000	x	-	5.1	-	-	390	240	160	95	-	5.9	-	320	220	145	100
	BS 594 - Base G	40-50	6.0	Crushed Rock	5.5	500*	32°F	1,000	x	-	5.3	-	-	390	240	160	95	-	5.9	-	490	310	210	140
	BS 594 - Base G	40-50	6.0	Crushed Rock	4.7	1,000*	50°F	1,000	x	-	5.0	-	-	390	240	160	95	-	5.9	-	340	230	160	110
	BS 594 - Base G	40-50	6.0	Crushed Rock	5.2	420*	68°F	1,000	x	-	3.4	-	-	390	240	160	95	-	4.6	-	195	120	66	38
	BS 594 - Base G	40-50	6.0	Crushed Rock	5.2	130*	86°F	1,000	x	-	3.5	-	-	-	-	-	-	-	4.9	-	100	64	40	25
	BS 594 - Base H	90-110	6.0	Crushed Rock	4.8	700*	50°F	1,000	x	-	3.2	-	-	700	330	170	76	-	4.0	-	360	200	120	62
	USA - Base L	90-100	4.2	Crushed Rock	6.2	1,100*	50°F	1,000	x	-	3.5	-	-	310	170	80	42	-	4.0	-	300	165	95	50
	Macadam - Base R	90-110	4.7	Crushed Rock	6.8	700*	50°F	1,000	x	-	3.3	-	-	390	190	96	48	-	4.1	-	230	135	75	42
	Macadam - Base S	190-210	4.3	Crushed Rock	6.5	860*	50°F	1,000	x	-	1.6	-	-	750	180	36	8	-	1.4	-	560	140	32	8
Macadam - Base T	190-210	4.7	Crushed Rock	6.1	600*	50°F	1,000	x	-	1.7	-	-	500	130	34	9	-	1.9	-	220	70	22	8	

*Approximate average stiffness.

Authors	Mix Designation	Asphalt Type	Asphalt Content	Grading and Aggregate Type	Air Voids	Stiffness, $\times 10^3$, psi	Temperature	Loading Rate Applications Per Minute	Controlled Stress Strain	K ₁	n ₁	Corr. Coef.	Mix $\epsilon - 10^{-6}$ in./in. at N			K ₂	n ₂	Corr. Coef.	Mix $\sigma - \text{psi}$ at N				
													10 ³	10 ⁴	10 ⁵				10 ⁶	10 ³	10 ⁴	10 ⁵	10 ⁶
Vallerga, Finn, Hicks	- - Unaged	85-100	6.0	Granite	3.3	168	80°F	100	x	-	-	-	-	-	-	5.4	-	-	145	90	58	38	
Vallerga, Finn, Hicks	- - Unaged	60-70	6.0	Granite	3.4	212	80°F	100	x	-	3.4	-	-	-	-	6.0	-	-	150	96	66	44	
Vallerga, Finn, Hicks	- - Unaged	40-50	6.0	Granite	3.6	278	80°F	100	x	-	-	-	-	-	-	4.8	-	-	250	160	92	56	
Vallerga, Finn, Hicks	- - Unaged	13	6.0	Granite	3.5	697	80°F	100	x	-	-	-	-	-	-	3.8	-	-	540	290	170	86	
Vallerga, Finn, Hicks	- - Aged	85-100	6.0	Granite	4.1	104	80°F	100	x	-	-	-	-	-	-	6.5	-	-	78	55	38	27	
Vallerga, Finn, Hicks	- - Aged	60-70	6.0	Granite	3.6	106	80°F	100	x	-	3.8	-	-	-	-	6.5	-	-	86	60	42	29	
Vallerga, Finn, Hicks	- - Aged	40-50	6.0	Granite	3.8	170	80°F	100	x	-	-	-	-	-	-	8.8	-	-	110	86	66	52	
Vallerga, Finn, Hicks	- - Aged	13	6.0	Granite	3.6	562	80°F	100	x	-	-	-	-	-	-	5.2	-	-	440	280	180	110	
Santucci & Schmidt	- - A-1	114	6.0	Granite	5.5	440-800	77°F	100	-	x	-	4.2	-	-	-	-	-	-	-	-	-	-	-
Santucci & Schmidt	- - A-2	112	6.0	Granite	5.5	300-450	77°F	100	-	x	-	4.1	-	-	-	-	-	-	1,200	680	390	230	-
Santucci & Schmidt	- - B-1	49	6.0	Granite	5.5	740-1000	77°F	100	-	x	-	3.8	-	-	-	-	-	-	1,000	560	400	170	-
Santucci & Schmidt	- - B-2	50	6.0	Granite	5.5	630-1100	77°F	100	-	x	-	5.9	-	-	-	-	-	-	880	580	390	280	-
Santucci & Schmidt	- - C	83	6.0	Granite	5.5	380-700	77°F	100	-	x	-	2.6	-	-	-	-	-	-	1,600	580	230	90	-
Santucci & Schmidt	- - D	47	6.0	Granite	5.5	1000-1350	77°F	100	-	x	-	3.2	-	-	-	-	-	-	580	280	140	75	-
Santucci & Schmidt	- - E	80	6.0	Granite	5.5	640-880	77°F	100	-	x	-	4.4	-	-	-	-	-	-	870	500	250	160	-
Santucci & Schmidt	- - F	82	6.0	Granite	5.5	340-500	77°F	100	-	x	-	2.5	-	-	-	-	-	-	2,300	880	360	130	-
Santucci & Schmidt	- - G	90	6.0	Granite	5.5	200-350	77°F	100	-	x	-	4.5	-	-	-	-	-	-	800	480	280	170	-
Santucci & Schmidt	- - H	66	6.0	Granite	5.5	650	77°F	100	-	x	-	-	-	-	-	-	-	-	-	-	-	-	-
Rathby & Sterling	- - Peil's G	45	6.0	Granite Sand	1-5	-	10°C	1,000	x	-	-	5.2	-	-	-	-	-	-	250	150	100	70	-
Rathby & Sterling	- - Peil's G	45	6.0	Granite Sand	1-5	110	25°C	1,000	x	-	-	5.2	-	-	-	-	-	-	120	75	50	32	-

Authors	Mix Designation	Asphalt Type	Asphalt Content	Grading and Aggregate Type	Air Voids	Stiffness, $\times 10^6$, psi	Temperature	Loading Rate Applications Per Minute	Controlled Stress Strain	K_1	v_1	Corr. Coef.	Mix $\epsilon - 10^{-6}$ in./in. at N	K_2	$\frac{1}{2}$	Corr. Coef.	Mix $\sigma - \text{psi}$ at N
													10^3 10^4 10^5 10^6				10^3 10^4 10^5 10^6
Papacian & Baker	- Chandragu	-	-	-	-	-	-	105	X	-	-	-	-	-	-	-	155 108 58 10
Papacian & Baker	-	60-70	7.4	Limestone, Sand	-	-	75°F	-	X	-	-	-	-	-	-	-	110 78 37 42
Jineez	-	85-100	7.5	Slag and Limestone	-	80,000	75°F	660	X	X	6.3	-	300 2,100 1,600 1,000	-	-	-	300 200 150 100
Layman & Phillippi	- Base Course Mixtures	AC-10	4.6	Gravel & Limestone	6.8	100 to 400	75°F	660	X	X	5.0	-	1,000 620 400 250	-	-	-	270 140 69 35
Layman & Phillippi	- Base Course Mixtures	AC-10	4.6	Screenings	-	-	90.5°F	660	X	X	4.3	-	1,400 800 470 280	-	-	-	180 60 25 19
Layman & Phillippi	- Base Course Mixtures	AC-10	4.6	Screenings	-	45	104°F	660	X	X	3.7	-	1,900 1,000 530 290	-	-	-	95 27 8 3
Bazin & Saunier	- Sandheet	40-50	9.5	Sandheet Rounded	4.1	1,400,000	-10°C to 10°C	3,000	X	-	5.25	-	750 468 310 210	-	-	-	-
Bazin & Saunier	- Dense Mix	40-50	6	Dense Crushed	6.5	1,400,000	10°C	3,000	X	-	4.3	-	490 280 170 95	-	-	-	-
Bazin & Saunier	- Lean Mix	40-50	4	Lean Mix Rounded	5.2	-	10°C	3,000	X	-	-	-	390 220 140 75	-	-	-	-
Bazin & Saunier	- Sandheet	180-220	9.5	Sandheet Rounded	3.9	-	10°C	3,000	X	-	-	-	760 410 260 150	-	-	-	-
Bazin & Saunier	- Dense	180-220	6	Dense Crushed	7.0	-	10°C	3,000	X	-	3.8	-	490 220 120 60	-	-	-	-
Bazin & Saunier	- Sandheet compstudy	Shell Lab compstudy	-	-	-	-	10°C	3,000	-	X	5.0	-	1,200 780 470 310	-	-	-	-
Bazin & Saunier	- Asphalt Concrete	Shell Lab compstudy	-	-	-	-	10°C	3,000	-	X	4.5	-	1,100 600 350 210	-	-	-	-
Kirk	- Grading I	180-200	5.5	Granite Limestone Filler	3.0	-	-5°C to 15°C	3,000	-	X	6.8	-	400 270 190 140	-	-	-	-
Kirk	- Grading I	80-100	15.2	Granite Limestone Filler	1.6	-	-	3,000	-	X	-	-	-	-	-	-	-
Kirk	- Grading I	80-100	12.9	Granite Limestone Filler	-	-	-	3,000	-	X	-	-	-	-	-	-	-
Kirk	- Grading I	80-100	11.0	Granite Limestone Filler	5.9	-	-	3,000	-	X	-	-	-	-	-	-	-
Kirk	- Grading I	80-100	9.0	Granite Limestone Filler	8.6	-	-	3,600	-	X	-	-	-	-	-	-	-
Kirk	- Grading I	180-200	13.3	Granite Limestone Filler	4.7	-	-	3,000	-	X	-	-	-	-	-	-	-
Kirk	- Grading I	46-50	13.1	Granite Limestone Filler	2.6	-	-	3,000	-	X	-	-	-	-	-	-	-
Kirk	- Grading I	10-20	12.7	Granite Limestone Filler	4.4	-	-	3,000	-	X	-	-	-	-	-	-	-
Kirk	- Grading I	Oxytized	12.9	Granite Limestone Filler	4.3	-	-	3,000	-	X	-	-	-	-	-	-	-
Kirk	- Grading II	80-100	9.8	Granite Limestone Filler	5.6	-	-	3,000	-	X	-	-	-	-	-	-	-
Kirk	- Grading III	60-100	6.5	Natural Fine Sand	38.0	-	-	3,000	-	X	-	-	-	-	-	-	-
Kirk	- Grading III	80-100	6.4	Natural Fine Sand	17.6	-	-	3,000	-	X	-	-	-	-	-	-	-
Kirk	- Limestone Filler	80-100	28.6	-	1.9	-	-	3,000	-	X	-	-	-	-	-	-	-
Kirk	- Quartz Filler	60-100	28.1	-	3.7	-	-	3,000	-	X	-	-	-	-	-	-	-
Kirk	- Grading I	80-100	10.8	Granite Limestone Filler	6.9	-	-	800	-	X	-	-	-	-	-	-	-
Kirk	- Grading I	80-100	14.7	Granite Limestone Filler	5.4	-	-	3,000	-	X	-	-	-	-	-	-	-
Kirk	- Grading I	80-100	12.3	Granite Limestone Filler	10.5	-	-	3,000	-	X	-	-	-	-	-	-	-
Kirk	- Grading I	80-100	10.2	Granite Limestone Filler	12.1	-	-	3,000	-	X	-	-	-	-	-	-	-

APPENDIX G

REDESIGN OF YGNACIO VALLEY ROAD USING GENERAL
FATIGUE CONSIDERATIONS

In the main section of the report a general procedure has been presented for the fatigue analysis of asphalt concrete in highway pavements using specific relationships to describe the fatigue behavior of California type mixes. This procedure (or subsystem) has been used in three forms to study two in-service pavements, Morro Bay and Folsom projects, and to design a new pavement, Ygnacio Valley Road. To evaluate the applicability of the more general fatigue relationships (Fig. 95) an extensive design study of the Ygnacio Valley Road was carried out and is described in this Appendix.

Two main objectives were incorporated into the study: (1) to obtain a comparison of fatigue life predicted by the specific relationships (described previously) and fatigue life using the general fatigue relationship, (2) to obtain a relationship between thickness of asphalt concrete and truck traffic intensity for the Ygnacio Valley Road environment and to compare the depth-traffic relationship with similar relationships derived from the Asphalt Institute's design procedure (as incorporated in MS-1(62)) from the Shell procedure (63) and from the State of California Design procedure (5).

Traffic

For the first comparison, the volume of truck traffic was seasonally varied as described in the main report, that is, the initial average annual daily truck traffic was 420 vehicles in the months of April and October, reduced to 80 percent of the average for the period November through March inclusive and increased to 120 percent of the average for the months May through September inclusive. The annual rate of increase in truck traffic was assumed to be five percent. For the second comparison, truck traffic volume was assumed uniformly distributed throughout the year. Annual average traffic volumes, expressed in terms of the Asphalt Institute traffic designation DTN, were varied to establish a relationship between thickness - traffic volume to cause failure. Truck traffic composition by axle configuration was the same for both conditions as follows:

<u>No. of Axles</u>	<u>Proportion - percent</u>
2	44.0
3	25.5
4	0.5
5	30.0

The daily distribution of truck traffic and wheel load factors used were as shown in Tables 37 and 38 respectively.

Climate

The climatic data used for the study were as previously presented in Table 43.

Materials

For both comparisons, a constant subgrade modulus of 5,000 psi was utilized and Poisson's ratio was assumed to be 0.5.

Stiffness moduli of the asphalt concrete as a function of temperature (at a time of loading of 0.015 sec) were determined using the Shell procedures and the following mixture data:

Recovered penetration of asphalt cement at 25°C	36 dmm
Ring and ball softening point	58°C
Unit weight, lb per cu ft	152
Air void content, percent	5
Volume concentration of aggregate, C_v	0.86

The resulting temperature vs. stiffness modulus relationship is shown in Fig. G1.

Thermal characteristics used in the pavement temperature calculations were:

Thermal conductivity, Btu per sq ft per hr, °F, ft	0.70
Specific heat, Btu per lb, °F	0.22
Surface coefficient, Btu per sq ft per hr, °F	0.85

Fatigue Characteristics of Asphalt Concrete. Fatigue curves for the mixture were determined from Fig. 95 for a range in stiffnesses. Moreover, based on data presented in the body of this report, it was assumed that strains less than 70×10^{-6} in. per in. would cause no fatigue damage. The resulting curves are shown in Fig. G2.

Structural Analysis. The structural section was represented as a two-layer system consisting of asphalt concrete on the subgrade. The CHEV5L program was used to analyze 140 different conditions, which included:

1. Four thicknesses of asphalt concrete: 8, 12, 16, 20 in.
2. Seven stiffness moduli for the asphalt concrete:
 5×10^4 , 1×10^5 , 3×10^5 , 6×10^5 , 9×10^5 , 1.5×10^6 , 3×10^6 psi
3. Five wheel loads: 1500, 2500, 3500, 4500, 5500 lbs.
 (At a tire pressure of 75 psi.)

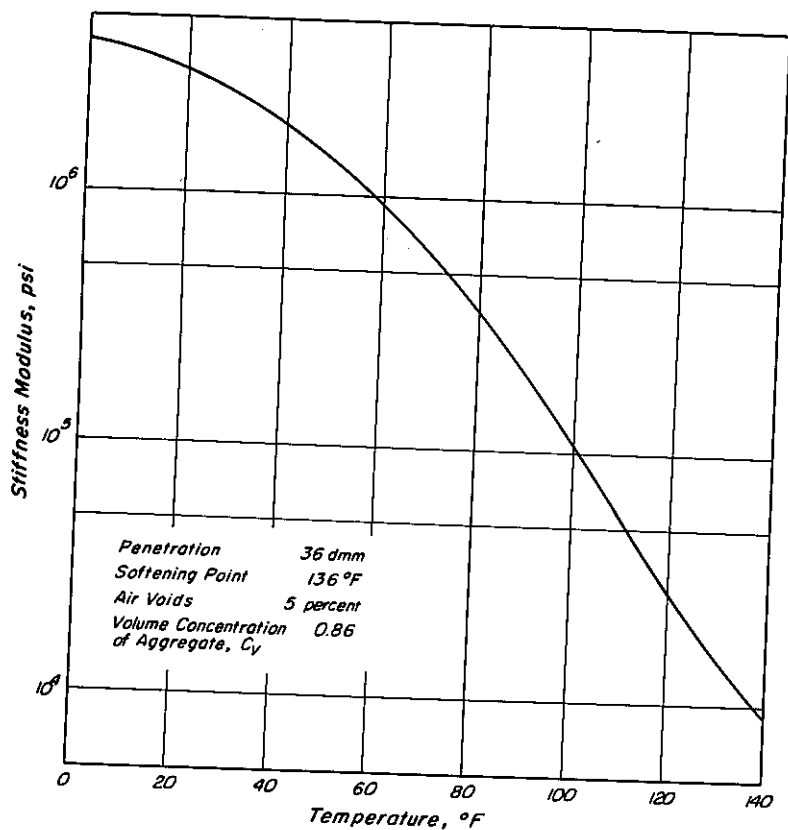


Fig. G1 - Stiffness vs. temperature relationship; asphalt concrete mixture Ygnacio Valley Road, California (time of loading - 0.0155).

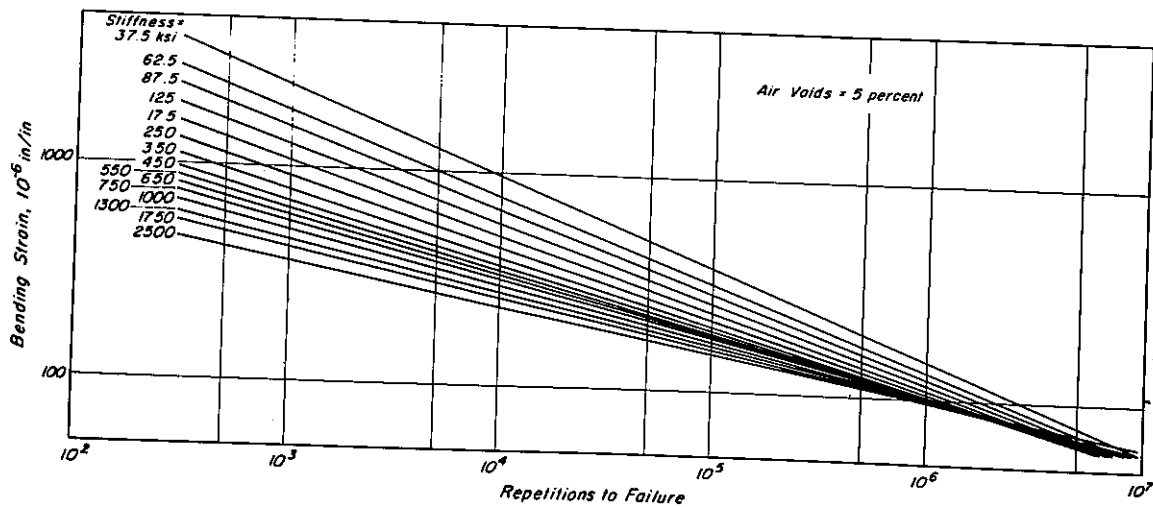


Fig. G2 - Strain vs. repetitions to failure for the general fatigue relationship.

Results of the computations are shown in Figs. G3 through G7 for the various axle loadings considered. This data was subsequently replotted in a more useful form as shown in Fig. G8.

Using the procedure described for the Folsom pavement (no consideration is given to mode factors) the frequency of the occurrence of stiffness moduli of the asphalt concrete were determined for the various thicknesses of asphalt concrete and the uniform traffic condition. Only the 12 inch thickness of asphalt concrete was considered with the seasonally varied traffic. The form of these frequency tabulations is shown in Table G1 for the 12 inch thickness and uniform traffic. Frequency data such as that shown in Table G1 can be weighted according to the truck traffic distribution of Table 37 and the results plotted as in Fig. G9. While this form is not used directly in the computations, it provides a visual indication of traffic related to stiffness conditions. For purposes of further comparison, Fig. G9 also shows data for two extremes of climate, Phoenix, Arizona and International Falls Minnesota and truck traffic distributions from Table 37.

Using graphs of the form of Figs. G2 and G7, tabulations such as Table G2 were prepared to show the relationship among stiffness, axle group, strain and fatigue life. These could then be incorporated into the fatigue life determination.

Fatigue Life Determination

Table G3 shows the distribution of axle loads for the seasonally varied traffic. Table G4 shows the seasonal damage and accumulated damage for the seasonally varied traffic and the 12 inch depth of asphalt concrete. As indicated in Table G4, the fatigue life is 19+ years compared to approximately 12 years for the procedure described in the main part of the report.

A comparison of thicknesses obtained from the fatigue subsystem with thicknesses from the Asphalt Institute, Shell and California Design procedures, for reasonably similar conditions, is shown in Fig. G10. It will be noted that for these conditions, the thicknesses determined using the fatigue subsystem are slightly larger than those by the Asphalt Institute procedures but substantially less (particularly at larger truck traffic intensities) than the California procedure.

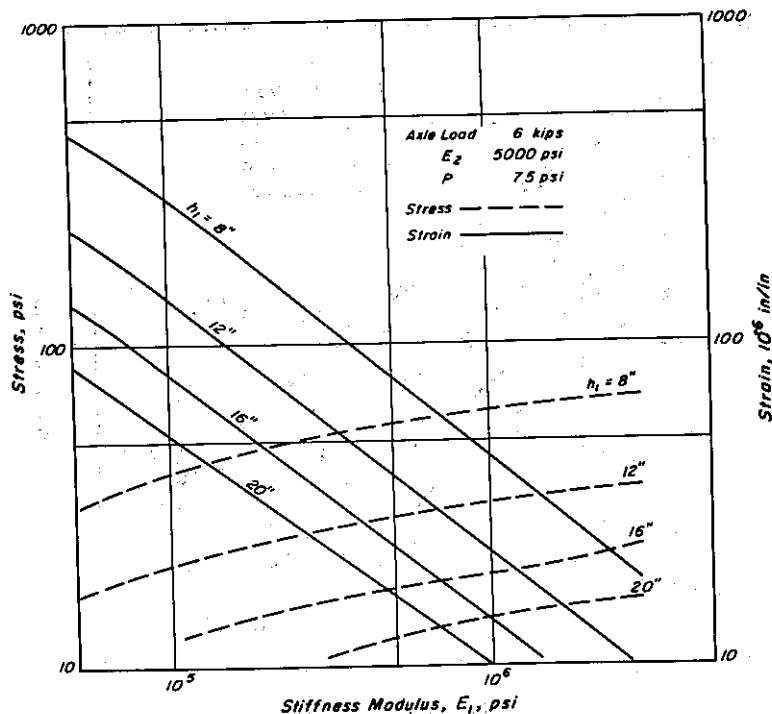


Fig. G3 – Computed stresses and strains for a range of thicknesses and stiffnesses of asphalt concrete for a 6,000 lb axle load.

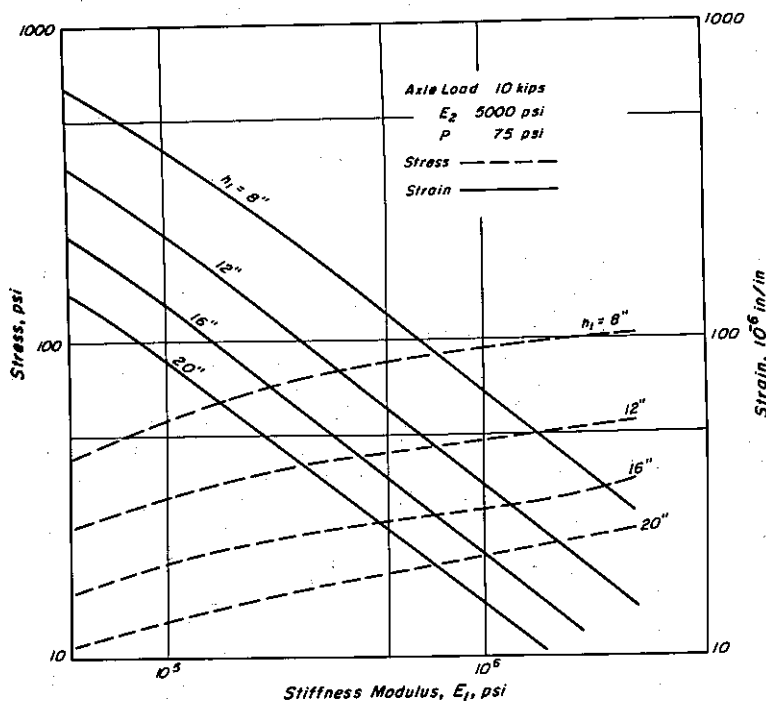


Fig. G4 – Computed stresses and strains for a range of thicknesses and stiffnesses of asphalt concrete for a 10,000 lb axle load.

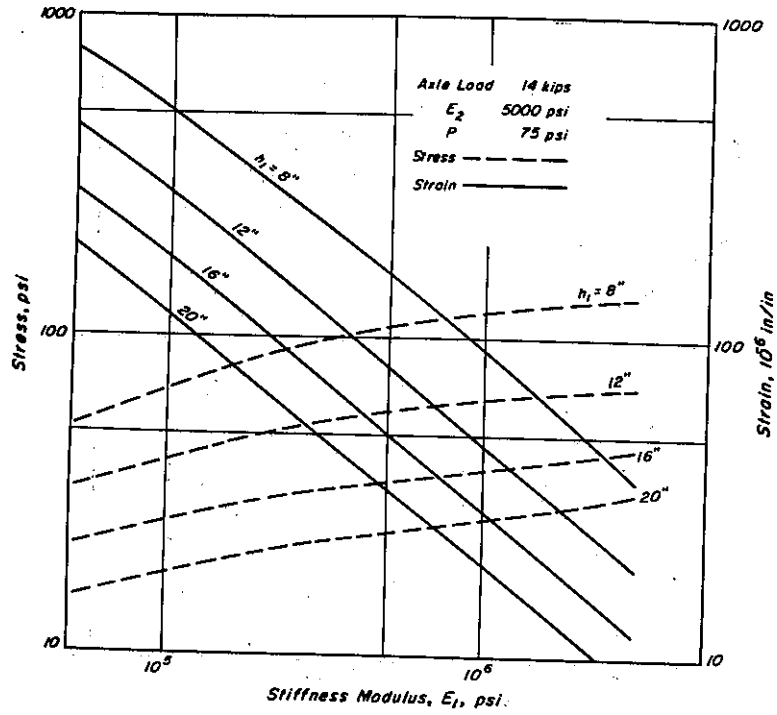


Fig. G5 - Computed stresses and strains for a range of thicknesses and stiffnesses of asphalt concrete for a 14,000 lb axle load.

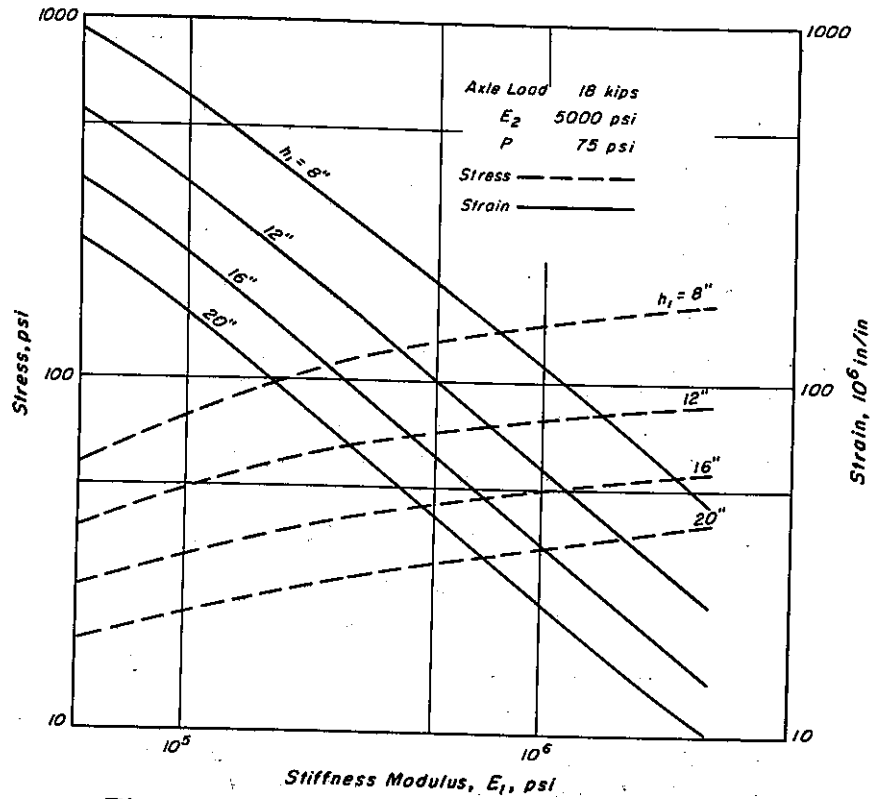


Fig. G6 - Computed stresses and strains for a range of thicknesses and stiffnesses of asphalt concrete for a 18,000 lb axle load.

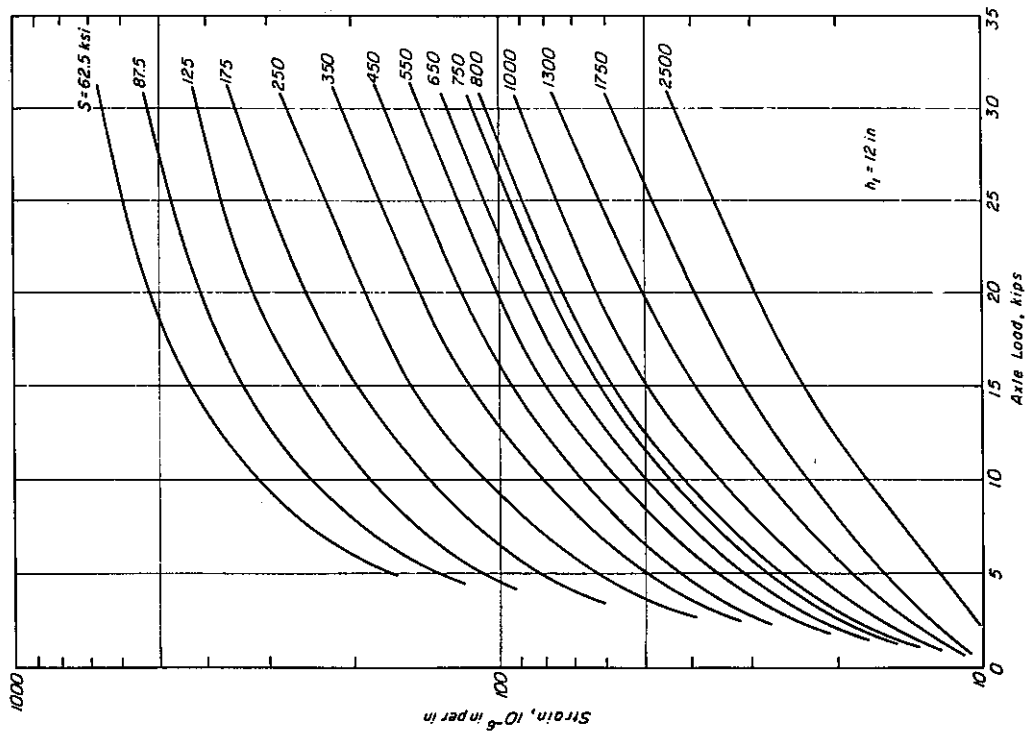


Fig. G8 - Computed strains vs. axle loads for 12 in. thick layer of asphalt concrete for a range in layer stiffnesses.

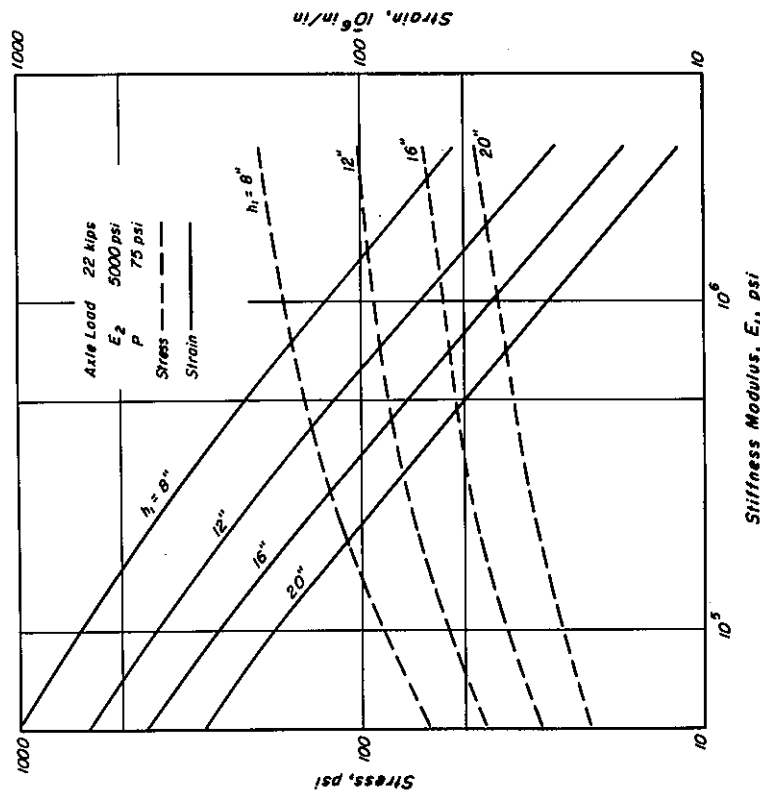


Fig. G7 - Computed stresses and strains for a range of thicknesses and stiffnesses of asphalt concrete for a 22,000 lb axle load.

TABLE G1 - FREQUENCY OF OCCURRENCE OF PAVEMENT STIFFNESS IN RANGE AND HOURLY INTERVAL DURING ONE YEAR: YGNACIO VALLEY ROAD
12 IN. LAYER OF ASPHALT CONCRETE

Time Interval	Stiffness Group - $\text{psi} \times 10^3$								
	200-300	300-400	400-500	500-600	600-700	700-900	900-1100	1100-1500	1500-2000
12 - 1 a. m.	0	2	2	0	2	1	2	1	2
1 - 2	0	2	2	0	2	1	1	2	2
2 - 3	0	2	1	1	1	2	1	2	2
3 - 4	0	1	1	2	0	3	0	3	2
4 - 5	0	1	1	2	0	3	0	3	2
5 - 6	0	1	1	2	0	3	0	3	2
6 - 7	0	1	1	2	0	3	0	3	2
7 - 8	0	1	1	2	0	3	0	3	2
8 - 9	0	2	0	2	0	3	0	3	2
9 - 10	0	2	1	1	1	2	1	2	2
10 - 11	0	2	2	0	2	1	1	2	2
11 - 12	0	2	2	0	2	1	2	1	2
12 - 1 p. m.	1	2	2	1	1	0	2	2	1
1 - 2	2	2	0	2	1	0	2	2	1
2 - 3	2	2	0	2	1	0	2	2	1
3 - 4	2	2	0	2	1	0	2	2	1
4 - 5	2	2	1	1	1	0	2	3	0
5 - 6	2	2	1	2	0	0	2	3	0
6 - 7	3	1	1	2	0	0	2	3	0
7 - 8	2	1	1	1	1	0	2	3	0
8 - 9	2	2	1	1	1	0	2	2	1
9 - 10	2	2	0	2	1	0	2	2	1
10 - 11	2	2	0	2	1	0	2	2	1
11 - 12	1	1	2	0	2	1	2	2	1

TABLE G2 — RELATIONSHIP AMONG STIFFNESS, AXLE LOAD, STRAIN
AND FATIGUE LIFE: YGNACIO VALLEY ROAD, 12 IN. THICK ASPHALT LAYER
 $E_{\text{subgrade}} = 5000 \text{ psi}$

Axle Load Group kips	Strain in. per in. $\times 10^{-6}$ Cycles to Failure	Stiffness Group - $\text{psi} \times 10^3$								
		200-300-	300-400	400-500	500-600	600-700	700-900	900-1100	1100-1500	1500-2000
< 3	ϵ	40*	36	31	27	24	20	17	15	14
	N_f	∞	∞	∞	∞	∞	∞	∞	∞	∞
3-7	ϵ	63	50	43	35	31	26	22	18	16
	N_f	∞	∞	∞	∞	∞	∞	∞	∞	∞
7-8*	ϵ	85	65	55	46	40	34	28	23	19
	N_f	2.1×10^6	∞	∞	∞	∞	∞	∞	∞	∞
8-12	ϵ	107	82	67	60	57	42	35	28	23
	N_f	1.0×10^6	2.2×10^6	∞	∞	∞	∞	∞	∞	∞
12-16	ϵ	145	108	88	76	65	56	46	36	29
	N_f	3.7×10^5	9.0×10^5	1.7×10^6	2.9×10^6	∞	∞	∞	∞	∞
16-18	ϵ	165	128	105	89	77	65	57	45	35
	N_f	2.5×10^5	5.0×10^5	8.6×10^5	1.65×10^6	3.1×10^6	∞	∞	∞	∞
18-20	ϵ	180	140	115	97	85	72	60	48	38
	N_f	1.9×10^5	3.5×10^5	6.2×10^5	1.2×10^6	2.0×10^6	4.2×10^6	∞	∞	∞
20-22	ϵ	195	150	125	105	93	77	65	53	41
	N_f	1.4×10^5	2.8×10^5	4.7×10^5	4.6×10^5	1.5×10^6	3.3×10^6	∞	∞	∞
22-24	ϵ	210	163	135	113	100	83	72	57	45
	N_f	1.1×10^5	2.1×10^5	3.5×10^5	6.4×10^5	1.1×10^6	4.0×10^6	∞	∞	∞
24-26	ϵ	228	175	145	122	108	90	76	62	48
	N_f	8.8×10^4	1.7×10^5	2.8×10^5	4.8×10^5	8.0×10^5	1.7×10^6	3.0×10^6	∞	∞
26-30	ϵ	255	195	160	135	120	99	85	71	69
	N	6.0×10^4	1.1×10^5	2.0×10^5	3.3×10^5	5.4×10^5	1.15×10^6	1.65×10^6	4.4×10^6	∞

*At strains less than 70×10^{-6} in. per in. fatigue life considered infinite.

TABLE G3 - ESTIMATED AXLE LOAD DISTRIBUTIONS -
YGNACIO VALLEY ROAD

Axle Load Group	Number per Month		
	Nov. - March ^a	May - Sept. ^b	April - Oct. ^c
< 3	338.5	544.0	423.1
3-7	3026.7	4864.4	3783.4
7-8	773.9	1243.8	967.4
8-12	1692.0	2719.3	2115.0
12-16	1256.1	2018.7	1570.1
16-18	777.6	1249.7	972.0
18-20	123.1	197.8	153.8
20-22	4.7	7.6	5.9
22-24	1.8	2.8	2.2
24-26	0.3	0.5	0.4
26-30	0.6	0.7	0.7

a. Based on initial ADTT = 336

b. Based on initial ADTT = 540

c. Based on initial ADTT = 420

TABLE G4 - FATIGUE ANALYSIS - YGNACIO VALLEY, CALIFORNIA

Year	Annual Damage				Accumulated Damage
	May - Sept.	April - Oct.	Nov. - March	Total	
1	0.03142	0.00097	Negligible	0.03239	0.03239
2	0.03299	0.00102	"	0.03301	0.06540
3	0.03464	0.00107	"	0.03571	0.10111
4	0.03637	0.00112	"	0.03749	0.14860
5	0.03819	0.00118	"	0.03937	0.18797
6	0.04010	0.00124	"	0.04134	0.22931
7	0.04211	0.00130	"	0.04341	0.27272
8	0.04421	0.00136	"	0.04557	0.31829
9	0.04642	0.00143	"	0.04785	0.36614
10	0.04874	0.00150	"	0.05024	0.41638
11	0.05118	0.00158	"	0.05276	0.46914
12	0.05374	0.00166	"	0.05540	0.52454
13	0.05643	0.00174	"	0.05817	0.58271
14	0.05925	0.00183	"	0.06108	0.64389
15	0.06221	0.00192	"	0.06413	0.70792
16	0.06533	0.00202	"	0.06735	0.77527
17	0.06859	0.00212	"	0.07071	0.84598
18	0.07202	0.00222	"	0.07424	0.92022
19	0.07563	0.00233	"	0.07796	0.99818
20	0.07941	0.00245	"	0.08186	1.08004

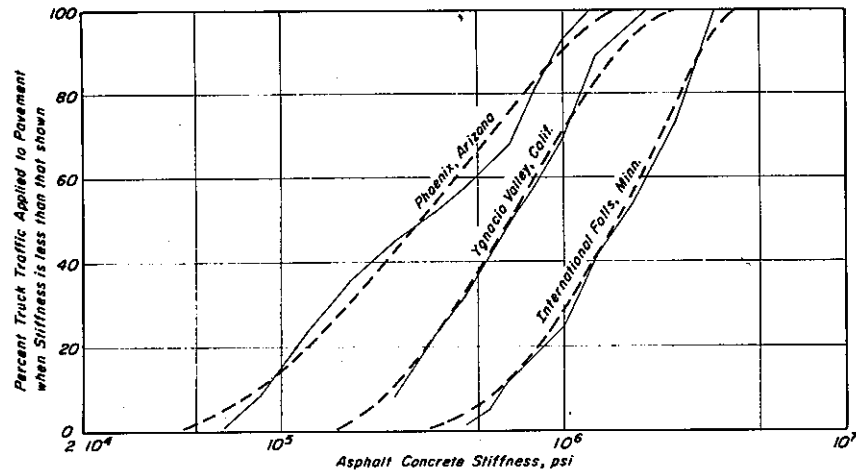


Fig. G9 – Stiffness variations with traffic applications – 12-in. thick asphalt concrete layer.

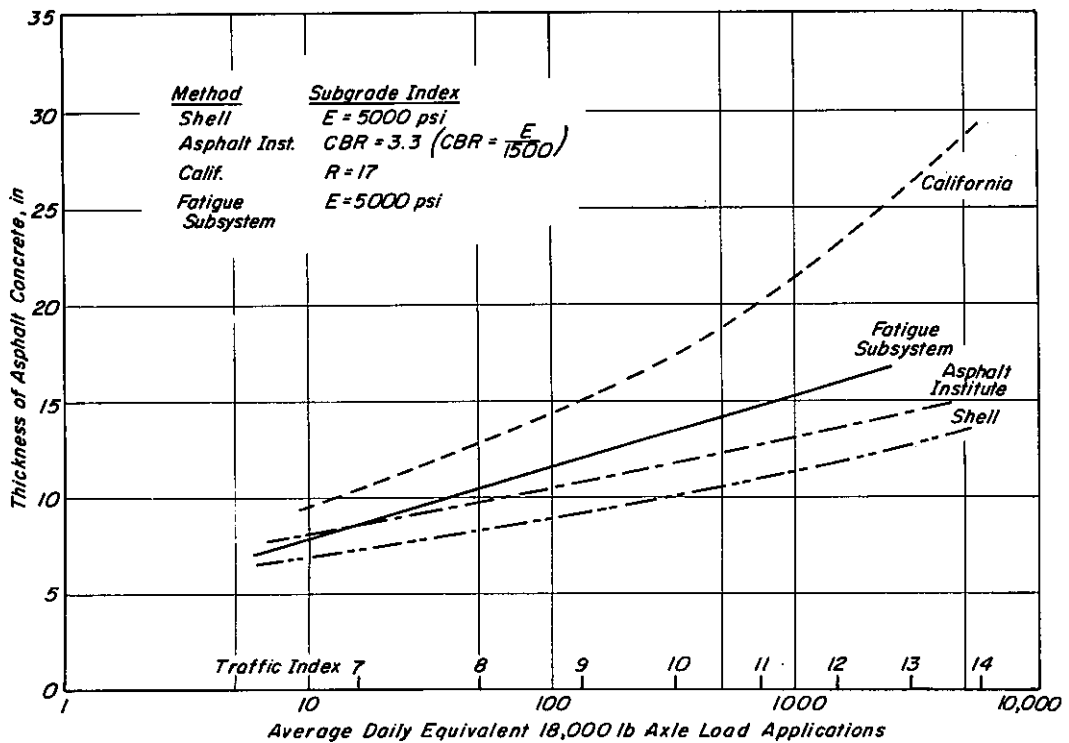


Fig. G10 – Comparison of thickness of asphalt concrete using one form of the fatigue subsystem with thicknesses determined by existing procedures.

APPENDIX H
COMPARISON OF TENSILE TEST RESULTS
WITH HEUKELOM'S RESEARCH

Heukelom (65) has presented a method whereby the stiffness of an asphalt can be used to describe its fracture properties and the fracture response of mixtures containing the asphalt.

A nomograph similar to that used to obtain stiffness values has been developed from which the elongation at fracture, of an asphalt cement may be determined using the penetration and softening point of the material. The strain at fracture may, in turn, be obtained by the use of the following expression:

$$\epsilon_{asp} = \ln(1 + \lambda) \dots \dots \dots (H1)$$

where:

$$\begin{aligned} \epsilon_{asp} &= \text{asphalt strain at fracture} \\ \lambda &= \text{elongation at fracture} \end{aligned}$$

Heukelom has also shown that the tensile strength of the asphalt is related to its stiffness, Fig. H1. Since the tensile strength of the asphalt is related to stiffness, the effect of temperature and loading time on the fracture properties of asphalts of various grades and origins is thus condensed into a single parameter, namely, stiffness.

Heukelom also suggests that the tensile strength of an asphalt mixture is a function of stiffness of the asphalt cement contained therein. Test results illustrating this point are shown in Fig. H2. The curve marked Type I is, according to Heukelom (65), an example of mixes with "poor grading and/or compaction" whereas Type II represents mixes with "better grading and/or compaction."

Superimposed on Fig. H2 are results of tensile tests obtained in this investigation (Table H2). In general, the results of this study which include mixtures containing various gradings, aggregates, asphalt type and content, and air voids correspond to the values reported by Heukelom as Type I mixes.

Heukelom further suggests that the stress and strain in the bitumen of a mix are proportional to the stress and strain applied to a given mix, i. e. :

$$\sigma_{mix} = M\sigma_{asp} \dots \dots \dots (H2)$$

where:

$$\begin{aligned} \sigma_{mix} &= \text{mixture stress at fracture, psi} \\ \sigma_{asp} &= \text{asphalt stress at fracture, psi} \\ M &= \text{mix factor} \end{aligned}$$

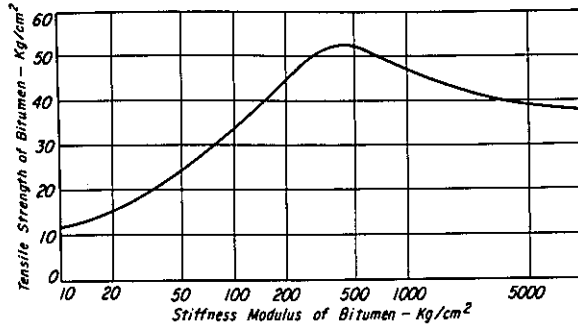


Fig. H1 - Tensile strength of asphalt vs. asphalt stiffness (after Heukelom).

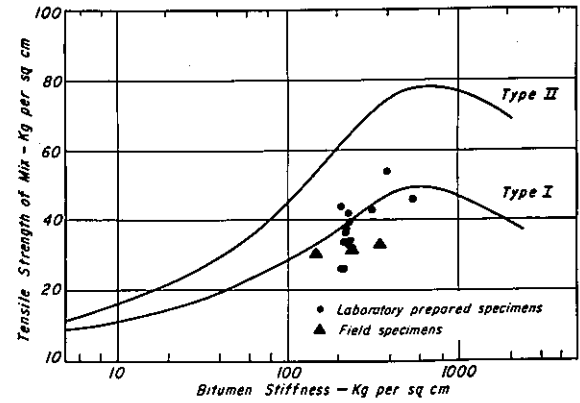


Fig. H2 - Tensile strength of asphalt mixtures vs. asphalt stiffness.

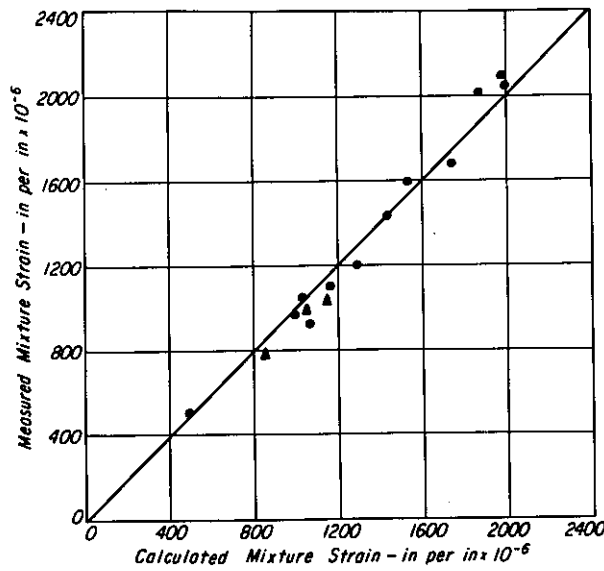


Fig. H3 - Relationship between calculated and measured mixture strains at fracture.

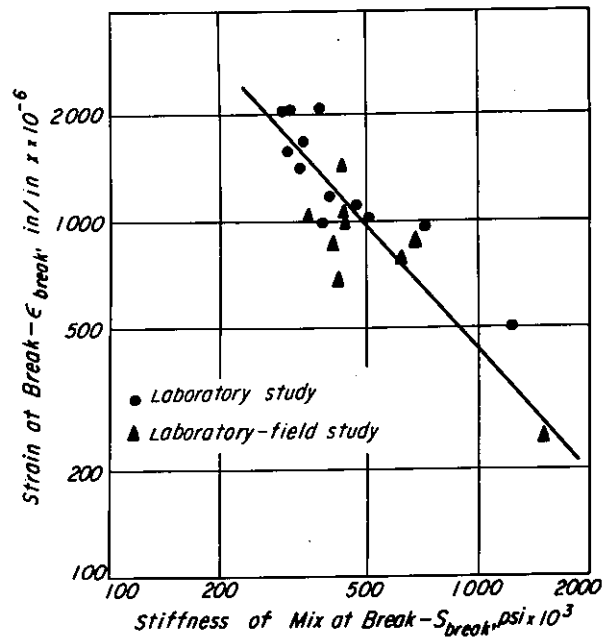


Fig. H4 - Relationship between strain at fracture and mixture stiffness.

TABLE H1 - DIRECT TENSION TEST RESULTS

Mix Designation	Asphalt Penetration	No. of Tests	Stress at Fracture psi	Strain at Fracture $\times 10^{-6}$ in./in.	Stiffness at Fracture $\times 10^3$ psi	Time to Fracture Range, sec.
California Coarse Granite Aggr.	85-100	5	479	1,593	301	.084 - .104
California Fine Granite Aggr.	85-100	7	775	2,100	369	.077 - .107
California Medium Granite Aggr.	85-100	7	596	2,027	294	.069 - .111
California Medium Granite Aggr.	60-70	8	626	2,054	305	.090 - .121
California Medium Granite Aggr.	40-50	7	611	505	1,210	.072 - .145
California Medium Basalt Aggr. 5.7% Asphalt	60-70	7	470	1,196	394	.083 - .138
California Medium Basalt Aggr. 6.7% Asphalt	60-70	6	513	1,112	461	.094 - .148
California Medium Basalt Aggr. 8.7% Asphalt	60-70	7	560	1,682	333	.099 - .128
California Medium Granite Aggr. 5.2% Asphalt	85-100	5	368	971	379	.110 - .136

TABLE F2 - PROPERTIES OF MIXES AND RECOVERED ASPHALTS

Mix Designation	Asphalt Grade	Properties of Recovered Asphalt				Mix Properties	
		Pen. @ 77°F dmm	R & B O _F	PI	Stiffness at t _m kg per cm ²	Tensile Strength at t _m kg per cm ²	Mean Fracture Time, t _m , sec.
Brit. Stand. 495 Granite Aggr.	40-50	21	60.0	-0.8	535	46	0.095
Calif. Coarse Granite Aggr.	85-100	36	51.7	-1.5	225	34	0.094
Calif. Fine Granite Aggr.	85-100	30	53.9	-1.4	347	54	0.092
Calif. Medium Granite Aggr.	85-100	37	52.8	-1.2	224	42	0.090
Calif. Medium Granite Aggr.	60-70	35	53.9	-1.0	204	44	0.105
Calif. Medium Granite Aggr.	40-50	26	55.6	-1.2	306	43	0.110
Calif. Medium Basalt Aggr. 5.7% Asphalt	60-70	32	58.0	-0.4	224	33	0.110
Calif. Medium Basalt Aggr. 6.7% Asphalt	60-70	32	58.0	-0.4	214	36	0.120
Calif. Medium Basalt Aggr. 8.7% Asphalt	60-70	32	58.0	-0.4	224	39	0.110
Calif. Medium Gran. Aggr. 5.2% Asphalt	85-100	34	52.8	-1.2	204	26	0.123
Calif. Medium Limestone	85-100	34	52.8	-1.2	225	33	0.110
Calif. Medium Crushed Gravel	85-100	34	52.8	-1.2	220	37	0.114

and the value of the mix factor, M , will depend upon the amount of asphalt cement, the grading of the aggregate, and the degree of compaction of the mix. Moreover M should be independent of time of loading, temperature, and type of asphalt since the stiffness of the asphalt is common to both the determination of the strength of asphalt and the strength of the mixture. Test results obtained in this study tend to reinforce some of the conclusions advanced by Heukelom.

Table H3 presents the values of the mix factor as determined from tests reported herein. Recovered properties of the asphalts were used to obtain the stiffness moduli of the asphalt cements. Stiffness was, in turn, used to estimate the strength of the asphalt. Mixture strength was obtained from tests the results of which are summarized in Table H1. The mix factor was then determined by dividing the strength of the mixture by the strength of the asphalt.

Effects of temperature and time of loading on the mix factor could not be investigated since both were maintained constant. The mixtures used to investigate the effect of asphalt type resulted in mix factors ranging from 0.86 to 0.98. While some difference is noted it is possible, as Heukelom suggests, that the effect of asphalt type on mix factor can be accounted for by the stiffness of the asphalt. Moreover, it would also appear that if the aggregate type and gradation, asphalt content, and air voids are fixed, the mix factor will have the same value regardless of the asphalt type used. Thus a single test series containing one asphalt for the above mixture conditions will permit determination of a mix factor for all types of asphalt to be used with that mixture. Other data (57) indicate a slight increase in mix factor with increase in asphalt content and that the mix factor may be affected by aggregate type.

Elongation at fracture of the asphalt for each of the mixes has been determined from the nomograph developed by Heukelom (65). Strain at fracture was then computed from equation (H1). The elongation and strain at fracture for the asphalt together with the strain in the mixture as measured during the test is reported in Table H4.

A value of the strain at fracture in the mixture may be calculated by substituting the relationship

$$\sigma_{\text{mix}} = S_{\text{mix}} \cdot \epsilon_{\text{mix}} \dots \dots \dots (H3)$$

where:

- S_{mix} = stiffness of mix, psi
- ϵ_{mix} = mixture strain at fracture

into equation (H2). The resulting equation

TABLE H3 — HEUKELOM'S MIX FACTOR AS DETERMINED FROM
DIRECT TENSION TEST RESULTS

Mixture Identification			Stiffness of Asphalt Kg per cm ² (1)	Strength of Asphalt psi (2)	Strength of Mixture psi (3)	Mix Factor M (4)
Designation	Asphalt Penetration, dmm	Asphalt Percent				
Granite British 594	40-50	7.9	535	745	654	0.878
Granite Coarse	85-100	6.0	225	660	479	0.725
Granite Fine	85-100	6.0	347	731	775	0.945
Granite Medium	85-100	6.0	224	660	596	0.905
Granite Medium	60-70	6.0	204	640	626	0.980
Granite Medium	40-50	6.0	306	710	611	0.862
Basalt	60-70	5.7	224	660	470	0.712
Basalt	60-70	6.7	214	650	513	0.790
Basalt	60-70	8.7	224	660	560	0.848
Granite	85-100	5.2	205	640	368	0.575
Limestone	85-100	4.7	225	660	465	0.705
Crushed Gravel	85-100	4.6	220	655	523	0.798
Morro Bay Field	85-100	5.9	145	549	433	0.790
Folsom - Shell Field	85-100	4.9	235	668	441	0.662
Folsom - Chevron Field	85-100	4.7	345	730	469	0.642

(1) Obtained from stiffness nomograph.

(2) Obtained from Fig. H1.

(3) Obtained from direct tension test.

$$(4) M = \frac{\sigma_{\text{mix}}}{\sigma_{\text{asp}}}$$

TABLE H4 - MEASURED AND CALCULATED VALUES OF BITUMEN AND MIXTURE-STRAINS AT FRACTURE

Designation	Mixture Identification		Bitumen Elongation at Fracture (1)	Bitumen Strain at Fracture in./in. (2)	Measured Mixture Strain at Fracture $\times 10^{-6}$ in./in. (3)	Calculated Mixture Strain at Fracture $\times 10^{-6}$ in./in. (4)
	Asphalt Penetration dmm	Asphalt Percent				
Granite British 594	40-50	7.9	0.12	0.113	916	1,060
Granite Coarse	85-100	6.0	0.22	0.199	1,593	1,530
Granite Fine	85-100	6.0	0.17	0.157	2,100	1,980
Granite Medium	85-100	6.0	0.21	0.190	2,027	1,870
Granite Medium	60-70	6.0	0.24	0.215	2,054	2,000
Granite Medium	40-50	6.0	0.17	0.157	505	490
Basalt	60-70	5.7	0.24	0.215	1,194	1,230
Basalt	60-70	6.7	0.25	0.223	1,112	1,160
Basalt	60-70	8.7	0.24	0.215	1,682	1,740
Granite	85-100	5.2	0.24	0.215	971	995
Limestone	85-100	4.7	0.23	0.207	1,427	1,430
Crushed Gravel	85-100	4.6	0.23	0.207	1,044	1,033
Morro Bay Field	85-100	5.9	0.32	0.278	986	1,050
Folsom - Shell Field	85-100	4.9	0.25	0.223	1,031	1,150
Folsom - Chevron Field	85-100	4.9	0.18	0.166	774	860

(1) Determined from elongation nomograph (after Heukelom).

(2) Obtained from Equation H1.

(3) Obtained from direct tension test.

(4) Obtained from Equation H7.

$$S_{\text{mix}} \cdot \epsilon_{\text{mix}} = M\sigma_{\text{asp}} \dots \dots \dots \text{(H4)}$$

may be arranged as follows:

$$\epsilon_{\text{mix}} = M \left(\frac{\sigma_{\text{asp}}}{S_{\text{mix}}} \right) \dots \dots \dots \text{(H5)}$$

$$\sigma_{\text{bit}} = S_{\text{asp}} \cdot \epsilon_{\text{asp}} \dots \dots \dots \text{(H6)}$$

where:

$$S_{\text{asp}} = \text{stiffness of asphalt, psi.}$$

The following expression may also be used:

$$\epsilon_{\text{mix}} = M \left(\frac{S_{\text{asp}}}{S_{\text{mix}}} \right) \epsilon_{\text{asp}} \text{(H7)}$$

Values of S_{asp} and ϵ_{asp} may be determined from the nomographs previously referred to. Mixture stiffness, S_{mix} , may be estimated using the Heukelom and Klomp procedure (35) or determined from measured values during the test while σ_{asp} as used in equation (H5) may be obtained from Fig. H1.

As shown previously (Fig. H2) the tensile strength of the mixes tested in this study are generally in the same range as those reported by Heukelom for his Type I mixes. Accordingly if one assumes that all of the mixes investigated herein are representative of Type I mixes, it is possible to estimate the tensile strength of a mix without measuring its actual value simply by determining the stiffness of the asphalt.

With the asphalt stiffness, a mix factor may then be calculated since the tensile strength of the asphalt may be obtained from Fig. H1. It is now possible with the use of equation (H7) to predict the tensile strain in a mixture at break from values which are determined from nomographs or figures presented by Heukelom. Utilizing this equation tensile strains at fracture have been estimated for the mixes tested in this investigation. Fig. H3 illustrates a comparison between the estimated and measured values with reasonable agreement indicated.

The relationships of mixture strength vs. mixture stiffness and strain at fracture vs. mixture stiffness were also investigated. While no discernible relationship exists between the mixture stiffness at fracture and the tensile strength of the mix, Fig. H4 indicates that the value of the strain at fracture decreases as the stiffness increases for the mixtures investigated.

APPENDIX I
COMPLIANCE CALIBRATIONS

Deflection Compliance

Fig. I1 illustrates the variation of the load-deflection curves with notch depths as obtained for mix M27 at 10⁰F. The deflection compliance, D, is obtained for each specimen utilizing the inverse slopes of these curves:

$$D = \frac{y \cdot b}{P}$$

where:

y = beam center deflection

P = applied load corresponding to y

b = width of beam = 1.5 in.

A normalized relationship (with respect to the value at zero notch depth) is shown in Fig. I2.

Crack Compliance

Crack opening displacement (C. O. D.) is directly related to notch depth and in turn is related to the fracture characteristics of a material (i. e., K_I).

The value of C. O. D. can be shown to be related to the state of stress by*:

$$v = \frac{8e_y a}{\pi} \ln \sec\left(\frac{\pi\sigma}{2\sigma_y}\right)$$

where:

v = C. O. D.

σ_y = yield stress

e_y = elastic yield strain σ_y/E

σ = uniform stress applied at a large distance from the crack

a = half crack length

Using a series expansion for the $\ln \sec$ expression and using only the first term:

$$v = \frac{\pi \sigma^2 a}{E \sigma_y}$$

*Burdekin, F. M., and D. E. W. Stone, "The Crack Opening Displacement Approach to Fracture Mechanics in Yielding Materials", Journal of Strain Analysis, Vol. 1, #2, pp. 145-153, 1966.

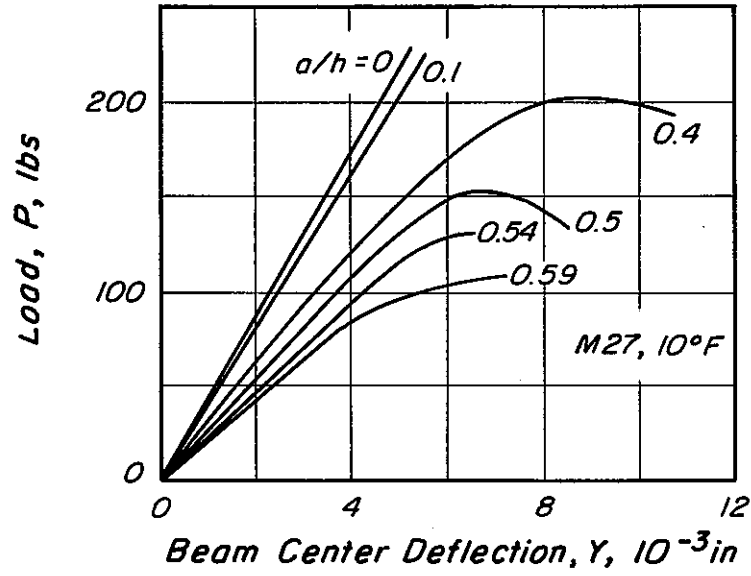


Fig. 11 - Variation of beam-center deflection with applied load for various notch depths.

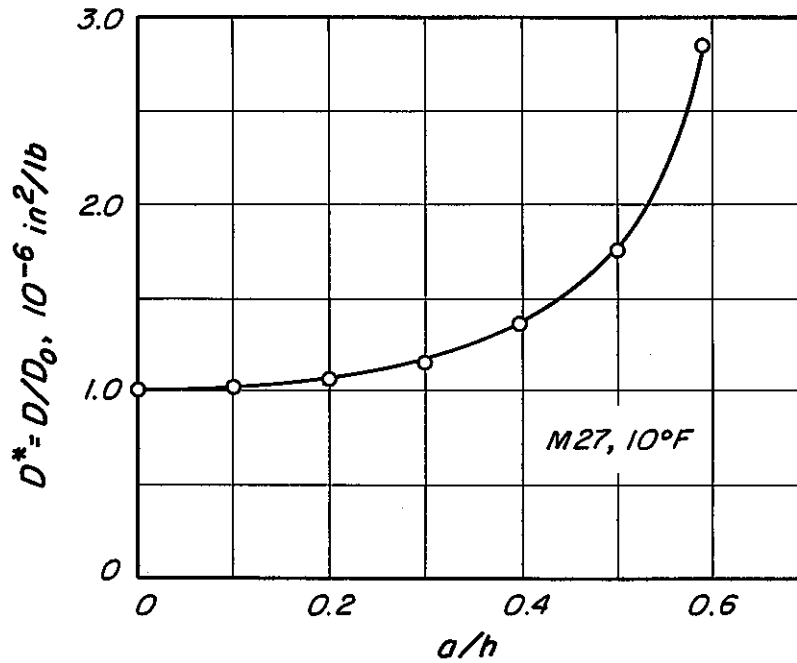


Fig. 12 - Normalized deflection compliance as a function of notch depth.

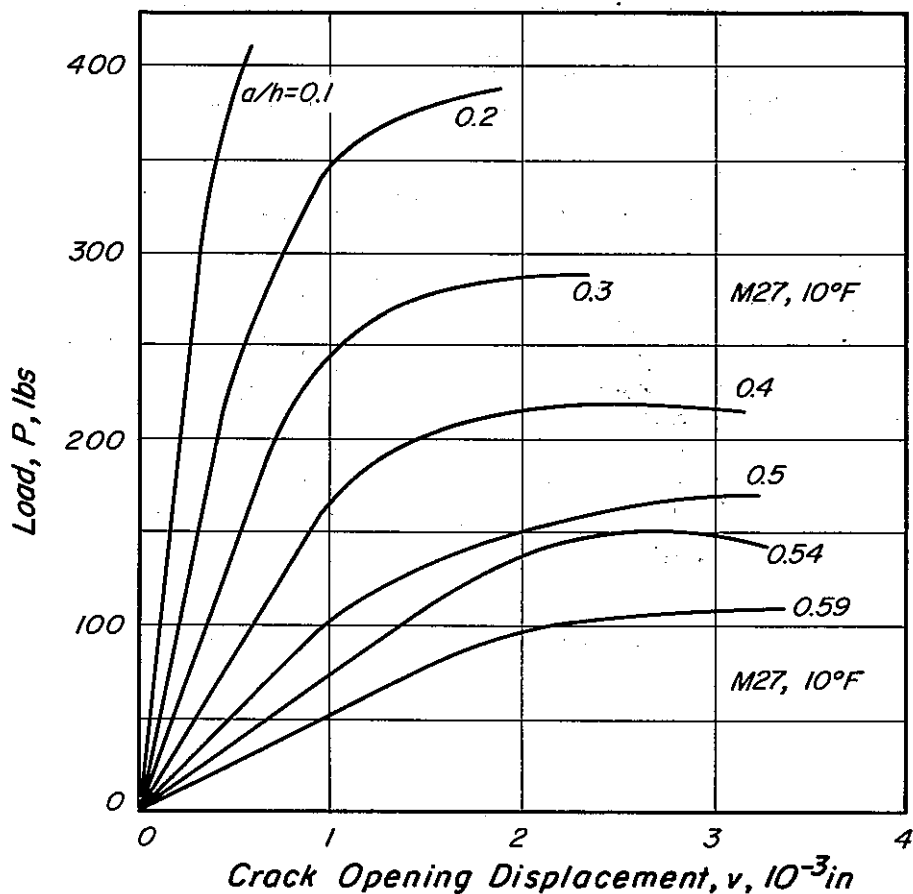


Fig. 13 - Variation of C. O. D. with applied load for various notch depths.

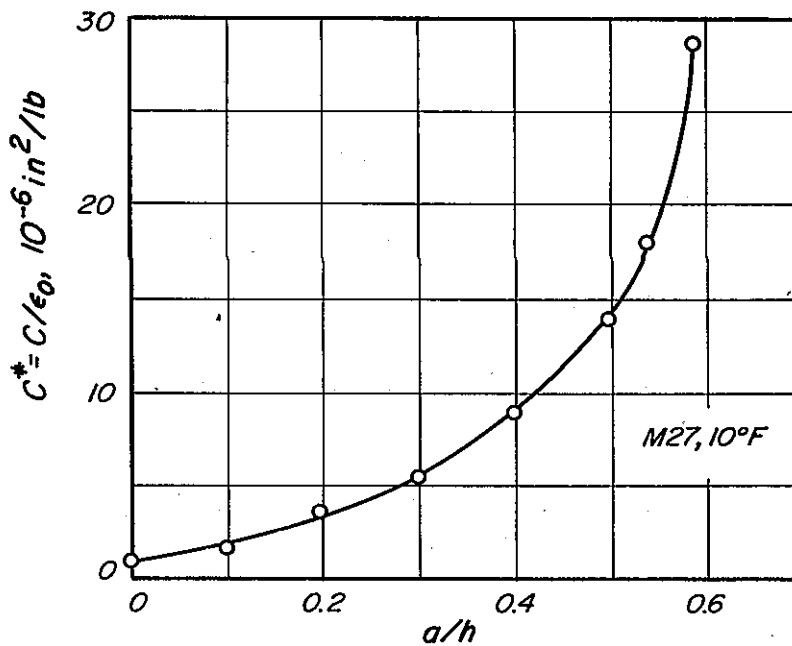


Fig. 14 - Normalized crack compliance as a function of notch depth.

This in turn is related to the fracture toughness:

$$v = \frac{1 - \nu^2}{E} \frac{K_I^2}{\sigma_y}$$

which indicates that the crack opening displacement is dependent upon K_I^2 .

Fig. 13 illustrates the influence of notch depth on the load vs. C. O. D. relationship for mix M27 at 10°F. The crack compliance can be computed for the inverse slopes of these curves in a manner similar to that for deflection compliance, i. e.

$$C(\text{crack compliance}) = \frac{v \cdot b}{P}$$

A normalized relationship is shown in Fig. 14. To plot this figure the initial value of crack compliance was taken as the strain value since C. O. D. measurements were taken over a 1 in. span in the vicinity of the notch.

